Spring 2007

Seagrass-Mediated Carbonate Dissolution and Early Diagenesis in Bahamas Bank Sediments

Xinping Hu
Old Dominion University

SEAGRASS-MEDIATED CARBONATE DISSOLUTION AND EARLY DIAGENESIS IN BAHAMAS BANK SEDIMENTS

by

Xinping Hu
B.S. July 1997, Beijing University

A Dissertation Submitted to the Faculty of
Old Dominion University in Partial Fulfillment of the
Requirement for the Degree of

DOCTOR OF PHILOSOPHY

OCEANOGRAPHY

OLD DOMINION UNIVERSITY
MAY 2007

Approved by:

David J. Burdige (Director)

Desmond Cook (Member)

Robert F. Dias (Member)

Richard C. Zimmerman (Member)

ABSTRACT

SEAGRASS-MEDIATED CARBONATE DISSOLUTION AND EARLY DIAGENESIS IN BAHAMAS BANK SEDIMENTS

Xinping Hu
Old Dominion University, 2007
Director: Dr. David J. Burdige

This dissertation presents the results of studies examining the role that seagrasses play in carbonate dissolution and early diagenesis of Bahamas Bank sediments. Three aspects of this problem are addressed: (1) stable carbon isotopes as an indicator of early diagenesis of carbonates, using results of a field study; (2) carbonate dissolution stoichiometry and carbonate reprecipitation, using the results from closed-system sediment incubation studies; (3) carbonate dissolution and reprecipitation across the broader Bahamas Bank. In Chapter II, I examined $\delta^{13}C$ in the dissolved inorganic carbon (DIC) of sediments with various degrees of seagrass densities. In low seagrass density and bare oolitic sand sediments, isotope mass balance could be explained by 1:1 mixing of DIC from carbonate dissolution and aerobic respiration. In contrast, pore water DIC in dense seagrass sediments was more enriched in ^{13}C than predicted by the simple mixing model. A carbonate dissolution/reprecipitation model was proposed to explain these observations. In Chapter III, a series of closed-system sediment incubation experiments was carried out under controlled oxygen input rates (i) to further test the carbonate dissolution/ reprecipitation model, (ii) to calculate reprecipitating carbonate phases, and (iii) to examine the relationship between the rates of oxygen consumption and carbonate dissolution in the these carbonate sediments. The carbonate reprecipitation model adequately explained pore water DIC ^{13}C enrichment when dissolution and reprecipitation occur. Furthermore, using pore water data and solid phase analyses and assuming a high magnesium calcite (HMC) phase with ~12 mole% Mg dissolved in these sediments, the reprecipitated carbonates had only a slightly lower Mg content than the starting material. Chapter IV presents the investigation of carbonate reprecipitation and dissolution mediated by seagrass based on an extensive pore water data set on the

Bahamas Bank scale. A numerical advection-diffusion-reaction (ADR) model was used to calculate depth integrated reaction rates (i.e., fluxes at the sediment-water interface). The carbonate dissolution flux was then further examined as a function of seagrass density and sediment permeability. Based on the model results, a positive linear correlation was found between carbonate dissolution and leaf area index (LAI), while carbonate dissolution and sediment permeability showed no significant correlation. Carbon dissolution was found to be the likely dominant carbonate removal mechanism that accounts for ~50% of gross carbonate production.

This thesis is dedicated to Li, and Jessica Danyang.

ACKNOWLEDGMENTS

First and foremost, I want to thank Dr. David J. Burdige for his direction during my Ph.D. study all these years. His tenacity toward the scientific truth has many times corrected the course of my study and prevented it from straying into the lost. I am grateful for his tireless help with my research work whenever I needed it and invaluable comments and suggestions on my writings.

I want to thank Dr. Richard C. Zimmerman. From the perspective of a biological oceanographer as well as a statistician, his view of scientific questions and tough criticisms often prompted me to rethink the problems I was trying to solve. I also truly enjoyed working with him during our three field trips together to the Bahamas.

Drs. Robert F. Dias and Desmond Cook both provided valuable instrument help and kindly allowed me sufficient time to finish up my enormous number of samples. I benefited a lot from the class - "Stable Isotope Geochemistry" that Dr. Dias taught, through critically examining the data interpretations in the literature he provided, and most importantly, his tough criticisms. I will never forget the times when he came to help with the instruments during weekends and holiday breaks. Dr. Cook offered valuable suggestions on my writing, which significantly improved the quality of my dissertation.

During my long time study here, I have bothered Drs. Gregory Cutter, Dennis Darby, Fred Dobbs, Donald Swift, and Mrs. Linda Cutter countless times for lab supplies and help with sample pre-treatments and analyses. Dr. Dobbs has also guided me through some complicated statistical mazes; he also pointed out a good reference for scientific writing, which helped me a lot in my dissertation writing. Joy Davis offered me selfless help with stable isotope measurements and always kindly answered my phone calls whenever I met problems. Drs. Lisa Drake at US Coast Guard Academy, Heidi Dierssen at University of Connecticut, Laura Bodensteiner at Moss Landing Marine Labs, and Scott Kline, Kimberly Krecek, and Kip Gardner at ODU all helped much with sample collection in the field as well as with sample analyses. Dave Winter at University of California Davis, Yongcheng Ji at Rutgers University, Mark Shaw at ODU Physics Department, and Dr. Zhongxing Chen at ODU Chemistry Department all kindly helped

me with sample analyses and their help is highly appreciated.

During the three field trips to the Bahamas, staff and crew members of both the Caribbean Marine Research Center (CMRC) and R/V *F. G. Walton Smith* provided valuable help with sample collections. Their companionship made the beautiful Bahamas even more so and those experiences will be a life-long asset in my professional life.

In correspondence with Drs. Frank Millero and Niel Plummer, both provided prompt replies regarding the problems I faced and I have gained a lot through communicating with them.

What makes my study at ODU unforgettable is the Department of Ocean, Earth and Atmospheric Sciences. The departmental staff - Dana Oblak, Toni Mason were all there whenever I needed help. I want to thank the department for the financial support during my first two years and the webmaster job during the last two years, which gave me a great peace of mind to concentrate on my study.

I also want to thank my dear friends - Bin Zhang, Drs. George Wong, Jianwu Tang, and Yingzhong Tang, who made the sometimes "boring" life at ODU much more enjoyable. I appreciate Dr. Wong's kind and always useful suggestions on my future career planning.

Finally, special thanks go to my wife - Li, daughter - Jessica Danyang, who have been quietly tolerating my frequent absence from home, and to my parents, who encouraged me to come to the US for further education. Without their long time unconditional firm support, the path leading to a Ph.D. would have never opened.

TABLE OF CONTENTS

LIST OF TABLES

Table Page

LIST OF FIGURES

Figure Page

Figure Page

CHAPTER I
INTRODUCTION

Dissolution of deep sea carbonate sediments has been recognized as a major buffering mechanism in the ocean to compensate for rising atmospheric CO_2 over long (10^3 years) time scales (Archer et al., 1998). Similarly, dissolution of tropical shallow water carbonate has also been proposed as a potential buffer to regulate atmospheric CO_2 on decadal time scales (Halley and Yates, 2004; Yates and Halley, 2006), although its importance remains controversial at present (Andersson and Mackenzie, 2004; Andersson et al., 2003; Morse et al., 2006). Carbonate sediments in shallow water tropical environments account for 30-40% of global oceanic carbonate production and accumulation although they cover only 3% of modern ocean area (Ku et al., 1999). On the Bahamas Bank and adjacent Florida Bay, the estimated gross water column carbonate production is ~5 mol/m^2/yr (Broecker and Takahashi, 1966; Milliman, 1993), of which ~50% accumulates in the sediments and the remaining ~50% may be removed either by export to surrounding deeper waters or by dissolution (Milliman, 1993; Walter and Burton, 1990). However, these estimates are highly uncertain due to different assumptions and techniques used in these studies. Therefore, further constraining the carbonate budget in these shallow water carbonate banks is necessary to better understand the role of these carbonate environments in regional to global carbon cycle.

Thalassia testudinum Banks ex König (turtle grass) is the dominant seagrass species and primary producer on the oligotrophic shallow water Bahamas Bank. Its biomass (dry weight, DW) can reach up to 1.1 kg DW/m^2 and it can have a net productivity of 2.5 kg DW/m^2/yr, as compared to the average phytoplankton productivity of 128 g DW/m^2/yr in the global ocean (Duarte and Chiscano, 1999; Tussenboek et al., 2006). Seagrass canopies reduce bottom water flow and can enhance the deposition of both particulate organic matter as well as fine-grained sediments from the water column to the sediments (Koch and Gust, 1999). The accumulation of particulate organic matter in seagrass beds promotes sedimentary microbial activity (Marbà et al., 2006). Seagrasses also transport

---

The journal model used in this dissertation is that of *Geochimica et Cosmochimica Acta.*

photosynthetic O_2 produced in the leaves through the root and rhizome to the below ground sediments (Bodensteiner, 2006; Borum et al., 2005; Enriquez et al., 2001; Jensen et al., 2005; Pedersen et al., 1998). Therefore seagrasses promote aerobic respiration of sedimentary organic matter, leading to "metabolic" CO_2 production in the sediments. This then drives down the pore water pH and carbonate ion concentration (Morse et al., 1987):

$$CO_2 + CO_3^{2-} + H_2O \Rightarrow 2HCO_3^- \quad (1)$$

On the Bahamas Banks, and many other shallow water carbonate platforms, the overlying waters are supersaturated with respect to all carbonate phases (Morse, 1985). As a result, rxn. (1) drives pore water toward carbonate undersaturation and once the pore waters are sufficiently undersaturated with respect to the most soluble carbonate phase, carbonate dissolution can occur (Burdige and Zimmerman, 2002; Ku et al., 1999; Morse et al., 1985; Walter and Burton, 1990). These reactions can be expressed in the following simplified fashion:

$$CH_2O + O_2 \Rightarrow CO_2 + H_2O \quad (2)$$

$$CO_2 + CaCO_3 + H_2O \Rightarrow Ca^{2+} + 2HCO_3^- \quad (3)$$

$$CH_2O + O_2 + CaCO_3 \Rightarrow Ca^{2+} + 2HCO_3^- \quad (4)$$

This dissolution driven by aerobic oxidation of organic carbon is generally referred to "metabolic carbonate dissolution" (Emerson and Bender, 1981).

In studies carried out in Florida Bay carbonate sediments, Walter and Burton (1990) observed a discrepancy between the amount of carbonate dissolution and the required amount of O_2 input to produce the necessary acid. These authors and Ku et al. (1999) further suggested that seagrass O_2 input in the root and rhizome zone might be the source of the O_2 needed to close the mass imbalance between O_2 input and the extent of carbonate dissolution. As the first study that quantitatively investigated the role of seagrass on addressing such mass imbalance, Burdige and Zimmerman (2002) found that diffusive O_2 input could only account for ~50% or less of the organic carbon oxidation/net carbonate dissolution calculated in the dense seagrass vegetated sediments. Therefore seagrass O_2 input presumably accounts for the "missing" O_2 source in the dense seagrass sediments. Although not quantitatively addressed in their study, pore

water advection was proposed as an important mass transport mechanism in these permeable sediments.

Based on the reaction stoichiometry in rxns. (2) to (4), one unit of O_2 consumption leads to one unit of metabolic carbonate dissolution, therefore a study of O_2 input mechanisms in these carbonate sediments is very important in terms of understanding carbonate dissolution. In addition to the seagrass O_2 input as discussed above, various physical factors may be responsible for O_2 delivery into the sediments. They include molecular diffusion (Berner, 1980) and pore water advection, which is also affected by sediment topography, grain size, and wave pumping (Huettel and Webster, 2001; Malan and McLachlan, 1991; Reimers et al., 2004). However, there are relatively few studies of pore water O_2 dynamics in coarse-grained carbonate sediments (Falter and Sansone, 2000; Rasheed et al., 2004) as compared to those in fine-grained continental margin and deep sea sediments (e.g., Cai and Sayles, 1996). Given the importance of O_2 in organic matter oxidation in the top centimeters of these coarse-grained sediments (Rasheed et al., 2004), the study of pore water O_2 input may provide a way to estimate the overall rate of sedimentary organic matter remineralization, as has been indicated in past studies of more fine-grained sediments (Cai and Reimers, 1995; Canfield et al., 1993). This can then be further linked back to carbonate metabolic dissolution caused by aerobic respiration in the sediments (Jahnke et al., 1997; Moulin et al., 1985; Wenzhoger et al., 2001).

Although metabolic dissolution occurs widely in the shallow water carbonate sediments (Burdige and Zimmerman, 2002; Ku et al., 1999; Morse et al., 1985; Walter et al., 1993; Walter and Burton, 1990), these carbonates also undergo "reprecipitation" (or "recrystallization" as is sometimes reported in the literature) at the same time, due to differences in the solubility of various carbonate phases. Carbonate reprecipitation has been confirmed both in natural environments (Hover et al., 2001; Macintyre and Reid, 1995; Macintyre and Reid, 1998; Morse and Mucci, 1984; Reid and Macintyre, 1998; Reid et al., 1992; Rude and Aller, 1991; Walter et al., 1993) and in laboratory studies (Mucci, 1987; Tribble and Mackenzie, 1998). In Bahamas Bank sediments, even though a highly soluble carbonate phase (such as high magnesium calcite, HMC) undergoes

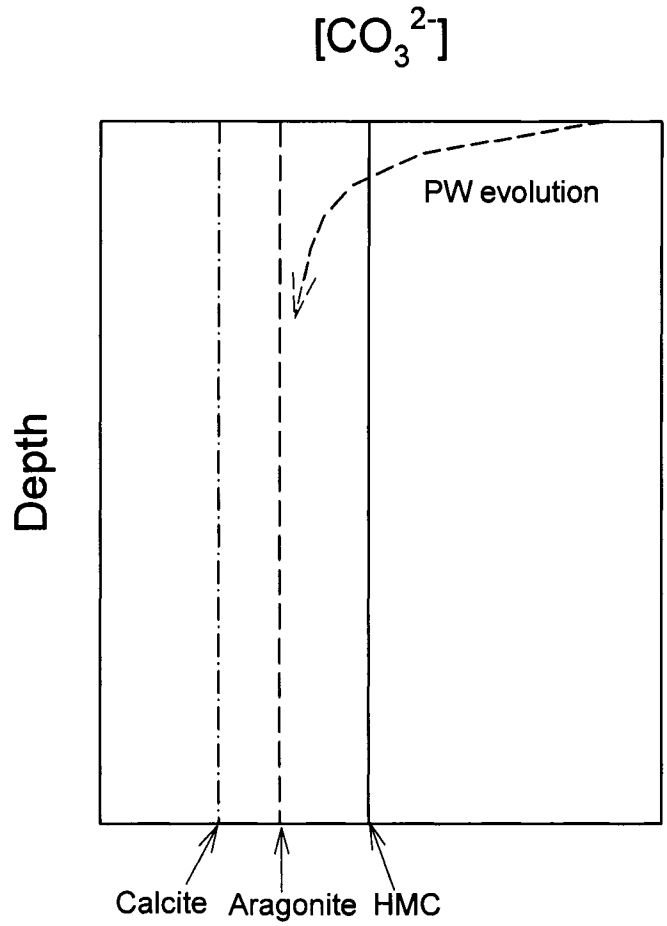

Fig. 1. A schematic illustration of how the pore water saturation state changes with depth across different carbonate solubility zones. Note that metabolic CO_2 decreases carbonate saturation state for all phases, although HMC will be the first phase to undergo dissolution (Morse et al., 2006). At the same time, however, the pore water may still remain supersaturated with respect to either calcite or aragonite.

dissolution, pore waters can still be supersaturated with respect to calcite and sometimes, even aragonite (Morse et al., 1985). Fig. 1 illustrates how the pore water saturation state changes as a result of microbial respiration.

Because of the difference in stable carbon isotope signatures ($\delta^{13}C$) of marine organic carbon (approx. -18 to -23‰ PDB) and calcium carbonate (approx. 0-4‰ PDB, e.g., McCorkle et al., 1985; Patterson and Walter, 1994, also see Fig. 1), the occurrence of rxn. (4) adds relatively light (i.e., depleted in ^{13}C) dissolved inorganic carbon (DIC) to sediment pore waters as compared to values of ~0-2‰ in the water just above the

sediments-interface (Dill, 1991; Patterson and Walter, 1994; Zeebe and Wolf-Gladrow, 2001).

Carbonate dissolution/reprecipitation could therefore potentially affect the isotopic composition of the carbonate minerals, and contaminate the carbonate sediment record. However, few studies have examined these processes in detail (e.g., Patterson and Walter, 1994; Turner et al., 1986). Furthermore, differences between the $\delta^{13}C$ of sediment organic matter and sediment carbonates implies that the $\delta^{13}C$ of pore water DIC should also provide information on the relative contributions of carbon pool from aerobic respiration and carbonate dissolution to the pore water DIC. Such analyses have been carried out successfully in both deep sea (e.g. Gehlen et al., 1999; Martin et al., 2000; McCorkle et al., 1985; Sayles and Curry, 1988) and continental margin (Presley and Kaplan, 1968) sediments. In contrast, in some shallow water marine environments the pore water DIC pool was found to be too enriched in ^{13}C and therefore could not be explained solely by these processes (Eldridge and Morse, 2000; McNichol et al., 1991).

Further study is clearly necessary to examine whether stable isotope techniques can be used in carbonate-rich sediments to differentiate DIC carbon sources to the pore waters.

This dissertation presents the results of research that is closely associated with an NSF-sponsored project to investigate the role of seagrasses in the dissolution and early diagenesis of carbonate sediments on the Bahamas Bank. In the following chapters I will address the problems introduced in the discussions here, and further expand our current understanding of this complex, yet fascinating, carbonate depositional environment. Chapter II presents an initial study of the $\delta^{13}C$ of pore water DIC, designed to examine the sources of DIC to the pore waters. This work also provided evidence for ^{13}C enrichment in pore water DIC in sediments underlying dense seagrass beds, and a coupled carbonate dissolution/reprecipitation model was proposed to explain this enrichment. Chapter III used the results from a series of closed-system incubation experiments to test the validity of the dissolution/reprecipitation model; and by manipulating the O_2 input to the experiments, the relationship between O_2 consumption and carbonate dissolution rates was also examined. Chapter IV examined carbonate dissolution/reprecipitation on a much larger geographic scale using pore water data.

Burdige et al. (submitted) proposed a pore water Advection-Diffusion-Reaction (ADR) numerical model based on our previous studies at Lee Stocking Island sediments. This model successfully combined O_2 input through three different mechanisms (i.e., seagrass input, advection and diffusion), and achieved mass balance among the depth-integrated fluxes of O_2 consumption, organic carbon oxidation, and carbonate dissolution. However, to further use this model on the bank scale to better constrain the carbonate dissolution budget, a study that covers a great expanse of the Bahamas Bank is therefore necessary. This ADR model was applied to the data in this chapter to investigate the reaction rates and O_2 transport mechanisms in these sediments, and using these results I have re-examined carbonate budget on the Bahamas Bank, as well as the global significance of carbonate dissolution on all carbonate banks and bays. Chapter V summarizes the conclusions drawn from Chapters II, III, and IV, and proposes further directions for the studies in these carbonate sediments-seagrass systems.

CHAPTER II

ENRICHED STABLE CARBON ISOTOPES IN THE PORE WATERS OF CARBONATE SEDIMENTS DOMINATED BY SEAGRASSES: EVIDENCE FOR COUPLED CARBONATE DISSOLUTION AND REPRECIPITATION

1. INTRODUCTION

Remineralization of sedimentary organic matter by aerobic respiration produces metabolic CO_2, and in undersaturated pore waters this CO_2 can react with carbonate sediments, causing their dissolution (see, e.g., Burdige and Zimmerman, 2002; Emerson and Bender, 1981, for further details). Approximating sediment organic matter as "CH_2O", these processes can be expressed as,

$$CH_2O + O_2 \rightarrow CO_2 + H_2O \quad (5)$$

$$CO_2 + CaCO_3 + H_2O \rightarrow Ca^{2+} + 2HCO_3^- \quad (6)$$

$$CH_2O + O_2 + CaCO_3 \rightarrow Ca^{2+} + 2HCO_3^- \quad (7)$$

and the coupling of aerobic respiration and carbonate dissolution implies that both processes can contribute to the pore water DIC pool. Our past studies (Burdige and Zimmerman, 2002) have also shown that seagrasses may enhance the dissolution of carbonate sediments when photosynthetically-produced O_2 is "pumped" into the sediments through root and rhizome tissues and therefore promotes aerobic respiration in the sediments (i.e., rxn. 5). This O_2 input by seagrasses may also help to resolve the mass balance problem observed in some carbonate sediments between the extent of sediment carbonate dissolution and the amount of oxidant needed to produce the necessary amount of acid (Ku et al., 1999; Walter and Burton, 1990).

This chapter is reprinted from *Geochimica et Cosmochimica Acta*, Vol. 71, X. Hu and D. J. Burdige, Enriched Stable carbon isotopes in the pore waters of carbonate sediments dominated by seagrasses: evidence for coupled carbonate dissolution and reprecipitation, pp. 129-144, Copyright (2007), with permission from Elsevier.

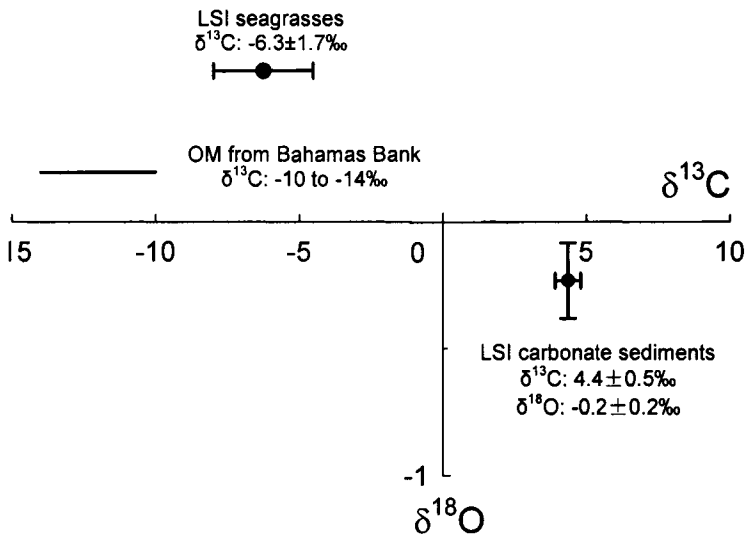

Fig. 2. $\delta^{13}C$ of carbonate sediments and seagrasses. Sedimentary organic matter (OM) $\delta^{13}C$ data are from the literature (Rasmussen et al., 1990; Scalan and Morgan, 1970).

Because of the difference in stable carbon isotope signatures ($\delta^{13}C$) of marine organic carbon (approx. -18 to -23‰ PDB) and calcium carbonate (approx. 0-4‰ PDB, e.g., McCorkle et al., 1985; Patterson and Walter, 1994; also see Fig. 2), the occurrence of rxn. (7) adds relatively light (i.e., depleted in ^{13}C) dissolved inorganic carbon (DIC) to sediment pore waters as compared to bottom water values of ~0-2‰ (Zeebe and Wolf-Gladrow, 2001); (also see Dill, 1991; Patterson and Walter, 1994). Furthermore, differences between the $\delta^{13}C$ of sediment organic matter and carbonates implies that the $\delta^{13}C$ of pore water DIC should provide information on the relative contributions of carbon to the pore water DIC pool from aerobic respiration and carbonate dissolution. Such analyses have been carried out successfully in both deep sea (e.g. Gehlen et al., 1999; Martin et al., 2000; McCorkle et al., 1985; Sayles and Curry, 1988) and continental margin (Presley and Kaplan, 1968) sediments. In contrast, in some shallow water marine environments the pore water DIC pool was found to be too enriched in ^{13}C and therefore could not be explained solely by these processes (Eldridge and Morse, 2000; McNichol et al., 1991).

In this paper I present results of pore water DIC stable isotope studies in Great Bahamas Bank (GBB) sediments, which suggest that both carbonate dissolution and reprecipitation are important in shallow water carbonate sediments, and also influence the isotopic composition of pore water DIC. The significance of such a dissolution/ reprecipitation process is further examined with a simple closed-system model, and all of the results are used to re-assess the importance of carbonate reprecipitation in the early diagenesis of carbonate sediments.

2. STUDY AREA AND METHODS

2.1. Sampling Locations

Pore water, sediments and seagrass samples were collected at sampling locations around Lee Stocking Island (LSI), Exuma Cays, Bahamas (Fig. 3), using the Caribbean Marine Research Center (CMRC) as the base of operation. The majority of the results

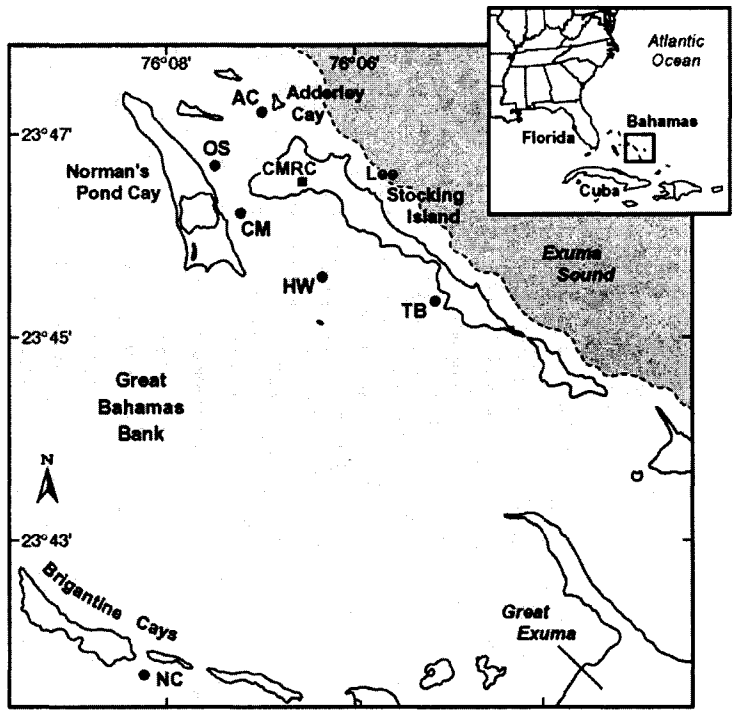

Fig. 3. A map of the LSI6 and LSI7 sampling sites.

described here were obtained in May-June 2003 (LSI 7), although some results from the May-June 2002 trip (LSI 6) are also described. Additional details about LSI sediments are presented in Section 3.1.

2.2. Sample Collection and Processing

Pore water were collected *in situ* by divers using sippers designed to collect pore waters from sandy sediments such as those around LSI (Burdige and Zimmerman, 2002). The sippers consist of a set of 10 ml Hamilton Gastight® syringes held in a rigid rack mounted on a small plate (6" x 12") with probes of different lengths (1-20 cm) that penetrate the sediments. The syringes are attached to metal springs that when released, slowly pull back on the plunger and draw the sample into the syringe. In this study, the sampling probes consisted of 18-gauge (ID 1.024 mm) Luer-lock needles that were cut to the appropriate lengths, silver soldered at the bottom end, and then rounded. Eight sample holes (0.38 mm ID) were drilled perpendicularly into the tube 2 mm from the tip (see Berg and McGlathery, 2001, for further details). The sampling probes are connected to the glass syringes with plastic 3-way stopcocks, which allow the divers to seal the syringes *in situ* immediately after pore water collection. The pore water volume retrieved with these samplers was usually 8-10 ml per sample. Additional details about the design and use of these sediment sippers can be found in Burdige and Zimmerman (2002).

Pore water samples collected in this fashion were returned to the lab at CMRC for processing within 1 hour of collection. First, dissolved O_2 was determined on unfiltered samples taken directly from the glass syringe (Burdige and Zimmerman, 2002; Hu and Burdige, unpubl. data). Samples were next filtered (0.45 μm. dia nylon disc filters) into appropriate storage vessels for analysis either at CMRC or back at ODU (Table 1).

2.3. Analytical Procedures

Total alkalinity was determined by Gran titration (Grasshoff et al., 1999) with automated end point detection (uncertainty, ±2%) using a Cole-Parmer pH electrode and a Metrohm 785 DMP Titrino automatic titrator. The titrant was certified 0.02N HCl, and Scripps Reference Seawater for CO_2 Measurement (Batch 51, 1999) was also used as an external reference standard (Dickson et al., 2003). Pore water DIC concentrations were

Table 1. Sample storage and processing.

Sample type	Sample Storage	Time of Analysis
DIC (concentration)	1.8 ml serum vials were filled completely and crimp-sealed with no headspace	Within 2 months (ODU)
DIC ($\delta^{13}C$)	Same as DIC (concentration)	Within 6 months (ODU)
Titration alkalinity	3 ml plastic syringe were partially filled with no headspace and sealed with 3-way stopcocks	Within 2 days (Bahamas)
Sulfide	Same as DIC (concentration)	Within 2 days (Bahamas)
Major Ions (Ca^{2+}, SO_4^{2-})	2 ml snap-cap vials were partially filled and sealed	Within 2-3 months (ODU)
Chlorinity	Same as major ions	Within 2-3 months (ODU)
Salinity	Measured by refractometer	During sample processing

determined coulometrically using a UIC Inc 5011 coulometer (DOE, 1994), with an uncertainty of <2%. Pore water chlorinity was determined by potentiometric titration using $AgNO_3$ with automatic end point detection (Grasshoff et al., 1999) using a Titrino™ titrator and a Metrohm® Ag-Titrode (Metrohm Ti Application Note No. T-1). The $AgNO_3$ titrant was standardized against IAPSO standard seawater. No significant chloride concentration variation (<1% of the average bottom water value of 571mmol/kg) was observed in the upper 20 cm of sediment pore waters. Sulfate was measured by ion chromatography with an uncertainty of 4% (Burdige and Zimmerman, 2002), while sulfide was determined using the spectrophotometric method described in Cline (1969) with an uncertainty of ~2%.

The $\delta^{13}C$ of pore water DIC was determined following the approach described in Salata et al. (2000). Briefly, 0.1 ml concentrated H_3PO_4 (75%) was first pipetted into 1.8 ml serum vials, and the vials were crimp-sealed with rubber serum stoppers and open top aluminum caps. The sealed vials were evacuated using a VacTorr™ 25 vacuum pump (Precision Scientific) for 3 minutes, and 0.8 ml of a pore water sample was then immediately injected into the vial using a 1 ml Hamilton Gastight® syringe flushed with

ultra pure He. Fast effervescence was observed upon sample injection. After sample acidification, the vials were equilibrated to atmospheric pressure with ultrapure He using a flow controller equipped with a manometer (see Salata et al. 2000, for details). All acidified sample vials were placed on a shaker table and agitated for 5 hours followed by headspace CO_2 isotopic analysis within 30 hours of acidification. The headspace gas was extracted using a 100µl Hamilton Gastight syringe by first injecting ultra pure He into the sample vials to compensate for changes in the headspace pressure caused by sample removal. The CO_2 in the headspace gas was separated from water vapor by gas chromatography and the $\delta^{13}C$ of the CO_2 was measured on a PDZ Europa® GEO 20-20 isotopic ratio mass spectrometer (IRMS) with a precision of 0.2‰. All samples were determined in duplicate by this procedure. The IRMS was calibrated using two different laboratory CO_2 gas standards.

Pore water DIC $\delta^{13}C$ values were calculated using the measured $\delta^{13}C$ of the headspace CO_2 corrected for the fractionation between the aqueous and gaseous phases. At 25°C, the isotopic fractionation ($10^3 ln\alpha$) for this exchange is 1.1‰ with the gaseous phase being enriched in ^{13}C (see Salata et al., 2000 and references therein). In preliminary studies examining this extraction procedure, I determined the $\delta^{13}C$ of the headspace CO_2 as a function of the time after acidification; within 5 to 30, the headspace gas reached equilibrium with the aqueous phase, and there was no apparent contamination or loss of headspace gas. The minimum equilibration time here (5 hours) is significantly shorter than the 15 hours in Salata et al. (2000), and indicates that agitation of the vials after acidification greatly enhances the rate of isotope exchange between the gaseous and aqueous phases.

Seagrass samples collected *in situ* by divers were separated into leaves and rhizome/root tissues, and first soaked for 30 minutes in 1N HCl to remove any attached carbonate. This was followed by a distilled water rinse to remove excess acid. After oven drying at 60°C, samples were ground into a powder (Craig, 1953; McMillan, 1980). High temperature combustion (HTC) in O_2 was used to convert organic carbon to CO_2 using an automated nitrogen/carbon (ANCA) elemental analyzer attached to the IRMS. Analytical uncertainty of these $\delta^{13}C$ measurements is 0.2‰. A subset of these samples were freeze dried at -20 °C *in vacuo* after an acid cleaning and then ground to a powder; no

significant differences were observed in measured seagrass $\delta^{13}C$ values between these two sample treatments. Both DIC and seagrass $\delta^{13}C$ values are reported relative to the PDB standard.

Isotopic analysis of sediment carbonate was carried out at the UC Davis Stable Isotope Lab. Dry sediments were first heated *in vacuo* at 75°C for 30 minutes and the CO_2 gas used for analysis was generated by acidification of the treated sediments in a heated (90°C) common acid bath (103% phosphoric acid). The resultant gas was then purified and introduced into a GVI Optima IRMS. The $\delta^{13}C$ values were calculated relative to V-PDB. Average precision (1σ) is ±0.04‰. Since the difference between V-PDB and PDB is negligibly small (Mook and Vries, 2001), the complete isotopic data set is internally consistent.

Carbonate mineralogy of the sediments was determined by X-ray diffraction using a Philips PW 1729 X-ray diffractometer with CuKa radiation generated at 40kV and 30 MA following the procedure of Morse et al. (1985). The scanning interval was 25° to 32°2' 2θ at a scanning speed of 0.02° 2θ per 2 second scanning step. The calcite and aragonite standards used for calibration were both of marine origin. *Porites* was used for the aragonite standard and *Crassostrea* was used for the calcite standard. The peak area method was used to quantify the relative amounts of aragonite and high and low magnesium calcite (HMC and LMC) (Milliman and Bornhold, 1973; Morse et al., 1985). The mole percent Mg content in HMC was calculated from the shift of the major calcite peak (near 29.8° 2θ) using the lattice parameters in Goldsmith et al. (1961). The precision of the XRD analysis of carbonate mineralogy I observed was 1.5%, although the accuracy of this method is widely considered to be ~3-5% (Andrews, 1991; Milliman et al., 1993; Morse et al., 1985). The precision of the analysis of Mg content in HMC by XRD was 0.5%, and the XRD-determined Mg content of HMC agrees well with analyses using wet chemistry (Walter and Morse, 1984).

3. RESULTS AND DISCUSSION

3.1. Results and General Trends in the Data

Sites around LSI include unvegetated, well-sorted oolitic sands and seagrass meadows (mostly *Thalassia testudinum* or turtlegrass) of densities exceeding 500

Table 2. Sample site mineralogy (unit: wt% for mineralogy) [a].

Station		Aragonite	HMC	LMC	mol% Mg in HMC
DG	AC	57.0±2.4	39.0±1.7	4.0±0.6	12.3±0.03
	CM	63.1±4.8	34.0±4.2	2.9±0.5	12.3±0.07
	NC	81.4±2.4	16.6±2.4	2.0±0.2	11.8±0.03
IG	HW	83.8±2.6	15.1±2.4	1.1±0.2	12.4±0.09
	TB	84.2±0.2	14.2±0.1	1.6±0.1	12.4±0.53
OS	OS	84.6±2.6	14.1±2.8	1.3±0.1	13.4±0.20

[a] At each station, samples from three depths were analyzed (a surface sample in the upper 5cm of sediment, a mid-depth sample near 10cm, and a deep sample, generally at 16-20cm depth). The values reported here for each station are averages and the uncertainties are standard deviations based on these three analyses.

shoots/m^2 (see below and discussions in Dill, 1991). Water depths range from ~2-10 m. Sediments in this area have a mean grain size of 200-750 μm (Stephens et al., 2003) and are comprised of biogenic calcareous skeletal debris, ooids, peloids and grapestones. The dominant minerals are aragonite (70-90 wt%) and high-Mg calcite (10-30 wt%) with a small amount of low-Mg calcite (generally <3-4 wt% of the bulk sediments). The Mg content of the HMC was consistently ~12 mol% (Table 2).

In this study I divided the sampling sites into three groups based on seagrass densities (Bodensteiner and Zimmerman, unpubl. data; see Burdige and Zimmerman, 2002, for a description of the methods used here). Dense seagrass sites (sites AC, CM and NC) have average shoot densities of 561±50 shoots/m^2 and LAI (leaf area index) values of 1.4±0.1 (note that LAI is defined as m^2-one sided leaf area per m^2-seafloor, e.g. Campbell and Norman, 1998). Intermediate density seagrass sites (sites HW and TB) have average shoot densities of 274±30 shoots/m^2 and average LAI values of 0.5±0.2. Finally, bare oolitic sands (site OS) have no seagrass (shoot density and LAI equal to zero).

At all sites examined, DIC concentrations increase with sediment depth in the upper 20 cm (Fig. 4 and Table 3) and the magnitude of this increase is greatest at dense seagrass

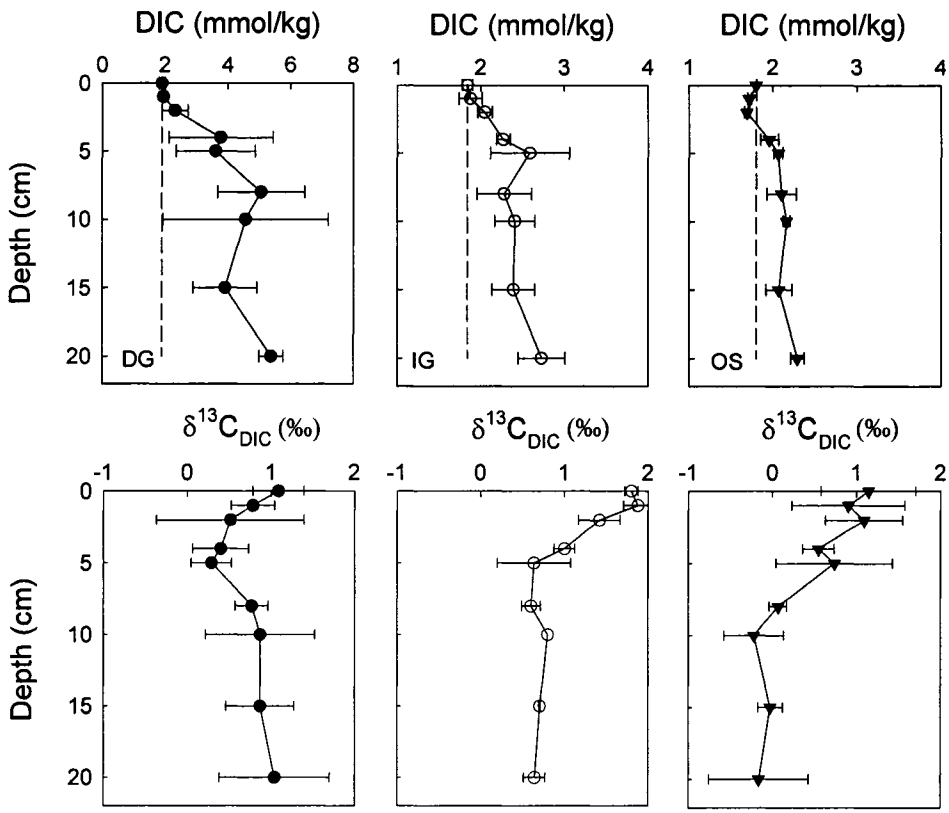

Fig. 4. Pore water depth profiles of DIC and the $\delta^{13}C$ of the DIC in dense and intermediate density seagrass sediments (DG and IG, respectively) and bare oolitic sand (no seagrasses, OS). The profiles shown here for each sediment type are average profiles based on individual profiles collected at different sites (n=4, 2, and 2 profiles for DG, IG and OS sites; respectively; see Table 3). In the upper DIC concentration profiles, the dashed line indicates the bottom water concentration. Uncertainties are standard deviations.

(DG) sites and smallest in the bare oolitic sands (OS). Intermediate density seagrass (IG) sites fell in-between the DG and OS sites, although they were closer in magnitude to the OS sites than the DG sites. These DIC concentration profiles in the seagrass vegetated sediments, along with alkalinity, Ca^{2+}, sulfate and O_2 profiles from LSI sediments (Hu and Burdige, unpubl. data) indicate that sediment carbonate dissolution occurs in the upper ~20cm of these sediments largely as a result of aerobic respiration sustained by seagrass O_2 input (or pumping) into this portion of the sediments (also see similar pore water profiles and discussions in Burdige and Zimmerman, 2002). Consistent with this

Table 3. Pore water data for LSI 6 and LSI 7 sampling trips.

Sites	Trip	Depth (cm)	pH	Cl^- (mmol/kg)	DIC (mmol/kg)	$\delta^{13}C$ (‰)	Alk (meq/kg)	Ca^{2+} (mmol/kg)	SO_4^{2-} (mmol/kg)	H_2S (mmol/kg)
DG										
AC	LSI7	0	8.03	588	1.84	1.41	2.00	10.93	28.5	0.00
		1	8.08	586	1.99	0.54	1.98	10.95	28.7	0.00
		2	7.52	581	2.65	0.37	2.64	10.89	26.7	0.00
		4	7.58	585	2.45	0.25	2.42	11.08	29.5	0.00
		5	7.41	580	2.63	0.15	2.84	11.48	27.5	0.38
		8	7.31	578	4.38	1.01	4.49	11.75	27.1	0.39
		10	7.50	568	2.32	0.44	2.39	11.22	23.3	0.93
		15	7.36	573	3.37	0.30	3.60	11.36	27.8	0.24
		20	7.31	576	5.13	1.01	5.33	11.80	29.2	1.29
CM	LSI7	0	7.95	597	2.03	1.04	1.95	10.80	30.6	-
		1	7.96	597	1.91	1.06	1.89	10.68	29.5	-
		2	8.01	594	1.88	1.59	1.80	10.91	30.7	-
		4	7.39	596	3.50	0.89	3.25	11.25	30.7	-
		5	7.34	591	5.04	0.01	2.97	11.75	30.5	-
		8	7.17	586	5.94	0.66	5.99	11.99	28.6	-
		10	7.36	582	3.95	0.48	3.73	11.38	31.1	-
		15	7.34	586	5.43	1.22	5.50	11.69	31.2	-
		20	7.29	583	5.94	1.59	5.96	11.65	30.2	-
CM	LSI6	0	8.08	576	1.95	0.69	2.29	10.74	29.7	-
		1	8.03	569	1.96	0.76	2.40	10.68	30.3	-
		2	7.96	571	2.03	0.66	2.33	10.66	30.4	-
		4	7.28	581	6.17	0.31	6.73	12.12	29.3	-
		5	7.03	584	4.29	0.47	4.13	11.44	30.5	-
		8	7.16	582	6.47	0.84	7.11	12.54	29.6	-
		10	7.09	586	8.37	1.83	8.73	12.84	29.6	-
		15	7.37	588	3.38	0.87	3.62	11.35	31.0	-
		20	7.19	586	5.11	1.43	5.44	11.93	30.7	-
NC	LSI7	0	7.89	581	1.80	1.21	2.06	10.74	29.4	0.00
		2	7.59	594	2.70	-0.55	3.02	11.10	28.9	0.01

Table 3. Continued.

Sites	Trip	Depth (cm)	pH	Cl- (mmol/kg)	DIC (mmol/kg)	$\delta^{13}C$ (‰)	Alk (meq/kg)	Ca^{2+} (mmol/kg)	SO_4^{2-} (mmol/kg)	H_2S (mmol/kg)
DG	LSI7	4	7.41	589	2.96	0.16	2.75	10.96	30.2	0.01
		5	7.44	588	2.47	0.50	2.43	10.77	29.4	0.60
		8	7.43	595	3.46	0.57	3.55	11.37	29.0	0.08
		10	7.41	588	3.62	0.72	3.62	11.25	28.5	0.00
		15	7.40	594	3.44	1.09	3.46	11.28	27.3	1.12
		20	7.38	596	5.35	0.12	5.15	11.64	28.9	0.77
IG										
HW	LSI7	0	7.80	577	1.88	1.88	2.13	10.60	-	-
		1	7.90	579	2.04	2.05	2.18	10.73	-	-
		2	7.75	584	1.97	1.67	2.08	10.75	-	-
		4	7.45	593	2.24	0.88	2.06	10.67	-	-
		5	7.34	593	3.11	0.20	3.22	11.02	-	-
		8	7.28	590	2.63	0.49	2.61	10.96	-	-
		15	7.38	588	2.68	0.71	2.73	10.92	-	-
		20	7.47	590	2.41	0.58	1.77	10.94	-	-
TB	LSI7	0	8.01	590	1.77	1.72	2.01	11.02	29.4	0.01
		1	7.98	590	1.81	1.71	1.97	10.96	28.0	0.01
		2	7.73	594	2.04	1.17	2.29	10.89	29.1	0.01
		4	7.54	591	2.21	1.13	2.04	10.82	29.4	0.01
		5	7.54	591	2.19	1.08	2.29	10.83	29.1	0.01
		8	7.51	592	2.23	0.72	2.24	10.74	29.2	0.01
		10	7.46	593	2.65	0.80	2.80	10.43	29.5	-
		15	7.49	594	2.19	0.70	2.14	11.22	29.6	0.02
		20	7.39	589	2.90	0.71	2.89	10.78	28.7	0.04
OS										
OS	LSI7	0	8.10	591	1.74	1.70	2.03	10.52	29.27	-
		1	7.94	593	1.66	1.58	1.95	10.71	28.64	-
		2	7.93	588	2.07	1.55	1.91	-	-	-
		4	7.56	582	2.01	0.36	2.18	10.64	28.91	-
		5	7.59	583	2.28	1.43	2.06	-	-	-

Table 3. Continued.

Sites	Trip	Depth (cm)	pH	Cl- (mmol/kg)	DIC (mmol/kg)	$\delta^{13}C$ (‰)	Alk (meq/kg)	Ca^{2+} (mmol/kg)	SO_4^{2-} (mmol/kg)	H_2S (mmol/kg)
OS	LSI7	8	7.59	584	2.20	-0.04	2.21	10.62	28.43	-
		10	7.64	583	2.23	-0.58	2.22	10.55	28.40	-
		15	7.60	582	2.21	0.12	2.19	10.69	28.32	-
		20	7.64	584	1.74	-0.76	2.28	10.77	27.78	-
OS	LSI6	0	7.57	632	1.80	0.58	1.92	11.43	32.3	-
		1	8.06	621	1.70	0.23	2.12	11.43	31.5	-
		2	8.08	613	1.72	0.63	2.20	11.21	31.7	-
		4	7.81	621	1.85	0.74	2.12	11.84	31.1	-
		5	7.73	590	2.12	0.04	2.43	11.09	30.1	-
		8	7.88	601	1.93	0.18	2.26	11.22	33.3	-
		10	7.79	599	2.12	0.13	2.42	11.03	30.8	-
		15	7.84	615	1.91	-0.17	2.25	11.20	31.7	-
		20	7.80	599	2.37	0.43	2.60	10.81	30.4	-

interpretation, more recent observations (Hu and Burdige, unpubl. data) indicate that >99% of the belowground seagrass biomass was distributed in the upper 20 cm of sediments.

At both the OS and IG sites, pore water DIC-$\delta^{13}C$ values decrease with sediment depth and reach constant values below ~10 cm (Fig. 4). However, the asymptotic $\delta^{13}C$ values at the OS site are slightly lighter than they are at the IG sites (approx. -0.1‰ vs. 0.7‰). In contrast, while pore water DIC-$\delta^{13}C$ values at the DG sites also initially decrease with depth, they then show a mid-depth minimum at ~5 cm, and return to near-bottom water values (~1‰) by the sediment depth of 20 cm.

3.2. Sources of Pore Water DIC

The isotopic composition of sediment carbonate and organic matter in Bahamas Bank sediments is shown in Fig. 2 and Table 4. Note that the $\delta^{13}C$ of organic matter in these sediments is heavier than "typical" marine organic matter (~-20‰) most likely due to the input of seagrass-derived organic matter (Rasmussen et al., 1990). Seagrass-derived organic matter is relatively heavy (e.g., LSI seagrasses are ~-6‰) because their photosynthetic carbon uptake shows less discrimination against heavy carbon than "typical" marine phytoplankton, despite the fact that seagrasses are also C_3 type plants (Anderson and Fourqurean, 2003; Hemminga and Duarte, 2000).

Both sediment organic matter remineralization and sediment carbonate dissolution may contribute DIC to the pore water pool. Given the distinct differences in the carbon isotope composition of these two sources (Fig. 2), the $\delta^{13}C$ of pore water DIC can be used to examine the relative contribution of these two sources to the pore water DIC pool. The

Table 4. Isotopic composition of seagrass and sedimentary carbonates (unit: ‰ PDB).

	DG	IG	OS
Seagrass [a]	-7.8±0.2	-4.5±0.2	-
Sediments	4.0±0.1	4.6±0.2	5.0±0.03

[a] There is no significant difference among isotopic values of seagrass leaves and rhizome/root tissues. Thus average values are reported here.

approach taken here is based on that presented by Sayles and Curry (1988) and Martin et al. (2000) in which they show that plots of (δ^{13}C-DIC)·[DIC] versus [DIC] are generally linear, and that the slope of such plots is the δ^{13}C of the DIC being added to the pore waters (defined here as $\delta^{13}C_{added}$; Fig. 5). Although not explicitly discussed in these works, this approach is very similar to that used to examine elemental ratios of the organic matter undergoing remineralization in marine sediments using pore water property-property plots (Berner, 1977; Burdige, 2006). However in the approach taken here, if I assume that total [DIC] is roughly equal to the pore water concentration of $DI^{12}C$ and that (δ^{13}C-DIC)•[DIC] is a "proxy" for $DI^{13}C$, then the slope of this line will yield the carbon isotopic composition of the DIC being added to the pore waters (see Appendix A for a more rigorous derivation).

Transport processes such as pore water advection or diffusion generally can impact the ability to use such property-property plots to examine these aspects of diagenetic processes in marine sediments (also see Hammond et al., 1999, for further details). For example, given the estimated permeability of LSI sediments (Burdige and Zimmerman, 2002), pore water advection through the sediments, due to near seabed pressure gradients caused by surface roughness or biogenic structures, is thought to be a significant transport process down to a depth of at least several centimeters (Huettel and Webster, 2001). This type of advection clearly affects concentrations of pore water solutes such as DIC and alkalinity, along with the ability to estimate rates of sediment processes from such pore water data without an accurate estimate of the magnitude of this advection. However, in terms of calculations such as those illustrated in Fig. 5, pore water concentrations will simply move "along" the mixing lines shown here as a function of pore water advection and DIC addition without changing the slope of the line (i.e. $\delta^{13}C_{added}$ will be largely independent of pore water advection).

Diffusion can also affect the interpretation of these property-property plots, although in most cases these effects are easily accounted for (Berner, 1980; Burdige, 2006). However, in the specific calculations presented here, the effects of diffusion may be slightly more complicated than that discussed in these references; nevertheless, this should not compromise the interpretation of the plots in Fig. 5.

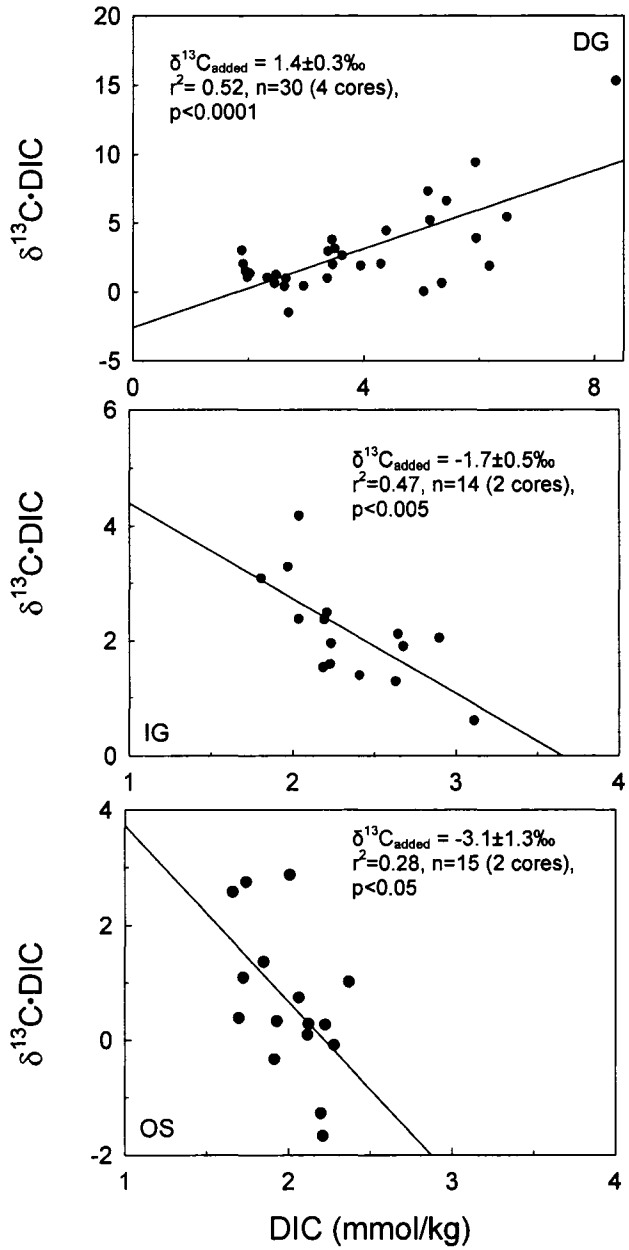

Fig. 5. Plot of DIC·$\delta^{13}C$ versus DIC for the three sediment types studied here. As discussed in the text, the slope of this line is the $\delta^{13}C$ of the DIC added to the pore waters ($\delta^{13}C_{added}$). Note the different axis scales on each figure.

Fits to the pore water data using this approach are shown in Fig. 5 and summarized in Table 5. Interpretation of these results in terms of eqns. (5) - (7) and possible sources of

Table 5. Isotopic composition of the DIC added to sediment pore waters.

	DG	IG	OS
$\delta^{13}C_{added}$ [a] (‰)	1.4±0.3	-1.7±0.5	-3.1±1.3
$\delta^{13}C_{OM}$ [b] (‰)	-1.2±0.5	-8.0±1.0	-11.1±2.6

[a] From Fig. 5. The uncertainties shown here are standard errors of the linear regressions in this figure.

[b] The calculated $\delta^{13}C$ of the sediment organic matter undergoing remineralization (see eqn. 9 and associated discussions in the text).

DIC to the pore waters requires that I make several assumptions. The first is that these sediments become sufficiently undersaturated below the sediment-water interface such that the coupling of eqns. (5)-(7) describes the processes that affect downcore variations in alkalinity, DIC and Ca^{2+} in these sediments. Evidence for this can be seen in Fig. 6 where I see the tight co-variance between increases in pore water alkalinity and DIC, consistent with these equations; similar trends are also seen with increases in pore water Ca^{2+} and DIC increases (Burdige and Zimmerman, 2002).

Another important assumption is that there is no net sulfate reduction in these sediments, since this process produces alkalinity and DIC at roughly equi-molar ratios in the absence of carbonate dissolution, as shown by the following reaction,

$$2CH_2O + SO_4^{2-} \rightarrow H_2S + 2HCO_3^- \qquad (8)$$

Several lines of evidence are consistent with the lack of net sulfate reduction occurring in these sediments. Previous work in LSI sediments (Burdige and Zimmerman, 2002), along with observations in this study (Fig. 7), demonstrate that pore water sulfate concentrations do not vary with sediment depth down to 20cm. These sulfate profiles also show no consistent downcore trends relative to bottom water values, as opposed to depth profiles of alkalinity, DIC and Ca^{2+} that increase "relatively" smoothly (and consistently) with depth (Fig. 4; Burdige and Zimmerman, 2002; also see Chapter IV). Finally, a property-property plot of ΔSO_4^{2-} vs. ΔAlkalinity (not shown here) has a slope that is indistinguishable from 0, and not the value of approx. -0.5 predicted by rxn. (8).

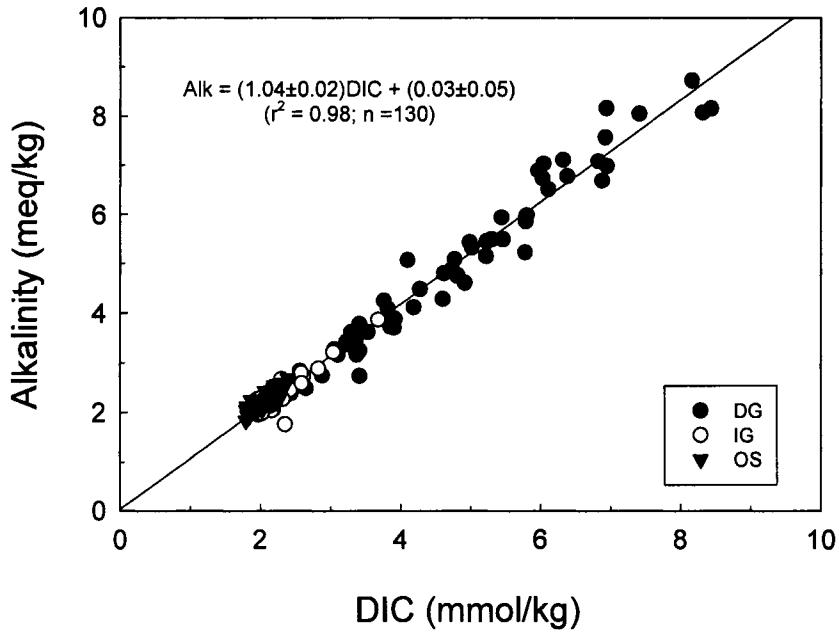

Fig. 6. Measured pore water alkalinity versus DIC in LSI sediments. The linear regression shown here was carried out using the data from sediment depths >2 cm (see discussions in Burdige and Zimmerman 2002 for details).

Given these observations, if I assume that contributions of DIC to the pore waters come from organic carbon oxidation and carbonate dissolution, then the following mass balance should be valid:

$$\delta^{13}C_{added} = f_{OM} \times \delta^{13}C_{OM} + f_C \times \delta^{13}C_C \qquad (9)$$

where f is the fraction of DIC input from either organic carbon oxidation (subscript *OM*) or carbonate dissolution (subscript *C*). Furthermore, if the rate of carbonate dissolution is fast relative to organic matter oxidation, i.e. reactions (5) - (7) are tightly coupled (Martin and Sayles, 2003), then $f_{OM} = f_C = 0.5$. With these assumptions then, I can calculate the $\delta^{13}C$ of the organic matter undergoing remineralization ($\delta^{13}C_{OM}$) based on the values of $\delta^{13}C_C$ from Table 4 and $\delta^{13}C_{added}$ from Table 5. These results are also shown in Table 5.

In the bare oolitic sands (OS site), the calculated $\delta^{13}C_{OM}$ value (-11.1±2.6‰) agrees well with the results from past studies of the $\delta^{13}C$ of organic matter in Bahamian sediments (approx. -10 to -14‰, Rasmussen et al., 1990; Scalan and Morgan, 1970). Furthermore, if I assume that water column particulate organic matter and/or benthic

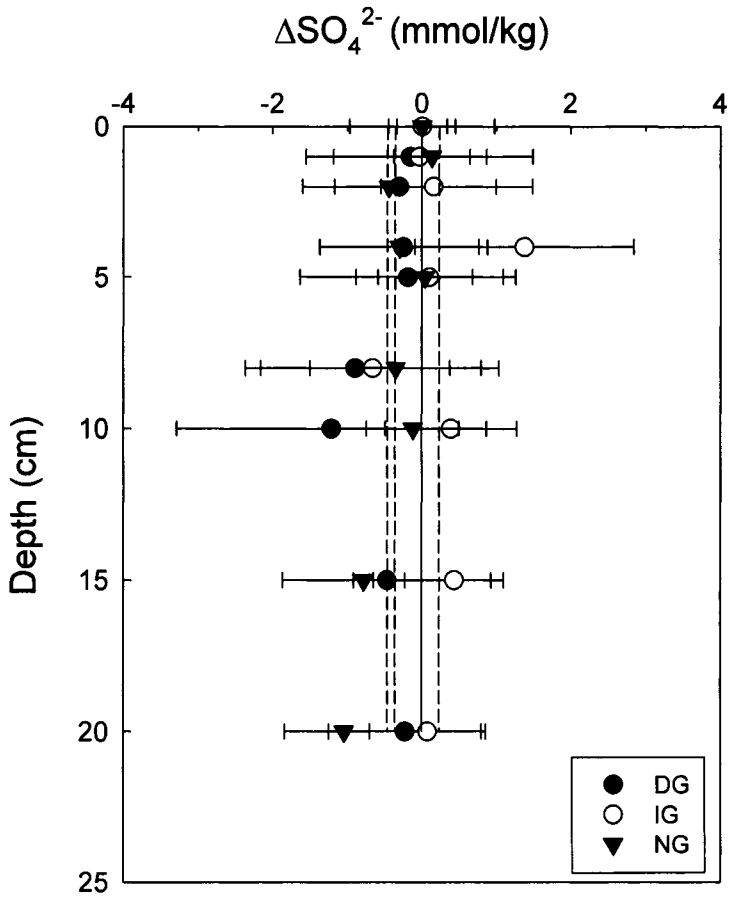

Fig. 7. Depth profiles of pore water ΔSO_4^{2-}, where $\Delta SO_4^{2-} = [SO_4^{2-}]_{pw} - [SO_4^{2-}]_{bw}/[Cl^-]_{bw} \cdot [Cl^-]_{pw}$ (subscripts *pw* and *bw* represent pore water and bottom water, respectively). This approach allows us to differentiate between small changes in sulfate concentration due to net sulfate reduction and those associated with change in pore water salinity. The dashed lines represent the average ΔSO_4^{2-} values in the DG, IG and OS sediments (-0.46±0.39, 0.23±0.57 and -0.36±0.40 mmol/kg, respectively, versus 0±1.12mmol/kg for bottom water samples). Similar results were obtained in these sediments by Burdige and Zimmerman (2002), and indicate that minimal net sulfate reduction occurs in these sediments.

algal production has $\delta^{13}C$ values that are in the range of -17 to -22‰ (e.g., Craig, 1953; Eadie and Jeffrey, 1973), this result suggests that the organic matter being remineralized in such bare sands is a mixture of non-seagrass derived organic matter and exported seagrass litter (with a presumed $\delta^{13}C$ value between -4 to -10‰; see Fig. 2).

In sediments underlying intermediate density seagrass beds (IG sites), the calculated value of $\delta^{13}C_{OM}$ (-8.0±1.0‰) is consistent with the range of $\delta^{13}C$ values for LSI

seagrasses (see Fig. 2). This suggests that seagrass-derived organic matter represents the major type of organic matter undergoing remineralization here. However, the $\delta^{13}C$ of seagrasses at the IG sites (-4.5 ± 0.2‰) is heavier than this value of $\delta^{13}C_{OM}$, suggesting that some fraction of the organic matter undergoing remineralization in the IG sediments could be either more typical detrital marine organic matter (as above), or lighter, exported seagrass litter from other nearby seagrass meadows (e.g., the DG sites; see Table 4).

In their studies of tropical seagrass sediments in coastal Thailand, Holmer et al. (2001) observed that the sediment bacterial biomass (based on the analysis of bacteria specific polar lipid derived fatty acids) has $\delta^{13}C$ values that are very close to that of the seagrass found at this site (ca. -12%), despite the existence of much lighter bulk sedimentary organic carbon (ca. -22‰), which is presumably detrital material of algal origin. Therefore it appears that organic matter remineralization in these sediments is largely driven by seagrass-derived organic matter, despite the fact that the presence of seagrasses (specifically the overlying leaf canopy) dampens water motion and promotes the deposition of inorganic and organic (detrital) particles from the water column to the sediments (e.g., Hemminga and Duarte, 2000; Koch and Gust, 1999). The remineralization of seagrass-derived materials in sediments such as these (as well as those at the DG sites) may occur through the incorporation of reactive seagrass litter into the bulk sediment organic matter pool, or through the release of seagrass-produced DOM from the roots and rhizomes of actively-growing plants (Holmer et al., 2001).

3.2.1. Sources of DIC in the pore waters of dense seagrass sediments.

At the OS and IG sites, pore water DIC isotopic mass balance appears to be satisfactorily explained by rxns. (5) - (7) given the likely sources of organic matter to these sediments. In contrast, the calculated $\delta^{13}C_{OM}$ in the dense seagrass sediments (DG sites) appears to be problematic ($\delta^{13}C_{OM}$ = -1.2±0.5‰), since no such heavy organic carbon existed in marine sediments that may be of biological origin. To the best of my knowledge, seagrasses have the heaviest organic carbon that is produced in shallow marine environments, with $\delta^{13}C$ values of up to -3‰ (Hemminga and Mateo, 1996). Seagrasses collected at the DG sites were in fact much lighter (-7.8±0.2‰).

These observations at the DG sites are not necessarily unique to these sediments, since other workers (Eldridge and Morse, 2000; McNichol et al., 1991) have similarly observed ^{13}C- enriched pore water DIC in coastal sediments that differ greatly from each other and from the DG sites (temperate, bioirrigated sediments in Buzzards Bay, MA, and highly sulfidic seagrass sediments in the negative estuary Laguna Madre, TX). One possible mechanism for this isotopic enrichment may involve the preferential diffusion of isotopically-heavy bottom water carbonate ion into the sediments (McNichol et al., 1991). This can occur because DIC and alkalinity are composed of several chemical species (e.g. carbonate and bicarbonate ions, as well as aqueous CO_2 [DIC only]), and changes with sediment depth in alkalinity and DIC can then lead to differing changes in dissolved carbonate and bicarbonate concentrations, and hence differential fluxes of these dissolved constituents across the sediment-water interface.

In particular, bottom waters at LSI are supersaturated with respect to all carbonate mineral phases present in the sediments (Burdige and Zimmerman, 2002), and for example, my calculations for LSI 6 and 7 indicate that the average bottom water saturation state with respect to aragonite ($\Omega_{aragonite}$), the dominant carbonate mineral in these sediments, is ~2.2. Therefore metabolic acid produced by aerobic respiration (rxn. 5) is first neutralized by reacting with dissolved carbonate producing bicarbonate according to:

$$CO_2 + H_2O + CO_3^{2-} \rightarrow 2HCO_3^- \qquad (10)$$

The consumption of CO_3^{2-} by this reaction lowers the saturation state of the pore water, and once the pore waters become sufficiently undersaturated, dissolution of the most soluble carbonate mineral occurs according to the coupled rxns. (5) - (7). This also results in a carbonate ion gradient across the sediment-water interface (Fig. 8), and bottom water carbonate can diffuse into the sediments despite the fact that there is a net flux of alkalinity and DIC (mainly in the form of bicarbonate) out of the sediments (also see discussions in Cai et al., 2000). Furthermore, because bottom water DIC is generally isotopically heavier than pore water DIC just below the sediment-water interface (e.g., see Fig. 4), this process may potentially lead to the enhanced diffusion of ^{13}C-enriched carbonate ion into the sediments.

In spite of these general trends, however, I do not feel that this process can significantly contribute to the heavy value of $\delta^{13}C_{added}$ seen in the DG sediments. First, an examination of Fig. 8 indicates that depth profiles of carbonate ion are roughly similar at all sites. It is thus unlikely that the diffusion of isotopically heavy carbonate ion into LSI sediments only occurs at DG sediments (however, I also note that a more rigorous examination of this problem requires an isotope-specific, reactive-transport model; e.g., Gehlen, et al., 1999). Furthermore, the shape of the pore water $\delta^{13}C$-DIC profile at the DG sites (Fig. 4) also argues against a water column source for this heavy DIC, since the apparent input here of heavy DIC into the pore waters does not occur at the sediment-water interface but at sediment depths below ~5cm. Finally, I also note that $[CO_3^{2-}]$ is essentially invariant below sediment depths of ~5 cm (Fig. 8, also see Burdige and Zimmerman, 2002). This implies that alkalinity production and DIC production must be tightly coupled at these sediment depths, because at the pH values of these sediments $[CO_3^{2-}] \approx$ Alkalinity – DIC, and if $\Delta[CO_3^{2-}] \approx 0$ then ΔAlkalinity $\approx \Delta$DIC. Again, this can only occur if carbonate dissolution is tightly coupled to aerobic respiration through rxns. (5) – (7), and the neutralization of metabolic CO_2 by downwardly-diffusing carbonate ion is of minor importance.

Another possible explanation of the observation that ^{13}C-enriched DIC is added to the pore water at the DG sites is that the reaction stoichiometry described above for metabolic carbonate dissolution (rxns. 5 - 7) is not valid in the DG sediments, and that in fact $f_C > f_{OM} \neq 0.5$. This then requires an additional acid source to dissolve sediment carbonate, in addition to the isotopically light metabolic CO_2 in order to produce the ^{13}C enriched DIC that is observed in the DG sediments. One possible mechanism by which this acid may be generated is through sulfide oxidation, either of dissolved sulfide or particulate sulfides such as iron monosulfide (FeS). While this possibility has been discussed by other workers (Ku et al., 1999; McNichol et al., 1991), there are several reasons why I believe that this is not likely important in LSI sediments.

In these sediments, and the Florida Bay sediments examined by Ku et al. (1999), net sulfate reduction appears to be minimal based on the lack of detectable pore water sulfate gradients (see Fig. 7 and Burdige and Zimmerman, 2002) and solid state accumulation. At the same time though, oxygen and sulfur stable isotope measurements in Florida Bay

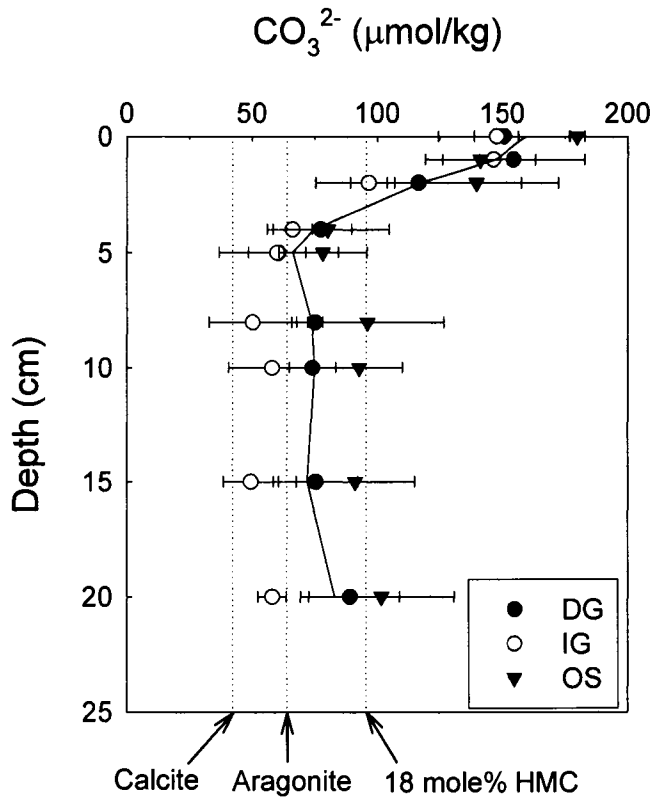

Fig. 8. Calculated carbonate ion concentrations in LSI sediments, determined using the program CO2SYS (Lewis and Wallace, 1998). The curve represents the average depth profile for pore water carbonate concentration in all three sediment types. The three arrows at the bottom of the figure represent the saturation carbonate ion concentrations for 18mol% HMC, aragonite and calcite. These concentrations were calculated using average pore water [Ca^{2+}] (Hu and Burdige, unpubl. data), [Mg^{2+}] calculated from chlorinity data, solubility constants for each mineral phase at 25°C (Mucci, 1983; Walter and Morse, 1984), and an average pore water salinity of 37.

sediments (Ku et al., 1999) and pore water sulfide measurements in LSI sediments (Fig. 9) both indicate that there is some amount of gross sulfate reduction in both of these sediments. This then implies that in these sediments there must be a tight coupling between sulfate reduction and sulfide oxidation. In LSI sediments, this coupling is largely mediated by the fact that seagrass O_2 input occurs down to depths of ~10-20cm, overlapping with depths where pore water sulfide data suggest sulfate reduction occurs. Furthermore, as Burdige and Zimmerman (2002) note, a tight coupling between sulfate reduction (and its resulting bicarbonate production) and sulfide oxidation (and its resulting proton production) simply results in the net production of H_2CO_3 (aqueous CO_2).

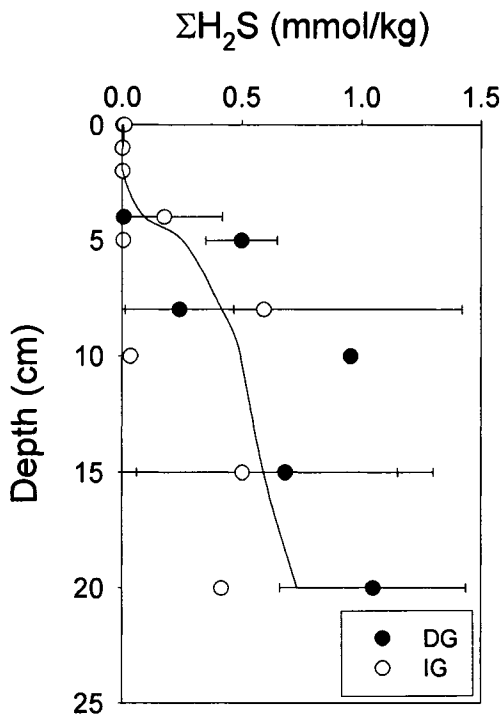

Fig. 9. Pore water depth profiles of total dissolved sulfide (ΣH_2S) in dense and intermediate density seagrass sediments.

Thus from the standpoint of the carbonate system and sediment carbonate dissolution, this is identical to that which occurs from aerobic respiration of sediment organic matter (rxn. 5).

In some coastal sediments however, there is net sulfate reduction that occurs during some portions of the year that involves seasonal storage of sulfide minerals during spring/summer. This is then followed by sulfide oxidation during fall/winter. This leads to a temporal uncoupling of sulfate reduction and sulfide oxidation, which then results in regular seasonal carbonate mineral saturation state (supersaturated during spring/summer and undersaturated in fall/winter, Green and Aller, 1998; Green and Aller, 2001; also see Sampou and Oviatt, 1991). However, several lines of evidence argue against this being an important process in LSI sediments, including the lack of this type of seasonality in biogeochemical processes occurring in these sediments versus that observed in temperate terrigenous sediments (e.g., Burdige and Zimmerman, 2002). The lack of significant Fe

in carbonate sediments such as these (e.g., Morse et al., 1985) also minimizes the ability to sequester any dissolved sulfide that is produced in these sediments as iron sulfides.

Finally, it is important to recognize that closed system calculations (Boudreau and Canfield, 1993; Stoessell, 1992) do indicate that small amounts of net sulfate reduction (~0.7 mM sulfate depletion) can lead to undersaturation with respect to either aragonite or some forms of high-Mg calcite (Walter and Morse, 1984). This amount of sulfate reduction may be within the uncertainty of the sulfate measurements, and it could represent another mechanism by which sediment organic matter remineralization processes may be coupled to carbonate dissolution. Open-system calculations (which allow for transport processes such as diffusion), however, suggest that the occurrence of this undersaturation during small amounts of sulfate reduction is unlikely in most marine sediments (Boudreau and Canfield, 1993). Furthermore and more importantly, recognizing that H_2S is likely to contribute only one proton towards carbonate dissolution at the pH values of typical marine sediments, then the coupling of sulfate reduction and carbonate dissolution may be approximately expressed as,

$$SO_4^{2-} + 2CH_2O + CaCO_3 \rightarrow Ca^{2+} + HS^- + 3HCO_3^- \qquad (11)$$

implying that here $f_{OM} \approx 0.67$ and $f_C \approx 0.33$. Since the resolution of the question of an extra acid source in DG sediments requires $f_C > f_{OM}$, the occurrence of a reaction such as rxn. (11), if it indeed occurs in an open sediment system, does not provide an explanation for the heavy value of $\delta^{13}C_{added}$ that is seen in the DG sediments.

3.2.2. Heavy values of $\delta^{13}C_{added}$ in DG sediments as a result of carbonate mineral reprecipitation.

Given the difficulties in explaining the ^{13}C enrichment of DIC in dense seagrass sediment pore waters by any of the above-discussed mechanisms, it is proposed that a coupling of carbonate dissolution and reprecipitation may actually explain these observations. A conceptual model for how this might occur is shown in Fig. 10. This somewhat over-simplified view of carbonate mineral diagenesis in these sediments recognizes that, because of differences in the solubility of carbonate phases in these sediments (calcite, aragonite and HMC), pore waters which are undersaturated with respect to one or more of the metastable phases (e.g., HMC) are still supersaturated with

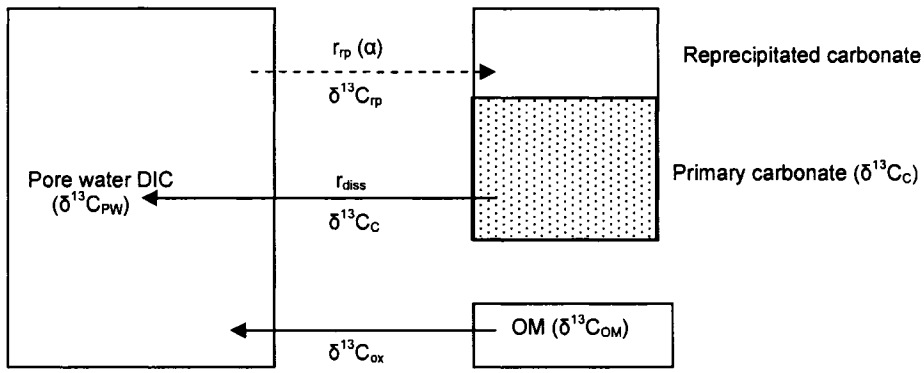

Fig. 10. A schematic illustration of the dissolution/reprecipitation mechanism discussed in the text, and its impact on the $\delta^{13}C$ of pore water DIC.

respect to calcite (or low-Mg calcite; e.g., see Fig. 8). Thus in these sediments there may be net dissolution of a more soluble carbonate phase along with reprecipitation of a more stable phase. Note that a further discussion of the phases that may actually be dissolving and reprecipitating in these sediments will be presented at the end of section 3.3.

Evidence for the occurrence of such coupled dissolution/reprecipitation processes has indeed been observed in many natural systems. Groundwater studies (Gonifiantini and Zuppi, 2003; Plummer and Sprinkle, 2001) have demonstrated that due to small Gibbs free energy differences, impure/less stable carbonate phases (analogous to HMC in these sediments) tend to dissolve and re-crystallize to form purer calcite phases. Evidence for carbonate dissolution/reprecipitation in Florida Bay and Bahamas Bank sediments have also been presented, using stable isotope, trace element analyses as well as microscopic observations (Hover et al., 2001; Patterson and Walter, 1994; Rude and Aller, 1991; Walter et al., 1993). A study carried out by Walter et al. (2006) in these sediments has also shown that an apparent isotope exchange enriches the pore water DIC pool with ^{13}C through carbonate reprecipitation.

Based on the above discussion, I suggest that net dissolution of a metastable carbonate phase such as HMC occurs in DG sediments through metabolic CO_2 production from the remineralization of seagrass-derived organic matter (as in the IG sediments); this process is ultimately driven by the fact that sediment pore waters become

undersaturated with respect to HMC just below the sediment-water interface. However, because the pore waters also remain supersaturated with respect to more stable carbonate phases, (e.g., calcite, see Fig. 8), there is a component of this gross dissolution that is balanced by the reprecipitation of one or more of these stable carbonate phases. As I will discuss below, this secondary carbonate phase presumably forms under chemical/isotopic equilibrium with respect to the pore water DIC.

This model for carbonate diagenesis then implies that the pore water DIC pool is more than a simple "reservoir" for the end-products of organic matter remineralization and carbonate dissolution. Rather, the pore waters also serve as an intermediate through which sedimentary carbonates cycle during dissolution/reprecipitation. As I will see below, recycling of the sedimentary carbonate through the pore water DIC pool has a dramatic effect on the (now) "apparent" $\delta^{13}C$ of the DIC being added to the pore waters. Furthermore, the net addition of light DIC from organic matter oxidation to the pore water DIC pool also implies that the secondary carbonate phase that forms will be isotopically lighter than the primary sediment carbonate (also see Walter et al., 2006).

To examine these processes more quantitatively, I will use a closed system model based on Fig. 10. In this model pore water DIC is affected by three processes: organic matter oxidation, carbonate dissolution and secondary carbonate reprecipitation. Changes in the concentration $DI^{12}C$ and $DI^{13}C$ are then given by

$$\frac{d[DI^{13}C]}{dt} = r_{diss} \times F_{sed} + r_{ox} \times F_{OM} - r_{rp} \times F_{rp} \tag{12}$$

$$\frac{d[DI^{12}C]}{dt} = r_{diss} \times (1 - F_{sed}) + r_{ox} \times (1 - F_{OM}) - r_{rp} \times (1 - F_{rp}) \tag{13}$$

where F_i is the isotopic abundance of ^{13}C in the original carbonate sediments (subscript *sed*), the sedimentary organic matter (subscript *OM*) and the secondary carbonate (subscript *rp*); r_{diss}, r_{ox} and r_{rp} are the rates of gross carbonate dissolution, organic matter remineralization and secondary carbonate reprecipitation, respectively. Fractionation among different dissolved carbonate species is ignored since the majority of the DIC exists in the form of bicarbonate.

Because the ultimate driving force for carbonate dissolution is CO_2 input from organic matter oxidation (metabolic dissolution), the net carbonate dissolution rate, (r_{diss} -

r_{rp}), must equal r_{ox} (e.g., based on the 1:1 stoichiometry shown in rxn. 7). I will also define the re-precipitation ratio R_{rx} as r_{rp}/r_{ox}. Finally I assume that there is no fractionation during organic matter oxidation or carbonate dissolution, and that recrystallization of secondary carbonate occurs under equilibrium conditions with pore water DIC pool. This then implies that

$$R_{rp} = \alpha \times R_{pw} \qquad (14)$$

where R_{rp} is the isotopic ratio ($^{13}C/^{12}C$) of the secondary carbonate, subscript *pw* represents pore water, and α is the fractionation factor between the secondary carbonate phase and bicarbonate ion. Isotopic fractionation ($10^3 \ln\alpha$) between calcite and bicarbonate is 0.9‰ at 25°C (Rubinson, 1969), and I have therefore used an α value of 1.0009 in these calculations. Finally, F_{rp} equals $R_{rp}/(1+R_{rp})$.

Eqns. (12) and (13) were solved using a 4th order Runge-Kutta method in the program Stella®. As can be seen in Fig. 11, an increase in the reprecipitation ratio R_{rx} leads to increasingly heavier pore water DIC because of the recycling of primary sediment carbonate (with a $\delta^{13}C$ of 4.0‰) through the DIC pool during dissolution/reprecipitation. Furthermore, if I combine the approach described in section 3.2 with these model calculations I can estimate the current "apparent" $\delta^{13}C$ of the DIC being added to the pore waters. As shown in Fig. 12, this value is a function of not only R_{rx} but also of the absolute rate of net dissolution r_{ox} (particularly for R_{rx} values greater than ~3).

For the dissolution rates in this figure, the value of $\delta^{13}C_{added}$ for the DG sediments "predicts" a value of R_{rx} (3.25-3.75) that is roughly consistent with the range of R_{rx} values for Florida Bay sediments. However, some care must be taken in interpreting this conclusion since it is not only based on a comparison between closed-system calculations and field observations, but it is also a comparison of two very different environments (i.e., "oligotrophic" LSI sediments versus more "eutrophic" Florida Bay sediments). Nevertheless, these model results do suggest that this dissolution/reprecipitation process could explain the $\delta^{13}C$-DIC results from the DG sediments. More detailed open-system modeling of these sediments using reactive-transport models that consider processes such as pore water advection or diffusion (e.g., Gehlen et al., 1999; McNichol et al., 1991) will be needed to further verify the conclusions reached here regarding carbonate

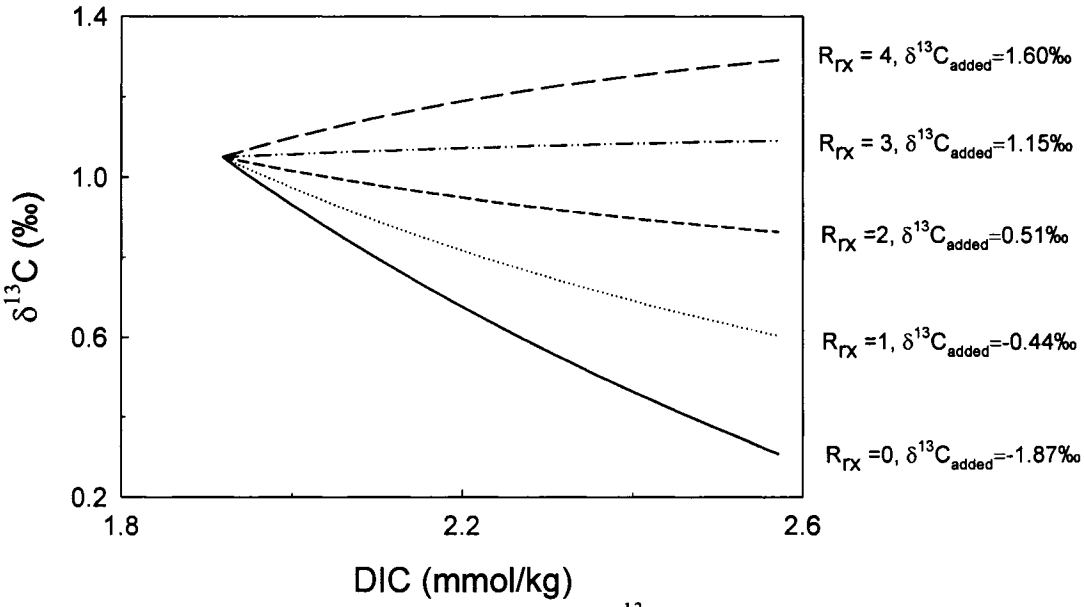

Fig. 11. The closed-system evolution of the $\delta^{13}C$ of pore water DIC with and without carbonate reprecipitation. All of these calculations start with bottom water values, i.e., [DIC] = 1.94 mmol/kg and $\delta^{13}C_{DIC}$ = 1.1‰. If no reprecipitation occurs, then the $\delta^{13}C$ of DIC added to the pore waters equals $(\delta^{13}C_{OM}+\delta^{13}C_C)/2$ = -1.9‰. In calculations where reprecipitation occurs, the net dissolution rate was fixed at 0.0163 mmol/kg/h, a value based on LSI sediment incubations studies (Chapter III). By varying R_{rx} this then change the gross rate of carbonate dissolution in each calculation.

reprecipitation in LSI sediments.

3.3. Why Does Evidence of Carbonate Reprecipitation Exists Only in DG Sediments?

The results from the DG sediments appear to provide evidence for the occurrence of carbonate mineral reprecipitation along with dissolution; in contrast no such evidence is seen in the OS and IG sediments. There are at least two explanations for these observations.

The first stems from an examination of the factors that appear to inhibit the inorganic precipitation of calcium carbonate from seawater. The sediment pore waters at these sites, along with much of the surface ocean, are supersaturated with respect to mineral phases such as calcite, and sometime aragonite (Fig. 8 in this study and Morse et al., 1985).

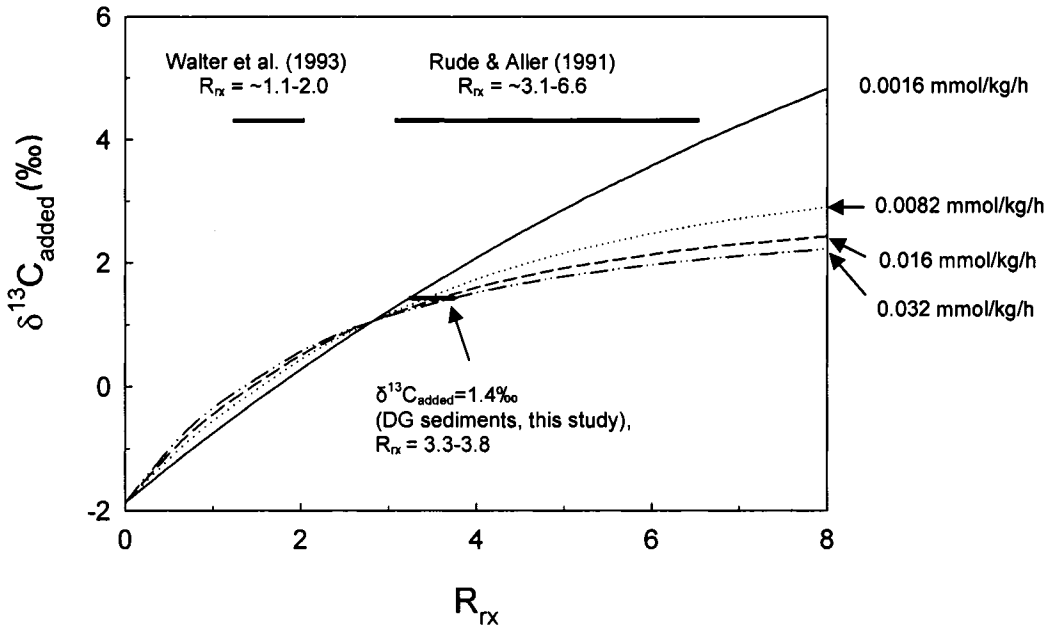

Fig. 12. $\delta^{13}C_{added}$ as a function of R_{rx} and r_{ox}. The two upper horizontal lines represent ranges of R_{rx} from previous studies in Florida Bay sediments (Walter et al., 1993; Ruder and Aller, 1991). Values on the right of the plot are r_{ox} values, i.e., net carbonate dissolution rates that range from 10% to 200% of dissolution rates I have observed in LSI sediments (Chapter III). The lower horizontal line represents the range in R_{rx} for these r_{ox} values based on the $\delta^{13}C_{added}$ value of 1.4‰ observed in the DG sediments.

However, results from a number of studies suggest that homogeneous precipitation (of calcite at least) is generally inhibited until seawater is even more supersaturated than surface ocean values (e.g., see discussions in Morse et al., 2003). Furthermore, heterogeneous carbonate mineral reprecipitation from supersaturated solutions may be inhibited because reprecipitation nucleation sites on sediment particles (e.g., carbonate grains) are poisoned by substances such as dissolved organic matter, phosphate, or Mg^{2+} that can adsorb to the nuclei surface (e.g., Berner et al., 1978; Morse and Mackenzie, 1990; Morse and Mucci, 1984; Mucci, 1987). However, in DG sediments with relatively high rates of net carbonate dissolution, the dissolution process may "cleanse" particle surfaces of these inhibitory substances and/or create new nucleation sites. As a result, this may act to overcome the inhibition of carbonate precipitation commonly seen in many laboratory and field studies.

Secondly, studies of carbonate dissolution and reprecipitation by Hover et al. (2001) suggest that the process may occur through what is termed "Ostwald ripening", in which smaller crystals dissolve and reprecipitate as larger crystals (also see Zullig and Morse, 1988). The driving force for this appears to be the decrease in surface free energy with increasing particle size. Expressed another way, smaller crystals have higher surface free energies and, in a given solution, are therefore more soluble than larger crystals (Walter and Morse, 1985). As a result, during Ostwald ripening crystals larger than a certain critical radius (representing particles in equilibrium with the solution saturation state) grow at the expense of the dissolution of crystals smaller than this critical radius. The relevance of this to results here may stem from the fact that the overlying seagrass canopy at the DG sites dampens water motion and may then enhance the deposition of fine-grained particles relative to that which occurs at the IG and OS sites. The presence of the seagrass canopy may also hinder resuspension and winnowing of fine-grained particles in these sediments. Consistent with these suggestions, Morse et al. (1987) observed that there was up to 3 times more fine-grained material (<52μm) in seagrass sediments relative to unvegetated sands in sites they studied in the Bahamas. The preferential dissolution of this fine-grained material may promote the overall Ostwald ripening of this material in the DG sediments.

Although evidence-to-date suggests that HMC preferentially undergoes net dissolution in LSI sediments (Burdige and Zimmerman, 2002; Chapter III), the results presented here provide no evidence regarding the composition of the carbonate phase(s) that reprecipitates. Interestingly, the two mechanisms discussed above have the potential to lead to the reprecipitation of different phases. In the first case (cleansing of nucleation sites), the dissolution of HMC might be expected to result in the reprecipitation of calcite (Rude and Aller, 1991). In contrast, Ostwald ripening might be expected to lead to the reprecipitation of HMC with a very similar (although perhaps slightly lower) Mg content to the original starting material (Cole and Chakraborty, 2001; Hover et al., 2001). More detailed studies of LSI sediments will be needed to further examine these possibilities.

3.4. Significance of These Results

Based on the discussion above, it is likely that carbonate dissolution/reprecipitation may also be responsible for the ^{13}C enrichment seen in the DIC of pore waters from other coastal sediments (Eldridge and Morse, 2000; McNichol et al., 1991). Similarly, carbonate dissolution and reprecipitation may occur in supralysoclinal carbonate-rich deep sea sediments (Broecker and Clark, 2003; Jahnke and Jahnke, 2004). Thus it appears that carbonate mineral reprecipitation may be more important than previously thought in the early diagenesis of a wide range of marine sediments.

Returning to shallow water carbonate sediments, these results demonstrate the impact that carbonate dissolution/reprecipitation may have on the isotopic composition of the sediment pore waters. Similar effects are also to be expected for trace elements such as Sr or F, which show differing degrees of incorporation into different carbonate mineral phases (e.g., Rude and Aller, 1991). Furthermore, if reprecipitation is extensive, then the composition of the solids should also evolve with depth (time of burial) from that of the original sediment material (e.g., Patterson and Walter, 1994; Walter et al., 1993). These processes therefore have the potential to significantly impact the paleo-records contained in stable isotope or trace element profiles in carbonate sediments (see discussions in Hover et al. 2001, and references therein). The role of these processes in the overall evolution of carbonate platforms (e.g., Melim et al., 2002) also remains to be further examined.

CHAPTER III
SHALLOW MARINE CARBONATE DISSOLUTION AND EARLY DIAGENESIS - IMPLICATIONS FROM AN INCUBATION STUDY

1. INTRODUCTION

Carbonate dissolution has been extensively studied in deep sea and continental slope/rise sediments. As a major process in the global carbon cycle, carbonate dissolution represents a negative feedback mechanism that may potentially compensate for rising atmospheric CO_2 by supplying excess alkalinity to the water column (Adler et al., 2001; Archer et al., 1989; Archer et al., 1998; Berelson et al., 1994; Caldeira and Rau, 2000; Emerson and Bender, 1981; Hales and Emerson, 1997; Jahnke et al., 1994; Jahnke et al., 1997; Jahnke and Jahnke, 2004; Martin and Sayles, 1996).

Shallow water carbonates (carbonate banks/bays, and continental shelves) represent the second largest carbonate pool on earth (~40% of global oceanic carbonate production and accumulation) although they cover only 8% of the area of the modern ocean (Milliman, 1993). Historically, only few studies in shallow water carbonate sediments have reported elevated pore water Ca concentrations as a result of sediment carbonate dissolution (e.g., Berner, 1966). Later, Aller (1982) observed carbonate shell dissolution caused by enhanced organic matter remineralization through biological irrigation and sediment reworking in Long Island Sound sediments. Similarly, sediments from carbonate banks (Florida-Bahamas Banks) that are traditionally considered to be net carbonate depositional environments (e.g., Broecker and Takahashi, 1966) have also been shown to undergo significant dissolution in association with both aerobic and anaerobic microbial respiration processes (Ku et al., 1999; Morse et al., 1985; Walter and Burton, 1990). It was estimated that as much as 20-50% of the gross carbonate production may be dissolved before the sediments are permanently buried (Ku et al., 1999; Sanders, 2003; Walter and Burton, 1990). In these sediments, microbial respiration of organic matter is the driving force for the occurrence of carbonate dissolution, despite the fact that the overlying waters are supersaturated with respect to the common carbonate minerals found in these sediments (e.g., Aller, 1982; Burdige and Zimmerman, 2002; Green and Aller,

1998; Green and Aller, 2001; Morse et al., 1985; Walter and Burton, 1990). Furthermore, seagrass vegetation in these sediments enhances benthic aerobic respiration through both seagrass O_2 pumping and increased organic matter input. Aerobic respiration in the sediments generates metabolic CO_2 and drives down the pore water saturation state; once the pore waters are sufficiently undersaturated, carbonate dissolution can occur (Chapter II; Burdige and Zimmerman, 2002; Ku et al., 1999; Morse et al., 1985; Walter and Burton, 1990). Here O_2 delivery eventually is an important controlling factor in sediment carbonate dissolution. The reactions can be written in the following simplified fashion:

$$CH_2O + O_2 \rightarrow CO_2 + H_2O \quad (15)$$

$$CO_2 + CaCO_3 + H_2O \rightarrow Ca^{2+} + 2HCO_3^- \quad (16)$$

$$CH_2O + O_2 + CaCO_3 \rightarrow Ca^{2+} + 2HCO_3^- \quad (17)$$

The pore waters in the Bahamas Bank sediments are generally supersaturated with respect to the dominant mineral - aragonite (see Fig. 6 in Morse et al., 1985), and high magnesium calcite (HMC) controls the pore water saturation state and is responsible for the observed dissolution (Morse et al., 2006). However, the composition of the dissolving carbonate phase(s) (i.e., mole% Mg in HMC) still remains unclear. Understanding the composition of the dissolving carbonate is important in terms of interpreting the diagenesis and preservation potential of modern carbonate sediments (Andrews, 1991).

In the previous work in Bahamas Bank sediments (Chapter II), I were able to achieve a stable carbon isotope mass balance with reasonable assumptions about the organic matter being remineralized in both intermediate seagrass and bare oolitic sand sediments. However, for the dense seagrass sediments, I observed that the pore water DIC pool was enriched in ^{13}C that could not be explained by the 1:1 mixing of DIC derived from sediment carbonate dissolution and organic matter oxidation as shown in eqn. (17). Several other studies have reported similar observations in other shallow water estuarine and coastal sediments (Eldridge and Morse, 2000; McNichol et al., 1991; Walter et al., 2006). In my work, a closed-system model was proposed to explain the pore water DIC ^{13}C enrichment based on the coupling between carbonate dissolution and reprecipitation (Chapter II). Qualitatively the model results agreed with the observations in the pore

water data. However it is desirable to carry out a closed-system study to more quantitatively verify this model.

In this paper, I will describe a series of closed-system incubation experiments using surface sediments from sites that have different seagrass densities. In these experiments, sediments were incubated under both oxic and anoxic conditions, and changes in pore water solute concentrations (e.g., O_2, alkalinity, DIC, calcium, sulfide) as well as the $\delta^{13}C$ of DIC were monitored, to examine dynamics of carbonate dissolution and reprecipitation and to gain a further understanding of the composition of dissolving carbonate phase(s). These data were also further used to verify the validity of the carbonate dissolution/ reprecipitation model in a closed-system setting.

2. MATERIALS AND METHODS

2.1. Site Descriptions

The experiments described here were carried out during a 2003 field expedition to Lee Stocking Island (LSI), Exuma Cays, Bahamas and on a cruise in 2004 on the R/V *F. G. Walton Smith* across the greater expanse of the Bahamas Bank (WS, see map in Fig. 13). In 2003, three sampling sites around LSI were studied – Channel Marker (CM), Halfway (HW) and Ooids Shoals (OS). Information about these sites can be found in Table 6 (also see Chapter II and Burdige et al. submitted). On the WS cruise studies were carried out at two sites - WS-3, located northwest of Andros Island (25°51.050'N, 78°43.899'W) and WS-13, located west of the Exuma Cays near Pipe Cay, (24°14.033N, 76°30.200'W) (Table 6).

The porosity of these sediments ranged from 45-65% (Table 6) with grain size of 200-800 μm (Burdige and Zimmerman, 2002 and Chapter IV). X-ray diffraction results showed that these sediments were predominantly aragonite (70-90%), with lesser amount of high magnesium calcite (HMC) (10-30%) and low magnesium calcite (LMC) (<3%). The Mg content in the HMC was fairly homogeneous among these sites, between 12-13.6 mol% (Table 7). Details about the X-ray diffraction procedures can be found in section 2.5 and Chapter II.

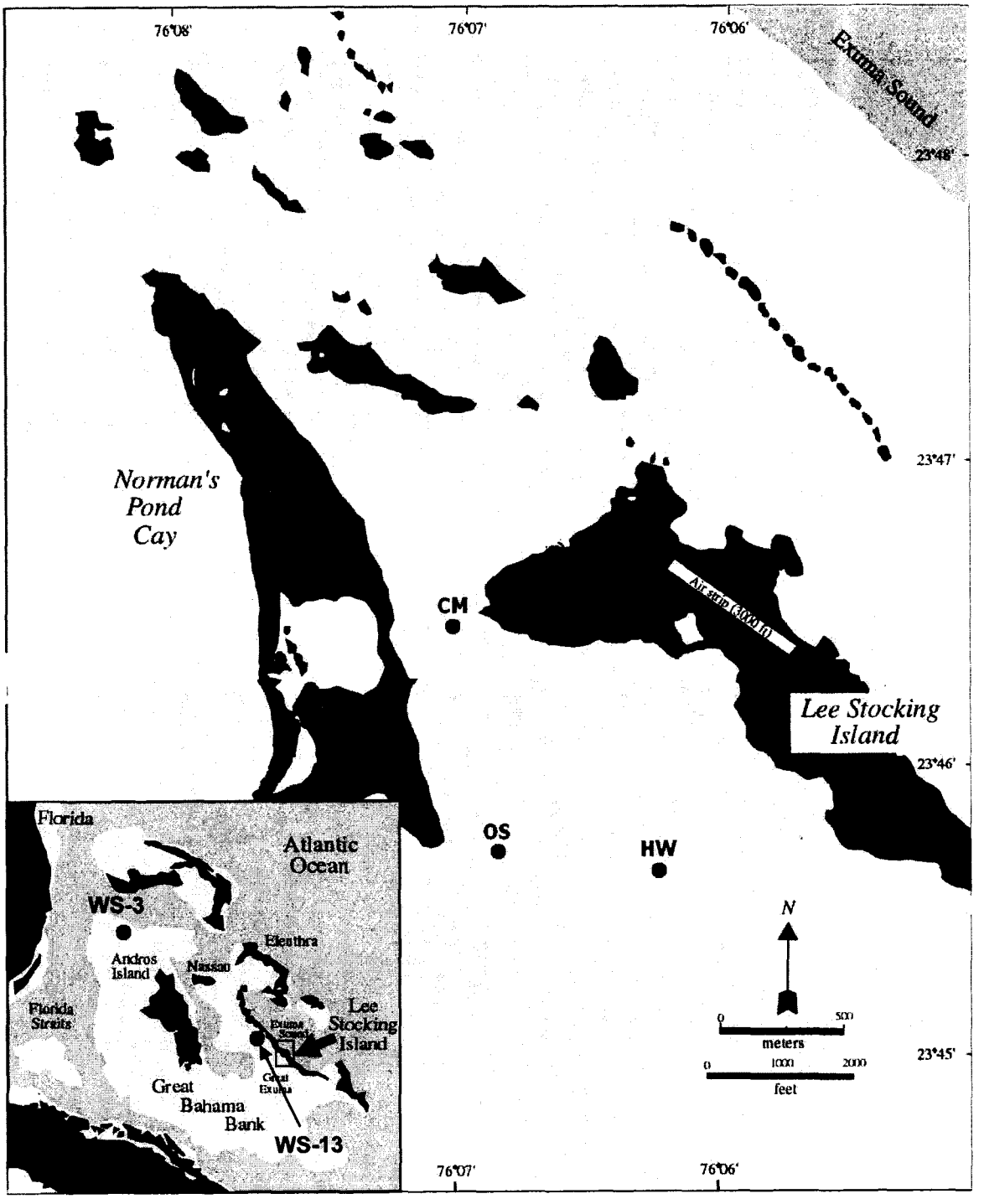

Fig. 13. A map of the sampling sites. Site names and abbreviations are as follows: Channel Marker (CM), Half Way (HW), Ooid Shoals (OS), Walton Smith Site 3 (WS-3), Walton Smith Site 13 (WS-13).

Table 6. Characterization of the sampling sites.

Station ID	Water Depth (m)	Seagrass vegetation	Leaf area index [a]	Porosity (φ)
CM	3.9	*Thalassia testudinum*	1.7±0.6	0.65±0.03
HW	3.0	*Thalassia testudinum*	0.6±.2	0.57±0.01
OS	2.8	None	0	0.47±0.01
WS-3	10.5	*Thalassia testudinum* *Syringodium filiforme*	1.3	0.57±0.02
WS-13	4.2	*Thalassia testudinum*	0.54±0.04	0.53±0.03

[a] Unit of leaf area index (LAI) is m^2-leaf/m^2-sediments, and the values of LAI are from Burdige et al. (submitted) and Bodensteiner (2006).

Table 7. Mineralogy of the incubated surface sediments [a].

Station ID	Aragonite (wt%)	HMC (wt%)	LMC (wt%)	Mg in HMC (mole%)
CM	64.3±1.4	32.4±1.9	3.3±2.0	12.2±0.1
HW	89.2	9.7	1.1	12.7
OS	87.3	11.2	1.4	13.6
WS-3	81.4±0.4	17.2±0.4	1.3±0.0	12.0±0.1
WS-13	91.2±0.1	7.8±0.1	1.0±0.2	12.3±0.1

[a] Errors are standard deviations (n=3) based on triplicate measurements of the same samples (WS-3 and WS-3) or three different samples (CM). WS-3 and WS-13 sediment samples were also used for isotope analysis as shown in Table 11.

2.2. Sediment Incubation Studies

Surface sediments (0-2 cm) from all sampling locations were collected by SCUBA divers with care taken to not mix surface sediments with deeper sediments. Seagrass and large mollusk debris were sieved out immediately after sampling using a plastic sieve (Φ=1 mm), and the sediments were then washed with surface seawater collected at the sampling sites. During processing the sediments were stirred continuously to ensure they were well oxygenated and homogenized.

The technique used in these incubation studies was modified from the approach described in Hulthe et al. (1998), and a schematic illustration is shown in Fig. 14. As will be discussed below, this approach allowed us to incubate the sediments at different O_2 delivery rates. Briefly, either Teflon tubing (I.D. 0.38mm, O.D. 0.8mm; all CM, HW, OS

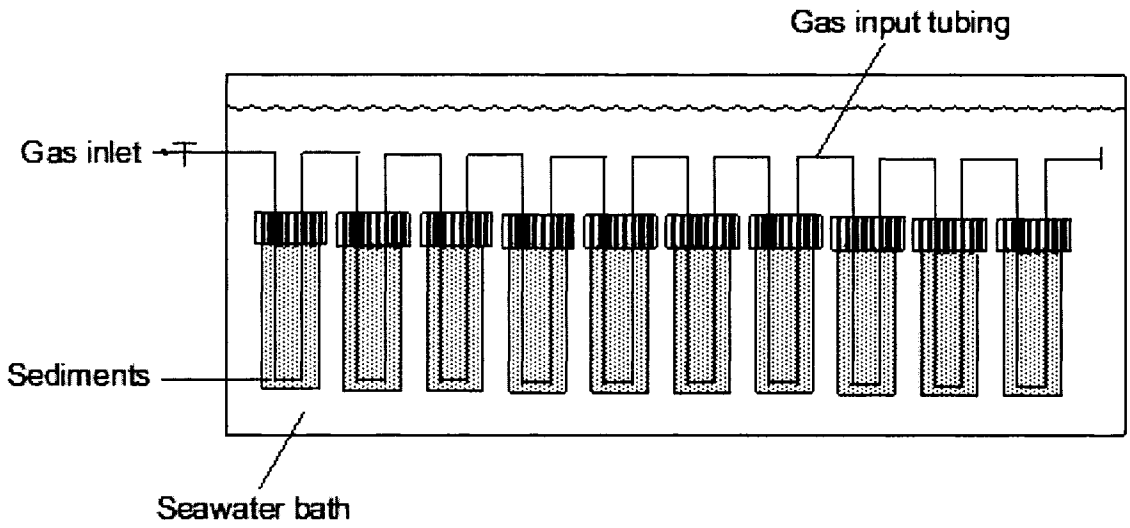

Fig. 14. A schematic illustration of the experimental set up.

incubations, and the 3-N, 13-N, and 13-L incubations) or Cole-Parmer® C-Flex™ tubing (I.D. 0.79mm, O.D. 2.38mm; the 3-L, 3-H, and 13-H incubations, Table 8) was passed through 10 Teflon- lined silicone septa and open-face caps to form a series of loops (exactly 20 cm in length), and the loops were inserted into 42 ml glass vials. Surface seawater (5.0 ml) was next added to each vial, and the vials were then filled with the well-mixed sediments. Finally the vials were sealed and the caps were wrapped with Parafilm® to further prevent contamination from atmospheric O_2. Aliquots of the sediment were sampled before, during the middle, and after the filling process, to determine the average porosity in the experimental sediments. Blank experiments using vials filled with N_2-purged seawater showed a net O_2 gain of ~1 μmol/kg/d. Therefore during a 4.5-5-day incubation there would have been a maximum net O_2 input of ≤5 μmol/kg, as compared with mmol/kg concentration changes of pore water solutes such as alkalinity or Ca^{2+}. Therefore this small amount of oxygen "leakage" into the vials is thus negligible.

After the vials were filled, the gas diffusion tube for each set of incubation vials was connected to a compressed N_2, O_2 or air tank through a Norgren® gas pressure regulator. The tubing was flushed with gas before the end of the tube was heat-sealed. The gas regulator was then set at the desired pressure. The vials were incubated in the dark at

constant temperature in a flowing seawater bath (Table 8). All incubations were maintained at constant gas pressures except 13-H, in which the O_2 pressure was first set at 20 psi, and then pressure was decreased to 10 psi after 56 hrs. Immediately after an experiment was set up, the first time point was collected by cutting the tubing between the last two vials and then sealing the open end of the shortened piece of tubing attached

Table 8. Experimental settings for sediment incubations and general trends in the data.

Station ID	Tube type	Gas Pressure (psi)/Gas Type	O_2 Input Rates (μmol/h) [a]	Incubation Designation [b]	Temperature (°C)	Case [c]
CM	Teflon	20/N_2	0	CM-G	28±1	1
		6/air	0.07	CM-P		2
		12/air	0.16	CM-R		2
		20/air	0.28	CM-B		2
		20/O_2	0.48	CM-W		2
HW	Teflon	20/N_2	0	HW-G	28±1	1
		2.5/air	0.03	HW-P		2
		5/air	0.06	HW-R		2
		10/air	0.14	HW-B		2
OS	Teflon	20/N_2	0	OS-G	28±1	1
		5/air	0.05	OS-P		2
		10/air	0.13	OS-R		2
		20/air	0.28	OS-B		2
WS-3	Teflon	20/N_2	0	3-N	22±2	1
	C-Flex	15/O_2	4.01	3-L		3
	C-Flex	25/O_2	6.71	3-H		3
WS-13	Teflon	20/N_2	0	13-N	23±1	1
	C-Flex	30/O_2	0.69	13-L		3
	C-Flex [d]	20/10/O_2	4.56/2.36	13-H		3

[a] O_2 input rates were calculated as discussed in section 2.3.

[b] G, P, R, B, and W were color coded and represented increasing O_2 delivery rates, N, L, and H stand for N_2, low O_2 and high O_2 input rates, respectively.

[c] Denotes the type of reaction in the incubation as discussed in section 3.1.

[d] In the 13-H incubation, the O_2 gas pressure was first set at 20 psi O_2 for the first 56 hours, and it was then changed to 10 psi for the rest of incubation.

to last of the remaining vials. Subsequent time points were then collected every ~12 hours for the next 4.5-5 days using the same procedure. Before pore water was collected from each vial, the vial was weighed to determine the total amount of sediment slurry in the vial. Dry sediment weight in each vial was then calculated using the porosity data described above.

For each time point, the sediments in the vials were first re-homogenized by manually agitating the vials, and the O_2 concentrations were determined by inserting an 18-gause stainless steel sleeved fluorescence optical oxygen sensor (Ocean Optics®) through the septa. The O_2 sensor was calibrated using two O_2 concentrations – N_2 purged oxygen-free seawater and air-saturated seawater at a known salinity and temperature. The O_2 concentration of the latter was calculated using the O_2 solubility equation in Pilson (1998). Detailed procedure in O_2 measurement can be found in Chapter IV.

The vials were next centrifuged at room temperature for 5 minutes in a clinical centrifuge at 3000 rpm to separate the pore water from the sediments. This water was drawn into a clean nylon syringe and filtered through 0.45 μm Gelman® Nylon Acrodisc filters. Samples for titration alkalinity (Alk_T), pH and total dissolved sulfide (TDS) were store in air-tight vessels (Chapter II) and analyzed within 2 hours of sampling. The remaining pore water was distributed into two crimp-sealed 2 ml serum vials (for DIC concentration and stable isotope analyses) with no headspace, and 2 ml plastic snap-cap vials (for major ion analyses). These samples were stored in the dark in a refrigerator and analyzed within 3 months of collection. Finally the residual sediments were removed from the vial and stored frozen at -20°C.

2.3. Calibration of the O_2 Diffusion Tubes

The O_2 delivery rate from the diffusion tube as a function of O_2 partial pressure was determined in the lab for each type of tubing using the same experimental set-up used in the field studies, with the exception that a vial that contained a 20 cm tubing loop was filled with N_2-purged seawater rather than sediments. After the tubing was flushed, sealed and the gas pressure set on the regulator, O_2 concentration in the vial was monitored with the optical oxygen sensor described above. The rate of O_2 concentration increase in the vial as a function of tubing gas (pure O_2 and air) pressure was determined and used to

construct calibration curves (O_2 delivery rate vs. regulator pressure) for both O_2 and air. For each type of tubing, O_2 delivery rate was a linear function of gas pressure for both pure O_2 and air (Hu and Burdige, unpubl. data).

2.4. Chemical and Isotopic Analyses

Total alkalinity (Alk_T) was determined by Gran Titration using a Metrohm automatic titrator combined with a Cole-Parmer pH electrode calibrated using pH 4.00, 7.00 and 10.00 NBS standards (Grasshoff et al., 1999). Total dissolved sulfide was determined using the spectrophotometric method described in Cline (1969). A Coulometer was used to determine dissolved inorganic carbon (DIC) for all samples (DOE, 1994). Dissolved calcium was determined on 0.1 ml pore water samples by automated EGTA titration with end point detection using a Thermo Orion Ca^{2+} ion-selective electrode (Kanamori and Ikegami, 1980). Chlorinity (chloride concentration) was also determined by automated titration with end-point detection by a Brinkman Ag Titrode™ (Metrohm Ti Application Note No. T-1). Both titrants (EGTA and $AgNO_3$) were standardized using IAPSO standard seawater (Grasshoff et al., 1999). Samples from the WS-3 and WS-13 incubations were analyzed for the $\delta^{13}C$ of the pore water DIC on a PDZ Europa 20-20 isotopic ratio mass spectrometer (IRMS), using a modification of the procedure of Salata et al. (2000) as described in Chapter II.

Oven dried (60 °C) sediment samples were analyzed for $\delta^{13}C$ of the sediment carbonate by acidification in a "Kiel" device using pure phosphoric acid at 90°C, with the resultant CO_2 gas then introduced into a PDZ Europa® GEO 20-20 isotopic ratio mass spectrometer (IRMS). Seagrass samples were also analyzed for the $\delta^{13}C$ of the organic carbon with a Carlo Erba NA1500 elemental analyzer (EA) interfaced with the IRMS. Before analysis, samples were acid cleaned and oven-dried at 60°C followed by grinding to fine powder with a mortar and pestle (Grice et al., 1996). All isotopic values are reported relative to the PDB standard. The seagrass C/N ratio was calculated based on EA peak intensity calibrated with an asparagine standard (Joy Davis, pers. comm.).

Uncertainties of these analyses are: alkalinity (±2%), DIC (±2%), Ca^{2+} (±1%), chlorinity (±0.2%), $\delta^{13}C$ (±0.2‰), TDS (±2%), O_2 (±3%).

2.5. Mineralogy

Crushed oyster shells (*Crassostrea*, calcite) and coral (*Porites*, aragonite) were used as carbonate standards in the analyses of sediment mineralogy. This approach is based on suggestions by Milliman (1974) that biogenic carbonates should be used in quantitative XRD analyses of marine carbonates due to the close resemblance of peak intensities among these materials relative to reagent grade carbonates, which often exhibit stronger XRD peaks at the same concentration level. A series of mixtures of these two carbonates (grain size <63μm) were prepared at different weight ratios, and 5 wt% NaCl was added to each mixture as an internal standard. XRD scans were carried out on a Philips PW 1729 X-ray generator with Cu-Kα nickel filtered radiation at 40 kV and 30 mA. Scans were run from 25° to 32° 2θ with a scanning speed of 0.02° 2θ and a measuring time of 2s per step. Additional details of these mineralogical studies can be found in Morse et al. (1985) and in Chapter II.

The uncertainty in these mineralogical measurements (i.e., %HMC, %LMC and %aragonite) was <1.5% (1σ, n=3), although the accuracy of this method is generally considered to be ±3-5% (Andrews, 1991; Milliman et al., 1993; Morse et al., 1985).

The Mg content of the HMC was also determined by XRD (Goldsmith et al., 1961) and the uncertainty of this measurement was <0.5%. Past studies have shown that the XRD-determined Mg content of HMC agrees well with bulk chemical analyses of HMC in natural carbonates (Walter and Morse, 1984).

3. RESULTS

3.1. Pore Water Chemistry

3.1.1. Overview of the Results

Closed-system incubations of carbonate sediments under different O_2 input rates essentially exhibit three types of behaviors: (1) anoxic remineralization, when the O_2 input rate is zero, (2) the apparent co-occurrence of oxic and anoxic remineralization, when O_2 input is low compared to O_2 consumption, and (3) oxic remineralization, when O_2 input is greater than or equal to O_2 consumption.

When the O_2 input rate is zero (see case 1 above, i.e., the diffusion tube was pressurized with N_2 gas), the incubated sediments become O_2 free shortly after the

experiments were set up and the first time points were taken (<1 hr). For example, although the initial sediment slurry was well-mixed and oxygenated during experimental setup, by the time the experiments were initiated and the first time points were collected, sediment O_2 levels were zero except in some of the incubations with high O_2 delivery rates. Sulfate then becomes the next major electron acceptor in organic matter remineralization, because nitrate, Mn oxides, and Fe oxides are all found at very low levels in these carbonate sediments (Burdige, 2006; Morse et al., 1985).

In the anoxic incubations, pore water alkalinity and DIC levels increase as a result of sulfate reduction. Pore water saturation states may initially decrease when there are low amounts of sulfate reduction (~0.7 mmol/kg loss of sulfate) and lead to slight amount of carbonate dissolution. However, as sulfate reduction progresses, the buildup of pore water alkalinity may lead to the precipitation of authigenic carbonate, as reflected by a Ca^{2+} depletion over time (Boudreau and Canfield, 1993; Burdige, 2006; Stoessell, 1992; Walter and Burton, 1990).

When O_2 consumption is rapid as compared to O_2 input through the diffusion tube (case 2), pore waters of the incubated sediments will have no dissolved O_2, and aerobic respiration and sulfate reduction can co-occur in microenvironments within the vials (i.e., aerobic respiration in regions close to the diffusion tube and sulfate reduction farther away). Some of the O_2 consumption is also likely involved in re-oxidation of sulfide to sulfate. The combination of sulfate reduction and sulfide oxidation is functionally equivalent to aerobic respiration according to:

$$2CH_2O + SO_4^{2-} \rightarrow 2HCO_3^- + H_2S \quad (18)$$

$$2O_2 + H_2S \rightarrow 2H^+ + SO_4^{2-} \quad (19)$$

$$CH_2O + O_2 \rightarrow CO_2 + H_2O \quad (20)$$

This implies that in these experiments O_2 input can simply be considered to solely drive aerobic respiration, which can then presumably mediate carbonate dissolution (rxn. 17). Due to the co-occurrence here of sulfate reduction and aerobic respiration, pore water alkalinity and DIC come from two sources, i.e., metabolic carbonate dissolution and sulfate reduction.

When the O_2 input rate is greater than or equal to the rate of sediment O_2 consumption (case 3), dissolved oxygen will be observed in the pore waters. Aerobic oxidation of organic matter and metabolic carbonate dissolution are the two dominant reactions that occur. Alkalinity, DIC, and Ca^{2+} concentrations are expected to increase, with the alkalinity increase essentially coming solely from carbonate dissolution.

3.1.2. O_2 Concentration Changes

All sediments used in these studies were initially well-mixed and oxygenated, and in all studies except those using N_2 as the diffusion gas, oxygen was continuously added to the sediments during the course of incubations. However, in many of the studies O_2 could not be detected in the sediments once the experiments were initiated (cases 1 and 2 above). These included all the CM, HW, OS incubations, both of the 3-N and 13-N incubations and the 13-L incubation. The oxic incubations that used C-Flex tubing (3-L, 3-H, and 13-H) all showed dissolved O_2 (case 3), which suggests that here aerobic respiration was the sole carbon oxidation mechanism. The O_2 concentration changes in the WS-3 and WS-13 incubations are shown in Fig. 15.

3.1.3. Titration Alkalinity, Total DIC, Calcium and Sulfide Concentration Changes

Changes in Alk_T, DIC, $[Ca^{2+}]$ and TDS during each set of incubations are shown in Figs. 16-19. These concentrations are expressed relative to starting concentrations, hence the Δ concentration notation is used in the following figures. Since these incubations were carried out under closed-system conditions, chlorinity (salinity) did not change significantly (Table 9).

Table 9. Changes in salinity for the incubations [a].

	CM	HW	OS	WS-3	WS-13
$[Cl^-]$ (mmol/kg)	584.6±2.6	592.6±3.9	589.0±3.0	571.0±1.5	581.1±3.9
Salinity	37.5±0.2	38.0±0.3	37.8±0.2	36.6±0.1	37.8±0.2
CV (%)	0.4	0.7	0.5	0.3	0.7

[a] For each site these are averages of all vials from all experiments, uncertainties are standard deviations of the analysis (n=9 for CM incubations and n=10 for all other incubations, uncertainties are standard deviations).

In such closed-system incubations, nonlinear concentration changes can occur (e.g., Rude and Aller, 1991), and in many of the incubations pore water solute concentrations initially increased and then leveled off with time. To describe the reaction rates and stoichiometry in these studies, linear regressions were calculated between Δ

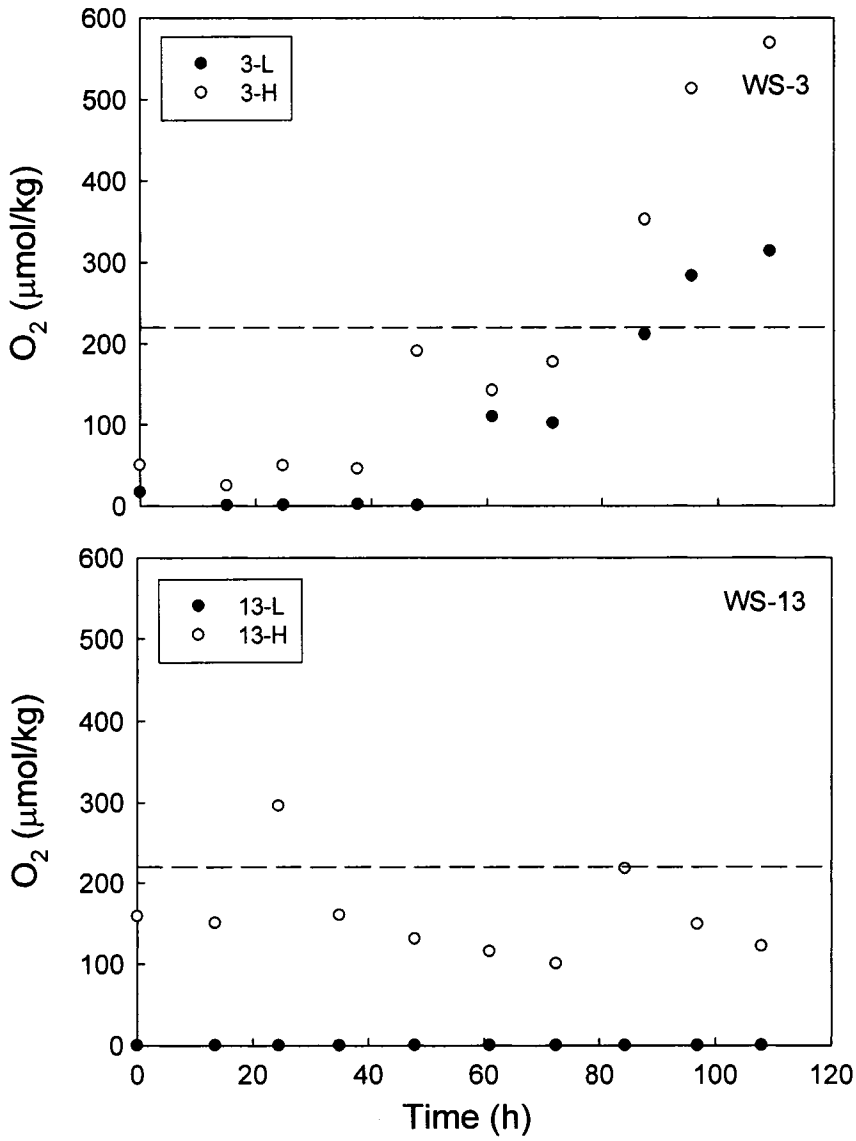

Fig. 15. Changes in pore water oxygen concentration in the WS-3 and WS-13 incubations. The dashed lines represent O_2 saturation at the experimental conditions (220 µmol/kg). Note the 13-L incubation used Teflon tubing as opposed to the much more permeable C-Flex tubing used in all other oxygenated incubations.

concentration and time for the linear portion of these times courses. The choice of the range of data points used here was based on the maximum range over which there was a statistically significant linear slope and a best-fit y-intercept equal to 0 ($\pm 1\sigma$) (Table 10). All incubations showed a slight decrease in pH (Appendix B). This observation agrees with the results of a closed-system organic carbon remineralization model for carbonate sediments (Boudreau and Canfield, 1993), in which both aerobic respiration (when O_2 is present) and sulfate reduction (when O_2 is depleted) lead to a decrease in pore water pH as the reactions progress.

In the CM experiments, TDS was observed even in some pore waters at the first time point, and all incubated CM sediments with or without O_2 input produced significant amount of TDS (0.9 - 2.1 mmol/kg at the end of each incubation; Fig. 19). Low levels of TDS were detected in HW experiments (10^{-2} mmol/kg). No TDS was detected in the OS incubations. A slight increase in TDS was observed in the 3-N incubation and no TDS was present in either the 3-L or 3-H incubation, consistent with the occurrence here of dissolved O_2 in the pore waters. In WS-13 incubations, significant TDS production was observed in the 13-N incubation, the 13-L incubation showed low level of TDS and the 13-H incubation showed no TDS.

According to rxns. (17) and (18), pore water alkalinity and DIC production rates should equal each other, regardless of the organic matter remineralization pathway (i.e., aerobic vs. anaerobic). Except for the CM incubations, this is indeed the case (Fig. 20). The reason for high alkalinity production rates in the CM incubations is unclear, although other production rates (i.e., DIC, Ca^{2+}) are consistent with the O_2 delivery rates (e.g., see discussion in section 4.5). These measured alkalinities are also consistent with calculated values of alkalinity (section 4.1).

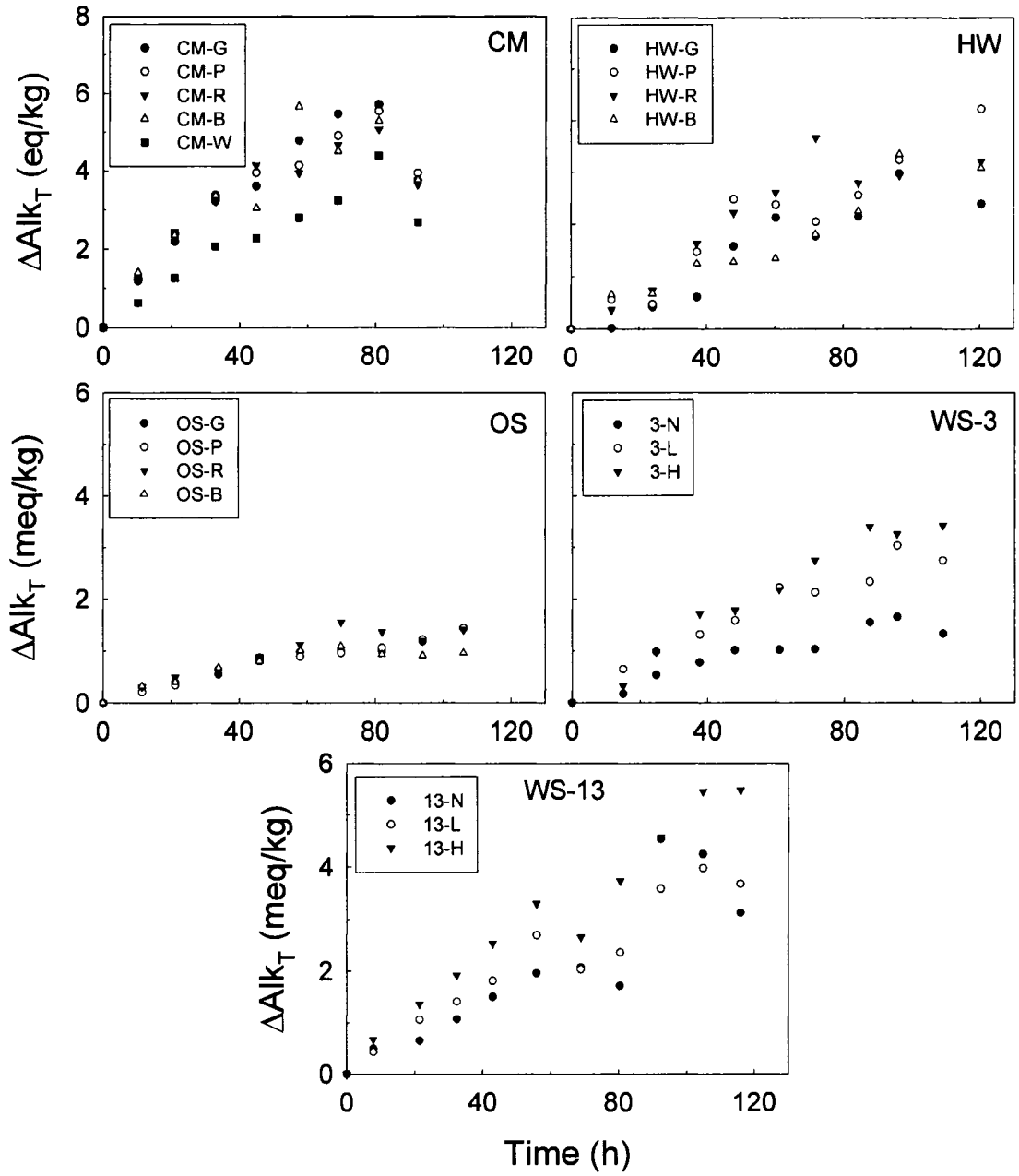

Fig. 16. Concentrations of total titration alkalinity versus time in the pore waters of all experimental incubations. Concentrations are expressed relative to starting pore water concentration (i.e., ΔAlk_T).

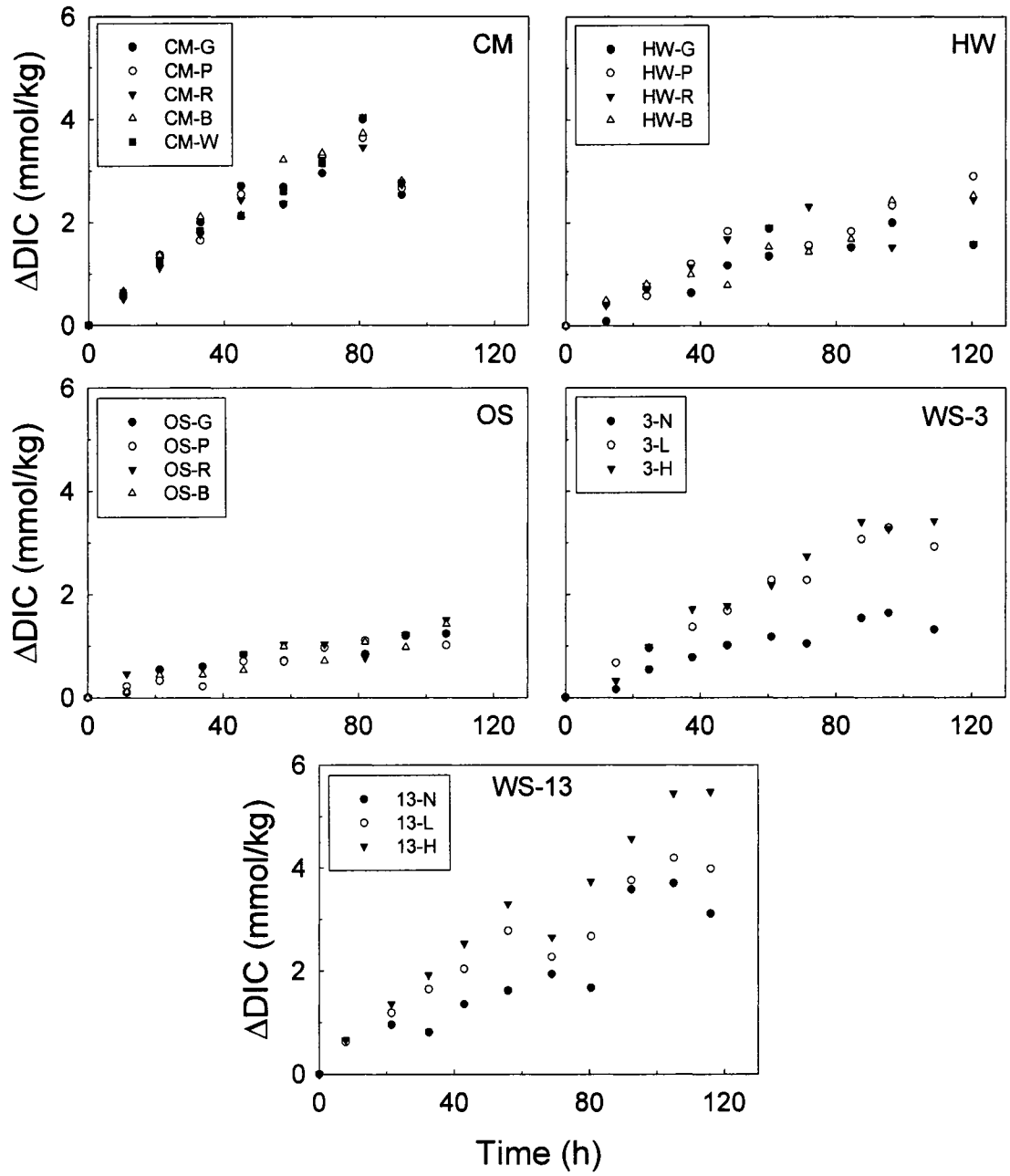

Fig. 17. Concentrations of total dissolved inorganic carbon versus time in the pore waters of all experimental incubations. Concentrations are expressed relative to starting pore water concentration (i.e., ΔDIC).

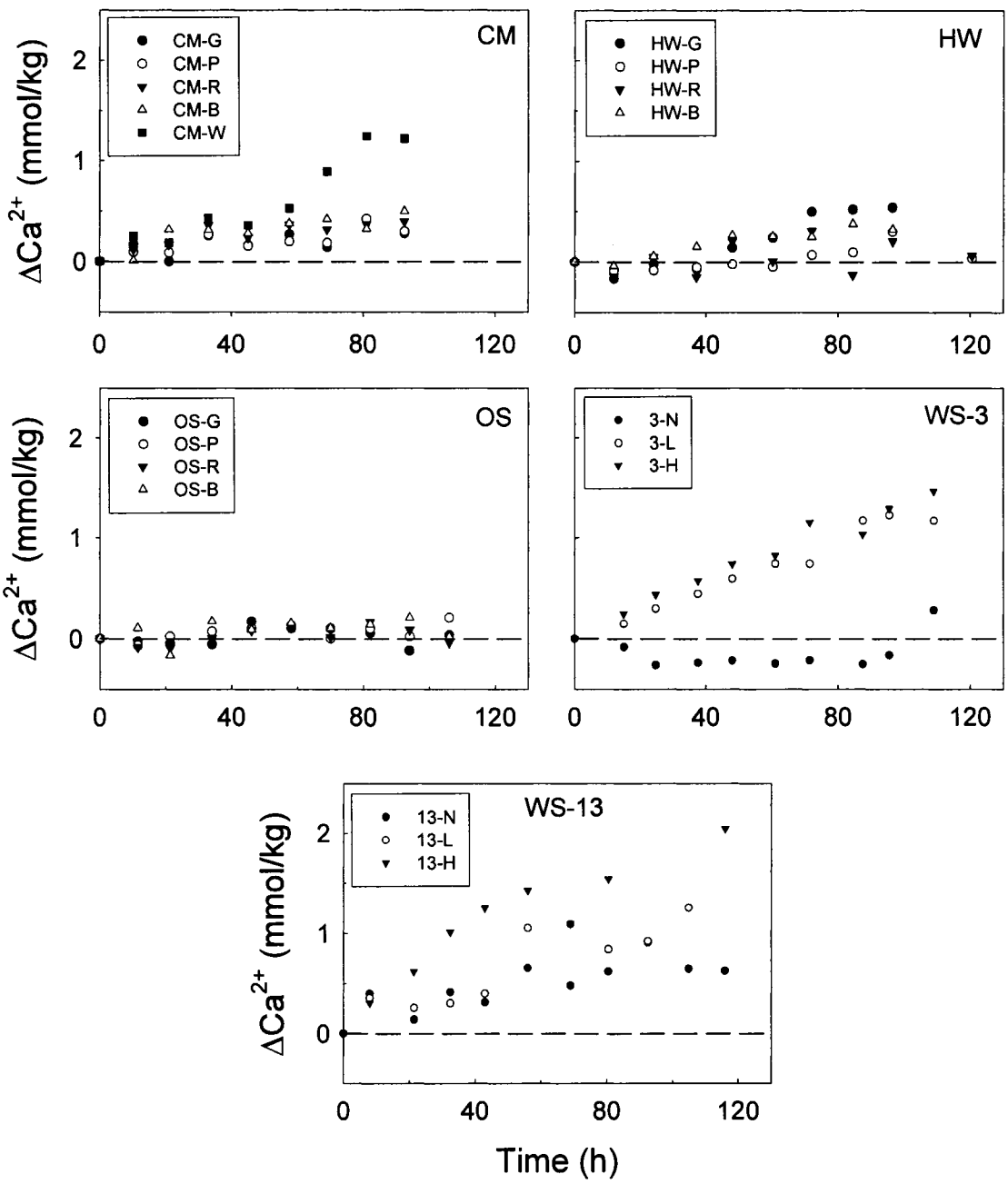

Fig. 18. Concentrations of calcium versus time in the pore waters of all experimental incubations. Concentrations are expressed relative to starting pore water concentration (i.e., ΔCa^{2+}).

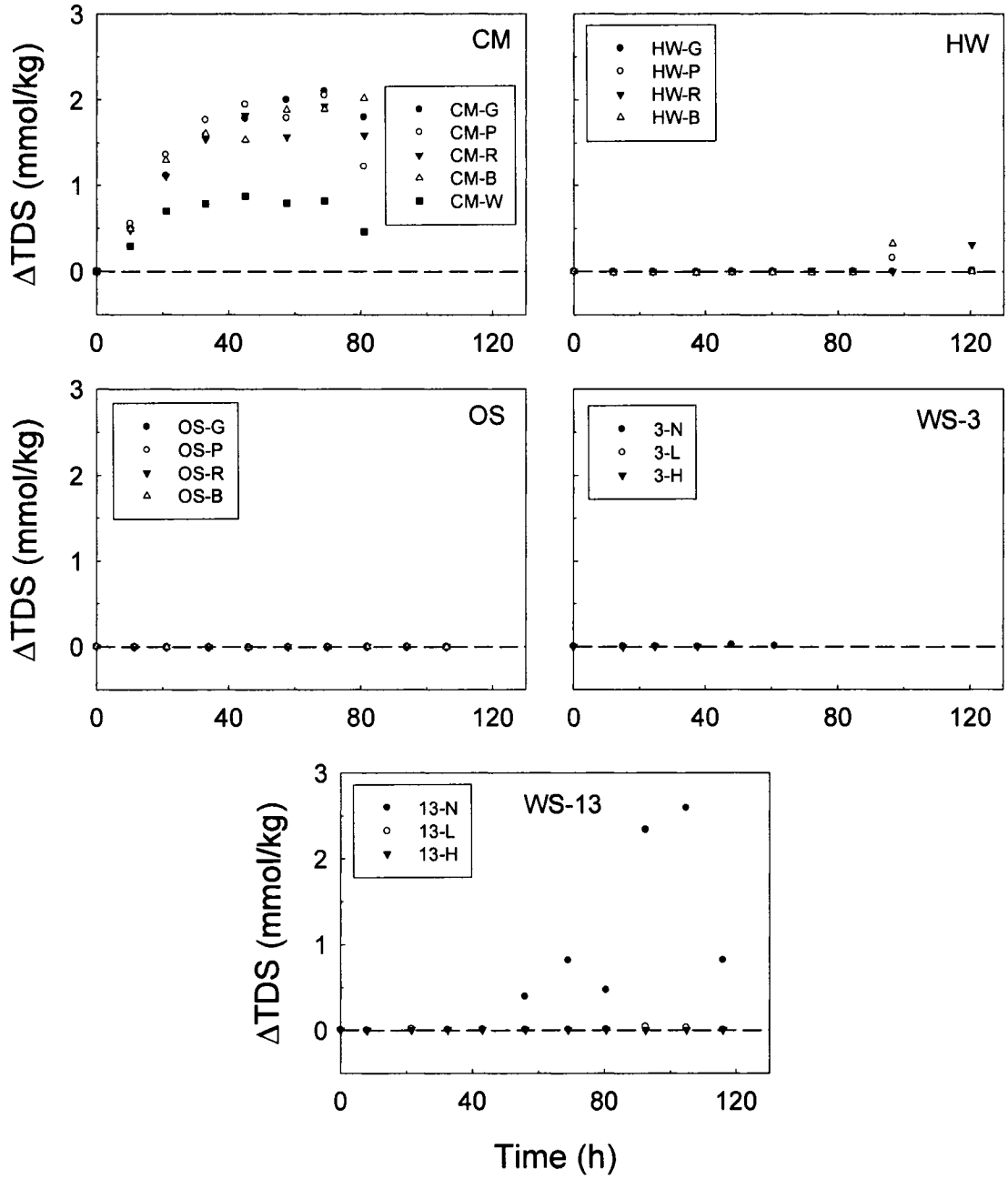

Fig. 19. Concentrations of total dissolved sulfide (TDS) versus time in the pore waters of all experimental incubations. Concentrations are expressed relative to starting pore water concentration (i.e., ΔTDS).

Table 10. Reaction rates in the sediment incubation experiments [a].

Experiment		Time range (h)	r_{alk} (μeq/kg/h)	Time range (h)	r_{DIC} (μmol/kg/h)	Time range (h)	r_{Ca} (μmol/kg/h)
CM	CM-G	0-33	97±5	0-45	61±2	0-57.5	[4±2]
	CM-P	0-33	102±6	0-45	54±4	0-57.5	4±1
	CM-R	0-21	116±4	0-33	54±1	0-69	5±1
	CM-B	0-33	100±9	0-33	64±1	0-69	6±1
	CM-W	0-33	63±1	0-33	60±2	0-81	13±2
HW	HW-G	0-128.5	26±4	0-104.5	20±2	0-60.3	[0±1]
	HW-P	0-80	35±7	0-68.3	33±3	0-84.5	2±1
	HW-R	0-92.5	42±6	0-80	31±1	0-72	4±2
	HW-B	0-104.5	29±3	0-45.3	26±4	0-72	5±1
OS	OS-G	0-58	17±1	0-46	19±3	0-70	[2±1]
	OS-P	0-58	16±1	0-94	13±1	0-58	3±1
	OS-R	0-70	20±1	0-58	16±2	0-58	[3±1]
	OS-W	0-46	17±2	0-58	15±3	0-58	[3±2]
WS-3	3-N	0-109	14±2	0-109	14±2	0-109	[-2±1]
	3-L	0-109	28±2	0-109	33±1	0-109	12±0
	3-H	0-109	34±2	0-109	35±3	0-109	15±1
WS-13	13-N	0-69	33±3	0-56	25±7	0-69	[8±4]
	13-L	0-56	42±2	0-69	47±2	0-69	14±5
	13-H	0-56	57±2/	0-56	62±2/	0-56	30±2/
		56-116	44±7	56-116	44±7	56-116	10±3

[a] Rate values in brackets denote that a significant linear regression ($P<0.05$) was not obtained from the available data; uncertainties in this table are standard errors derived from the linear regressions.

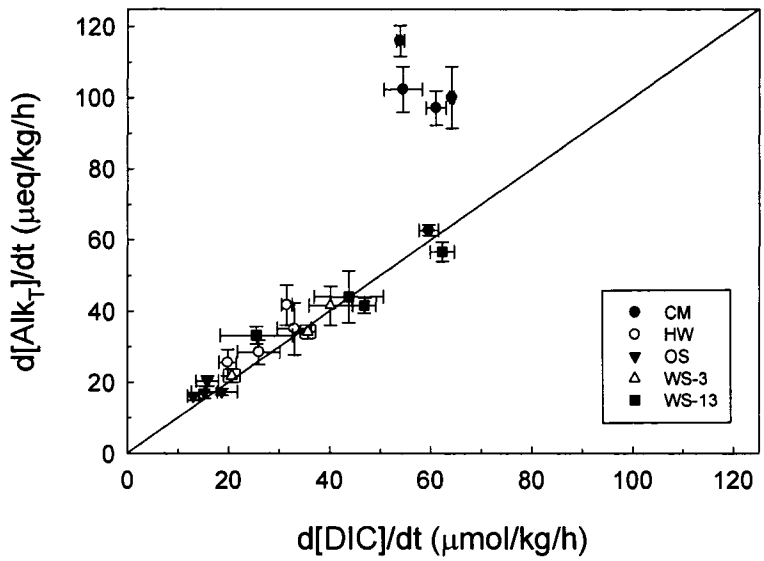

Fig. 20. Production rates of alkalinity and DIC in all incubations (taken from Table 10). The solid line is the 1:1 line. The data points that deviate from 1:1 relationship are from CM-G, CM-P, CM-R, and CM-B incubations. Uncertainties are standard errors of the linear regressions.

3.1.4. Pore Water Saturation State

The ion concentration product (ICP) for experimental time points was calculated using $[Ca^{2+}]$ and $[CO_3^{2-}]$, with the latter being determined with pH and DIC concentration data using the Excel® version of the program CO2SYS (Millero, pers. comm., Lewis and Wallace, 1998). The calculated ICP values were then divided by the stoichiometric solubility constant of aragonite ($K'_{sp\text{-}arag}$) calculated using the constants in Mucci (1983) at experimental temperatures and salinity. This results in the saturation index (Ω_{arag}) of the pore waters, or

$$\Omega_{arag} = \frac{[Ca^{2+}][CO_3^{2-}]}{K'_{sp-arag}} \qquad (21)$$

From Fig. 21, it appears that all pore waters in these experiments were either supersaturated or close to saturation with respect to aragonite.

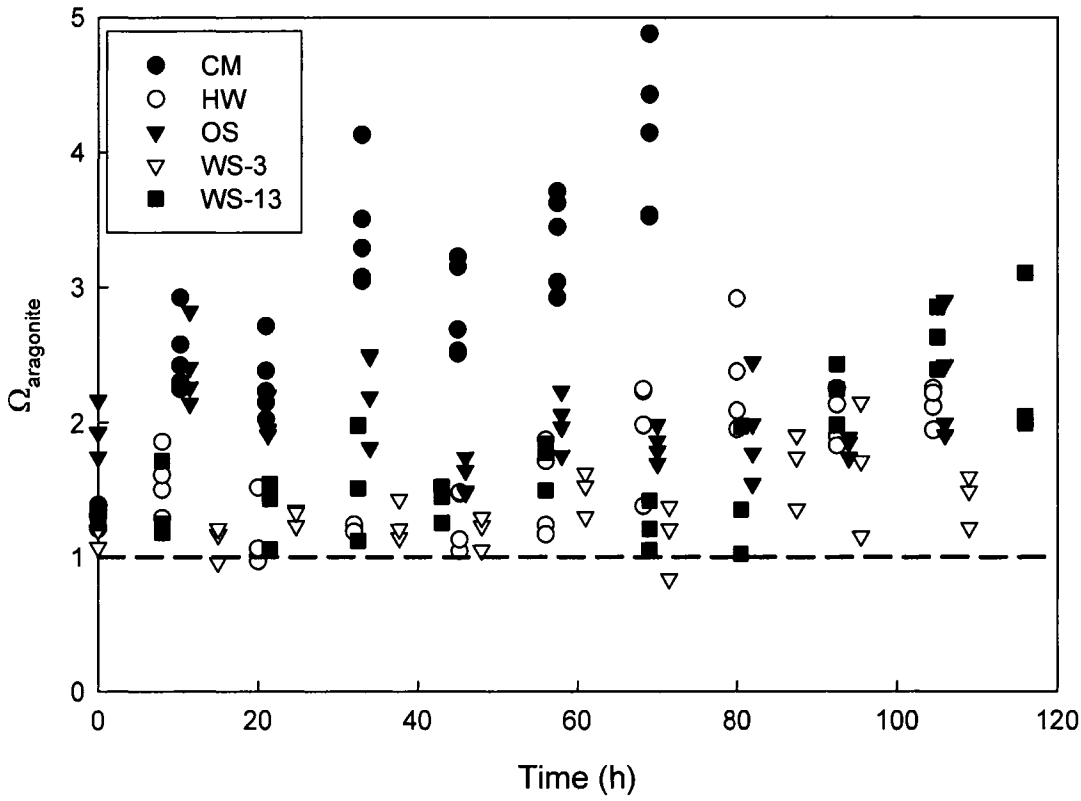

Fig. 21. The pore water aragonite saturation index (Ω_{arag}) in all incubations. Ω_{arag} was calculated as the calcium carbonate ion concentration product (ICP) in the pore waters divided by the stoichiometric solubility constant ($K'_{sp\text{-}arag}$) at incubation salinity and temperature.

3.2. Stable carbon isotopes

Isotopic values of both carbonate sediments and seagrass are shown in Table 11.

Table 11. Isotopic composition (‰) of seagrass and carbonate sediments.

	$\delta^{13}C_{carbonate}$ [a]	$\delta^{13}C_{Thalassia}$	$\delta^{13}C_{Syringodium}$
WS-3	4.20±0.04	-9.7±0.7	-6.0±0.7
WS-13	3.93±0.01	-4.9±0.5	-

[a] See Table 7 for information on the mineralogy of these sediments, uncertainties are standard deviations of the measurements (n=3).

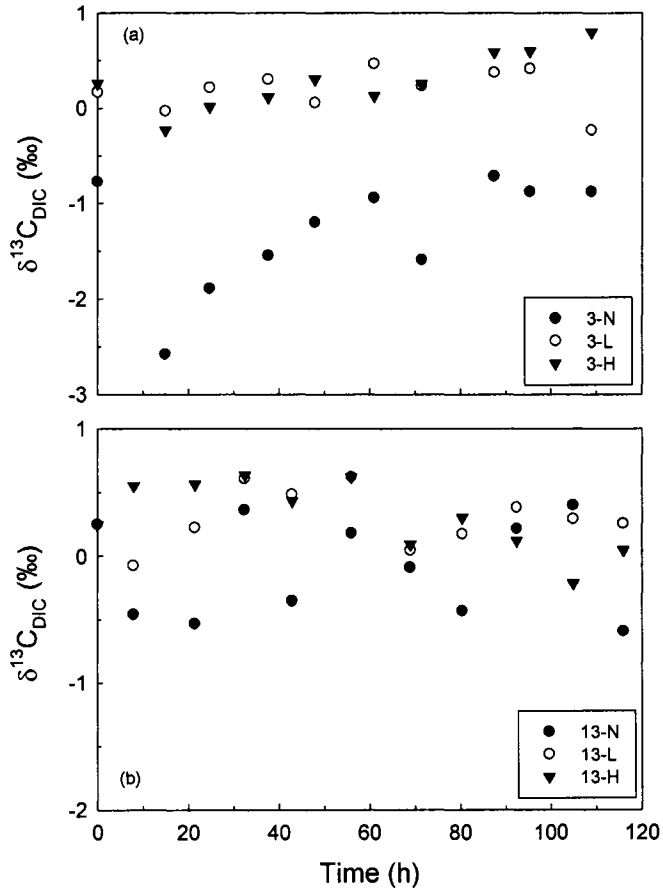

Fig. 22. Co-evolution of pore water DIC $\delta^{13}C$ and DIC concentration in (a) WS-3, and (b) WS-13 incubations.

Pore water DIC $\delta^{13}C$ changes with time in WS-3 and WS-13 experiments are shown in Fig. 22 and listed in Appendix B. DIC $\delta^{13}C$ values in WS-3 pore waters first showed a drop from the initial value and then gradually increased as DIC concentration increased. DIC $\delta^{13}C$ values in WS-13 pore waters (0-56 hrs) increased slightly in both the 13-L and 13-H incubations, with no obvious trend observed in the 13-N incubation.

4. DISCUSSIONS

4.1. Reaction Stoichiometry

In the tropical coastal sediments of Ban Pak Klok, Thailand, that are inhabited by seagrasses, Holmer et al. (2001) observed that microbial respiration is closely coupled

with organic matter production by the dominant seagrasses *Cymodocea rotundata* and *Thalassia hemprichii*; a similar observation was also made in Lower Laguna Madre (LLM) sediments vegetated by *T. testudinum* (Jones et al., 2003). Analogous to the LLM environment, the water column in the Bahamas is also largely oligotrophic and seagrasses are the dominant primary producers (Hemminga and Duarte, 2000). In the previous study (Chapter II), organic matter that is being remineralized in both bare oolitic sand and intermediate seagrass sediments could be attributed to either seagrass/detrital carbon mixture or seagrass carbon. Furthermore in the carbonate dissolution/reprecipitation model proposed to explain the unusual enrichment of ^{13}C in pore water DIC pool of the dense seagrass sediments, seagrass carbon was assumed to be the sole type of organic carbon undergoing remineralization (see detailed discussions in Chapter II). In these closed-system incubations, I also assume that seagrass is the only organic carbon source that contributes to the pore water DIC pool. Based on this assumption, seagrass elemental ratios (C/N/P) and stable carbon isotopic composition will be used in the calculations in this section and in section 4.2.

The C/N ratios determined in this study (Table 12) were generally higher than previously reported values for *T. testudinum* in Florida Bay (average elemental ratio C:N:P = 106:5.8:0.1 and C:N = 18.3, Fourqurean et al., 1992). These carbonate sediments are P-limited and the C/P ratio may be up to 1000 or higher (Hemminga and Duarte, 2000), therefore P is a negligible source that contributes to pore water alkalinity during organic matter remineralization. A C/P ratio of 106:0.1 was adopted here and the average value of the seagrass C/N ratio at each site was used to calculate x in the ratio $106/x$ (Table 12) in seagrass organic matter remineralization reaction equations. For anaerobic respiration, the reaction is:

Table 12. C/N ratio of seagrasses at the sampling sites.

Station ID	*T. testudinum*		*S. filiforme*	
	Leaf	Root	Leaf	Root
CM	16	30	-	-
HW	40	58	-	-
WS-3	30	45	33	89
WS-13	36	69	-	-

$$\frac{1}{53}(CH_2O)_{106}(NH_3)_x(H_3PO_4)_{0.1} + SO_4^{2-} + \frac{x}{53}H^+ \rightarrow$$
$$2HCO_3^- + H_2S + \frac{x}{53}[NH_4^+] + \frac{0.1}{53}H_3PO_4 \quad (22)$$

where the alkalinity increase here is caused by sulfate reduction only. Since [Ca^{2+}] increases were small in the anoxic incubations, net carbonate dissolution appeared to be minimal, and pore water alkalinity increases were predominantly derived from sulfate reduction. From eqn (22), one unit of sulfate reduction produces slightly more than two units of alkalinity:

$$\Delta Alk_T \cong \Delta Alk_S = 2 \times \Delta TDS + \Delta[NH_4^+] = (2 + \frac{x}{53})\Delta TDS \quad (23)$$

During aerobic respiration, one unit of organic carbon oxidation also yields slightly more than two units of carbonate alkalinity if the strong acids (HNO_3 and H_3PO_4) produced in this process also react with carbonate. However the strong acids produced here are negligible given the high C/N/P ratio of seagrass (Table 12). Aerobic respiration is written here as:

$$\frac{1}{53}(CH_2O)_{106}(NH_3)_x(H_3PO_4)_{0.1} + \frac{106+2x}{53}O_2$$
$$\rightarrow 2H_2CO_3 + \frac{x}{53}HNO_3 + \frac{0.1}{53}H_3PO_4 + \frac{x}{53}H_2O \quad (24)$$

$$H_2CO_3 + MCO_3 \rightarrow M^{2+} + 2HCO_3^- \quad (25)$$

where M is the divalent ions (Ca^{2+}, Mg^{2+}) in the carbonate phases.

Pore water alkalinity composition can be expressed in the following equation (e.g., Dickson, 1981):

$$Alk = [HCO_3^-] + 2[HCO_3^{2-}] + [B(OH)_4^-] + [HS^-] + 2[S^{2-}] + [NH_4^+] - [H^+] +$$
$$[OH^-] + [HSO_4^-] + [H2PO_4^-] + 2[HPO_4^{2-}] \quad (26)$$

In experiments where anaerobic respirations occur in the sediments with or without aerobic respiration, pore water alkalinity is dominated by carbonate alkalinity (HCO_3^- and CO_3^{2-}), sulfide alkalinity (HS^- and S^{2-}), ammonium alkalinity (NH_4^+), and borate alkalinity ($B(OH)_4^-$). This assumption was tested by independently estimating the total alkalinity concentrations using this equation using eqn. (26) and comparing these estimates with measured values. As shown in Fig. 23, calculated alkalinity values are in

good agreement with the measured values for all incubations except HW, which showed a lower regression slope (0.66) than that for the rest of the data (1.07) using ANCOVA (MS = 16.8, MS err = 0.1, F = 165.24, df = 1, 179, P<0.0001). Thus except the data from HW incubations, there was good internal consistency within rest of the data set. The low calculated alkalinity values for HW incubations could be due to inaccurate sulfide measurements.

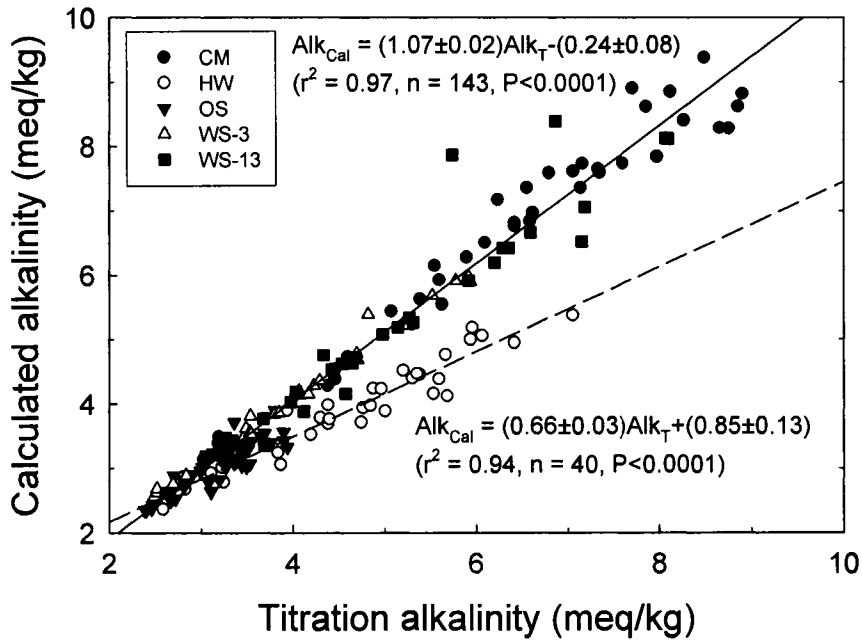

Fig. 23. Calculated alkalinity versus measured titration alkalinity for all incubations. Calculated alkalinity was determined using the following equation $Alk = [HCO_3^-] + 2[HCO_3^{2-}] + [B(OH)_4^-] + [HS^-] + 2[S^{2-}] + [NH_4^+] - [H^+] + [OH^-] + [HSO_4^-] + [H_2PO_4^-] + 2[HPO_4^{2-}]$ (e.g., Dickson, 1981). In this calculation, alkalinity contributions from H^+, OH^-, phosphates, and HSO_4^- were assumed to be negligible and were not included in the calculations. Carbonate and bicarbonate concentrations were calculated with measured values of DIC and pH using the program CO2SYS (Lewis and Wallace, 1998); borate alkalinity was calculated using salinity corrected total borate concentration and pH; sulfide alkalinity was calculated from total dissolved sulfide concentration and pH; ammonium alkalinity was calculated using sulfide concentrations and the reaction stoichiometry in rxn (22). All dissociation constants used in these calculations are from Millero (2001). The solid and the dashed lines are linear regression of calculated alkalinity vs. titration alkalinity for all incubations except the HW incubations, and the HW incubations, respectively.

To differentiate alkalinity sources in CM experiments (carbonate dissolution versus sulfate reduction) when both types of respirations (aerobic and anaerobic) occur, the following equation was used (cf. Berner et al., 1970):

$$\Delta Alk_T \cong \Delta Alk_C + \Delta Alk_S \quad (27)$$

where ΔAlk_C is the alkalinity produced through aerobic metabolic carbonate dissolution (rxns 15-17), and ΔAlk_S is the alkalinity produced through sulfate reduction. Since borate alkalinity changes were small (data not shown), their contribution to the changes in total alkalinity was neglected. Therefore the total alkalinity production minus the alkalinity produced by sulfate reduction (ΔAlk_S) yields alkalinity produced by carbonate dissolution (ΔAlk_C).

Using ΔTDS and eqn. (23), ΔAlk_S can be calculated, and then with eqn. (27) ΔAlk_C can be calculated. Finally, ΔAlk_C versus $\Delta[Ca^{2+}]$ can then be used to calculate the Ca content of the apparent carbonate phase dissolving in each incubation, where this Ca content equals to $2\times(\Delta[Ca^{2+}]/\Delta Alk_C)$, and $\Delta[Ca^{2+}]/\Delta Alk_C$ is the slope of the regression line through the data. As discussed in section 3.1.1 (case 3), when there is no sulfate reduction $\Delta Alk_S=0$ and $\Delta Alk_C= \Delta Alk_T$.

In all HW, OS, and CM incubations except the CM-W incubation, Ca^{2+} concentration changes were relatively low and regressions of $\Delta[Ca^{2+}]$ versus ΔAlk_C yielded slopes with large errors and high P values (>0.05). Therefore these results are not included in the discussion here. In the CM-W incubation, the regression of $\Delta[Ca^{2+}]$ versus ΔAlk_C yielded a value of 0.37±0.01 (Fig. 24), thus the apparent dissolving carbonate phase has the composition of $Ca_{0.74}Mg_{0.26}CO_3$. In the 3-L and 3-H incubations, the regression slopes of $\Delta[Ca^{2+}]$ versus ΔAlk_C for each incubation were not significantly different from each other (Student's t-test, P>0.05), therefore the pooled data were used to calculate a combined $\Delta[Ca^{2+}]/\Delta Alk_C$ ratio (Fig. 24). This value is 0.39±0.01, and the apparent dissolving phase thus has the composition of $Ca_{0.79}Mg_{0.21}CO_3$. In the WS-13 incubations, the first 6 data points (0-56 hrs) for both oxic incubations showed a good linear relationship between $\Delta[Ca^{2+}]$ and ΔAlk_C and were used in these regressions (note that this approach is consistent with the isotope mass balance calculations in the next section, and 56 hrs also represents the time at which the O_2 gas pressure was reduced from 20 psi to 10 psi). The calculated $\Delta[Ca^{2+}]/\Delta Alk_C$ values are 0.32±0.05 (r^2=0.91, p<0.005) for 13-L, and

0.47±0.02 (r^2=0.99, p<0.0001) for 13-H. The plots of these regressions are shown in Fig. 24 and the $\Delta[Ca^{2+}]/\Delta Alk_C$ ratio values are listed Table 13. Neither the 3-N nor the 13-N incubation yielded significant Ca^{2+} production ($d\Delta[Ca^{2+}]/dt \approx 0$, Table 10), which is indicative of no net dissolution. Thus these incubations were not used in these calculations. However, additional information about carbon cycling in these sediments is discussed in the next section where isotope mass balance calculations using the results from these anoxic incubations are carried out.

From another prospective, all pore waters of these incubated sediments were either supersaturated or close to saturation with respect to aragonite (see Fig. 21). It is therefore likely that a soluble carbonate phase(s) (most likely HMC) with greater or similar solubility as aragonite was dissolving in response to metabolic CO_2 production. These results agree with previous studies that HMC is preferentially dissolved in carbonate sediments such as these (Burdige and Zimmerman, 2002; Morse et al., 2006; Morse and Mackenzie, 1990; also see Walter and Morse, 1984).

On the other hand, the Mg content of the HMC in the sediments measured using XRD techniques was much lower than that calculated from the pore water results (i.e., 100% minus the mole% Ca) from the CM and WS-3 sediments (12.6 and 12.0 mole% vs. 26 and 21 mole% Mg). In contrast this same comparison in the WS-13 sediments was rather equivocal (Table 7 and 13), since the 13-L and 13-H incubations yielded a Mg content in HMC phase that was between 36% and 7% (versus 12.3 mole% Mg based on the XRD results).

Two possible reasons may contribute to the discrepancy between the Mg content of the HMC that is dissolving (based on the pore water data) and the Mg content of the HMC in the sediments (based on XRD results). The first is that a more soluble HMC with a higher Mg contents (21-26 mole% Mg) was actually dissolving, since HMC solubility increases with increasing Mg concentration in the natural carbonate minerals (Bischoff et al., 1993; Bischoff et al., 1987; Plummer and Mackenzie, 1974). Furthermore, because the XRD spectra of these carbonate sediments usually showed a broadened 104 peak as compared to that obtained with pure biogenic calcite standards, the HMC in these sediments was possibly a mixture of carbonates with a range of Mg contents such that the average value was ~12 mole% (Berner, 1966). However, when comparing these results

with tabulated results in the literature of the Mg content of HMC in Bahamian sediments (e.g., Morse et al., 1985), the Mg contents based on the pore water data are at the high

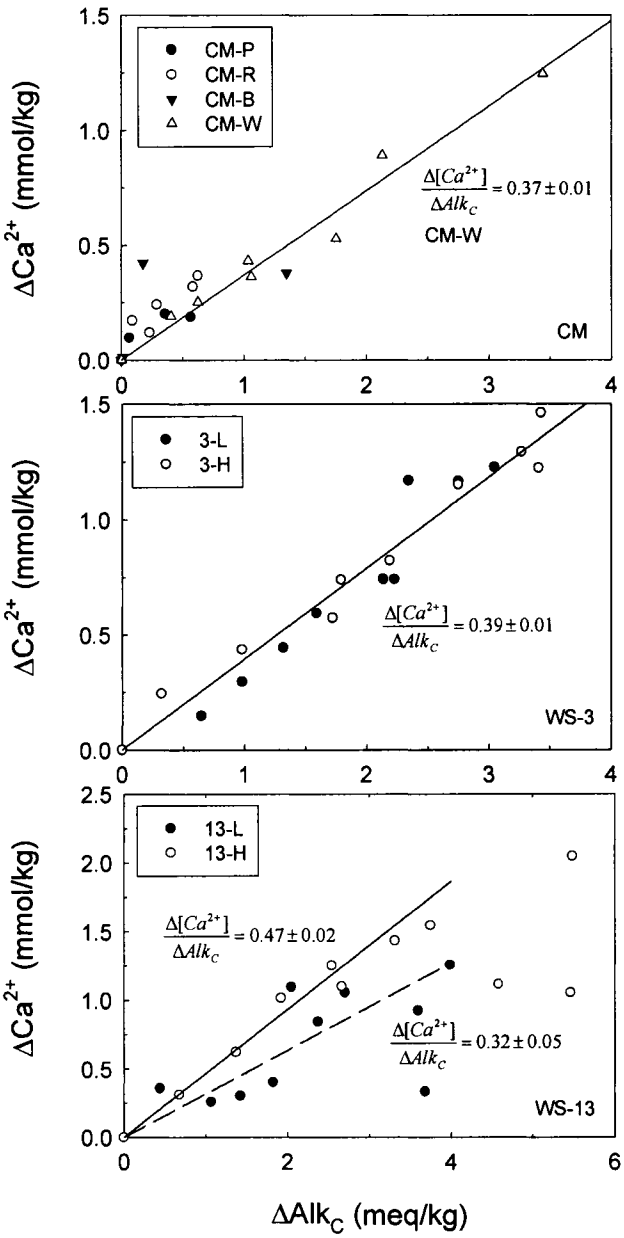

Fig. 24. The regression of $\Delta[Ca^{2+}]$ vs. ΔAlk_C for the CM, WS-3 and WS-13 incubations. Since the y-intercepts of these linear regressions are not significantly different from zero, the regression lines were all forced through the origin. Note that in the CM incubation, only the data from CM-W incubation was used to generate the regression. See the text and Table 13 for details.

Table 13. Composition of the apparent dissolving phase in the CM, WS-3 and WS-13 incubations [a].

	CM	3-L & 3-H	13-L	13-H
$\Delta[Ca^{2+}]/\Delta Alk_C$	0.37±0.01	0.39±0.01	0.32±0.05	0.47±0.02
r^2	0.97	0.97	0.76	0.98
P	<0.0001	<0.0001	<0.001	<0.0001

[a] Uncertainties were standard errors obtained from the linear regressions (Fig. 24).

end of this range, especially for the CM sediments (26 mole% Mg).

Alternatively, if HMC with ~12 mole% Mg was indeed dissolving, then a secondary carbonate phase with a lower Mg content may be reprecipitating (for example, Rude and Aller, 1991). Such a scenario could then sustain the disproportional increase in production of $[Ca^{2+}]$ relative to the Ca/Mg ratio in the sediment HMC. These two possible explanations will be revisited in section 4.3 after discussing the stable isotope mass balance in section 4.2.

4.2. Stable Carbon Isotope Mass Balance

Due to distinct difference between the carbon isotopic composition ($\delta^{13}C$) of sedimentary organic matter and carbonate sediments, carbon isotopes have been used extensively in marine geochemical studies to differentiate between carbon sources that contribute to the pore water DIC pool (Chapter II; Gehlen et al., 1999; Martin et al., 2000; McCorkle et al., 1985; McNichol et al., 1991; Sayles and Curry, 1988). However, in some coastal sediments (Eldridge and Morse, 2000; McNichol and Druffel, 1992), discrepancies are observed between the observed $\delta^{13}C$ values and those derived from the 1:1 stoichiometric mixing of organic and inorganic carbon (rxn. 17) as discussed in Chapter II.

Following the procedure in Chapter II, the $\delta^{13}C$ of the DIC being added to the pore waters of these incubations ($\delta^{13}C_{added}$) was calculated through a linear regression of $\delta^{13}C{\cdot}DIC$ vs. DIC (see Appendix A for a detailed derivation).

In the WS-3 incubations, the calculated $\delta^{13}C_{added}$ values in both the 3-L and the 3-H incubations were not significantly different from each other (Student's t-test, $P>0.05$),

therefore the data of these incubations were pooled together and a single $\delta^{13}C_{added}$ value was calculated for the pooled data set. However, the regression of the data from the anoxic incubation yielded a higher $\delta^{13}C_{added}$ value (Fig. 25). For the WS-13 incubations, because $\delta^{13}C$·DIC vs. DIC showed a good linear relationship over the first half of the oxic incubations (0-56 hr, see section 4.1), only these data points were included in the linear regression. The regression in the 13-N incubation was not significant ($P>0.05$), although the calculated $\delta^{13}C_{added}$ is still used in the following discussion for comparison with the results from the oxic incubations (Fig. 26). All $\delta^{13}C_{added}$ values derived from these linear regressions are shown in Table 14.

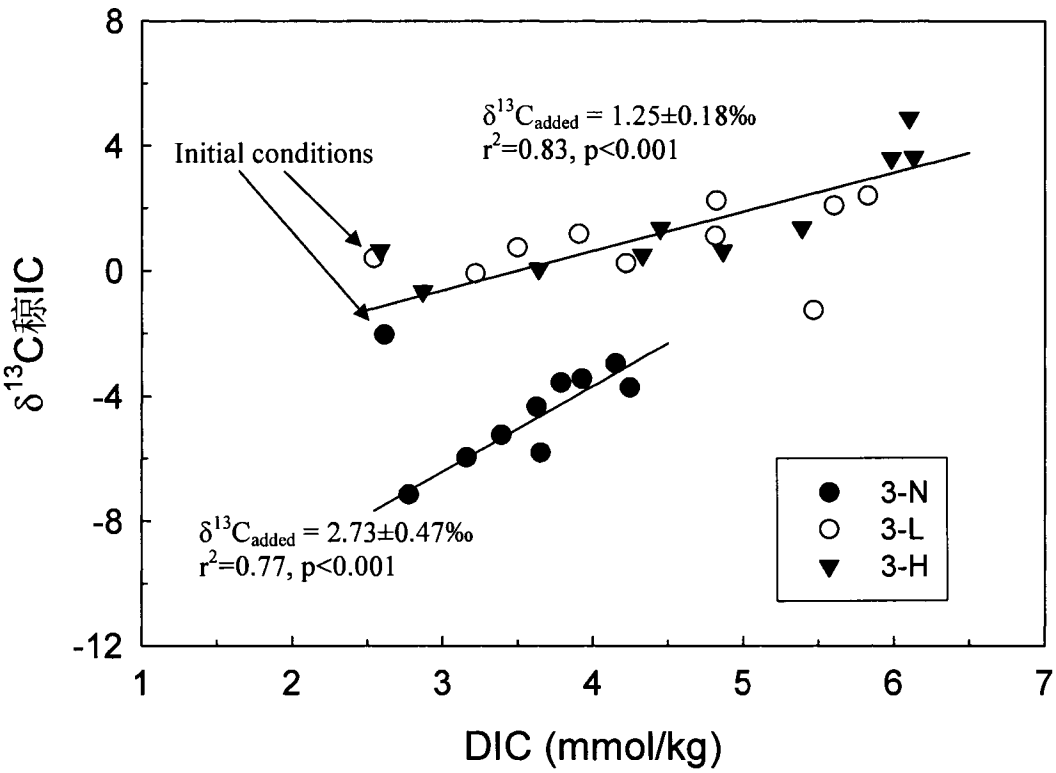

Fig. 25. Regression of $\delta^{13}C$·DIC vs. DIC in the WS-3 incubations. Note that the regression lines did not include the initial set of data points, to account for the equilibration of the sediment-water mixture after the initial setup of the experiment. The data from the 3-L and 3-H incubations were pooled together since regression slopes ($\delta^{13}C_{added}$) of each individual incubation were not statistically different from each other but both were lower than that of the anoxic incubation (ANCOVA test, $P<0.05$, and $\delta^{13}C_{added\text{-}3\text{-}L} = \delta^{13}C_{added\text{-}3\text{-}H} < \delta^{13}C_{added\text{-}3\text{-}N}$).

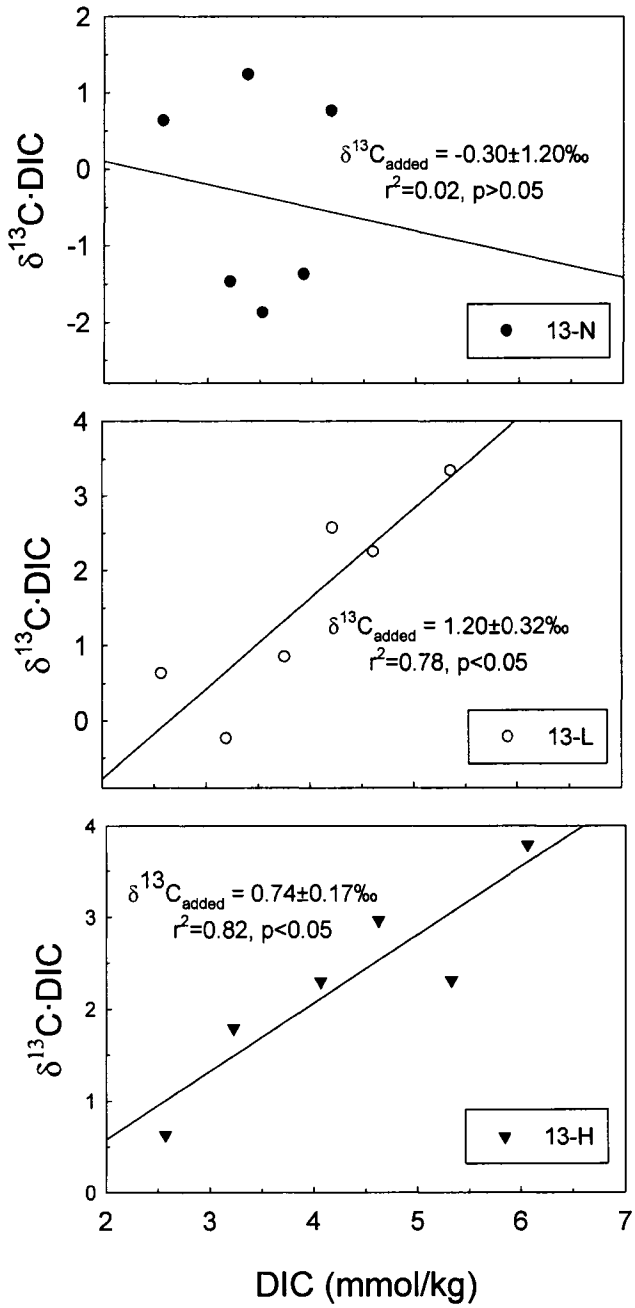

Fig. 26. Regression of $\delta^{13}C{\cdot}DIC$ vs. DIC in the WS-13 incubations. In the 13-N incubation, the regression slope was not significant (see Table 14).

One unit of CO_2 production should yield approximately the same amount of carbonate dissolution under aerobic conditions (ignoring the minor dissolution caused by nitric and phosphoric acid productions, see rxns. 24-25). Therefore $\delta^{13}C_{added}$ can be

Table 14. Values of $\delta^{13}C_{added}$ for the WS-3 and WS-13 incubations.

	3-N	3-L & 3-H	13-N	13-L	13-H
$\delta^{13}C_{added}$ [a]	2.73±0.47	1.25±0.18	-0.3±1.2	1.20±0.32	0.74±0.17
r^2	0.83	0.77	0.02	0.78	0.82
P	<0.001	<0.0001	>0.05	<0.05	<0.05
$\delta^{13}C_{OM}$ [b]	-1.70±0.36	-2.00±0.71	-2.42±1.80	-1.53±0.64	-2.45±0.34
	(a)	(o)	(a)	(o)	(o)

[a] Uncertainties were standard errors obtained from the linear regressions (Figs. 25-26).

[b] $\delta^{13}C_{OM}$ values were calculated using the 1:1 (oxic incubation, (o)) and 2:1 (anoxic incubations (a)) mixing ratios between organic carbonate and carbonate carbon, assuming no other processes contribute to the DIC $\delta^{13}C$ changes.

described using the following equation:

$$\delta^{13}C_{added} = f_C\delta^{13}C_C + f_{OM}\delta^{13}C_{OM} \quad (28)$$

where the f values are DIC contributions from carbonate dissolution and organic matter oxidation, and $f_C = f_{OM} = 50\%$. In the case of the anoxic incubation, if assume that H_2S produced by sulfate reduction can contribute 1 proton towards carbonate dissolution, therefore $f_{OM} \approx 0.67$ and $f_C \approx 0.33$ (eqn. 29)

$$SO_4^{2-} + 2CH_2O + CaCO_3 \rightarrow Ca^{2+} + HS^- + 3HCO_3^- \quad (29)$$

If I assume no other processes affect the DIC isotopic composition, using the calculated $\delta^{13}C_{added}$ values (Table 14) and the measured values of $\delta^{13}C_C$ in WS-3 and WS-13 sediments (Table 11) I can then use eqns. (28) and (29) to back-calculate $\delta^{13}C_{OM}$. These results are also shown in Table 14. It is clear that the simple mixing model is inadequate to explain pore water DIC ^{13}C enrichment since the calculated $\delta^{13}C_{OM}$ values were all greater than the $\delta^{13}C$ values of seagrasses at the respective sites, and any other types of natural organic carbon in these environments or the adjacent ocean (Hofmann et al., 2000; Rasmussen et al., 1990).

To explain similar enrichments of ^{13}C in the pore water DIC of LSI sediments, I must invoke a closed-system model based on a carbonate dissolution and reprecipitation mechanism (Fig. 27, and Chapter II). In the following discussion, this model is applied to the data from these incubations.

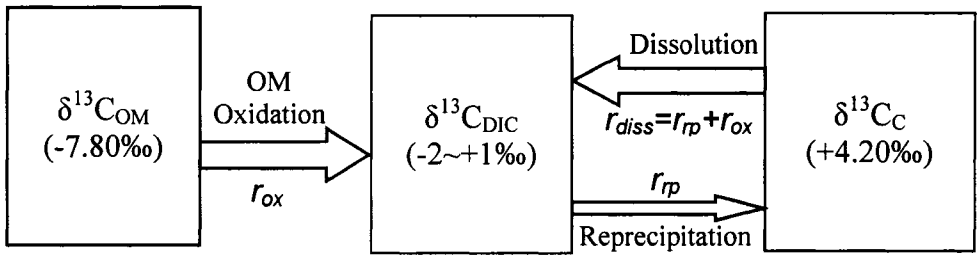

Fig. 27. Carbonate dissolution/reprecipitation model. The dissolution rate (r_{diss}) shown here represents the "gross" dissolution rate equal to the sum of the metabolic dissolution rate (driven by CO_2 release) and the reprecipitation rate ($r_{ox} + r_{rp}$), see Chapter II for details.

In the dissolution/reprecipitation model, several assumptions are explicitly made: (1) no isotope fractionation occurs during carbonate dissolution (Martin et al., 2000), since carbonate dissolution involves either partial or complete destruction of the dissolving carbonate phase; (2) reprecipitation of the secondary carbonate occurs under equilibrium conditions (Patterson and Walter, 1994), and the isotopic fractionation during reprecipitation is taken to be $\varepsilon_{calcite\text{-}HCO3^-} = 0.9‰$ (Rubinson, 1969); (3) diffusion processes that causes isotope gradients on the mineral surface are negligible, i.e., the pore waters are isotopically homogeneous so that the secondary carbonate produced at any given time has the same isotopic composition throughout the incubations vial.

No TDS was observed in incubations 3-L, 3-H, and 13-H, therefore aerobic respiration was the only remineralization process. Although the 13-L incubation had low level of TDS (<0.05 mmol/kg), when compared to the magnitude of DIC production in this incubation (up to 4 mmol/kg), sulfate reduction is thus negligible. Therefore in the following discussion, I will also treat 13-L as an aerobic incubation. Carbonate dissolution and reprecipitation in the model equations can be expressed as:

$$\frac{d[^{13}C]}{dt} = r_{diss} \times F_C + r_{ox} \times F_{OM} - r_{rp} \times F_{rp} \tag{30}$$

$$\frac{d[^{12}C]}{dt} = r_{diss} \times (1 - F_C) + r_{ox} \times (1 - F_{OM}) - r_{rp} \times (1 - F_{rp}) \tag{31}$$

$$R_{rp} = \alpha \times R_{pw} \tag{32}$$

where r is the rate of a reaction; subscripts *diss*, *ox*, and *rp* represent gross dissolution, organic matter oxidation and reprecipitation; and F is the isotopic abundance of the reactants - carbonate (*C*), organic carbon (*OM*) and the secondary carbonate (*rp*). Based on the discussion in Chapter II, the "net" dissolution rate (r_{diss}') equals r_{ox} (Table 15), and therefore

$$r_{ox} = r_{diss} - r_{rp} \tag{33}$$

Based on rxn. (25), r_{ox} can be calculated through the regression of DIC versus incubation time:

$$r_{ox} = r_{diss}' = \frac{1}{2}\frac{d[DIC]}{dt} \tag{34}$$

Note that carbonate dissolution rates calculated using alkalinity production rates agreed well with DIC-derived rates (Table 10).

In the two anoxic incubations, the linear regression of $\Delta[Ca^{2+}]$ vs. time yielded a slope of -2±1 μmol/kg/h (P>0.0.5) in the 3-N incubation, and 8±4 μmol/kg/h (P>0.05) in the 13-N incubation (Table 10). This suggests that net carbonate dissolution was negligible in these anoxic incubations. Thus, when compared with the model used for the oxic incubations, here net dissolution (r_{diss}') is equal to 0 and any carbonate dissolution must be exactly balanced by reprecipitation ($r_{diss} = r_{rp}$). Eqns. (30)-(31) become:

Table 15. Reaction rates and secondary carbonate compositions in WS-3 and WS-13 experiments [a].

Rate (μmol/kg/h)	3-N	3-L & 3-H	13-N	13-L	13-H
r_{ox}	14±2	16±1	25±5	24±1	31±1
r_{diss}'	0	16±1	0	24±1	31±1
r_{rp}	32±5	33±6	39±47	32±23	28±14
R_{rx} [b]	-	2.1±0.5	-	1.4±0.6	0.9±0.5
x [c]	0.93±0.31	0.92±0.42	0.61±1.94	1.06±1.02	0.82±0.99

[a] Uncertainties are standard errors from either linear regressions (r_{ox}) or model calculations (r_{rp}, R_{rx}, and x).

[b] x is the calculated Ca content in the secondary carbonate phase.

[c] R_{rx} is the rate ratio of carbonate reprecipitation and net dissolution (r_{rp}/r_{diss}').

$$\frac{d[^{13}C]}{dt} = r_{rp} \times F_C + r_{ox} \times F_{OM} - r_{rp} \times F_{rp} \quad (35)$$

$$\frac{d[^{12}C]}{dt} = r_{rp} \times (1 - F_C) + r_{ox} \times (1 - F_{OM}) - r_{rp} \times (1 - F_{rp}) \quad (36)$$

and r_{ox} is:

$$r_{ox} = \frac{d[DIC]}{dt} \quad (37)$$

Both the oxic model (eqns. 30-34) and the anoxic model (eqns. 35-37) were solved using the 4th order Runge-Kutta method in the program Stella®.

The data for each incubation were fit to the model by taking r_{ox} and r_{diss}' values in Table 15 and adjusting the r_{rp} value to obtain the calculated $\delta^{13}C_{added}$ values for that incubation. The resulting r_{rp} values are also shown in Table 15. The co-evolution of pore water DIC concentration and its $\delta^{13}C$ in all incubations is shown in Figs. 28 and 29.

In Figs. 28 and 29, it can be seen that the carbonate dissolution/reprecipitation model generally reproduces the co-evolution of the pore water DIC $\delta^{13}C$ and concentration in these incubations, and this modeling exercise further indicates that such model can be used in the interpretation of ^{13}C enrichment in the carbonate sediment pore waters.

The average composition of the HMC in WS-3 and WS-13 sediments determined through XRD was $Ca_{0.88}Mg_{0.12}CO_3$ (Table 7). If I assume this HMC is the dissolving phase, the model results for the incubations with these sediments are further examined in the following discussion.

4.3. The Composition of the Secondary Carbonate Phase

4.3.1. Oxic Incubation

Here, the gross dissolution rate (r_{diss}) can be calculated with eqn. (33) based on the calculated value of r_{rp} and r_{ox} in Table 15. If I assume that the reprecipitated carbonate has the composition of $Ca_xMg_{(1-x)}CO_3$, then the dissolution and reprecipitation processes can be written as follows:

$$Ca_{0.88}Mg_{0.12}CO_3 + CO_2 + H_2O \xrightarrow{r_{diss}} 0.88Ca^{2+} + 0.12Mg^{2+} + 2HCO_3^- \quad (38)$$

$$xCa^{2+} + (1-x)Mg^{2+} + 2HCO_3^- \xrightarrow{r_{rp}} Ca_xMg_{(1-x)}CO_3 + H_2O + CO_2 \quad (39)$$

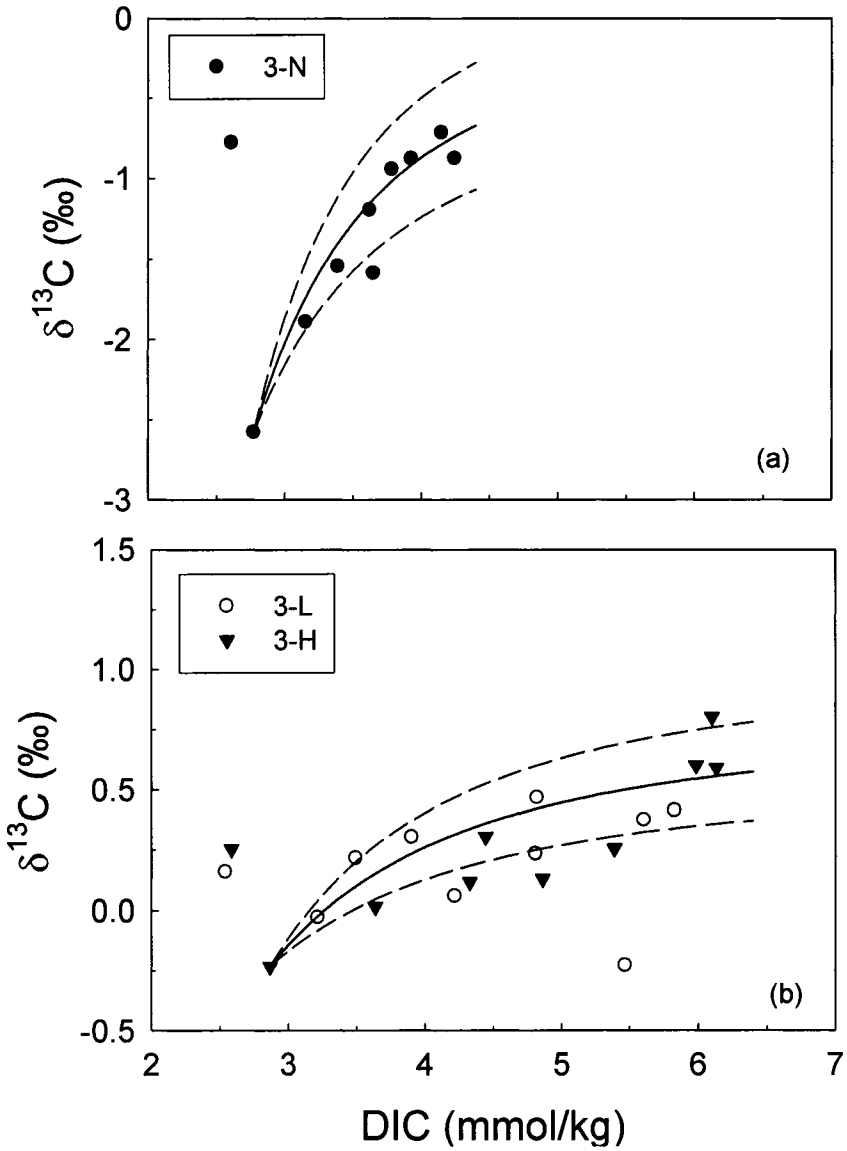

Fig. 28. Results of the carbonate dissolution/reprecipitation model applied to the WS-3 incubations. The solid lines represent model results obtained with an r_{rp} value that predicts the regressed values of $\delta^{13}C_{added}$ from Fig. 25. The dashed lines are model results based on the upper and lower uncertainties (95% confidence interval) of $\delta^{13}C_{added}$.

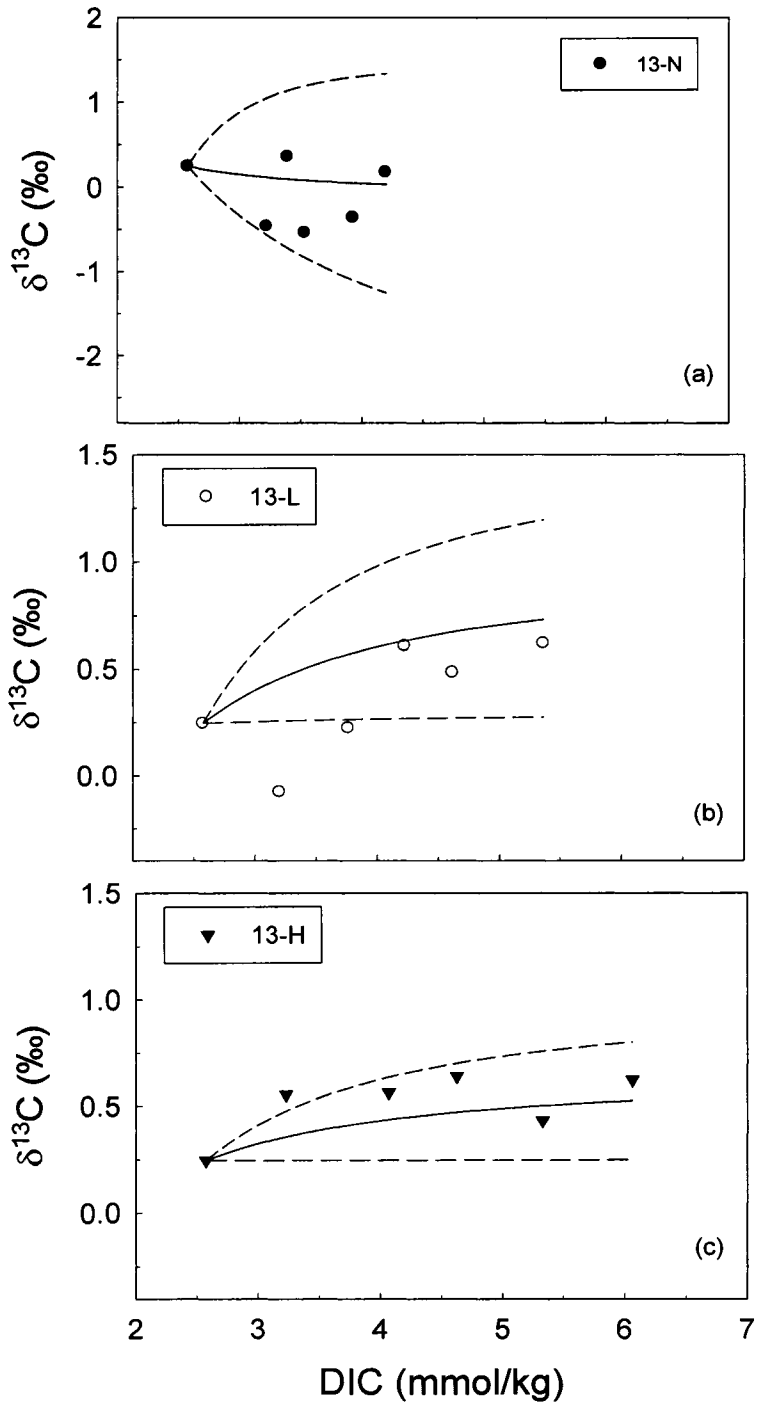

Fig. 29. Results of the carbonate dissolution/reprecipitation model applied to the WS-13 incubations. The solid lines represent model results obtained with an r_{rp} value that predicts the regressed value of $\delta^{13}C_{added}$ from Fig. 26. The dashed lines are the model results based on the upper and lower uncertainties (95% confidence interval) of $\delta^{13}C_{added}$.

Furthermore the concentration changes for Ca^{2+} and alkalinity are given by:

$$d[Ca^{2+}] = r_{diss} \times 0.88 - r_{rp} \times x \quad (40)$$

$$dAlk = 2r_{diss} - 2r_{rp} \quad (41)$$

and the linear regression of $\Delta[Ca^{2+}]$ versus ΔAlk will have slope equal to:

$$\frac{d\Delta[Ca^{2+}]}{d\Delta Alk} = \frac{r_{diss} \times 0.88 - r_{rp} \times x}{2(r_{diss} - r_{rp})} \quad (42)$$

From eqn. (42), I can then solve for x, the Ca content of the secondary carbonate phase, since all other parameters are known in this equation (Table 15).

4.3.2. Anoxic Incubation

As has been discussed in section 4.1, there was minimal net carbonate dissolution in the incubations; therefore any changes in Ca^{2+} presumably came from carbonate dissolution/reprecipitation. If I again assume that $Ca_{0.88}Mg_{0.12}CO_3$ is the dissolving phase, then from the rate of $[Ca^{2+}]$ change, I can calculate the composition of the reprecipitated carbonate ($Ca_xMg_{(1-x)}CO_3$) in these experiments in conjunction with eqns. (38)-(39):

$$\frac{dCa^{2+}}{dt} = r_{diss} \times 0.88 - r_{rp} \times x \quad (42)$$

Again re-arranging this equation allows me to solve for x. However, the linear regressions of $[Ca^{2+}]$ vs. time were not significant for both the 3-N or 13-N incubations. Therefore some caution must be taken in interpreting the values of *x* calculated here.

4.3.3. The Reprecipitating Carbonate Composition - Results

For the WS-3 incubations, these calculations imply that the carbonate phase which reprecipitates has the composition $Ca_{0.92}Mg_{0.08}CO_3$ (Table 15). This agrees with the composition of HMC overgrowths (~8 mole% Mg) which formed on the surface of Iceland spar (crystallized calcite mineral) buried in Bahamian sediments (Morse and Mucci, 1984; Mucci and Morse, 1983). However, the propagated errors through my calculations were on the order of ~30-40% for the calculated Ca content. Therefore the apparent agreement between the calculated composition of the secondary carbonate phase in the WS-3 sediments and these literature results may be fortuitous. Similarly, for the

WS-13 incubations, the calculated Ca contents of the reprecipitating phase have even large errors, particularly for 13-N, but an average x value for the 13-L and 13-H incubations is 0.94±0.72. Again these results qualitatively agree with the literature results despite of their large errors.

Although some caution must be taken in the interpretation of these calculations, when these results are looked in the context of the discussion in section 4.1, it appears likely that reprecipitation in these sediments produces a new carbonate phase with only a slightly lower Mg content than the starting materials. Therefore these results agree with the studies by Bischoff et al. (1987) and Hover et al. (2001) that HMC diagenesis may lead to reprecipitation of a carbonate phase with similar or slightly lower Mg content, as a result of "Ostwald ripening", in which smaller carbonate grains dissolve at the expense of secondary carbonates that form on the surface of larger grains. Furthermore, little elemental and isotopic composition changes are expected for the solid phase in these incubated sediments, given the short experimental duration and large solid/aqueous ratios. Therefore to observe such changes in the solid phase, incubation times that are relatively longer than those used in this study are necessary (such as the long term burial study by Patterson and Walter, 1994).

4.4. Reaction Rates - Further Considerations

Seagrass materials appeared to be the dominant organic carbon source for microbial respiration in these oligotrophic sediments, and fresh seagrass litter is generally considered to be "labile" (Boschker et al., 2000; Holmer et al., 2001; Jones et al., 2003), Therefore it appears that there was no difference in the rates of aerobic versus anaerobic organic matter remineralization during these short term incubations (Table 15). This observation is consistent with previous findings in the literature regarding organic carbon remineralization rates under different redox conditions (see Burdige, 2006, for a review).

When examining the ratio of carbonate reprecipitation and net carbonate dissolution rates (R_{rx}) in WS-3 and WS-13 incubations, I observed that the values ranged from 0.9-2.1. Given all the assumptions made here and in Chapter II, this range appears to be very similar to other values in the literature (e.g., 1.1-2.0 in Walter et al., 1993; 3.1-6.6 in Rude and Aller, 1990), even though both of these earlier studies used distinctively

different approaches than I used (^{45}Ca and trace elemental [F, Sr] combined numerical modeling approaches). It is noted, however, that care needs to be taken when comparing the results from incubation and field studies. Nonetheless, the agreement among all of these studies appears encouraging, and a combination of both methods therefore may be potentially useful in the future to address the dissolving and reprecipitating carbonate phase problems.

From this study I have further confirmed the validity of the carbonate dissolution/ reprecipitation model developed in Chapter II to help interpret pore water data from Lee Stocking Island sediments. These observations further reinforce the fact that carbonate dissolution/reprecipitation may be an important process in carbonate diagenesis. It is likely that carbonate reprecipitation may have also caused the pore water DIC $\delta^{13}C$ enrichment in other shallow water sediments (for example, Eldridge and Morse, 2000; McNichol et al., 1991). Furthermore, I predict that pore water DIC $\delta^{13}C$ should also exhibit enrichment in deep sea sediments where carbonate reprecipitation may occur (Broecker and Clark, 2003; Jahnke and Jahnke, 2004).

4.5. Role of O_2 Input on Carbonate Dissolution

One goal of this study was to use these results to examine the stoichiometric relationship between the rates of O_2 consumption and net carbonate dissolution. Both alkalinity and Ca^{2+} production rates can be used to calculate the net carbonate dissolution rate. Here pore water calcium production rates for all incubations were used in this analysis. To convert these rates to carbonate dissolution rates, two end member approaches were taken, based on assumptions regarding the Ca content of the phase undergoing dissolution: (1) a minimum Ca value was obtained by assuming that the Ca content of the HMC could be obtained from pore water $\Delta[Ca^{2+}]/\Delta[Alk_C]$ (Table 13, see section 4.1), (2) a maximum value was obtained by assuming that the HMC undergoing dissolution has a Ca content based on XRD results (100% minus mole% Mg in HMC, Table 7). Carbonate dissolution rates were then calculated using $[Ca^{2+}]$ production rates and corrected using these two conversion factors. Average values of the dissolution rate for each incubation are plotted versus O_2 consumption rate (Fig. 30). For the incubations

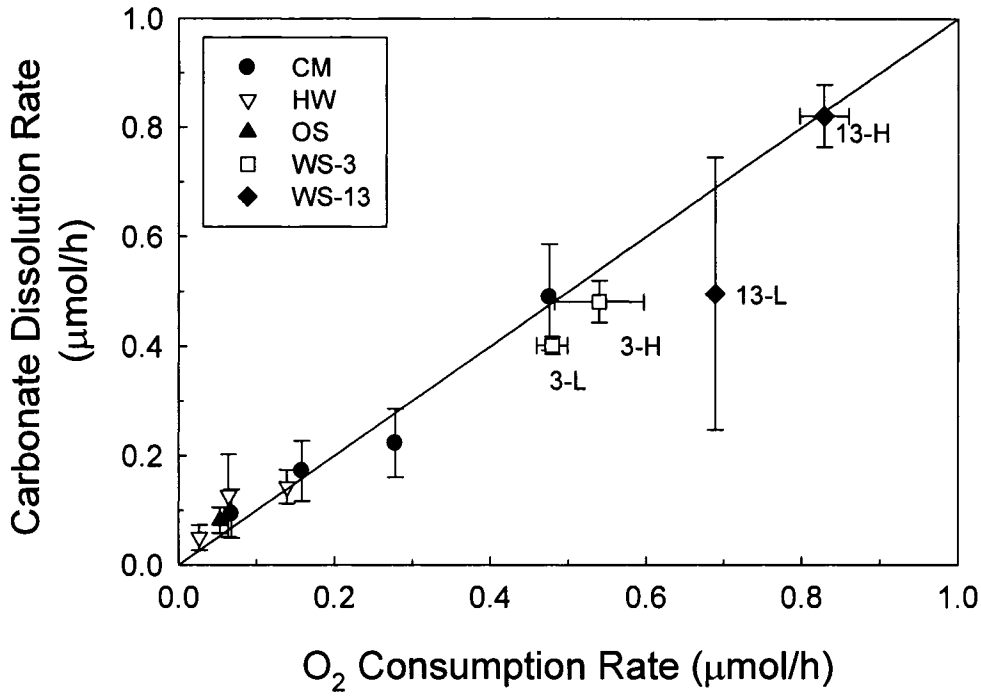

Fig. 30. Carbonate dissolution rate vs. oxygen consumption rate. The carbonate dissolution rates are average values based on two end-members for the Ca concentration of the dissolving carbonate phase (see section 4.5 for details). The solid line represents the 1:1 line between the carbonate dissolution and oxygen consumption rates. In all incubations except 3-L, 3-H, and 13-H, O_2 consumption rates equaled O_2 delivery rates from the gas diffusion tube (see Table 8 and Fig. 20). In these three incubations O_2 consumption was estimated as discussed in the text. Uncertainties were standard errors.

with no dissolved O_2 observed in the pore waters, O_2 consumption rates equaled the O_2 delivery rates through the diffusion tubes.

In all incubations except for the 3-L, 3-H, and 13-H incubations (Fig. 30), there was a 1:1 relationship between O_2 consumption and carbonate dissolution rates. In these three incubations, O_2 consumption rates based on the O_2 delivery rates from the diffusion tubes (4.0, 6.7, 4.6 μmol/h) initially appeared to be much greater than the carbonate dissolution rates (0.4, 0.4, 0.9 μmol/h). Taken at face value, this apparent high O_2 consumption would seem to suggest an uncoupling of aerobic respiration and carbonate dissolution (rxn. 15-17), i.e., when aerobic respiration is sufficiently fast, carbonate dissolution becomes the rate-limiting step. However, if this were the case, I would expect to see the

uncoupling of alkalinity and DIC production, with DIC production greatly exceeding that of alkalinity. In contrast though the results in Fig. 20 show that this uncoupling was not observed, and the production rates of alkalinity and DIC in the 3-L, 3-H, and 13-H incubations were equal to one other. Therefore the O_2 input rates for these three incubations probably were likely overestimated based on the calibration curve determined in section 2.3. The soft nature of the C-Flex tubing (as opposed to the rigid Teflon tubing used in all other incubations) may have contributed to this overestimation, since the tubing may have been pinched during experimental setup. Therefore the gas pressure on the regulator may not have represented the true gas pressure in the sealed tubing. Thus for these incubations O_2 consumption rates were calculated as one half of the DIC production rate (eqn. 34). Furthermore, it also appears that the O_2 input in these three incubations "saturated" the sedimentary microbial respiration in these incubations where dissolved oxygen was detected (Fig. 15). Metabolic CO_2 production thus is the actual rate-limiting step in the dissolution process, consistent with other results from the literature where it has been observed that carbonate dissolution rates are faster than organic carbon oxidation rates in marine sediments (Martin et al., 2000; Martin and Sayles, 2003).

In coastal sediments, O_2 penetration depth is controlled by the organic matter input rate as well as microbial activity, and the value is usually on the order of several millimeters, if bioturbation is absent (Cai and Sayles, 1996). The root and rhizome of the seagrasses in Bahamian sediments, however, penetrate up to ~20 cm into the sediments, and therefore O_2 supply from the plant tissues will be much deeper than that from physical processes alone (diffusion and advection). Bodensteiner (2006) suggested that below ground O_2 flux for *T. testudinum* under light-saturated condition is 1.2 mmol/m^2-leaf/h in this environment. If I assume that the daily average photosynthetic time is 9 hours (Burdige et al., submitted) and the leaf area index (LAI) is 1 m^2-leaf/m^2-sediments, then the total O_2 input would be ~10.8 mmol/m^2/d. This O_2 input rate is significantly higher than the diffusion controlled O_2 input rates in the sediments I have studied (Chapter IV; Burdige et al., submitted; Burdige and Zimmerman, 2002). Besides, it is likely that production of metabolic acid (CO_2) at depth may have more reaction time with the carbonate sediments and therefore is much less affected by bottom water-pore water exchange that commonly affects metabolic dissolution efficiency (MDE) in carbonate

sediments (note MDE is defined by the ratio of dissolving carbonate flux and the metabolic acid production flux across the sediments-water interface; Jahnke and Jahnke, 2004). Further study of mass transport mechanisms at the sediment-water interface of these carbonate sediments is necessary to quantitatively examine the dissolution rates.

5. CONCLUSIONS

Using closed-system incubations, I have further confirmed that HMC with a solubility similar to or higher than that of aragonite is preferentially dissolved in carbonate sediments on the Bahamas Bank as a result of sedimentary microbial respiration.

The carbonate dissolution/reprecipitation model proposed in Chapter II was applied to the results from these closed-system incubations to explain the apparent enrichment of ^{13}C in the pore water DIC pool, and the results from this modeling exercise suggest that carbonate reprecipitation occurs over the relatively short time scales of these experiments. Thus pore waters represent a sensitive sedimentary diagenetic indicator that can be used in addition to other geochemical techniques (such as XRD) to study carbonate diagenesis in recently deposited sediments. The ratio of carbonate reprecipitation/dissolution (i.e., R_{rx}, 0.9-2.1) calculated here agrees well with literature reported values (Chapter II; Walter et al., 1993; Rude and Aller, 1990), despite the fact that this study employed a different approach than used previously.

The composition of the reprecipitated carbonate in WS-3 and WS-13 sediments was calculated using a combination of the pore water data and the results from the carbonate dissolution/reprecipitation model. Although the results were equivocal, they suggest that the reprecipitated carbonate in these experiments may have a Mg content that is similar to or slightly lower than that of the dissolving carbonate phase, which resembles "Ostwald ripening" that widely occurs in the carbonate sediments.

Finally, carbonate dissolution and O_2 consumption showed a robust 1:1 linear relationship over a wide range of reaction rates. This observation suggests that microbial metabolic activity that produces CO_2 controls the rate of carbonate dissolution, consistent with literature reported results that organic carbon oxidation is the rate limiting step in metabolic carbonate dissolution.

CHAPTER IV
CARBONATE SEDIMENT DISSOLUTION AND REPRECIPITATION IN BAHAMAS BANK SEDIMENTS - A BANK SCALE SYNOPSIS

1. INTRODUCTION

Shallow marine environments, including coral reefs, carbonate banks/bays, and continental shelves that are largely located in tropical and subtropical areas, cover only 8% of the area of the modern ocean, yet they account for ~40% of the global oceanic carbonate production and accumulation (Milliman, 1993). Because these environments are located well above the lysoclines of the common carbonate minerals formed in the oceanic environment, little attention has historically been paid to the dissolution of these carbonate sediments (e.g., Berner, 1966).

Recent studies have, however, shown that carbonate dissolution may occur in carbonate banks sediments as a result of microbial respiration, despite the occurrence of net carbonate accumulation in these environments (Chapter II; Broecker and Takahashi, 1966; Burdige et al., submitted; Burdige and Zimmerman, 2002; Halley and Yates, 2004; Ku et al., 1999; Morse et al., 2006; Morse et al., 1985; Sabine and Mackenzie, 1995; Walter et al., 1993; Walter and Burton, 1990; Yates and Halley, 2006). This dissolution is caused by production of metabolic CO_2 through aerobic respiration, which first drives down the pore water saturation state, and once the pore waters are sufficiently undersaturated with respect to the most soluble carbonate phase, carbonate dissolution can occur (Chapter II; Burdige and Zimmerman, 2002; Ku et al., 1999; Morse et al., 1985; Walter and Burton, 1990). Assuming that the organic carbon being remineralized can be expressed as CH_2O, then the reactions can be written as:

$$CH_2O + O_2 \rightarrow CO_2 + H_2O \quad (44)$$

$$CO_2 + CaCO_3 + H_2O \rightarrow Ca^{2+} + 2HCO_3^- \quad (45)$$

$$CH_2O + O_2 + CaCO_3 \rightarrow Ca^{2+} + 2HCO_3^- \quad (46)$$

Interest in shallow water carbonate sediment dissolution stems from the suggestion that this dissolution may be able to compensate for the anthropogenic CO_2 increase in the atmosphere by neutralizing this CO_2 (Andersson and Mackenzie, 2004; Andersson et al., 2003; Droxler et al., 1986; Halley and Yates, 2004; Morse et al., 2006; Sabine and Mackenzie, 1995; Yates and Halley, 2006). Therefore a thorough knowledge of carbonate dissolution in shallow water carbonate depositional environments enhances our understanding of the role that this process may play in the global carbon cycle.

At the same time, carbonate budgets for such shallow water environments are poorly constrained. According to the landmark review by Milliman (1993), ~50% total carbonate production is lost through export to surrounding environments or dissolution, although this estimate is poorly constrained (also see Walter and Burton, 1990). Furthermore, recent studies in both Bahamas Bank and Florida Bays sediments suggested that carbonate dissolution alone may be sufficient to account for the magnitude of carbonate loss from the banks and bays (Burdige et al., submitted; Yates and Halley, 2006). These studies, however, were focused on relatively restricted environments. Therefore, a study that covers a greater expanse of the Bahamas Bank is desirable to further examine this problem.

Seagrasses, a group of aquatic angiosperms, are widely distributed in many shallow marine environments. Current estimates indicate that seagrasses cover up to ~10% of the coastal ocean (0.15% of the ocean as a whole) with very high net productivity (average ~10^3 g DW /m^2/yr), as compared to the average phytoplankton productivity of 128 g DW /m^2/yr in the global ocean (Duarte and Chiscano, 1999). Overall then, seagrasses account for ~1% of total marine net primary production (Hemminga and Duarte, 2000). The dominant seagrass on the Bahamas Bank, *Thalassia testudinum*, can have biomass and net productivity of 1.1 kg DW/m^2 and 2.5 kg DW/m^2/yr. Seagrass-derived organic carbon stored in the sediments is estimated to be ~15% of the total carbon stored in the marine environment (Hemminga and Duarte, 2000). Moreover, seagrasses enhance organic carbon input into the sediments of many otherwise oligotrophic areas through their own production. At the same time, the "baffling effect" of the seagrass canopy slows water motion and thereby enhances the deposition of fine-grained materials including

particulate organic matter (POM) from the water column to the sediments (Koch and Gust, 1999; Koch et al., 2006).

In many temperate sediments, seagrasses transport photosynthetic O_2 below ground to maintain low sulfide levels (Pedersen et al., 1998). In more oligotrophic sediments settings this below-ground O_2 transport by seagrasses can potentially enhance remineralization of sedimentary organic matter. Although an earlier study by Morse et al. (1987) suggested that there was no linkage between sediment chemistry and the presence of seagrass in coarse grained Bahamian sediments, later studies (Burdige and Zimmerman, 2002; Ku et al., 1999; Walter and Burton, 1990) suggested that seagrasses not only enhance carbonate dissolution but may close sediment carbonate dissolution budget (see Chapter I for details).

More detailed studies have followed up this work (Chapters II and III; and Burdige et al., submitted), and this chapter discusses this problem on a much larger geographic scale, based on a 2004 cruise to the Great Bahamas Bank on board the R/V *F. G. Walton Smith* (WS). The sites examined on this cruise had a range of seagrass densities as well as different sediment types (i.e., fine-grained aragonite muds or coarse-grained carbonate sands or grapestones).

In Chapters II and III, pore water DIC was found to be enriched in ^{13}C in densely seagrass vegetated sediments both in field studies and in incubation experiments, and the 1:1 mixing between DIC derived from organic carbon oxidation and carbonate dissolution could not solely explain this enrichment. Rather, a carbonate dissolution/ reprecipitation model was invoked to explain both the field observations (Chapter II) and the results of closed-system incubation studies (Chapter III). In this chapter I will first use pore water DIC $\delta^{13}C$ data to further examine the occurrence of carbonate dissolution and reprecipitation across the greater expanse of the Bahamas Bank.

Next, this approach will be coupled with an inverse advection-diffusion-reaction model (Burdige et al., submitted) applied to the complete data set, to calculate the rates of carbonate dissolution and reprecipitation, as well as sediment O_2 input. Together, these results will be used to explore the factors that control carbonate reprecipitation in these sediments.

2. MATERIALS AND METHODS

2.1. Study Sites

The study was carried out in March, 2004 using R/V *F. G. Walton Smith* as the sampling platform. A number of sites (Fig. 31) with various seagrasses densities and sediment types were sampled across the Bahamas Bank. The dominant seagrass species were *Thalassia testudinum* and *Syringodium filiforme*, with the latter observed to be significant only at sites WS-1 (WS-25) and WS-3 (Bodensteiner, 2006). Water depths at these sites ranged from 4 to 10 m with the average depth of ~6 m. Visual inspection of the sediments showed that the sediment types ranged from very fine-grained carbonate muds on the west side of Andros Island, to coarse-grained oolitic carbonate sand and grapestone in the northern part of the Bank and on the eastern arm of the Bank along the Exuma Cays (Neuweiler, per. comm., Table 16).

2.2. Sample Collection and Analytical Methods

Pore water samples were collected *in situ* using sediment sippers, and sampling techniques and sample processing are described in detail elsewhere (Chapters II and III; Burdige and Zimmerman, 2002). A bottom water sample and three sets of pore water profiles were collected at each site, the latter from sediment depths of 1, 2, 4, 5, 8, 10, 15, and 20 cm. After pore waters were collected and returned to the ship, the water samples were equilibrated at lab temperature for 30 min, and O_2 concentrations were measured using an optode (FOXY-18G, Ocean Optics®) connected to a SF2000 spectrophotometer (Ocean Optics). For this analysis, a pore water sample was overfilled into a N_2 flushed 1.8 ml serum vial containing a stir bar, and the vial was sealed using an open-faced cap and a Teflon-lined silicone septum. The septum was then pierced by the optode, and the O_2 concentration was determined after 1 minute (Ocean Optics Tech Notes). The optode was calibrated every 0.5 hr at lab temperature in both N_2-bubbled and air-saturated surface seawater with known salinity using a standard, linear (Stern-Volmer) two-point calibration (Wang et al., 1999). The remaining samples were filtered using 0.45 μm nylon disc filters and then preserved in appropriate storage vessels at 4°C for further analyses (Chapter II).

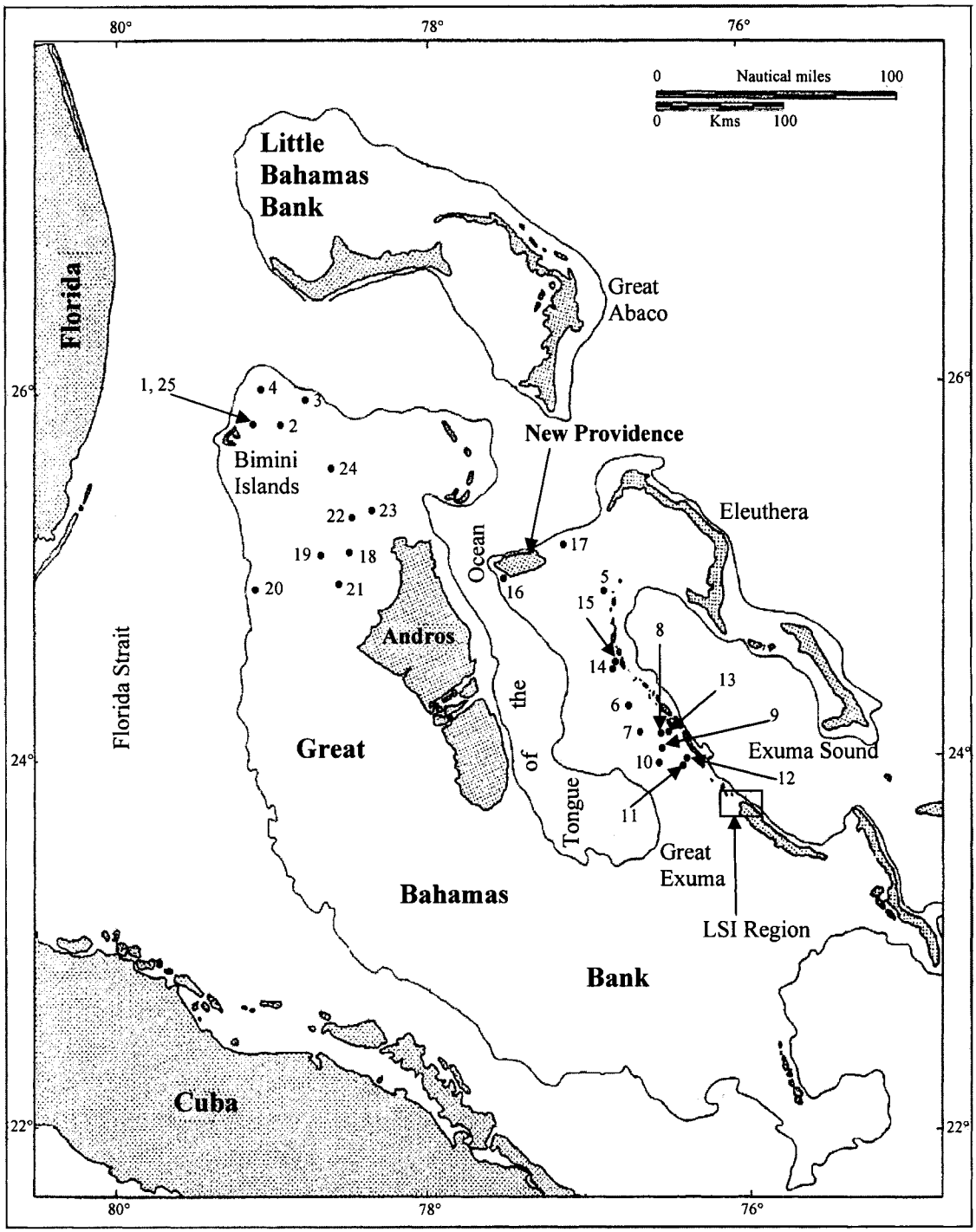

Fig. 31. Map of the sampling sites on the Bahamas Bank (Bathurst, 1971). Numbers in the figure are site designations as shown in Table 16.

Table 16. Sampling sites and their descriptions.

Site ID	Location	Water Depth (m)	Description	Seagrass LAI (m^2/m^2)
WS-1	25°48.236'N, 79°6.776'W	5.2	Ooid sand	3.73±0.40
WS-2	25°47.536'N, 78°55.595'W	6.0	Ooid sand	0.96±0.04
WS-3	25°51.050'N, 78°43.899'W	10.5	Pellet mud	1.37±0.08
WS-4	25°58.650'N, 79°4.391'W	9.5	Coarse ooids	1.72±0.06
WS-5	24°48.680'N, 76°50.016'W	5.6	Grapestone/ooid	0.03±0.02
WS-6	24°21.440'N, 76°46.304'W	7.9	Grapestone/ ooid	0
WS-7*	24°14.083'N, 76°43.953'W	5.3	-	0
WS-8	24°13.875'N, 76°31.233'W	5.0	Grapestone/cryptocrystal-line mud	0.19±0.03
WS-9	24°7.293' N, 76°32.341'W	5.2	Pellet grapestone sand	0
WS-10	23°5.340' N, 76°32.724'W	5.7	Pellet grapestone sand	0.02±0.00
WS-11	23°56.239'N, 76°23.829'W	5.6	Pellet grapestone/fine grain sand	0.07±0.01
WS-12	23°56.366'N, 76°23.756'W	5.3	Pellet mud	1.40±0.05
WS-13	24°14.033'N, 76°30.200'W	4.2	Ooid sand	0.53±0.04
WS-14	24°34.909'N, 76°49.812'W	5.5	Ooid sand	0.41±0.02
WS-15	24°35.077'N, 76°48.982'W	3.7	Pellet sand/ooid/grapestone	0.86±0.04
WS-16	24°59.298'N, 77°29.928'W	5.6	Coarse sand	0
WS-17	25°4.336' N, 77°4.335' W	7.5	Ooid sand	0.33±0.01
WS-18	25°7.033' N, 78°28.423'W	4.9	Pellet mud	0.17±0.01
WS-19*	25°3.090' N, 78°42.324'W	5.6	Pellet mud	0
WS-20	24°55.923'N, 79°4.462' W	6.7	Ooid/grapestone	0.77±0.04
WS-21	24°56.624'N, 78°30.540'W	5.4	Pellet mud	0.07±0.01
WS-22	25°21.340'N, 78°30.003'W	4.8	No sediments collected	0.64±0.07
WS-24	25°36.030'N, 78°36.956'W	6.2	Ooid/grapestone	0.25±0.02
WS-25#	25°48.410'N, 79°6.814' W	5.4	Ooid sand	3.73±0.40

* No pore water samples were collected at sites WS-7 and WS-19.

WS-25 is the same "site" as WS-1; differences in the coordinates simply indicate differences in where the ship was anchored at the time of sampling.

Titration alkalinity (Alk_T) was determined on board the ship by automated Gran titration using Scripps Reference Seawater as an external standard (Dickson et al., 2003). pH (NBS) and sulfide (Cline, 1969) were also analyzed on board the ship. Alk_T and pH were also analyzed in all three sets of pore water samples from each site, while sulfide was measured in one set. DIC was analyzed with a UIC 5011 coulometer (DOE, 1994) back at ODU using Scripps Reference Seawater as the reference material. $\delta^{13}C$ of the pore water DIC was also determined back at ODU following the procedure described in Chapter II, using a PDZ Europa® GEO 20-20 isotopic ratio mass spectrometer (IRMS).

Pore water samples (0.1 ml) were analyzed for Ca^{2+} concentration by automated titration using EGTA as the titrant and a Thermo-Orion Calcium ion selective electrode (ISE) to detect the end-point. Chlorinity (pore water chloride concentration) was

determined by automated titration using $AgNO_3$ as the titrant and a Brinkman Ag Titrode™ to detect the end-point. All titrations were performed using a Metrohm® automatic titrator. Sulfate was analyzed on a Dionex ion chromatography (IC). IAPSO standard seawater (salinity 34.996) was used to standardize both titrants (EGTA and $AgNO_3$) as well as to construct the sulfate standard curve (Grasshoff et al., 1999).

Seagrasses, benthic macro algae, and sediment samples were collected by divers at selected sites. Epiphytes were first removed from seagrass and algae samples, which were then soaked in 1N HCl for 30 minutes to remove attached or skeletal carbonate. The residual plant materials were rinsed with distilled water to remove excess acid, oven dried at 60°C overnight, and then ground into powders using mortar and pestle (Chapter II; Craig, 1953; McMillan, 1980). High temperature combustion (HTC) in O_2 was used to convert organic carbon to CO_2 using an automated nitrogen carbon (ANCA) elemental analyzer attached to the IRMS. A subset of the acid-treated and washed seagrass samples were freeze dried at -20°C *in vacuo* and then ground to powder; no significant differences in measured seagrass $\delta^{13}C$ values were observed among these two treatment methods (data not shown).

Sediment samples were oven dried at 60°C overnight, and then were ground to powder using mortal and pestle. Isotopic analyses of the sediment carbonate were carried out at the UC Davis Stable Isotope Lab. The CO_2 gas used for analysis was generated by acidification of the treated sediments in a heated (90°C) common acid bath (103% phosphoric acid). The resultant gas was purified and introduced into a GVI Optima IRMS. These $\delta^{13}C$ values were calculated relative to V-PDB. Since the difference between V-PDB and PDB is negligibly small (Mook and Vries, 2001), the complete isotope data set is then internally consistent.

Alkaline earth elemental ratios (Sr^{2+}/Ca^{2+} and Mg^{2+}/Ca^{2+}) were determined in both pore waters and carbonate sediments at selected sites. In past studies of shallow water carbonate sediments no obvious diagenetic alteration of sediment mineralogy has been observed in the top 20-30 cm of sediment (e.g., Berner, 1966; Morse et al., 1985). Thus here a single sediment sample (8-10 cm sediment depth) was analyzed and assumed to be representative of the composition of the upper 20 cm of surface sediments at each site. The sediments were first dried at 50°C over night, then 0.500 g of sediment was dissolved

in 30 ml of 1N HCl followed by dilution to 100 ml with deionized water (Robinson, 1980). Pore water samples and sediment acid extracts were analyzed on an inductively coupled plasma optical emission spectrometer (ICP-OES) at Rutgers University. Briefly, two different standard solutions were prepared from three new single element standards - High Purity® Ca (1000 ± 3 ppm), Mg (1000 ± 3 ppm), and Sr (1000 ± 3 ppm). The mixed standard solutions were prepared by spiking the appropriate volumes (determined gravimetrically) of the Mg, Ca and Sr standards directly into 3% HNO_3. Multi-element standards at target concentrations between 5 and 10 times greater than elements in the sample solutions were made, and then a matrix-matched standard curve using three-point internal standardization was constructed, i.e., three-point standard additions were prepared by adding varying amounts of the multi-element standard to the sample matrix. To control for instrument sensitivity drift during the run, Indium (In) was used during these analyses as an internal standard to which signal intensities for each element (i.e., Mg, Sr and Ca) were normalized. An internal standard of 10 ppb In was prepared in 10% HNO_3 (v/v) and 100 uL were added to each sample, blank and standard, yielding a final concentration of 1 ppb In. Sensitivity and stability of the instrument were adjusted to optimum conditions before sample analysis, and monitored using 1ppb In.

All surface sediments were wet-sieved for grain size analysis. The sieve sizes used here were 2mm, 600 μm, 125 μm, and 63 μm. The <63μm fraction was defined as the fine fraction (Bennett et al., 1990). Mean grain size was calculated using the equation $d=\Sigma f_n d_n$, where f is the weight percent of a size fraction, and d is the median grain size in that fraction. For the >2 mm and <63 μm size fractions, median grain sizes of 2.25 mm and 31.5 μm were assumed (D. Swift, pers. comm.). Porosity was calculated using an empirical relationship between percent fine fraction (<0.063 mm) and measured porosity reported in Bennett et al. (1990). Sediment permeability was calculated using the Carman-Kozeny equation (Boudreau, 1997). Permeability values calculated with this equation agree well with measured permeabilities (Burdige, 2006).

The uncertainties of all analyses were: alkalinity (±2%); DIC (±2%); pH (±0.02 pH units); Ca^{2+} (±1%); Cl^- (±0.2%), $\delta^{13}C$ (DIC, organic carbon, and carbonate carbon) ±0.2‰, ±0.1‰, and ±0.04‰; $\delta^{18}O$ (±0.06‰), sulfate (±3%); sulfide (2%).

3. RESULTS

The complete set of pore water data from this cruise is listed in Appendix D. Depth profile of pore water O_2, alkalinity, DIC, calcium, aragonite saturation index ($\Omega_{aragonite}$), pH, sulfate, total dissolved sulfide (TDS), and $\delta^{13}C$ of the DIC from six representative sites across the Bank are shown in Figs. 32-34. In general, O_2 concentration and pH decrease with depth in these sediments, accompanied by increases in alkalinity, DIC, and Ca^{2+}. Such profiles are consistent with the occurrence of metabolic carbonate dissolution in the sediments (Chapter II; Burdige and Zimmerman, 2002). At the same time, the lack of net sulfate reduction and sulfide accumulation are also consistent with these previous studies, indicating no net sulfate reduction or sulfide accumulation in these sediments.

3.1. Pore Water Chemistry

3.1.1. Oxygen

In the upper 1-2 cm, O_2 profiles showed relatively flat gradients (i.e., no significant concentration decrease). Between these depths and 5 cm, O_2 concentration decreased with depth at all site studied. Below ~5 cm, O_2 concentrations either gradually approached zero or remained relatively constant at 50±20 μmol/kg.

3.1.2. Alk_T, DIC, Ca^{2+}

Pore water Alk_T, DIC, and Ca^{2+} concentrations were generally elevated relative to bottom water concentrations. Similar to the O_2 profiles, profiles of these solutes had relatively flat gradients in the upper 1-2 cm as well. The profiles also showed considerable variations at each individual site, indicating spatial heterogeneity of these sediments at small (within site) scales (<100 m radius).

Fig. 35 shows that there is an tight linear relationship between ΔAlk_T and ΔDIC at these sites with a small negative y-intercept ($r^2 = 0.94$). A similar property-property plot of ΔCa^{2+} vs. ΔDIC shows greater scatter, although the correlation is still significant ($r^2 = 0.56$, Fig. 36). A plot of ΔCa^{2+} vs. ΔAlk_T also showed a significant correlation with a slope similar to that observed in the plot of ΔCa^{2+} vs. ΔDIC (results not shown). All of these observations are consistent with the results from previous LSI studies (Chapter II; Burdige and Zimmerman, 2002).

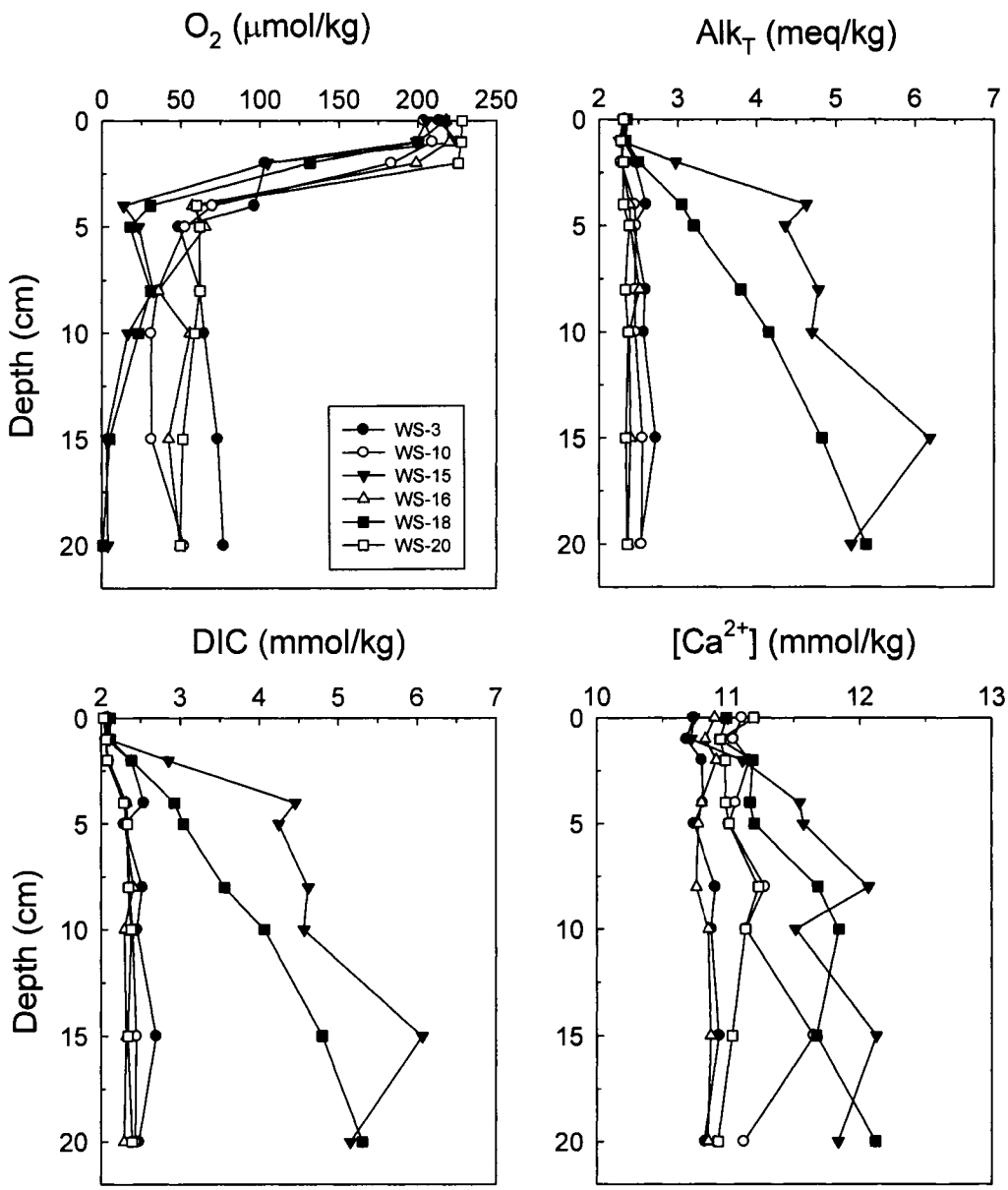

Fig. 32. Pore water profiles of O_2, alkalinity, DIC, and Ca^{2+} at six representative sampling sites on the Bahamas Bank (WS-3, WS-10, WS-15, WS-16, WS-18, and WS-20).

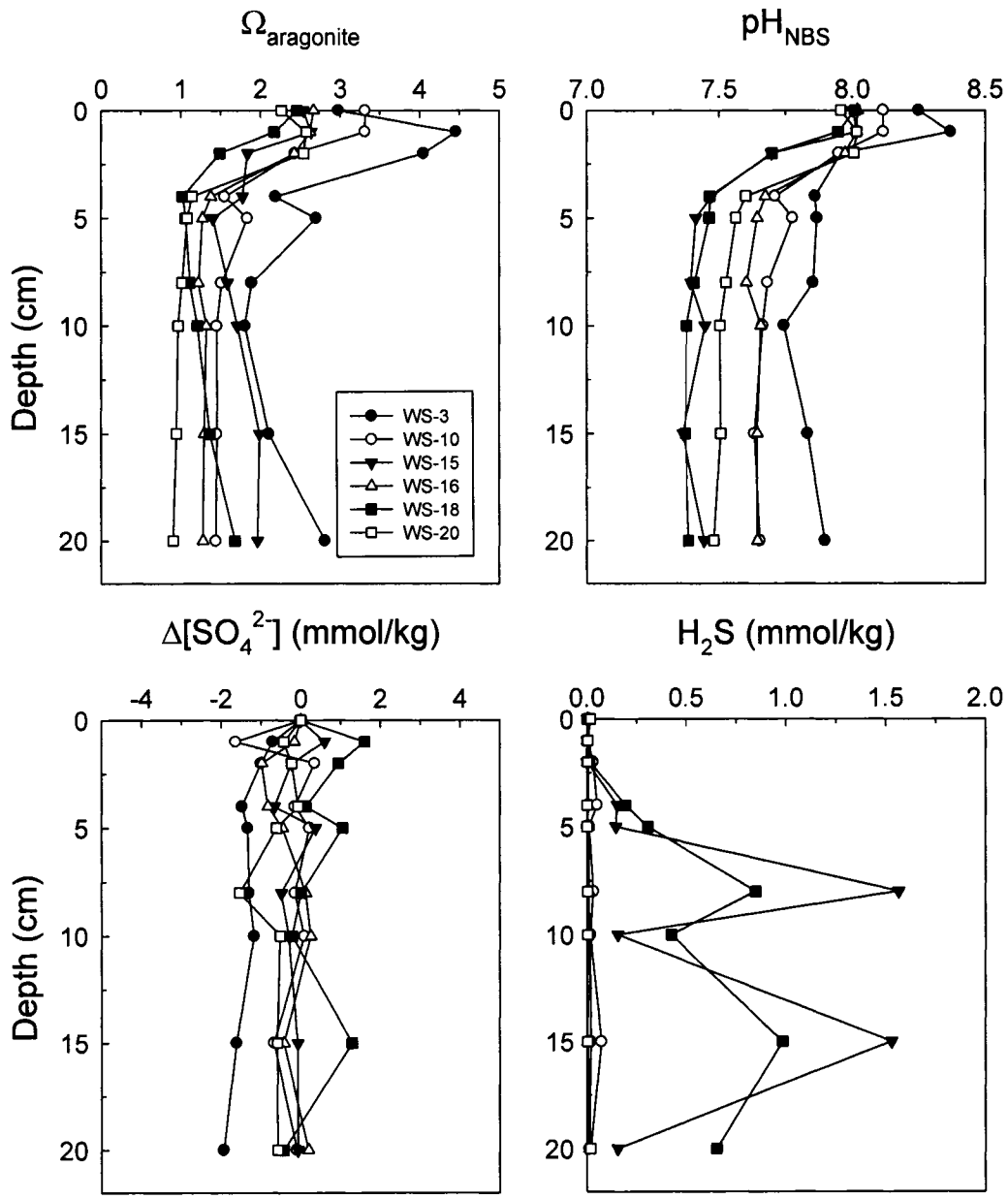

Fig. 33. Pore water saturation state, pH, $\Delta[SO_4^{2-}]$, and total dissolved sulfide (TDS) at six representative sampling sites on the Bahamas Bank (WS-3, WS-10, WS-15, WS-16, WS-18, and WS-20). Δ concentrations are pore water solute concentrations relative to bottom water values and are calculated as $\Delta[S] = [S]_{PW} - [S]_{BW} \times \frac{Sal_{PW}}{Sal_{BW}}$, in which [*S*] is the measured solute concentration, *Sal* is the salinity (calculated from titration chlorinity), and the subscripts *PW* and *BW* indicate pore water and bottom water concentrations at the sampling sites.

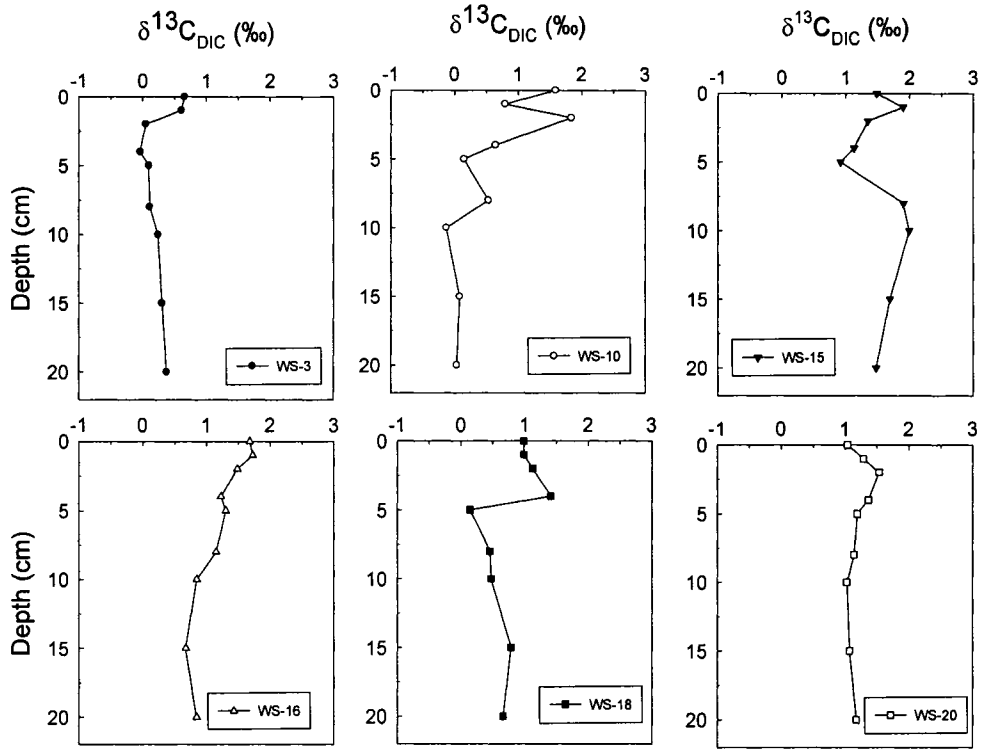

Fig. 34. $\delta^{13}C$ of pore water DIC at six representative sampling sites on the Bahamas Bank (WS-3, WS-10, WS-15, WS-16, WS-18, and WS-20)

3.1.3. pH and Pore Water Saturation States

Pore water pH generally decreased below the sediment-water interface with the steepest gradients in the upper 5 cm (Fig. 33). With depth the pH values were relatively constant at (~7.3-7.7).

Similar to the approach taken in Morse et al. (1985), calculated equilibrium lines for calcite, aragonite and 18 mole% Mg HMC are plotted on a pH-DIC diagram (Fig. 37). These lines represent the saturation CO_3^{2-} concentrations for these three minerals at different pH and DIC values. For calcite and aragonite, they were calculated using the following equations:

$$[CO_3^{2-}]_{aragonite} = \frac{K'_{aragonite}}{[Ca^{2+}]} \quad (47)$$

$$[CO_3^{2-}]_{calcite} = \frac{K'_{calcite}}{[Ca^{2+}]} \quad (48)$$

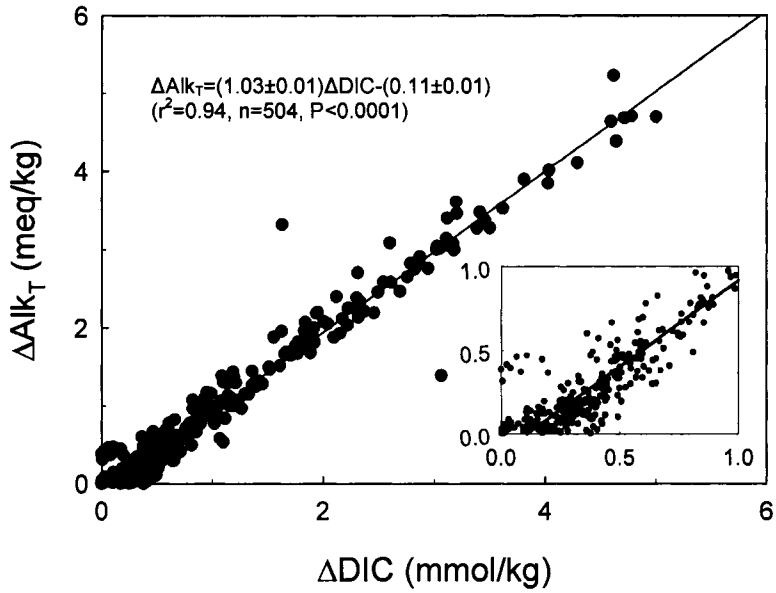

Fig. 35. Changes in pore water titration alkalinity (ΔAlk_T) and DIC (ΔDIC) relative to bottom waters in Bahamas Bank sediments. The linear regression (solid line) produces a best fit at the $P<0.0001$ level.

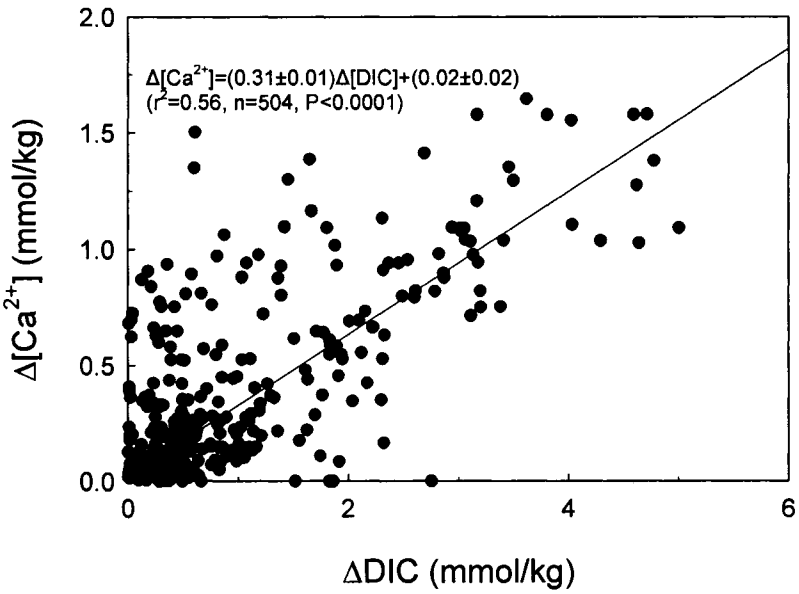

Fig. 36. Relationship between pore water Ca^{2+} and DIC concentration changes in the Bahamas Bank sediments. The linear regression (solid line) produces a best fit at $p<0.0001$ level.

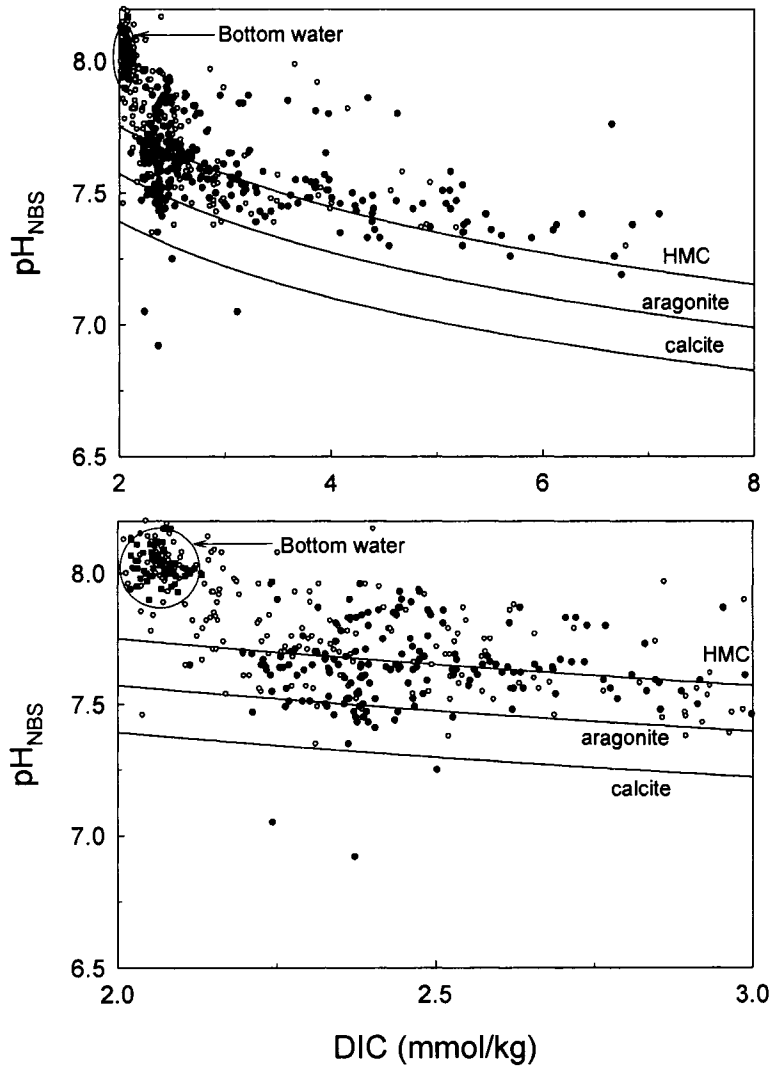

Fig. 37. Plot of pore water pH and DIC concentration. Open circle represent samples from ≤5cm and filled circles represent the deeper samples (from 8 cm and below). Bottom water values are shown in filled squares. The three saturation lines are described in the text. The upper panel includes all data and the lower panel illustrates data in the DIC range 2-3 mmol/kg.

where $[Ca^{2+}]$ was assumed to be 10.9 mmol/kg (extrapolated to salinity 37 based on a $[Ca^{2+}]$ = 10.3 mmol/kg in standard seawater of salinity 35). K_a' and K_c' are the stoichiometric dissolution constants of aragonite and calcite that were calculated with the equations in Mucci (1983); at 25°C and salinity 37 these values are 6.95×10^{-7} and

4.59×10^{-7}, respectively. For HMC (18 mol% Mg), an equilibrium constant (1.15×10^{-8}) from Walter and Morse (1984a) was used, and the saturation [CO_3^{2-}] was calculated using the equation

$$[CO_3^{2-}]_{HMC} = \frac{K_{Mg_{0.18}Ca_{0.82}CO_3}}{(\gamma_{Ca^{2+}}[Ca^{2+}])^{1-x}(\gamma_{Mg^{2+}}[Mg^{2+}])^{x}} \times \frac{1}{\gamma_{CO_3^{2-}}} \quad (49)$$

where the γ values are activity coefficients calculated using the program CO2BRINE (F. J. Millero, pers. comm.); the resulting values were $\gamma_{Mg^{2+}} = 0.2193$, $\gamma_{Ca^{2+}} = 0.2152$ and $\gamma_{CO_3^{2-}} = 0.0381$. [$Ca^{2+}$] at salinity 37 was determined as discussed above, while [Mg^{2+}] at salinity 37 was extrapolated from its concentrations in standard seawater (52.8 mmol/kg at salinity 35); the resulting value for [Mg^{2+}] was 55.9 mmol/kg. Note that the stoichiometric dissolution constants of both aragonite (K_a') and calcite (K_c') were determined in seawater media, while that for HMC ($K_{Mg_{0.18}Ca_{0.82}CO_3}$) was determined in solutions at lower ionic strength (I=0.18 instead of 0.7, which is the ionic strength of salinity 35 seawater, see Walter and Morse, 1984a). Due to enhanced ionic interactions when higher concentrations of salt are present, the solubility of HMC in these sediments may be greater than the literature reported values (Millero, 2001; Mucci, 1983), moving the HMC saturation line in Fig. 37 upward. Therefore the HMC saturation line in Fig. 37 represents a lower limit of the actual solubility of 18 mol% HMC in these sediment pore waters.

After the equilibrium carbonate ion concentrations for each of the three carbonate phases were calculated with eqns (47)-(49), equilibrium concentrations of bicarbonate and carbonic acid were calculated as a function of pH using the following equations

$$[HCO_3^-] = \frac{[H^+][CO_3^{2-}]}{K_2'} \quad (50)$$

$$[H_2CO_3] = \frac{[H^+][HCO_3^-]}{K_1'} \quad (51)$$

where K_1' and K_2' are the stoichiometric dissociation constants of carbonic acid (Millero, 2001). Equilibrium DIC concentrations were then determined as the sum of these three concentrations,

$$DIC = [H_2CO_3] + [HCO_3^-] + [CO_3^{2-}] \quad (52)$$

The resulting saturation lines along with values of pH and DIC for the pore water and bottom water samples are shown in Fig. 37. Similar to observations in Morse et al. (1985), the majority of the data points fall above the aragonite saturation line. In the deeper samples (closed circle), when DIC concentrations were greater than ~4 mmol/kg, the pore waters appeared to be saturated or perhaps supersaturated with respect to HMC, although based on the discussion above, this interpretation is highly dependent on the extent to which the HMC solubility line moves upward at the higher ionic strength of these pore waters.

3.1.4. Sulfate and Sulfide

Pore water sulfate profiles did not show any downcore trend (Fig. 33). Pore water sulfide levels were generally low, ranging from 10^{-3} to ~1 mmol/kg and at only 4 sites (WS-13, WS-14, WS-15, and WS-18) did sulfide levels increase with depth (1.1-1.6 mmol/kg). Thus, little or no net sulfate reduction occurred in the upper 20 cm of these sediments. These observations were similar to previous findings in LSI sediments (Chapter II; Burdige et al., submitted; Burdige and Zimmerman, 2002) and those from sediments in analogous environments such as Florida Bay (Ku et al., 1999; Walter and Burton, 1990).

3.2. Stable Carbon Isotopes

3.2.1. $\delta^{13}C$ of the Organic Matter and Carbonate Sediments

Stable isotope ratios in seagrasses, benthic algae, and sediment carbonate are listed in Tables 17 and 18. In this study *Thalassia* had $\delta^{13}C$ values that ranged from -4.9 to -9.7‰, and these values agreed with values reported in the literature for *Thalassia* in similar environments (Fourqurean et al., 2005; Hemminga and Mateo, 1996; Lin et al., 1991; McMillan, 1980). *Syringodium* had $\delta^{13}C$ values that ranged from -6.0 to -7.7‰ and the values agreed well with the values reported in the literature (Hemminga and Mateo, 1996). Organic matter from benthic algae had $\delta^{13}C$ values that were in general agreement with values for calcareous algae in this region as reported by Craig (1953). However, they were relatively enriched in ^{13}C as compared to phytoplankton carbon in the surrounding Atlantic Ocean, which have $\delta^{13}C$ values of ~-21‰ (Hofmann et al., 2000).

Table 17. Stable isotope compositions of seagrasses and some benthic macroalgae [a].

Species	Sampling sites	$\delta^{13}C_{OM}$ (‰)
Seagrasses		
Thalassia testudinum	WS-1, WS-25	-9.31±0.02
	WS-2	-6.32±0.12
	WS-3	-9.66±2.22
	WS-4	-8.92±0.19
	WS-11	-7.11±0.12
	WS-12	-5.63±0.09
	WS-13	-4.86±0.17
	WS-20	-6.29±0.06
Syringodium filiforme	WS-1, WS-25	-7.67±0.16
	WS-3	-5.95±0.26
Benthic Algae		
Penicillus sp.	WS-2	-15.77±0.03
Rhipocephalus sp.	WS-2	-12.76±0.08
Penicillus sp.	WS-4	-15.15±0.05
Rhipocephalus sp.	WS-4	-16.31±0.12
Udotea sp.	WS-4	-13.71±0.05

[a] The $\delta^{13}C$ values of the seagrasses are average values of the leaf and rhizome/root tissues. All results were based on triplicate analyses of pooled.

Sediment carbonate had $\delta^{13}C$ and $\delta^{18}O$ values that showed a close resemblance with literature values (Bathurst, 1971; Swart and Eberli, 2005). At some sites $\delta^{13}C$ values showed slight down core variability (up to 1‰) but did not show any consistent trend with depth.

3.2.2. Thalassia $\delta^{13}C$ and Water Depth Relationship

Values of $\delta^{13}C$ for *Thalassia* were negatively correlated with water depth at the study sites on the Bahamas Bank and at the LSI sites (Hu and Burdige, unpubl. data). At only one site (WS-1) did the data significantly fall outside the 95% confidence interval of the regression (Fig. 38). In contrast, no similar correlation was observed between the values of bottom water DIC $\delta^{13}C$ and water depth (Fig. 38).

Table 18. Stable isotope compositions of the Bahamas Bank carbonate sediments.

Sampling Sites	Depth (cm)	$\delta^{13}C$	Avg.	$\delta^{18}O$	Avg
WS-1	1	4.92	4.57±0.33	-	
	7	4.28		-	
	15	4.52		-	
WS-2	1	4.05	4.17±0.18	-0.58	-0.54±0.05
	9	4.09		-0.55	
	16	4.38		-0.48	
WS-3	1	4.20	4.18±0.07	-	-
	7	4.20		-	
	16	4.14		-	
WS-4	1	4.66	4.11±0.48	-0.54	-0.68±0.13
	6	3.89		-0.78	
	12	3.79		-0.74	
WS-5	1	4.09	4.58±0.45	-0.59	-0.39±0.18
	6	4.69		-0.32	
	15	4.96		-0.25	
WS-6	1	3.81	4.48±0.58	-0.38	-0.11±0.23
	9	4.73		0.02	
	15	4.88		0.02	
WS-8	1	4.19	4.19±0.19	-	-
	7	4.00		-	
	15	4.37		-	
WS-9	1	4.42	4.68±0.24	-0.22	-0.15±0.06
	7	4.75		-0.12	
	12	4.88		-0.11	
WS-10	1	4.36	4.34±0.02	-	-
	6	4.34		-	
	12	4.32		-	
WS-11	1	4.48	4.68±0.21	-0.13	-0.04±0.08
	3	4.66		-0.01	
	5	4.89		0.03	

Table 18. Continued.

Sampling Sites	Depth (cm)	$\delta^{13}C$	Avg.	$\delta^{18}O$	Avg
WS-12	1	4.32	4.28±0.29	-	-
	6	3.98		-	
	10	4.55		-	
WS-13	1	3.91	3.93±0.01	-	-
	5	3.94		-	
	10	3.93		-	
WS-14	1	4.28	4.35±0.35	-0.30	-0.22±0.16
	5	4.73		-0.04	
	10	4.04		-0.32	
WS-15	1	4.47	4.40±0.06	-	-
	5	4.35		-	
	10	4.38		-	
WS-16	1	3.89	3.89	-	-
WS-17	1	4.91	4.71±0.19	-	-
	5	4.69		-	
	10	4.52		-	
WS-18	1	4.52	4.62±0.15	0.12	0.16±0.07
	7	4.56		0.12	
	10	4.80		0.25	
WS-20	1	4.48	4.49±0.15	-	-
	5	4.35		-	
	10	4.65		-	
WS-21	1	4.51	4.64±0.14	0.28	0.25±0.03
	6	4.64		0.21	
	10	4.78		0.25	
WS-24	1	5.09	4.70±0.35	-0.14	-0.28±0.12
	4	4.45		-0.37	
	10	4.54		-0.33	

3.2.3. $\delta^{13}C$ of Pore Water DIC and Calculation of $\delta^{13}C_{added}$

Pore water DIC $\delta^{13}C$ values were generally lower than bottom waters values (Fig. 34). At some of the sites, $\delta^{13}C$ first decreased and then increased with sediment depth, thus showing a mid-depth minimum. The profiles observed here are similar to previous observations in LSI sediments (Chapter II).

DIC in the pore waters is altered by reprecipitation and metabolic carbonate dissolution. Following the approach in Chapter II, the isotopic composition of the DIC added to the pore waters ($\delta^{13}C_{added}$) was calculated using the linear regression of ($\delta^{13}C$-DIC)×[DIC] versus [DIC]. The results of these regressions are shown in Table 19. Fig. 39 shows three plots of such regression at sites that represent different seagrass densities (i.e., WS-2, WS-10, and WS-25). In the literature, there is an alternative approach used to calculate $\delta^{13}C_{added}$ by regressing $\delta^{13}C_{DIC}$ versus the reciprocal of the DIC concentration, based on the following equation (see Ogrinc and Faganeli, 2003, for details):

$$\delta^{13}C_{DIC} = \delta^{13}C_{added} + B'\frac{1}{DIC} \qquad (53)$$

Here the y-intercept is $\delta^{13}C_{added}$. Values of $\delta^{13}C_{added}$ values obtained using eqn. (53) were not significantly different from those calculated using the regression of ($\delta^{13}C$-DIC)×[DIC] vs. [DIC] (Paired t-test, $P>0.05$, data not shown), and the RMS error between these two sets of $\delta^{13}C_{added}$ values was ~0.14‰, less than the analytical uncertainty of isotope measurements pore water DIC (0.2‰). Therefore the following discussion of $\delta^{13}C_{added}$ will be based on values calculated from the regressions of ($\delta^{13}C$-DIC)×DIC vs. DIC, to maintain consistency with Chapter II.

Among the 20 sites with available pore water DIC $\delta^{13}C$ data, linear regressions for eight sites yielded statistically significant values ($P\leq0.05$). The $\delta^{13}C_{added}$ values for these regressions ranged from -5.41±1.66‰ (WS-10) to 1.63±0.31‰ (WS-15). For most regressions that were not statistically significant ($P>0.05$), $\delta^{13}C_{added}$ values were essentially indistinguishable from 0‰.

Table 19. Pore water DIC stable carbon isotope regression [a].

Site	$\delta^{13}C_{added}$	P [b]	Cal'd $\delta^{13}C_{OM}$	$\delta^{13}C_{seagrass}$ (m)	$\delta^{13}C_{seagrass}$ (c)
WS-2	1.63±0.22	0.00	-0.92±0.25	-6.32±0.12	
WS-3	-3.83±1.50	0.02	-11.83±2.96	-7.80±2.22 [c]	
WS-4	0.61±1.64	0.72	-2.89±2.80	-8.92±0.19	
WS-5	-4.50±1.24	0.01	-13.58±2.03		-6.67±1.64
WS-6	-0.18±1.05	0.87	-4.83±1.52		-7.94±1.95
WS-8	0.53±0.85	0.56	-3.12±1.52		-6.34±1.55
WS-9	1.34±2.60	0.63	-1.99±4.97		-6.45±1.58
WS-10	-5.41±1.66	0.01	-15.15±3.31		-6.73±1.65
WS-11	1.43±0.28	0.00	-1.81±0.34	-7.11±0.12	
WS-12	3.93±1.98	0.09	3.57±3.67	-5.63±0.09	
WS-13	1.10±0.27	0.00	-1.73±0.52	-4.86±0.52	
WS-14	-0.09±0.57	0.88	-4.52±0.79		-6.62±1.62
WS-15	1.63±0.31	0.00	-1.13±0.55		-5.63±1.38
WS-16	-1.07±1.62	0.52	-6.04±3.14		-6.67±1.64
WS-17	-0.30±27.11	0.99	-5.30±54.04		-7.72±1.89
WS-18	0.56±0.44	0.23	-3.51±0.75		-6.29±1.54
WS-20	-1.77±0.77	0.10	-8.03±1.38	-6.29±0.06	
WS-24	-0.92±1.34	0.52	-6.54±2.33		-7.01±1.72
WS-25	-2.54±0.57	0.00	-9.66±0.82	-8.49±1.38 [b]	

[a] $\delta^{13}C_{seagrass}$ (m) values were measured (Table 17), and $\delta^{13}C_{seagrass}$ (c) values were calculated using the linear relationship between water depth and seagrass $\delta^{13}C$ (Fig. 38) at sites with no seagrass samples collected. See section 4.3.1 for details.

[b] P values were power of the linear regressions used to calculated $\delta^{13}C_{added}$ at each site.

[c] WS-3 and WS-25 seagrass $\delta^{13}C$ values were calculated from both *Thalassia* and *Syringodium* $\delta^{13}C$ values at these sites, at all other sites *Thalassia* was the dominant seagrass species.

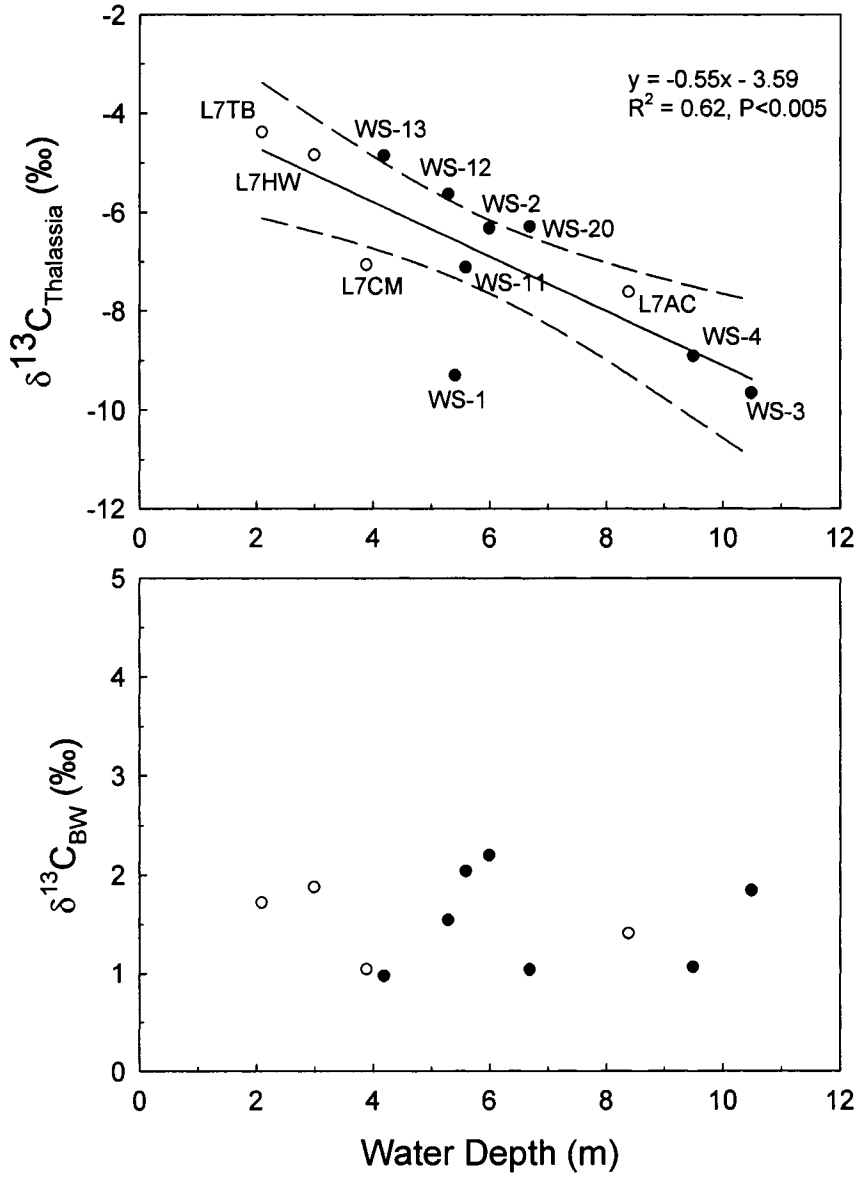

Fig. 38. Compilations of the $\delta^{13}C$ values of (a) *Thalassia* and (b) bottom water DIC versus water depth. The filled circles are values obtain in this study, and the open circles are LSI seagrass $\delta^{13}C$. The dashed lines represent the 95% confidence interval of the linear regression.

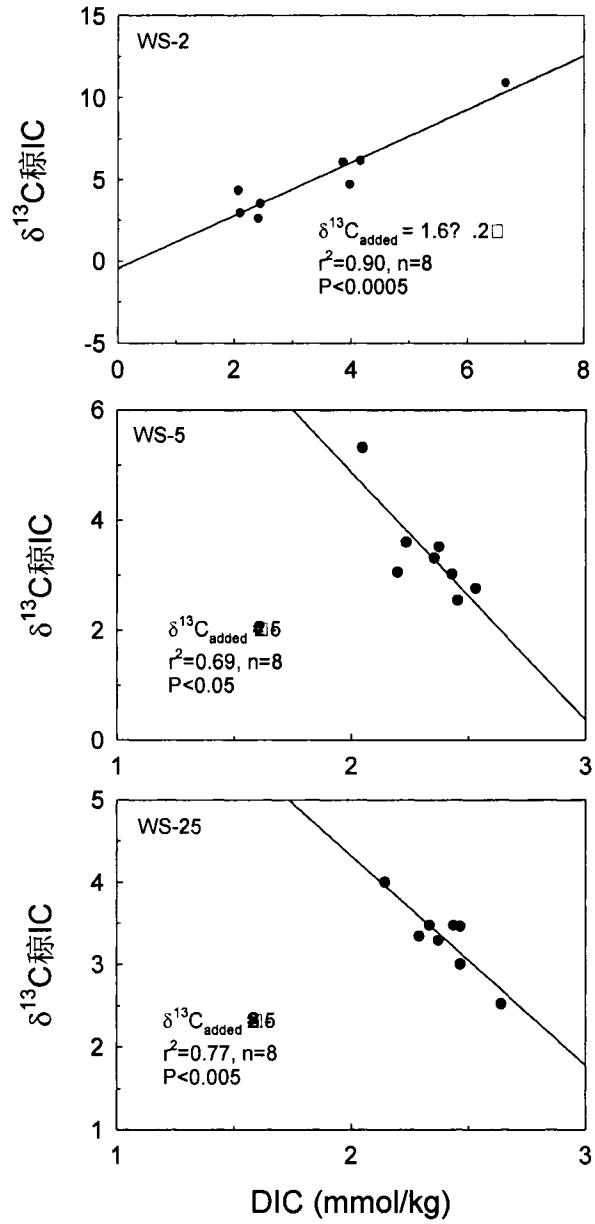

Fig. 39. Plots of linear regression of $\delta^{13}C$·DIC versus DIC in three representative sites in Bahamas Bank sediments (WS-2, WS-5, and WS-25).

3.3. Sr/Ca and Sr/Mg ratios

Similar to observations in other shallow water carbonate sediments (e.g., Berner, 1966), pore water cation ratios (Sr/Ca, Sr/Mg) did not show any significant downcore trends in the upper 20cm of sediments when compared to their respective water column values (Table 20). The pooled Sr/Ca values in all pore waters and bottom waters

($(8.97\pm0.18)\times10^{-3}$) was slightly higher than the Atlantic Ocean water value of 8.55×10^{-3} (Villiers, 1999) but similar to the IAPSO standard seawater value of 8.81×10^{-3} (Pilson, 1998)}. The Sr/Mg ratio was $(1.71\pm0.06)\times10^{-3}$ and also agreed with the IPASO value of 1.72×10^{-3}.

The solid phase Sr/Ca ratio (Table 21) showed a much higher Sr concentration than that expected from equilibrium inorganic precipitation of either aragonite or calcite under sea water conditions, consistent with the observations by Berner (1966). The partitioning coefficients of Sr (eqn. 54) for aragonite and calcite are 1.12±0.04 and 0.14±0.02, respectively (Bathurst, 1981),

$$K_{Sr} = \frac{(mSr^{2+} / mCa^{2+})_{solid}}{(mSr^{2+} / mCa^{2+})_{solution}} \qquad (54)$$

while the average molar concentration ratio between solid and aqueous phases in these sediments was 1.40±0.14. The sediment Sr/Ca ratios (11-13 mmol/mol) are similar to those of Long Island Sound (LIS) and Florida Bay sediments (e.g., ~10 in Green and Aller, 2001; 9-12 mmol/mol in Rude and Aller, 1991), despite differences in the carbonate content of these sediments, e.g., carbonate content is 2 wt% in LIS sediments vs. >95 wt% in Florida Bay-Bahamas Bank sediments.

3.4. Sediment Grain Size, Porosity and Permeability

In the majority of these sediments grain sizes ranged from 200 to 800 μm, although sediments at WS-5, 10 and 16 were much coarser (2-6 times) than those at all other sites. The corresponding permeability values in these sediments were therefore 4-8 times larger than those at the other sites ($16\text{-}39\times10^{-10}$ m^2 vs. $2.2\text{-}8.5\times10^{-10}$ m^2). The calculated permeability values for the WS sediments were greater than *in situ* permeabilities measured at sites on the Bahamas Bank near WS-21 in this study (0.03-0.8×10-10 m^2, Bennett et al., 1990). However, they were similar to those calculated for LSI sediments ($>2\times10^{-10}$ m^2; Burdige and Zimmerman, 2002). The calculated sediment porosities at the WS sites were not significantly different among the sites (45% to 56%, Table 22) and were similar to the *in situ* porosities reported in Bennett et al. (1990; 36-61%).

Table 20. Pore water cation ratios (unit mol/mol).

Site	Depth (cm)	Sr/Ca ($x10^3$)	Sr/Mg ($x10^3$)	Mg/Ca
WS-3	0	8.936	1.690	5.288
	1	9.109	1.734	5.253
	4	9.164	1.685	5.438
	10	8.900	1.666	5.341
	15	8.988	1.735	5.180
	20	8.925	1.660	5.378
WS-13	0	9.122	1.716	5.315
	1	8.796	1.688	5.212
	2	8.952	1.735	5.159
	5	8.812	1.719	5.127
	8	9.030	1.743	5.180
	10	9.146	1.826	5.010
	15	9.121	1.796	5.078
	20	9.226	1.871	4.930
WS-21	0	8.975	1.618	5.546
	1	9.028	1.663	5.430
	2	8.962	1.694	5.292
	4	8.801	1.674	5.257
	5	8.594	1.659	5.181
	8	8.975	1.720	5.218
	10	9.046	1.696	5.335
	15	8.306	1.709	4.860
	20	8.954	1.780	5.030
WS-25	0	9.051	1.709	5.296
	1	8.915	1.714	5.200
	2	9.090	1.705	5.331
	5	9.220	1.642	5.614
	8	8.996	1.671	5.383
	10	8.984	1.727	5.204
	20	8.888	1.620	5.486
L7 CM	0	8.806	1.664	5.291
	2	8.650	1.635	5.291
	5	8.878	1.737	5.111
	10	8.756	1.689	5.185
	15	8.799	1.824	4.824
	20	8.757	1.781	4.916

Table 21. Solid phase cation concentrations (unit: ppm) [a].

Sediment #	Ca	Mg	Sr	Sr/Ca (mmol/mol)
WS-3-1	339387	8671	9306	13
WS-3-2	363026	6580	9780	12
WS-3-3	357727	6146	9758	12
WS-3	364821	7024	9729	12
WS-13	374944	3058	11448	14
WS-21	367464	4705	10559	13
WS-25	358916	4377	10428	13
L7 AC	351700	11533	8188	11
L7 CM	354409	9465	8857	11
L6 OS	374249	5000	10986	13

[a] Note that WS-3-1, WS-3-2, and WS-3-3 are replicate surface (1-2cm) sediments collected before, during the middle, and after filling process from the WS-3 incubation experiment in Chapter III. All other samples are from 8-10 cm depth at the different sites (see section 2.2).

4. DISCUSSION

In previous studies of LSI sediments, the sediments were categorized into three broad classes based on seagrass density (Chapter II; Burdige and Zimmerman, 2002). However, this study included sampling sites across a much wider range of geographical locations and sediment types, as opposed to a relatively restricted study area around LSI. Therefore, that approach was not used here.

Previous studies of LSI sediments (Chapter II; Burdige et al., submitted; Burdige and Zimmerman, 2002) suggested that seagrasses can significantly enhance metabolic carbonate dissolution through below-ground O_2 input and organic carbon deposition. However, the extent to which these findings are significant over the larger area of the Bahamas Bank is unknown. Thus it is necessary to examine relationships between seagrass density and carbonate dissolution or carbonate reprecipitation across a much broader geographical setting on the Bahamas Bank, to better understand the role of seagrasses in these sediment biogeochemical processes.

Table 22. Sediment grain size distribution in the Bahamas Bank sediments [a].

Site ID	%wt size fraction [b]					Mean Grain size (μm)	Porosity	Permeability ($\times 10^{10}$ m^2)
	>2	0.6-2	0.125-0.6	0.063 -0.125	<0.063			
WS-2	0	9	78	8	5	409	49	4.4
WS-3	0	3	45	40	12	238	56	2.8
WS-4	3	19	74	3	1	587	46	6.3
WS-5	19	55	15	9	2	1201	46	28.1
WS-6	1	34	63	2	1	691	45	8.2
WS-8	0	20	71	6	3	521	48	6.4
WS-9	3	28	67	1	1	678	45	7.8
WS-10	16	72	8	2	3	1319	48	39.0
WS-11	0	3	92	5	0	374	45	2.3
WS-12	1	2	51	40	6	272	51	2.2
WS-13	0	9	76	11	4	406	49	4.1
WS-14	0	23	72	4	1	558	46	5.9
WS-15	0	4	76	12	8	340	53	4.1
WS-16	6	50	42	0	1	940	46	16.0
WS-17	0	8	80	10	1	406	46	3.0
WS-18	6	8	57	20	9	458	54	8.5
WS-20	0	10	78	9	3	423	48	3.9
WS-21	0	4	63	17	16	306	58	6.0
WS-24	0	17	79	4	1	503	46	4.6
WS-25 (1)	0	11	71	13	5	425	50	4.8

[a] Porosity and permeability calculations are described in section 3.3.
[b] size fractionation have units of mm.

4.1. Pore Water Chemistry

As shown in section 3.1, carbonate dissolution end-products (alkalinity, DIC, and Ca^{2+}) concentrations all increased with depth, whereas O_2 concentration, pH, pore water saturation states decreased with depth. The linear relationship (1:1) between pore water alkalinity and DIC (Fig. 35), in conjunction with the lack of sulfate reduction and sulfide accumulation (Fig. 33), suggests that carbonate dissolution in these sediments was driven primarily by aerobic respiration, and that sulfate reduction, if it occurred, was tightly coupled with sulfide re-oxidation. As discussed previously the overall effect of these two processes is equivalent to aerobic respiration (e.g., Chapter II; Burdige and Zimmerman, 2002; Ku et al., 1999). In general, the pore water chemistry observed across the Bank was consistent with the results from previous studies (Chapter II; Burdige et al., submitted; Burdige and Zimmerman, 2002).

Burdige et al. (submitted) observed a strong positive correlation at the LSI sites between pore water solute (alkalinity, DIC and Ca^{2+}) accumulation and seagrass density (e.g., LAI), indicating that seagrasses enhance carbonate dissolution. In contrast, no significant correlation between pore water solute accumulation and LAI (Fig. 40) or permeability (data not shown) was observed across these sites on the Bank. Instead, relatively low concentrations of the solutes were present at some sites with high seagrass densities; for example, WS-1, WS-3, WS-4, WS-12, and WS-25 all had alkalinity concentrations increases at depth that were less than ~1 mmol/kg despite LAI values that were greater than 1. Similarly, high solute concentration at depth were observed in some sediment with intermediate or even low LAI values, for example, WS-2, WS-13, WS-14, and WS-15 that had LAI of 0.4-1; or WS-8, WS-11, WS-18, WS-21 that had LAI of 0.07-0.19, all these sites had maximum alkalinity concentration increase greater than 1 mmol/kg.

Calculated sediment permeability values (Table 22) suggest that pore water advection probably played an important role in sediment-water mass exchange processes at these WS sites (Burdige et al., submitted; Burdige and Zimmerman, 2002; Huettel and Webster, 2001; Jahnke et al., 2005; Rasheed et al., 2004; Reimers et al., 2004; Rusch et al., 2006). Flat pore water gradients in the upper ~1-4 cm of the sediments are also consistent with this type of advection (Figs. 32 and 33). Because rapid pore water advection can remove

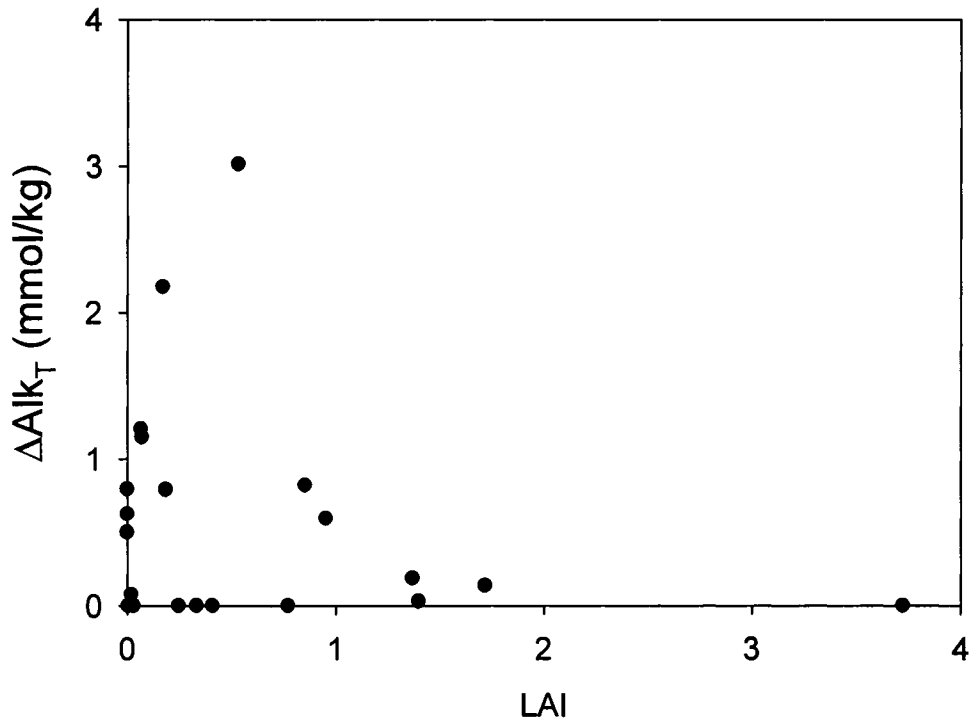

Fig. 40. Pore water solute accumulation (ΔAlk_T) versus LAI. ΔAlk_T is defined as the difference between the average alkalinity between 10 and 20 cm and bottom water value.

respiration and metabolic dissolution end-products from the pore waters of the sediments, pore water gradients near the sediment-water interface do not accurately reflect reaction rates in these advection-controlled systems (Burdige et al., submitted). Therefore to use these pore water profiles to estimate rates of sediment processes and sediment-water mass exchange, a modeling approach is required; this will be presented in detail in section 4.4.

4.2. Dissolving Carbonate Phase

4.2.1. Implications from Pore Water $\Omega_{aragonite}$

The dominant carbonate minerals in Bahamas Bank sediments are aragonite and high-magnesium calcite (HMC) (e.g., Chapters II and III; Morse and Mackenzie, 1990; Walter and Burton, 1990). In contrast, low magnesium calcite (LMC, typically less than 4 mol% or 1 wt% of $MgCO_3$ content, Milliman, 1974) does not represent a major phase in these

sediments (<5%, Chapter III) and also has a lower solubility than either HMC and aragonite. Therefore, its dissolution is of less concern here.

Solubility and dissolution kinetics of different carbonate materials have been extensively studied (e.g., Hales and Emerson, 1997; Keir, 1980; Mucci, 1983; Plummer and Mackenzie, 1974; Walter and Morse, 1984a; Walter and Morse, 1984b; Walter and Morse, 1985). Studies carried out by Walter and coworkers examined the factors controlling the solubility of many biogenic carbonate phases (including grain size, microstructures etc), and concluded that the general solubility order is 18 mol% HMC > 12 mol% Mg HMC ≈ aragonite > calcite. Droxler (1986), however, suggested that 12 mol% Mg HMC is more soluble than aragonite, based on carbonate mineral distribution in deep waters around the Bahamas Bank.

Based on these studies, the factors controlling carbonate dissolution rates are solubility (thermodynamic) and microstructure (kinetic). In particular, solubility control determines which mineralogical phase is dissolved; microstructure represented by "reactive surface area" controls how fast the carbonates dissolve when the saturation condition is met. In low latitude shallow marine environments, both water column and pore waters are generally close to, or supersaturated, with respect to aragonite (Bernstein and Morse, 1985; Morse et al., 1985; Sabine and Mackenzie, 1995; Walter and Burton, 1990). Since little or no net sulfate reduction occurred in the pore waters at all sampling sites (Table 17 and Fig. 33), regressions of ΔAlk_T and ΔDIC as well as ΔCa^{2+} vs. ΔDIC (Fig. 35 and 36) clearly indicate net carbonate dissolution in these sediments following rxns. (44)-(46).

The positive x-intercept (107±3 μmol/kg ΔDIC) of the regression line in Fig. 35 can be thought of as the titration of the existing CO_3^{2-} in the pore waters by metabolic CO_2 to a carbonate ion concentration such that the carbonate saturation state is low enough for dissolution to occur (Burdige and Zimmerman, 2002; Moulin et al., 1985). To examine this problem I used the program CO2SYS (Lewis and Wallace, 1998) to first estimate an average bottom water [CO_3^{2-}] value (185 μmmol/kg) assuming an average bottom water DIC concentration (2.07 mmol/kg) and pH (8.04). If I then add 107 μmmol/kg of CO_2 to this water, the resulting [CO_3^{2-}] will decrease to 120 μmmol/kg, a value close to the

equilibrium [CO_3^{2-}] for 18 mol% Mg HMC (96 μmmol/kg) and similar to the asymptotic pore water [CO_3^{2-}] calculated for the WS sediments (80-140 μmmol/kg).

Pore water profiles (Figs. 32 and 33) and pore water property-property plots (Figs. 35 and 36) both suggest that metabolic carbonate dissolution is occurring in these sediments. At the same time, these sediment pore waters are supersaturated with respect to aragonite, although as the discussion in section 3.1.3 indicates, the saturation state with respect to HMC is equivocal. Therefore carbonate phases more soluble than aragonite (and are most likely HMC) are dissolving in these sediments, consistent with observations in the literature (e.g., Morse, 1985; Walter and Burton, 1990). Discussion in the following sections will more quantitatively support this suggestion.

4.2.2. Implications from Pore Water $\Delta Ca^{2+}/\Delta DIC$ Stoichiometry

In muddy, diffusion-controlled sediments, i.e., where advection can be neglected, pore water property-property plots are often used to calculate reaction stoichiometry (Berner, 1977). However, as noted above (section 4.1), mass transport near the sediment-water interface of the Bahamas sediments was advection-controlled due to the high sediment permeability at these sites. In sites where biological advection occurs (i.e., bio-irrigation), Hammond et al. (1999) have shown that this same approach can be used to calculate reaction stoichiometry with pore water property-property plots (also see related discussion in Chapter II). Therefore, it appears that these property-property plots can be used to examine reaction stoichiometry in permeable sediments. Thus the pore water $\Delta Ca^{2+}/\Delta DIC$ ratio in the sediments presumably represents the production ratio of these two solutes, and can be used to estimate the composition of the dissolving carbonate phase. Based on Fig. 36, apparently 1 unit of DIC production was associated with 0.31 units of Ca^{2+} production. According to rxn (44)-(46), assuming dissolution was homogeneous (Turner et al., 1986), then the apparent dissolving carbonate should have a composition of $Ca_{0.62}Mg_{0.38}CO_3$.

However, the Mg content of HMC phases in carbonate sediments range from 8 mole% in abiotic carbonate precipitates , to ~20 mole% in some calcareous organisms, although in some red algae the Mg content of the skeletal carbonate can reach up to ~25 mole% due to the presence of brucite ($Mg(OH)_2$; Milliman, 1974; Morse and Mackenzie,

1990; Walter and Morse, 1984a). In Chapters II and III, XRD results showed that the Mg content of the HMC in LSI and WS sediments (WS-3 and WS-13) was ~12 to 13 mole%; similar Mg concentrations were also observed for sediment HMC in other sediments both on the Bahamas Bank and in nearby Florida Bay (Berner, 1966; Morse et al., 1985). Taken together, it seems that the dissolving carbonate phase in the WS sediments had a higher Mg content than that in the actual solid phase.

The apparent discrepancy between the pore water calcium and DIC production ratio and the sediment Ca content calls upon a possible incongruent dissolution mechanism, in which HMC dissolves at the same time that reprecipitation generates a secondary low-Mg carbonate (Macintyre and Reid, 1998; Morse and Mucci, 1984; Mucci, 1986; Mucci, 1987; Mucci and Morse, 1983; Reid and Macintyre, 1998; Tribble and Mackenzie, 1998; Walter et al., 1993). In Chapter III, I showed that if the dissolving carbonate phase was 12 mole% Mg, then the secondary carbonate was estimated to be 8 mole% HMC, consistent with observations from Bahamas Bank sediments (Morse and Mucci, 1984; Mucci, 1987). In the following discussion I will try to estimate the rates of reprecipitation using the production rates of DIC and calcium and a mass balance calculation (section 4.4).

4.3. Stable Carbon Isotope Mass Balance

4.3.1. The Relationship between Seagrass $\delta^{13}C$ and Water Depth

On the Bahamas Bank I have observed that *Thalassia* organic matter becomes more ^{13}C-depleted (i.e., $\delta^{13}C$ values become more negative) with increasing water depth (Fig. 38). Given a narrow temperature range (22-24 °C) among these sites, and the fact that $\delta^{13}C$ values of bottom water DIC did not co-vary with water depth (Fig. 38), it seems unlikely that such factor could explain these observations. However, a similar relationship between seagrass $\delta^{13}C$ and light intensity has been observed for other seagrass species (Cooper and DeNiro, 1989; Grice et al., 1996), and here, light intensity controlled by water depth could explain these observations. Because the growth of the seagrasses is CO_2-limited, decreasing rates of photosynthesis with increasing water depth lead to greater isotopic fractionation, therefore seagrass organic carbon was more depleted in ^{13}C at deeper depths (Durako and Hall, 1992; Durako and Sackett, 1993;

Hemminga and Mateo, 1996; Zimmerman et al., 1997). In contrast though, seagrass growth rates at the study sites on the Bahamas Bank were likely not light-limited, because *in situ* values of photosynthetically active radiation (PAR) were above the saturation values for these seagrasses (Zimmerman, pers. comm.). This therefore seems contradictory to the irradiance control on seagrass carbon isotopic fractionation described above. Further study is clearly needed to determine the actual controls on seagrass carbon isotopic fractionation on the Bahamas Bank. Nevertheless, for the modeling exercise in the next section it appears reasonable to use the empirical relationship in Fig. 38 to estimate seagrass $\delta^{13}C$ values for sites at which no seagrass samples were collected. These values are also listed in Table 19.

4.3.2. Stable Carbon Isotope Evidence for Carbonate Reprecipitation

If carbonate dissolution and organic carbon oxidation are the sole processes contributing DIC to the pore waters, then the following mass balance equation can be written (also see Chapters II and III):

$$\delta^{13}C_{added} = f_{OM} \times \delta^{13}C_{OM} + f_C \times \delta^{13}C_C \quad (55)$$

where $f_{OM} = f_C = 0.5$ based on metabolic carbonate dissolution (i.e., rxn 44-46). Based on the values of $\delta^{13}C_{added}$ determined in section 3.2.3 (Table 19) and the measured values of $\delta^{13}C_C$ (Table 18), $\delta^{13}C_{OM}$ values can then be back-calculated using eqn (55). These are also shown in Table 19.

Seagrass detritus is generally considered to be the dominant carbon source for microbial respiration in seagrass vegetated sediments in oligotrophic tropical environments, where other types of carbon sources (for example, algal detritus) are limited (Boschker et al., 2000; Holmer et al., 2001; Jones et al., 2003). Therefore if I compare the calculated values of $\delta^{13}C_{OM}$ with either the measured or estimated values of $\delta^{13}C_{seagrass}$ I see that these sediments can be roughly divided into 3 groups: (1) $\delta^{13}C_{OM} > \delta^{13}C_{seagrass}$, at sites WS-2, 4, 6, 8, 9, 11, 12, 13, 14, 15, and 18; (2) $\delta^{13}C_{OM} \approx \delta^{13}C_{seagrass}$, at sites WS-3, 16, 17, 20, 24, and 25; (3). $\delta^{13}C_{OM} < \delta^{13}C_{seagrass}$, at sites WS-5 and WS-10. If I define $\delta^{13}C_{seagrass} - \delta^{13}C_{OM}$ as $\Delta^{13}C_{seagrass\text{-}OM}$ and then plot $\Delta\delta^{13}C_{seagrass\text{-}OM}$ versus LAI, no clear trend was observed. However $\Delta\delta^{13}C_{seagrass\text{-}OM}$ showed a weak, but significant

positive correlation with sediment grain size (Fig. 41). This will be further discussed in section 4.4.

Based on Chapters II and III, if the calculated $\delta^{13}C_{OM}$ is greater than the $\delta^{13}C_{seagrass}$ as in Group (1) sediments, then presumably there is coupled dissolution/ reprecipitation occurring in the sediment. This process enriches the pore water DIC pool with ^{13}C as a results of "heavy" carbonate carbon ($\delta^{13}C$ approx. 4-5‰) passing through the DIC pool during this coupled process. An alternate explanation of these results is that there is an organic carbon source to these sediments that is heavier than the seagrasses on the Bahamas Bank. This seems particularly unlikely since both benthic algae and phytoplankton produce organic carbon that is isotopically lighter than seagrasses (Table 17; also see Hofmann et al., 2000). Therefore even if lighter carbon were contributing to the organic carbon pool, this would only increase the difference between the calculated value of $\delta^{13}C_{OM}$ and the mixed $\delta^{13}C$ value of the materials being remineralized.

For the two Group (3) sediments, the calculated $\delta^{13}C_{OM}$ values were similar to those of benthic algal materials, although LAI values were not zero at either site and seagrass material could likely contribute to the pool of organic matter being remineralized. On the other hand, the sediments at these sites were the coarsest among all studied sites (Table 22), and soft-bodied green macro-algae were clearly visible at WS-10 (F. Neuweiler, pers. comm.). Thus it appears that either benthic algal carbon or a mixture of seagrass/algal carbon may be remineralized at these two sites. A detailed mechanism for the transport of algal materials into these sediments is discussed in section 4.4.

In Group (2) sediments, the calculated values of $\delta^{13}C_{OM}$ seemed to suggest that 1:1 mixing of the two carbon sources (seagrass vs. carbonate) could adequately explain the pore water $\delta^{13}C$ results. However, with some uncertainty of the exact organic carbon source (algae vs. seagrass, for example in the Group (3) sediments), it is difficult to unequivocally ascertain whether carbonate dissolution alone was occurring in these sediments. Furthermore, Group (2) sediments included sites WS-3 and WS-25, where very high seagrass densities were observed. This observation appeared to contradict our previous findings in LSI sediments where carbonate reprecipitation occurred solely in densely-vegetated sediments (Chapter II). To further examine this discrepancy, a

diagenetic modeling approach is needed in addition to these stable isotope isotopic mass balance calculations. This will be presented in the next section 4.4.

4.4. Coupled O_2 input and Carbonate Dissolution Model

In fine-grained sediments, diagenetic models that consider diffusion, bioturbation and

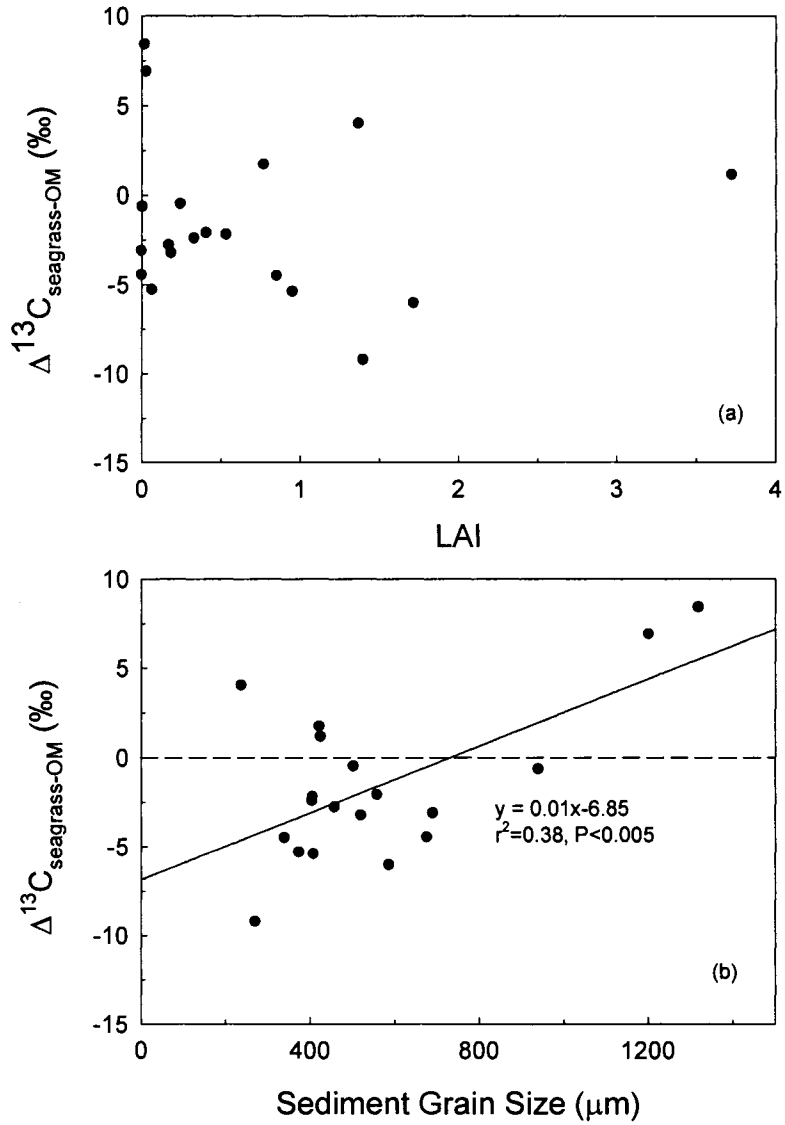

Fig. 41. The relationships between $\Delta^{13}C_{seagrass-OM}$ and (a) seagrass LAI, (b) mean grain size. The solid line in (b) is the linear regression that produces the best fit at the $P<0.005$ level, and the dashed line defines where the calculated $\delta^{13}C_{OM}$ using the mass eqn. (55) equals $\delta^{13}C_{seagrass}$.

bioirrigation are well developed and have been widely used (e.g., Boudreau, 1997; Burdige, 2006). However, in the coarse grained sediments such as theses at the WS sites, both seagrass O_2 input at sediment depth and high sediment permeability (Table 22, Huettel and Webster, 2001) makes it difficult to apply such commonly-used models, because transport processes associated with permeability are not well-understood or quantified. Nevertheless, empirical models describing non-diffusive solute transport in permeable sediments have been recently reported in the literature and provided reasonable fits to field data (e.g. Jahnke et al., 2005).

To address the apparent mass imbalance between the extent of carbonate dissolution and O_2 input (Burdige and Zimmerman, 2002; Ku et al., 1999; Walter and Burton, 1990), Burdige et al. (submitted) developed an advection-diffusion-reaction (ADR) model and applied it to LSI sediments to estimate carbonate dissolution rates. Here this model will be further used to study the reaction rates across a broader expanse of the Bahamas Bank.

4.4.1. Model Description

The ADR model is discussed in detail in Burdige et al. (submitted) and will be briefly presented here. The ADR equations for O_2 and other solutes (alkalinity, DIC, Ca^{2+}) are written as follows

$$0 = D_s \frac{\partial^2 C}{\partial z^2} + P(z) - A(z) - R(z) \tag{56}$$

$$0 = D_s \frac{\partial^2 C}{\partial z^2} - A(z) + R(z) \tag{57}$$

Eqn. (56) is the O_2 ADR equation, and eqn. (57) is the ADR equation for alkalinity, DIC and Ca^{2+}. In these equations D_s is the molecular diffusion coefficient corrected for tortuosity (Burdige, 2006), C is pore water concentration, z is sediment depth starting at the sediment-water interface, *P(z)* is below-ground seagrass O_2 input, *R(z)* is O_2 consumption (eqn. 56) or solute production (alkalinity, DIC, and Ca^{2+}, eqn. 57), and *A(z)* is the term describing the non-local advective transport defined as:

$$A(z) = \alpha_z (C - C_0) \tag{58}$$

In this equation C_0 is the bottom water concentration, and α_z is the non-local exchange coefficient defined as:

$$\alpha_z = \alpha_o e^{-\beta z} \quad (59)$$

where α_0 and β are constants that define the depth attenuation of α_z (e.g., Reimers et al., 2004). Note that in a few studies (e.g., McNichol et al., 1988; Ogrinc and Faganeli, 2003) α_z is assumed to be a constant over some fixed sediment interval, hence β then equals to 0.

Below-ground O_2 flux (*P(z)*) is obtained from the seagrass LAI and below-ground biomass distribution (Fig. 42), assuming a 9-hr average daily solar irradiance at light-saturated level and a "per plant" below ground seagrass O_2 input rate of 1.2 mmol/m^2_{leaf}/h (Bodensteiner, 2006). Note that although both *Thalassia* and *Syringodium* were observed in WS-3 and WS-25 sediments, to a first order approximation, only the below-ground biomass distribution of *Thalassia* was used to calculate depth-dependent O_2 input by seagrasses. However at these sites O_2 input was calculated using the combined LAI of *Thalassia* and *Syringodium*.

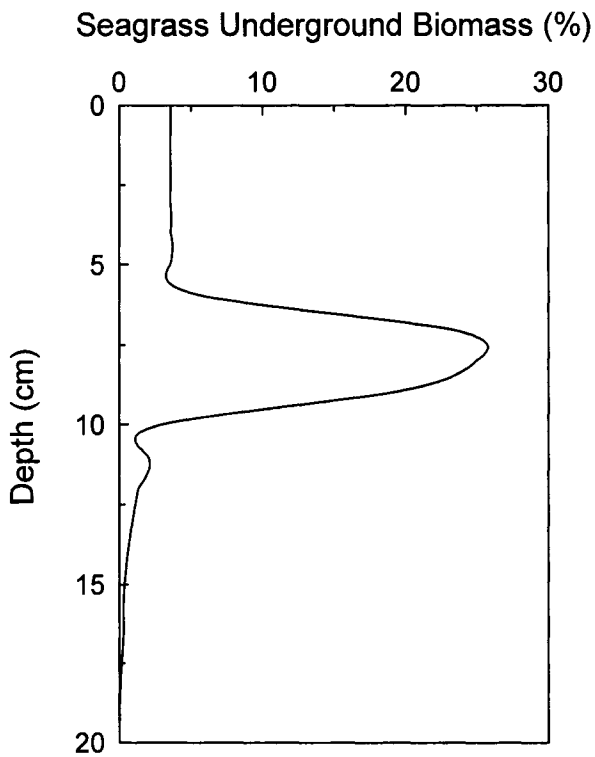

Fig. 42. *Thalassia* plant underground biomass distribution.

This model can be used to calculate depth-dependent reaction rates (i.e., O_2 consumption, alkalinity, DIC, and Ca^{2+} production). Then from the integration of the reaction rates to studied depth (i.e., 20 cm), I can obtain the depth-integrated rates. Given the way that the model is formulated, the only variables in this model are α_0 and β. Therefore the "best-fit" values of α_0 and β should predict depth-integrated rates that satisfy the following mass balance constraints:

$$2 \cdot DIRO = DIRD = DIRA \quad (60)$$

in which *DIRO*, *DIRA*, *DIRD*, and *DIRC* are the depth-integrated rates for O_2 consumption, alkalinity, DIC, and Ca^{2+} productions, respectively. α_0 and β values were arbitrarily constrained to the ranges of 0-20 d^{-1} and 0-1 cm^{-1} based on discussions in the literature (Burdige et al., submitted; Jahnke et al., 2005), and then the model was solved by varying α_0 and β values at 0.01 d^{-1} and 0.01 cm^{-1} step sizes, to achieve the minimum error (*err*) value as defined below

$$err = \frac{1}{3}\left\{\frac{|2DIRO - DIRA|}{0.5(2DIRO + DIRA)} + \frac{|2DIRO - DIRD|}{0.5(2DIRO + DIRD)} + \frac{|DIRD - DIRA|}{0.5(DIRD + DIRA)}\right\} \quad (61)$$

where each term inside the bracket represents the "error" of each of the three mass balance constraints (eqn. 60). A MatLab® script (Appendix E) was used in the model calculations following the approach in Burdige et al. (submitted). Note that depth integrated reaction rate is equivalent to the flux at sediment water interface (Burdige, 2006). As shown in rxn. (46), 1 unit of metabolic carbonate dissolution produces 2 units of alkalinity and DIC and consumes 1 unit of O_2. Therefore, carbonate dissolution flux (*CD*) was calculated as

$$CD = 0.5DIRA = 0.5DIRD = DIRO \quad (62)$$

The error in *CD* is defined as the standard deviation of the three *CD* values calculated using the different approaches in eqn. (62).

Depth integrated calcium production (*DIRC*) was not used in the fitting process, since based on Chapters II and III and studies by others (Rude and Aller, 1991; Walter et al., 1993; Walter et al., 2006) the occurrence of carbonate dissolution/ reprecipitation leads to unproportional pore water [Ca^{2+}] changes compared to the solid phase composition. Furthermore, the ability to incorporate this observation into mass balance constraints such as those in eqn. 60 requires accurate knowledge of the compositions of both the

dissolving phase as well as the secondary carbonate that reprecipitates. However, *DIRC* may be used to help better constrain the compositions of these phases as discussed in section 4.4.3.

4.4.2. Results of the Model Calculations - O_2 Consumption and Metabolic Dissolution

Metabolic O_2 consumption in the sediments (*DIRO*) is driven by three processes that deliver O_2 to the sediments - diffusion across the sediment-water interface, below-ground O_2 input from seagrasses, and permeability-related advection. The results are listed in Table 23.

The relationships between DIRO and LAI for LSI and WS sediments were found to be not significantly different by ANCOVA (MS = 171, MS err = 41, F = 4.17, df = 1, 25, P = 0.052). Similarly, relationships between CD and LAI for these two sets of sediments were not significantly different either by ANCOVA (MS = 163, MS err = 41, F = 4, df = 1, 25, P = 0.057). Therefore combing the WS results with previous LSI results (Burdige et al., submitted), *DIRO* and CD were both found to be positively correlated with seagrass density (Fig. 43a and Fig. 44). The slopes of the linear regression lines were significant ($P<0.0001$) and the y-intercepts were not significantly different from zero ($P>0.05$). While advective O_2 input in WS sediments was positively correlated with LAI (Fig. 43b), a negative slope exists for the LSI sediments. These relationships were found to be significantly different by ANCOVA (MS = 174, MS err = 41, F = 4.27, df = 1, 25, P = 0.049). Diffusive O_2 input is a minor contributor to *DIRO* (6% or less, at most) and was not correlated with LAI (Fig. 43c). This observation further confirmed earlier discussion that O_2 diffusion played a negligible role in the total O_2 input to these sediments (vs. advection and seagrass pumping, Table 24). Due to the approach with which seagrass O_2 input was defined, this input is a linear function of seagrass LAI (Fig. 43c).

In the LSI study, Burdige et al. (submitted) observed a negative correlation between advective O_2 input and seagrass LAI in vegetated sediments, while Fig. 43(b) shows that such a relationship was positive in the WS sediments. Burdige et al. (submitted) attributed this inverse relationship to a decreased pressure gradient at the sediment water interface with increasing LAI, caused by a reduction in horizontal flow through the

Table 23. O_2 input through diffusion, advection and seagrass pumping (unit: mmol/m^2/d) [a].

Site	LAI	DIRO	Advection	Diffusion	Plant
WS-2	0.96±0.04	12.5	2.2 (18%)	0.0 (0%)	10.3 (82%)
WS-3	1.37±0.08	41.8	27.0 (65%)	0.0 (0%)	14.8 (35%)
WS-4	1.72±0.06	57.1	38.5 (67%)	0.0 (0%)	18.6 (33%)
WS-5	0.03±0.02	3.2	2.9 (90%)	0.0 (0%)	0.3 (10%)
WS-6	0	nc	nc	nc	nc
WS-8	0.19±0.03	2.7	0.6 (22%)	0.08 (3%)	2.0 (75%)
WS-9	0	6.5	6.4 (98%)	0.11 (2%)	0.0 (0%)
WS-10	0.02±0.00	1.4	1.2 (84%)	0.01 (1%)	0.2 (15%)
WS-11	0.07±0.01	1.4	0.7 (45%)	0.07 (5%)	0.7 (50%)
WS-12	1.40±0.05	20.9	5.7 (27%)	0.07 (0%)	15.1 (72%)
WS-13	0.53±0.04	7.1	1.3 (19%)	0.0 (0%)	5.8 (81%)
WS-14	0.41±0.02	5.3	0.9 (16%)	0.01 (0%)	4.4 (83%)
WS-15	0.86±0.04	10.5	1.3 (12%)	0.00 (0%)	9.2 (88%)
WS-16	0	nc	nc	nc	nc
WS-17	0.33±0.01	nc	nc	nc	nc
WS-18	0.17±0.01	2.6	0.7 (26%)	0.08 (3%)	1.9 (71%)
WS-20	0.77±0.04	nc	nc	nc	nc
WS-21	0.07±0.01	1.2	0.4 (31%)	0.08 (6%)	0.8 (62%)
WS-24	0.25±0.02	15.7	12.9 (82%)	0.12 (1%)	2.7 (17%)
WS-25	3.73±0.40	80.1	39.8 (50%)	0.0 (0%)	40.2 (50%)

nc=no convergence.

The ADR model did not converge for the data from WS-6, WS-16, WS-17, and WS-20 sites using the ranges of α_0 and β values described in the text (see section 4.4.1 for details).

[a] The data in parentheses are percentage of O_2 input by each of the transport mechanisms (see eqn. 56 and section 4.4.1 for details).

Table 24. Reaction rates calculated using the ADR model (units: mmol/m^2/d) [a].

Site	LAI	DIRO	DIRA	DIRD	err	CD	DIRC	J_{rp} (1.0)	J_{rp} (0.92)
WS-2	0.96±0.04	12.5	26.3	24.0	3%	12.6±0.3	6.9	34.9	104.8
WS-3	1.37±0.08	41.8	81.0	86.4	2%	41.8±0.8	31.9	40.8	122.4
WS-4	1.72±0.06	57.1	113.9	114.2	0%	57.0±0.1	63.4	hm	hm
WS-5	0.03±0.02	3.2	3.5	6.4	39%	2.7±0.5	2.7	hm	hm
WS-6	0	nc	nc	nc	nc	nc	nc	nc	nc
WS-8	0.19±0.03	2.7	5.3	5.6	2%	2.7±0.0	1.4	7.9	23.64
WS-9	0	6.5	13.0	13.2	1%	6.5±0.1	nn	nn	nn
WS-10	0.02±0.00	1.4	2.8	2.9	0%	1.4±0.0	0.1	9.3	27.9
WS-11	0.07±0.01	1.4	2.9	2.9	1%	1.5±0.0	28.9	hm	hm
WS-12	1.40±0.05	20.9	41.7	41.8	0%	20.9±0.0	51.9	hm	hm
WS-13	0.53±0.04	7.1	14.1	14.3	0%	7.1±0.0	5.0	10.6	31.7
WS-14	0.41±0.02	5.3	10.5	10.7	1%	5.3±0.0	4.5	1.0	3.1
WS-15	0.86±0.04	10.5	20.9	21.8	3%	10.6±0.3	7.3	16.8	50.4
WS-16	0	nc	nc	nc	nc	nc	nc	nc	nc
WS-17	0.33±0.01	nc	nc	nc	nc	nc	nc	nc	nc
WS-18	0.17±0.01	2.6	5.1	5.4	1%	2.6±0.0	1.5	6.4	19.3
WS-20	0.77±0.04	nc	nc	nc	nc	nc	nc	nc	nc
WS-21	0.07±0.01	1.2	2.6	2.4	2%	1.2±0.0	0.7	3.4	10.2
WS-24	0.25±0.02	15.7	31.4	31.4	0%	15.7±0.0	7.8	50.0	149.8
WS-25	3.73±0.40	80.1	159.8	161.0	0%	80.2±0.4	56.7	115.5	346.6

nc=the model did not converge for the data from these sites (WS-6, WS-16, WS-17, and WS-20, i.e., see Table 23);
nn=a negative value of DIRC was obtained (WS-9);
hm=using the calculated DIRC, a secondary carbonate phases with a lower Ca content than the starting phase was predicted. This is not supported by experimental evidences (see section 4.4.3 for details).

* The two sets of J_{rp} values were calculated assuming two different secondary carbonate, i.e., $CaCO_3$ (1.0) and $Ca_{0.92}Mg_{0.08}CO_3$ (0.92).

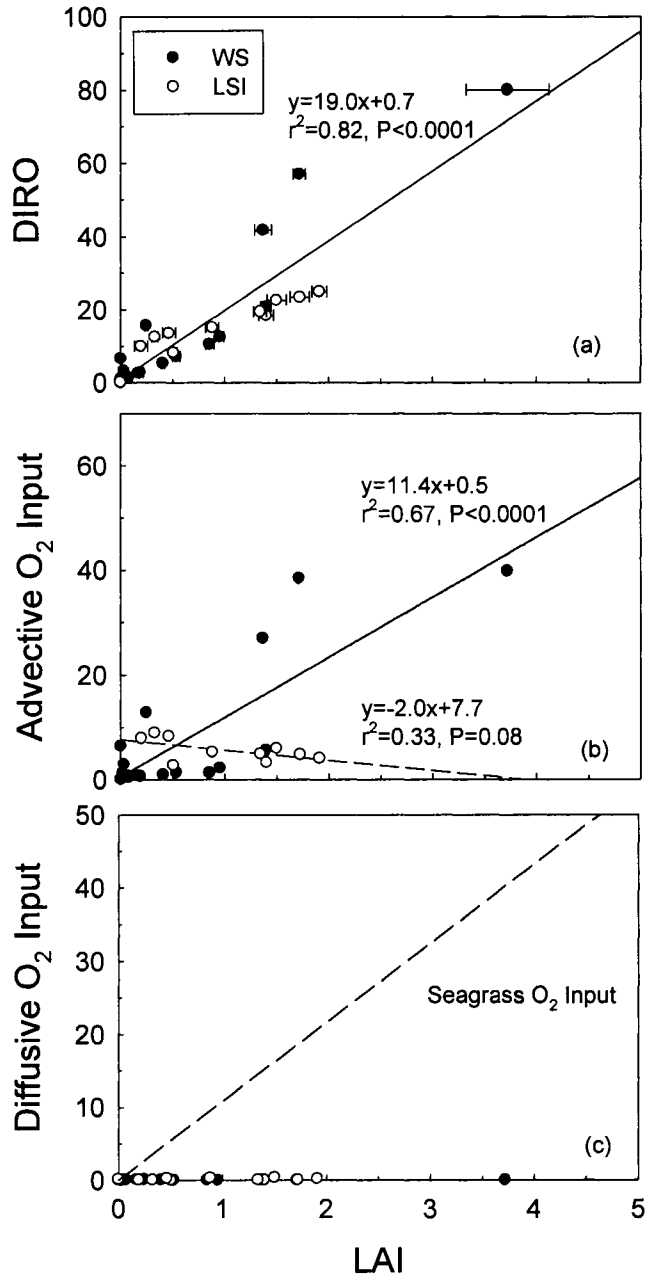

Fig. 43. The relationships between LAI and (a) DIRO, (b) advective O_2 input, and (c) diffusive O_2 input. The closed circles represent the result from this study (WS; Bahamas Bank sediments) and the open circles are from Burdige et al. (submitted) from LSI sediments. All fluxes on y-axes are mmol/m^2/d. Note the inverse relationship between advective O_2 input and LAI for LSI sediments.

canopy as seagrass density increases. This can be seen in Darcy's Law, which shows that advective pore water flow is a linear function of the near seabed pressure gradient,

$$q = \frac{k}{\varphi\eta}\frac{\partial P}{\partial z} \quad (63)$$

where q is pore water flow rate, k is permeability factor, φ is sediment porosity, η is pore water viscosity, and $\partial P/\partial z$ is the near-seabed pressure gradient (Boudreau, 1997). This explanation therefore resembles a scenario in Koch and Gust (1999), in which a tide-dominated system (unidirectional flows) leads to "skimming flows" over the seagrass canopy, thus decreasing the mixing between the water above and within the meadow. Similar effect may also impact the exchange of pore waters and bottom waters within the meadow since the deflection of the bottom water motion by the seagrass canopy renders this portion of the water column in the meadow relatively static. Therefore the pressure gradients are expected to decrease as the density of the seagrasses increases. Consistent with this explanation is the fact that water flow around the LSI sites is strongly dominated by diurnal tidal flow, due to the location of these sites near cuts between the Exuma Cays and Exuma Sound.

On the other hand, the WS sites are farther away from land masses (Fig. 31; for a comparison of site locations see Fig. 2 in Chapter II) and tidal motion presumably is much less important in terms of generating pressure gradients that facilitate advective pore water flow. However, a different hydrodynamic situation, namely wave-dominated motion (oscillatory flow), may occur at these sites. This motion actually increases the exchange between the water above and within the meadow by "opening" and "closing" the canopy during this oscillatory flow (Koch and Gust, 1999), and may subsequently enhance the pore water-bottom water exchange. The strong prevailing winds on the Bahamas Bank that persisted throughout our WS cruise may have also further contributed to bottom water motion at these studied sites (Dierssen et al., ms. in prep.). In shallow waters, such strong winds are known to generate Langmuir "supercells", as the wind strength increases, eventually leading to oscillatory water motion that reaches the full depth of the water column and may even cause resuspension of fine grained sediments (Gargett et al., 2004).

The model results showed that total, advective, diffusive O_2 input, and carbonate

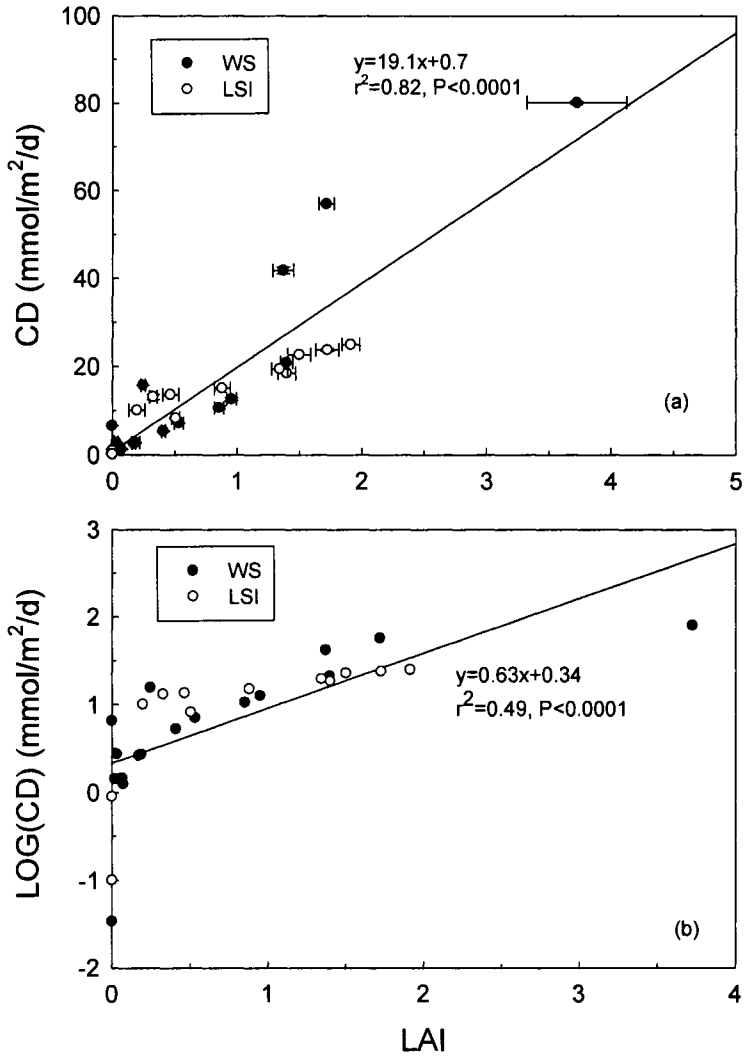

Fig. 44. The relationship between carbonate dissolution and seagrass LAI. Linear regressions (solid lines) produce the best fit at P<0.0001 level. The upper panel shows a linear regression between CD and LAI (a); and the lower panel shows a linear regression between the log-transformed CD and LAI (b). In (b) the data satisfy normality and constant variance tests.

dissolution rate do not show any correlation with sediment permeability, and the high permeability sediments at WS-5 and WS-10 (28×10^{-10} m^2 and 39×10^{-10} m^2) show low overall O_2 input rates and rates of carbonate dissolution (Fig. 45). Although Darcy's Law indicates that the pore water advective flow is a linear function of sediment permeability (eqn. 63), this flow is also controlled by hydrodynamic activity, benthic topography, and

seagrass vegetation that may all potentially affect the near seabed pressure gradient (i.e., the term $\partial P/\partial z$ in eqn. 63; Falter and Sansone, 2000; Huettel and Webster, 2001; Jahnke et al., 2005; Koch and Gust, 1999; Rasheed et al., 2004; Walter and Burton, 1990). Therefore the lack of observed correlation between the modeled rates and sediment permeability is not necessarily surprising.

Based on above discussion, it is clear that more field studies are needed. In particular, the application of a recently developed eddy correlation technique (Berg et al., 2003) can be used to measure sediment O_2 uptake in a non-invasive way in these coarse grained sandy sediments. These results can then be compared with the model-derived estimates of sediment O_2 uptake to further constrain results from the ADR model.

4.4.3. Results of the Model Calculations - Carbonate Reprecipitation

Pore water $\Delta[Ca^{2+}]/\Delta DIC$ plots (Fig. 36) suggest that the apparent dissolving carbonate phase(s) has a much lower Ca content (62 mole%) than that of the HMC in these sediments (88 mole% Ca, see section 4.2.2), and the lower net Ca^{2+} production rates in the pore waters may be explained by incongruent carbonate dissolution (section 4.2.2). Therefore from the depth integrated Ca^{2+} production and carbonate dissolution rates (*DIRC* and *CD*), the following equation can be written based on the discussion in Chapter III (eqn. 40):

$$DIRC = a \times (CD + J_{rp}) - b \times J_{rp} \qquad (64)$$

where J_{rp} is depth integrated reprecipitation rate, and a and b are the calcium content in the original and reprecipitated carbonates, respectively. In solving this equation for J_{rp}, I assume that the dissolving carbonate had a Ca content based on our XRD results in Chapter II and III (i.e., a=0.88). J_{rp} was then calculated using eqn. (64) assuming two possible compositions for the reprecipitated carbonate phase - $Ca_{0.92}Mg_{0.08}CO_3$ (i.e., b=0.92) and $CaCO_3$ (i.e., b=1). The former phase corresponds to the composition of the HMC overgrowth formed in Bahamian sediments (Morse and Mucci, 1984; Mucci, 1987) and is also consistent with the composition of the secondary carbonate phase predicated by the results of the incubation studies in Chapter III. The latter is a carbonate phase with no Mg (i.e., calcite). It is noted, however, that for some sites (e.g., WS-4, WS-5, WS-11, and WS-12) the calculated *DIRC/CD* ratios were greater than 0.88 (the Ca content in the

dissolving materials). Although eqn. (64) is still mathematically valid, it requires the reprecipitated carbonate to have a lower Ca content than the dissolving phase. Since this is not supported by experimental evidences (Morse and Mucci, 1984; Mucci, 1987; Tribble and Mackenzie, 1998), J_{rp} was not calculated for these sites.

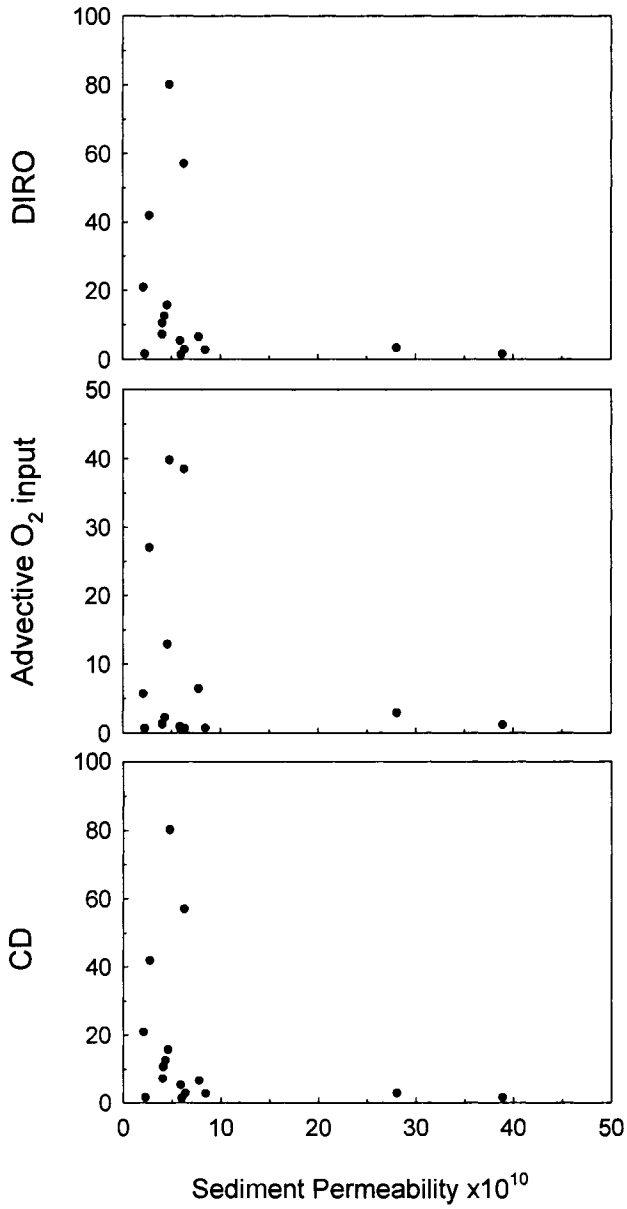

Fig. 45. The relationships between sediment permeability and (a) DIRO, (b) advective O_2 input, and (c) carbonate dissolution. All fluxes on the y-axes are mmol/m^2/d.

The calculated carbonate reprecipitation fluxes (J_{rp}) ranged from 1.0-3.1 mmol/m^2/d at site WS-14 to 116-347 mmol/m^2/d at site WS-25. In studies of Florida Bay sediments, Rude and Aller (1991) calculated that the calcite reprecipitation flux was 17.4 mmol/m^2/d when there was no fluorapatite formation, and a much higher J_{rp} was also calculated at the same time for a scenario with fluorapatite formation (46 mmol/m^2/d). Similarly, Walter et al. (1993) estimated a carbonate reprecipitation flux of 400 μmol/cm^2/yr (equivalent to 11.0 mmol/m^2/d) through ^{45}Ca isotope exchange experiments in both Florida Bay and Bahamas Bank sediments.

At any site the estimates of J_{rp} depend on the choice of the secondary carbonate phase that is assumed to reprecipitate (i.e., $CaCO_3$ or $Ca_{0.92}Mg_{0.08}CO_3$). These reprecipitation calculations are also very sensitive to the assumed composition of the dissolving carbonate. For example, if the dissolving HMC phase is assumed to be 15 mole% Mg (e.g. Bischoff et al., 1993), then the range in J_{rp} becomes 0 to 76 mmol/m^2/d for $CaCO_3$ and 0 to 164 mmol/m^2/d for $Ca_{0.92}Mg_{0.08}CO_3$. Therefore the reprecipitation rates here are taken at a relative sense and their relationship with seagrass densities and sediment properties can only be used in a qualitative fashion. For the simplicity of the following discussion, the J_{rp} values based on $Ca_{0.92}Mg_{0.08}CO_3$ reprecipitation were used.

J_{rp} increased with increasing seagrass density (i.e., LAI, Fig. 46), consistent with our previous field study in LSI sediments; and the rate did not show any significant correlation with sediment permeability (Table 24). When plotting J_{rp} and *CD* together, a positive correlation clearly exists (Fig. 47). Note the LSI sites with significant amounts of reprecipitation were all densely vegetated sites (AC, CM, and NC, see Burdige et al., submitted, for details). The correlation between carbonate dissolution and reprecipitation supports the suggestion in Chapter II that enhanced metabolic activity (i.e., metabolic carbonate dissolution) may cleanse the carbonate grain surfaces that are coated with dissolved organic matter that can inhibit precipitation (e.g., Berner et al., 1978; Mucci, 1987, Morse, 1984); this will then facilitate the reprecipitation process.

More importantly, the results in Fig. 47 indicates that J_{rp} /*CD* is roughly constant (= 4.4) in both the WS and LSI sediments. This ratio is also the same as R_{rx} (the reprecipitation ratio) discussed in Chapters II and III, and Table 25 clearly indicates that

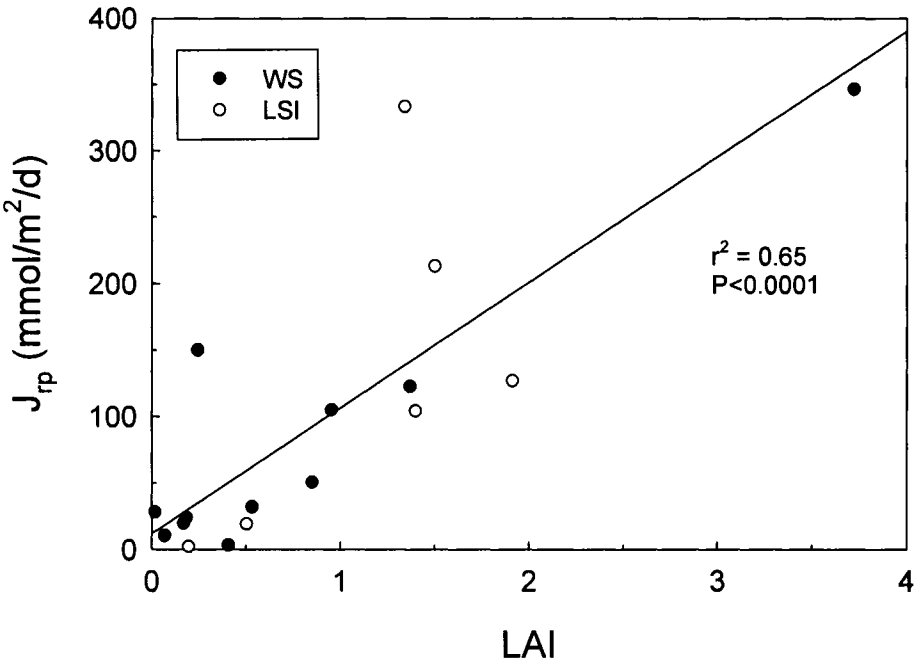

Fig. 46. The relationship between the carbonate reprecipitation flux and seagrass LAI. The solid line is the best-fit straight line through all data points. Assume $Ca_{0.92}Mg_{0.08}CO_3$ is the secondary carbonate. The closed circles are from this study, and the open circles are from Burdige et al. (submitted).

Table 25. Reprecipitation ratio (R_{rx}) in carbonate sediments.

Location	R_{rx} (or J_{rp}/CD)	Method	Source
LSI [a]	3.3-3.8	Carbon isotope model	Chapter II
WS [b]	0.9-2.1	Carbon isotope model	Chapter III
WS and LSI [c]	4.4±0.9	ADR model	This study
Florida Bay/Bahamas Bank [d]	1.1-2.0	Calcium isotope model	(Walter et al., 1993)
Florida Bay [e]	3.1-6.6	Trace element (F)	(Rude and Aller, 1990)

a. Derived from the application of a closed-system model to pore water profiles.
b. Derived from closed-system incubations.
c. Calculated using the pore water ADR model and Ca mass balance.
d. Derived from a closed-system incubation.
e. Derived from a trace element (F) study.

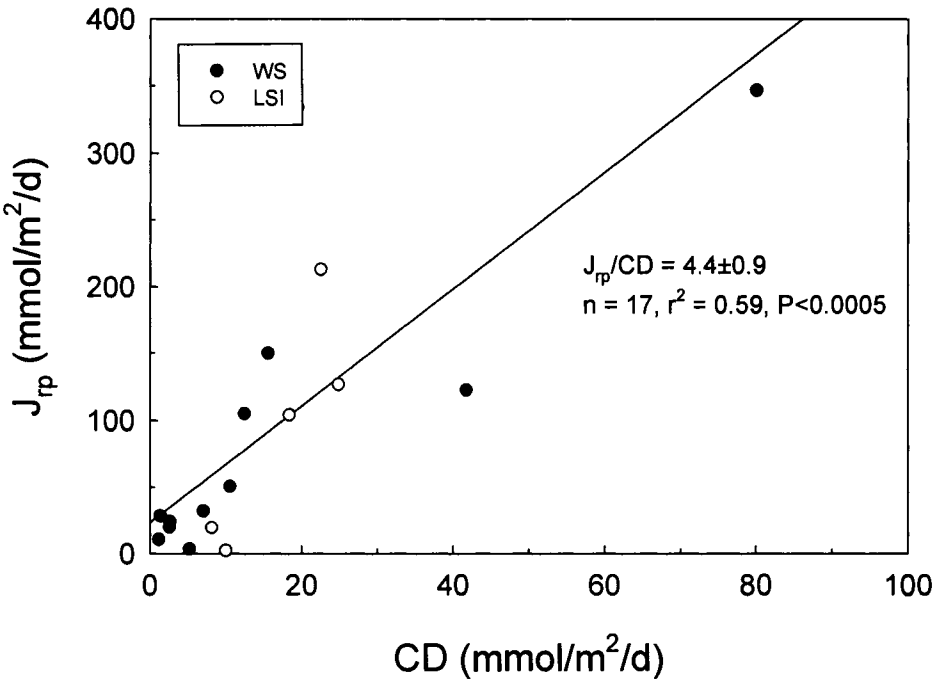

Fig. 47. Carbonate reprecipitation versus dissolution. The solid line is the best-fit straight line through all data point. The solid line is the best-fit straight line through all data points. Assume $Ca_{0.92}Mg_{0.08}CO_3$ is the secondary carbonate. The closed circles are from this study, and the open circles are from Burdige et al. (submitted).

the values are roughly consistent no only with each other, but with literature reported values (Walter et al., 1993; Rude and Aller, 1990). Despite the distinctively different approaches used in all of these studies, this agreement suggests that carbonate reprecipitation has a common feature in carbonate diagenesis in these tropical shallow water carbonate sediments, i.e., the rate of reprecipitation is rather constant relative to the rates of net dissolution, as well as gross dissolution.

4.4.4. The Controlling Factors of Carbonate Dissolution/Reprecipitation

Seagrass vegetation appears to be the dominant controlling factor in metabolic carbonate dissolution (Fig. 43a and Fig. 44), further confirming previous suggestions that seagrasses play an important role in resolving the mass balance problem between the O_2 input and amount of carbonate dissolution (Ku et al., 1999; Walter et al., 1993; Walter and Burton, 1990). The results of this study were also consistent with our previous work

in LSI sediments (Burdige et al., submitted). Seagrass not only enhances O_2 input, but they also directly or indirectly enhance organic matter deposition in the sediments, which also enhance carbonate dissolution.

According to the carbonate dissolution/reprecipitation model, when reprecipitation occurs pore water DIC becomes more enriched in ^{13}C, and the apparent $\delta^{13}C$ of the organic carbon undergoing remineralization ($\delta^{13}C_{OM}$ in eqn. 55) is greater than that of the seagrass organic matter. Based on the calculations using the ADR model, Group (1) sediments all showed moderate to high carbonate reprecipitation fluxes (3.1-104.8 mmol/m^2/d, Table 26), and these results agreed well with prediction using the pore water DIC ^{13}C data that carbonate reprecipitation occurs in these sediments. Due to the small and irregular [Ca^{2+}] changes (Δ[Ca^{2+}] ~0.2 mmol/kg) in the Group (3) sediments, the *DIRC* calculation was imprecise, making the calculation of reprecipitation flux (J_{rp}) unreliable and its occurrence in these sediments unreliable.

In the Group (2) sediments, mass balance calculation with the $\delta^{13}C$ of pore water DIC showed no evidence of carbonate reprecipitation, assuming that only seagrass organic matter undergoes remineralization in these sediments (section 4.2). However, for two densely vegetated sites (WS-3 and WS-25) and a moderately vegetated site (WS-24, the ADR model yielded high carbonate reprecipitation fluxes at these sites (122-347 mmol/m^2/d). A possible explanation for this observation is that if seagrass organic matter is remineralized and reprecipitation also occurs, then a lighter carbon source (e.g., algal carbon) must also be remineralized, to counter the heavy carbon being added to the pore waters by carbonate dissolution and reprecipitation. When examining the locations of the Group (2) sites, it can be seen that all are located along the Bank margin to the northwest of Andros Island. Abundant nutrient supply from the adjacent oceanic waters in this region may support relatively higher algal production as compared to the generally oligotrophic Bahamas Bank waters, and consistent with this, the highest seagrass LAI values observed were on this portion of the Bank (Table 16). Therefore remineralization of a mixture of organic matter (algal and seagrass carbon) will contribute DIC to the pore water DIC pool that is lighter than that resulting solely from the remineralization of seagrass material. The supply of ^{13}C-depleted organic carbon to the sediments may originate from the wind-driven Langmuir supercell as discussed above. It is noted,

Table 26. A comparison between the predictions of carbonate reprecipitation in the Bahamas Bank sediments using the stable isotope technique and the ADR model.

Group	Site	LAI	$\delta^{13}C_{OM}$ (‰) [a]	$\delta^{13}C_{seagrass}$ (‰) [a]	CD [b]	J_{rp} (0.92) [b]
(1)	WS-2	0.96±0.04	-0.92±0.25	-6.32±0.12	12.6±0.3	104.8
	WS-4	1.72±0.06	-2.89±2.80	-8.92±0.19	57.0±0.1	hm
	WS-6	0	-4.83±1.52	-7.94±1.95	nc	nc
	WS-8	0.19±0.03	-3.12±1.52	-6.34±1.55	2.7±0.0	23.64
	WS-9	0	-1.99±4.97	-6.45±1.58	6.5±0.1	nn
	WS-11	0.07±0.01	-1.81±0.34	-7.11±0.12	1.5±0.0	hm
	WS-12	1.40±0.05	3.57±3.67	-5.63±0.09	20.9±0.0	hm
	WS-13	0.53±0.04	-1.73±0.52	-4.86±0.52	7.1±0.0	31.7
	WS-14	0.41±0.02	-4.52±0.79	-6.62±1.62	5.3±0.0	3.1
	WS-15	0.86±0.04	-1.13±0.55	-5.63±1.38	10.6±0.3	50.4
	WS-18	0.17±0.01	-3.51±0.75	-6.29±1.54	2.6±0.0	19.3
(2)	WS-3	1.37±0.08	-11.83±2.96	-7.80±2.22	41.8±0.8	122.4
	WS-16	0	-6.04±3.14	-6.67±1.64	nc	nc
	WS-17	0.33±0.01	-5.30±54.04	-7.72±1.89	nc	nc
	WS-20	0.77±0.04	-8.03±1.38	-6.29±0.06	nc	nc
	WS-24	0.25±0.02	-6.54±2.33	-7.01±1.72	15.7±0.0	149.8
	WS-25	3.73±0.40	-9.66±0.82	-8.49±1.38	80.2±0.4	346.6
(3)	WS-5	0.03±0.02	-13.58±2.03	-6.67±1.64	2.7±0.5	hm
	WS-10	0.02±0.00	-15.15±3.31	-6.73±1.65	1.4±0.0	27.9

Note nc, nn, and hm are defined in Table 24.

[a] $\delta^{13}C$ values of the organic matter apparently undergoing remineralization ($\delta^{13}C_{OM}$) and seagrasses ($\delta^{13}C_{seagrass}$) are from Table 19.

[b] Carbonate dissolution and reprecipitation rates are from Table 24.

however, that if the input of algal materials indeed plays a role in sedimentary organic carbon remineralization, then the mixing of seagrass carbon and algal carbon should demonstrate a seasonal pattern, since the wind speeds on the Bahamas Bank vary over a annual cycle (strongest in the Spring and Fall, see Dierssen et al., ms. in prep.).
In the context of the discussion above, when Fig. 41 is re-examined, it shows that the apparent $\delta^{13}C_{OM}$ becomes more enriched in ^{13}C as sediment grain size decreases. Expressed another way, it appears that reprecipitation that contribute heavy DIC to the pore waters becomes more evident in the finer-grained sediments. This observation is consistent with Ostwald ripening process, in which smaller grains dissolve and secondary carbonate forms on larger grains, thereby reducing carbonate surface energy (Hover et al., 2001; Walter et al., 1993).

Nevertheless, on a much broader expanse of the Bahamas Bank, it seems that it is not always appropriate to assume that seagrass carbon is the sole carbon source being remineralized in the sediments. Therefore to gain the knowledge of the exact $\delta^{13}C$ value of the remineralizing carbon, compound-specific isotope studies on bacterial biomass such as those in Holmer et al. (2001) may help to better constrain the actual organic carbon being remineralized in the sediments and help to improve the application of stable carbon isotopes in such mass balance studies.

4.5. Carbonate Dissolution on the Bahamas Bank - the Regional Significance

Our previous study of LSI sediments (Burdige et al., submitted) used a relationship between LAI and carbonate dissolution rate (CD) such as that in Fig. 44a to predict the carbonate dissolution flux for the entire Bahamas Bank. The result agreed reasonably well with literature reported values (Ku et al., 1999; Milliman, 1993; Rude and Aller, 1991; Walter and Burton, 1990; Yates and Halley, 2006). Here the data set from the larger geographic expanse of the Bahamas Bank will be used to re-evaluate the dissolution flux.

Using the same approach as in Burdige et al. (submitted), if I assume that the average LAI in the seagrass sediments on the Bahamas Bank is 0.7, and that the areas of vegetated vs. unvegetated sediments are equal to each other, then the regression line in Fig. 44 predicts that the average carbonate dissolution flux for the Bahamas Bank is 2.7

mol/m^2/yr, as compared to the values of 3-5 mol/m^2/yr calculated in Burdige et al. (submitted).

The carbonate dissolution flux calculated here suggests that *in situ* carbonate dissolution is an important removal process in the carbonate budget on the Bahamas Bank. In particular, if I assume that the bank wide gross carbonate production rate is 5 mol/m^2/yr (Broecker and Takahashi, 1966; Milliman, 1993), then dissolution may equal or exceed carbonate export flux to deeper waters (Burdige et al., submitted; also see, Yates and Halley, 2006). Furthermore, the rough estimate by Milliman (1993) that 50% of the gross carbonate production is exported to the surrounding waters may be an overestimate; alternatively, if this export flux is as large as Milliman (1993) assumes, then the gross carbonate production rate may be higher than the presently accepted values under steady-state conditions. The possibility also exists that the system is not in steady-state and is currently losing carbonate (Sanders, 2003).

Integrating this carbonate dissolution flux over the area of the Bahamas Bank (~210,000 km^2, Bathurst, 1971), and assuming that the system is at steady-state, then the total alkalinity production in these sediments due to carbonate dissolution is ~1.1×10^{12} mol/yr. This value is similar to the alkalinity export from the Mississippi River due to continental weathering (Raymond and Cole, 2003). If this carbonate dissolution flux is further scaled up to include all carbonate banks around the globe (assuming 800,000 km^2 of shallow water carbonate banks and bays), then this alkalinity production is 4.1×10^{12} mmol/yr. Compared with the global oceanic alkalinity production rate of $50\text{-}72\times10^{12}$ mmol/yr (Chen, 2002), carbonate banks and bays contribute 6-8% of the global oceanic alkalinity production, although they only account for ~0.2% of the modern ocean surface area (Milliman, 1993). Therefore they represent a potentially significant alkalinity source to the oceanic environment.

At the same time though, calcium carbonate formation in the water column both consumes carbonate alkalinity and generates CO_2 according to:

$$Ca^{2+} + 2HCO_3^- \rightarrow CaCO_3 + CO_2 + H_2O \qquad (65)$$

Therefore while the deposition of carbonate sediments in the shallow water carbonate banks act as a source of CO_2 to the atmosphere (Zeebe and Wolf-Gladrow, 2001), any

subsequent carbonate dissolution in shallow water areas thus mitigates the role of these areas as CO_2 sources.

Based on discussions here (also see rxn. 46), ~50% of the inorganic carbon associated with alkalinity production from metabolic carbonate dissolution comes from the oxidation of organic matter that is largely derived from seagrass photosynthesis (Chapter II; Holmer et al., 2001). Furthermore, ~70% of the inorganic carbon for seagrass photosynthesis comes from CO_2 (e.g., Zimmerman et al., 1997). As a result, the coupling between seagrass production and metabolic carbonate dissolution acts as a "carbon shuttle" that transfers atmospheric CO_2 into marine DIC pool.

Given these observations, an additional situation may arise, because the growth of seagrasses in tropical carbonate sediments is generally P-limited (Fourqurean and Zieman, 2002; Fourqurean et al., 1992; Jensen et al., 1998). With increasing atmospheric CO_2 due to anthropogenic activities, seagrass production may increase and subsequently enhance carbonate dissolution, which further liberates carbonate-bound phosphate. In return, the release of this phosphate may promote further seagrass production that takes up more CO_2 and then enhances carbonate dissolution. Overall then, this series of reactions may exert a negative feedback on rising atmospheric CO_2 (see Burdige et al., submitted, for a more detailed discussion).

5. CONCLUSIONS

Pore water saturation state calculations indicate that a carbonate phase more soluble than aragonite, presumably HMC, is undergoing dissolution in Bahamas Bank sediments.

Seagrass vegetation enhances both carbonate dissolution and pore water carbonate reprecipitation. At three sites with moderate to dense seagrass vegetation, an inverse pore water model suggests that carbonate reprecipitation was occurring, although the calculated $\delta^{13}C$ values of the organic matter apparently undergoing remineralization appeared to be similar to that of the seagrass carbon at these sites. Input of light carbon such as that from algae might contribute to the pore water DIC pool, which then counters the ^{13}C enrichment of pore water DIC caused by carbonate dissolution/reprecipitation. Furthermore, carbonate reprecipitation versus net dissolution ratio appears constant

across the Bank, suggesting that carbonate reprecipitation has a common feature in carbonate diagenesis in these tropical shallow water carbonate sediments

Sediment permeability did not show any obvious correlation with the reaction rates (O_2 consumption and metabolic carbonate dissolution). This is expected since solute transport rates not only depend on sediment permeability, but also near seabed pressure gradients.

Different relationship between pore water advection and LAI were found in LSI and WS sediments. Such difference may be caused by different types of bottom water flow at the two sets of sampling sites, i.e., wave-dominated oscillatory flow at the WS sites, and tidal-dominated skimming flow at the LSI sites.

Integration of carbonate dissolution rate across the Bahamas Bank suggests that dissolution, rather than export, may dominate carbonate removal after deposition in these shallow water environments. Alkalinity production through metabolic carbonate dissolution in the tropical carbonate bank and bays contributes significantly to global oceanic alkalinity production, despite their small area in the modern ocean. At the same time, syndepositional carbonate dissolution mitigates the role of the shallow water carbonate banks and bays as a CO_2 source to the atmosphere. The mechanism by which seagrasses enhance carbonate dissolution potentially exerts a negative feedback on rising atmospheric CO_2, by enhancing CO_2 uptake during the carbonate dissolution process.

CHAPTER V
SUMMARY

This dissertation presented three independent, yet closely related, studies focusing on the role that the seagrasses play in carbonate dissolution and early diagenesis of shallow water carbonate sediments. This chapter summarizes the major conclusions drawn from these studies.

First, in Chapter II, in a relatively restricted environment (LSI), ^{13}C enrichment in the pore water DIC pool was found to be associated with high seagrass densities, while sediments with no or low seagrass densities did not show such enrichment. This ^{13}C enrichment was successfully explained by a carbonate dissolution/reprecipitation mechanism, during which a more soluble metastable carbonate phase dissolves at the same time that a less soluble and more stable phase precipitates.

In the closed-system incubation study described in Chapter III, this carbonate dissolution/reprecipitation process was more quantitatively examined using a model developed in the previous chapter, and was found to adequately explain the experimental results (i.e., the model could adequately explain the occurrence of ^{13}C enrichment in pore water DIC as a result of dissolution/reprecipitation). These results further indicated that the reprecipitated secondary carbonate phase was only slightly depleted in Mg relative to the original HMC that dissolved. The results of this study also confirmed the 1:1 reaction stoichiometry between O_2 consumption and carbonate dissolution. Organic carbon remineralization was therefore found to be the rate limiting step in metabolic carbonate dissolution.

Finally, to study the extent to which carbonate dissolution/reprecipitation occurs across a much broader area of the Bahamas Bank, an inverse pore water model was applied to set of pore water profiles to examine rates of sediment biogeochemical processes at sites with a range of seagrass densities and sediment types (Chapter IV). The results of this study showed that the rates of both carbonate dissolution and reprecipitation correlate significantly with seagrass density (LAI). These findings support the conclusion derived from the LSI study that seagrass vegetation has a significant

impact on the geochemistry of shallow water carbonate platforms. However, the assumption that seagrass carbon is the sole carbon source for sediment remineralization may not be appropriate over the larger geographical settings of the Bahamas Bank. There is probably significant input of algal detritus to the sediments in some of the sampling sites. Relationships between LAI and pore water advection showed distinctively different patterns for the Bank sites and the LSI sites. This appeared to be related to difference in the types of bottom water flow at the two sets of sampling sites. Based on the results from this chapter, I also determined a better constrained carbonate loss term for a shallow water carbonate budget, i.e., ~50% of gross carbonate production is being dissolved in the shallow water sediments. At the same time, when the carbonate dissolution flux was integrated over all shallow water banks and bays on a global scale, significant alkalinity production (6-8% of global production) was observed. This dissolution also has the potential to mitigate the CO_2 input from carbonate depositional environments to the atmosphere that occurs as a result of carbonate precipitation.

In light of these observations, further investigations of the following problems are necessary, to better understand the biogeochemistry of carbonate sediments and the associated sediment-seagrasses interactions, as well as the impacts of these sedimentary processes on the regional and global carbon cycle:

1. Studies of mass transport mechanisms. Since sediments on the Bahamas Bank are highly permeable, advection is the dominant mass transport processes near the sediment-water interface. In Bahamas Bank and LSI sediments, two distinctively different relationships between seagrass density and pore water advection were observed. To better understand pore water advection in these coarse-grained sediments, physical processes such as wave action, tidal forcing, and Langmuir circulation need to be better quantified and further examined in the context of pore-bottom water exchange. A detailed understanding of this exchange will help us to better define the alkalinity flux from carbonate dissolution. This information can be used in models of carbon and carbonate cycle in these types of environments.

2. Studies of the isotopic composition of the organic carbon consumed in sedimentary respiration processes, preferably using bacteria specific polar lipid derived fatty acids (PLFA). Across the broader Bahamas Bank, I have found that the simple assumption that

seagrasses dominate the organic carbon supply to seagrass vegetated sediments was not always appropriate. Instead, remineralization of other lighter carbon sources (e.g., algal carbon) may also contribute to the pore water DIC pool in these sediments. Therefore to address the problem about what "types" of carbon are being remineralized in the sediments, a direct approach is to study the microbes that consume this organic carbon as well as produce the metabolic CO_2.

3. Dissolution kinetics and solubility of HMC. Because questions about the solubility of HMC in seawater remain unresolved, the dissolution kinetics of HMC, which is a function of the degree of pore water undersaturation, is unclear. A more quantitative understanding of solubility and dissolution rate of HMC in seawater may help further constrain the calculated carbonate dissolution rate used in future pore water models.

REFERENCES

Adler, M., Hensen, C., Wenzhofer, F., Pfeifer, K., and Schulz, H. D. (2001) Modeling of calcite dissolution by oxic respiration in supralysoclinal deep-sea sediments. *Mar. Geol.* **177**, 167-189.

Aller, R. C. (1982) Carbonate dissolution in nearshore terrigenous muds: The role of physical and biological reworking. *J. Geol.* **90**, 79-95.

Anderson, W. T. and Fourqurean, J. W. (2003) Intra- and interannual variability in seagrass carbon and nitrogen stable isotopes from south Florida, a preliminary study. *Org. Geochem.* **34**, 185-194.

Andersson, A. J. and Mackenzie, F. T. (2004) Shallow-water oceans: a source or sink of atmospheric CO_2. *Front. Ecol. Environ.* **2**, 248-353.

Andersson, A. J., Mackenzie, F. T., and Ver, L. M. (2003) Solution of shallow-water carbonates: an insignificant buffer against rising atmospheric CO_2. *Geology* **31**, 513-516.

Andrews, J. E. (1991) Geochemical indicators of depositional and early diagenetic facies in Holocene carbonate muds, and their preservation potential during stabilisation. *Chem. Geol.* **93**, 267-289.

Archer, D., Emerson, S., and Reimers, C. (1989) Dissolution of calcite in deep-sea sediments: pH and O_2 microelectrode results. *Geochim. Cosmochim. Acta* **53**, 2831-2845.

Archer, D., Kheshgi, H., and Maier-Reimer, E. (1998) Dynamics of fossil fuel CO_2 neutralization by marine $CaCO_3$. *Global Biogeochem. Cycl.* **12**, 259-276.

Bathurst, R. G. C. (1971) *Carbonate sediments and their diagenesis*. Elsevier.

Bathurst, R. G. C. (1981) Early diagenesis of carbonate sediments. In *Sediment Diagenesis* (eds. A. Parker and B. W. Sellwood), D. Reidel Publishing Company.

Bennett, R. H., Li, H., Lambert, D. N., Fischer, K. M., and Walter, D. J. (1990) *In situ* porosity and permeability of selected carbonate sediment: Great Bahama Bank Part 1: Measurements. *Mar. Geotechnol.* **9**, 1-28.

Berelson, W. M., Hammond, D. E., McManus, J., and Kilgore, T. E. (1994) Dissolution kinetics of calcium carbonate in equatorial Pacific sediments. *Global Biogeochem. Cycles* **8**, 219-235.

Berg, P. and McGlathery, K. J. (2001) A high-resolution porewater sampling for sandy sediments. *Limnol. Oceanogr.* **46**, 203-210.

Berg, P., Røy, H., Janssen, F., Meyer, V., Jørgensen, B. B., Huettel, M., and De Beer, D. (2003) Oxygen uptake by aquatic sediments measured with a novel non-invasive eddy-correlation technique. *Mar. Ecol. Prog. Ser.* **261**, 75-83.

Berner, R. A. (1966) Chemical diagenesis of some modern carbonate sediments. *Am. J. Sci.* **264**, 1-36.

Berner, R. A. (1977) Stoichiometric models for nutrient regeneration in anoxic sediment. *Limnol. Oceanogr.* **22**, 781-786.

Berner, R. A. (1980) *Early diagenesis - A Theoretical Approach.* Princeton University Press, Princeton, N.J.

Berner, R. A., Scott, M. R., and Thomlinson, C. (1970) Carbonate alkalinity in the pore waters of anoxic marine sediments. *Limnol. Oceanogr.* **15**, 544-549.

Berner, R. A., Westrich, J. T., Graber, R., Smith, J., and Martens, C. S. (1978) Inhibition of aragonite precipitation from supersaturated seawater: A laboratory and field study. *Am. J. Sci.* **278**, 816-837.

Bernstein, L. D. and Morse, J. W. (1985) The steady-state calcium carbonate ion activity product of recent shallow water carbonate sediments in seawater: A comparison of field observations and laboratory experiments. *Mar. Chem.* **15**, 311-326.

Bischoff, W. D., Bertram, M. A., Mackenzie, F. T., and Bishop, F. C. (1993) Diagenetic stabilization pathways of magnesian calcites. *Carbonates Evaporites* **8**, 82-89.

Bischoff, W. D., Mackenzie, F. T., and Bishop, F. C. (1987) Stabilities of synthetic magnesian calcites in aqueous solution: Comparison with biogenic materials. *Geochim. Cosmochim. Acta* **51**, 1413-1423.

Bodensteiner, L. B. (2006) The impact of light availability on benthic oxygen release by the seagrasses - *Thalassia testudinum* (Banks ex König) and *Zostera marina.* California State University.

Borum, J., Pedersen, O., Greve, T. M., Frankovich, T. A., Zieman, J. C., Fourqurean, J. W., and Madden, C. J. (2005) The potential role of plant oxygen and sulphide dynamics in die-off events of the tropical seagrass, *Thalassia testudinum*. *J. Ecol.* **93**, 148-158.

Boschker, H. T. S., Wielemaker, A., Schaub, B. E. M., and Holmer, M. (2000) Limited coupling of macrophyte production and bacterial carbon cycling in the sediments of *Zostera* spp. meadows. *Mar. Ecol. Prog. Ser.* **203**, 181-189.

Boudreau, B. P. (1997) *Diagenetic Models and Their Implementation - Modelling Transport and Reactions in Auqatic Sediments*. Springer.

Boudreau, B. P. and Canfield, D. E. (1993) A comparison of closed- and open-system models for porewater pH and calcite-saturation state. *Geochim. Cosmochim. Acta* **57**, 317-334.

Broecker, W. S. and Clark, E. (2003) Pseudo dissolution of marine calcite. *Earth Planet. Sci. Lett.* **208**, 291-296.

Broecker, W. S. and Takahashi, T. (1966) Calcium carbonate precipitation on the Bahama Banks. *J. Geophys. Res.* **71**, 1575-1602.

Burdige, D. J. (2006) *Geochemistry of Marine Sediments*. Princeton University Press.

Burdige, D. J., Hu, X., and Zimmerman, R. C. Estimating rates of darbonate dissolution in permeable platform sediments. ms. submitted to *Limnol. Oceanogr.*

Burdige, D. J. and Zimmerman, R. C. (2002) Impact of seagrass density on carbonate dissolution in Bahamian Sediments. *Limnol. Oceanogr.* **47**, 1751-1763.

Cai, W.-J. and Reimers, C. E. (1995) Benthic oxygen flux, bottom water oxygen concentration and core top organic carbon content in the deep northeast Pacific Ocean. *Deep-Sea Res. I* **42**, 1681-1699.

Cai, W.-J. and Sayles, F. L. (1996) Oxygen penetration depths and fluxes in marine sediments. *Mar. Chem.* **52**, 123-131.

Cai, W.-J., Zhao, P., and Wang, Y. (2000) pH and pCO_2 microelectrode measurements and the diffusive behavior of carbon dioxide species in coastal marine sediments. *Mar. Chem.* **70**, 133-148.

Caldeira, K. and Rau, G. H. (2000) Accelerating carbonate dissolution to sequester carbon dioxide in the ocean: Geochemical implications. *Geophys. Res. Lett.* **27**, 225-228.

Campbell, G. and Norman, J. (1998) *An Introduction to Environmental Biophysics*. Springer.

Canfield, D. E., Jørgensen, B. B., Fossing, H., Glud, R., Gundersen, J., Ramsing, N. B., Thamdrup, B., Hansen, J. W., Nielsen, L. P., and Hall, P. O. J. (1993) Pathways of organic carbon oxidation in three continental margin sediments. *Mar. Geol.* **113**, 27-40.

Chen, C.-T. A. (2002) Shelf- vs. dissolution-generated alkalinity above the chemical lysocline. *Deep-Sea Res. II* **49**, 5365-5375.

Cline, J. D. (1969) Spectrophotometric determination of hydrogen sulfide in natural waters. *Limnol. Oceanogr.* **14**, 454-458.

Cole, D. R. and Chakraborty, S. (2001) 2. Rates and Mechanisms of Isotopic Exchange. In *Stable Isotope Geochemistry* (eds. J. W. Valley and D. R. Cole), Mineralogical Society of America, Washington DC, pp. 83-223.

Cooper, L. W. and DeNiro, M. J. (1989) Stable carbon isotope variability in the seagrass *Posidonia oceanica*: evidence for light intensity effects. *Mar. Ecol. Prog. Ser.* **50**, 225-229.

Craig, H. (1953) The geochemistry of the stable carbon isotopes. *Geochim. Cosmochim. Acta* **3**, 53-92.

Dickson, A. G. (1981) An exact definition of total alkalinity, and a procedure for the estimation of alkalinity and total inorganic carbon from titration data. *Deep-Sea Res.* **28**, 609-623.

Dickson, A. G., Afghan, J. D., and Anderson, G. C. (2003) Reference materials for oceanic CO_2 analysis: a method for the certification of total alkalinity. *Mar. Chem.* **80**, 185-197.

Dierssen, H. M., Zimmerman, R. C., and Burdige, D. J. Windrows and whitings: Benthic and optical processes in the shallow Bahamas Bank shaped by wind-driven Langmuir supercells. ms. in prep.

Dill, R. F. (1991) Subtidal stromatolites, ooids and crusted-lime mud beds at the Great Bahama Bank Margin, *From shoreline to abyss*. SEPM Spec. Pub. No. 46.

DOE (1994) Handbook of Methods for Analysis of the Various Parameters of the Carbonate Dioxide System in Seawater. (eds. A. M. Dickson and C. Goyet), Oak Ridge National Laboratory, Oak Ridge, TN, USA.

Droxler, A. W., Morse, J. W., and Kornicker, W. A. (1986) Controls on carbonate mineral accumulation in Bahamian Basins and adjacent Atlantic Ocean sediments. *J. Sed. Petrol.* **58**, 120-130.

Duarte, C. M. and Chiscano, C. L. (1999) Seagrass biomass and production: a reassessment. *Aquat. Bot.* **65**, 159-174.

Durako, M. J. and Hall, M. O. (1992) Effects of light on the stable carbon isotope composition of the seagrass *Thalassia testudinum*. *Mar. Ecol. Prog. Ser.* **86**, 99-101.

Durako, M. J. and Sackett, W. M. (1993) Effects of CO_2(aq) on the carbon isotopic composition of the seagrass *Thalassia testudinum* Banks ex Konig (Hydrocharitaceae). *J. Exp. Mar. Biol. Ecol.* **169**, 167-180.

Eadie, B. J. and Jeffrey, L. M. (1973) $\delta^{13}C$ analyses of oceanic particulate organic matter. *Mar. Chem.* **1**, 199-209.

Eldridge, P. M. and Morse, J. W. (2000) A diagenetical model for sediments-seagrass interactions. *Mar. Chem.* **70**, 89-103.

Emerson, S. and Bender, M. (1981) Carbon fluxes at the sediment-water interface of the deep-sea: calcium carbonate preservation. *J. Mar. Res.* **39**, 139-162.

Enriquez, S., Duarte, N. M. C. M., Van Tussenbroek, B. I., and Reyes-Zavala, G. (2001) Effects of seagrass *Thalassia testudinum* on sediment redox. *Mar. Ecol. Prog. Ser.* **219**, 149-158.

Falter, J. L. and Sansone, F. J. (2000) Hydraulic control of pore water geochemistry within the oxic-suboxic zone of a permeable sediment. *Limnol. Oceanogr.* **45**, 550-557.

Forja, J. M., Ortega, T., DelValls, T. A., and Gomez-Parra, A. (2004) Benthic fluxes of inorganic carbon in shallow coastal ecosystems of the Iberian Peninsula. *Mar. Chem.* 85, 141-156.

Fourqurean, J. W., Escorcia, S. P., Anderson, W. T., and Zieman, J. C. (2005) Spatial and seasonal variability in elemental content, $\delta^{13}C$, and $\delta^{15}N$ of *Thalassia testudinum* from South Florida and its implications for ecosystem studies. *Estuaries* **28**, 447-461.

Fourqurean, J. W. and Zieman, J. C. (2002) Nutrient content of the seagrass *Thalassia testudinum* reveals regional patterns of relative availability of nitrogen and phosphorus in the Florida Keys USA. *Biogeochemistry* **61**, 229-245.

Fourqurean, J. W., Zieman, J. C., and Powell, G. V. N. (1992) Phosphorus limitation of primary production in Florida Bay: Evidence from C : N : P ratios of the dominant seagrass *Thalassia testudinum*. *Limnol. Oceanogr.* **37**, 162-171.

Gargett, A., Wells, J., Tejada-Martinez, A. E., and Grosch, C. E. (2004) Langmuir supercells: A mechanism for sediment resuspension and transport in shallow seas. *Science* **306**, 1925-1928.

Gehlen, M., Mucci, A., and Boudreau, B. (1999) Modelling the distribution of stable carbon isotopes in porewaters of deep-sea sediments. *Geochim. Cosmochim. Acta* **63**, 2763-2773.

Goldsmith, J. R., Graf, D. L., and Heard, H. C. (1961) Lattice constants of the calcium-magnesium carbonates. *Am. Mineral.* **46**, 453-457.

Gonifiantini, R. and Zuppi, G. M. (2003) Carbon isotope exchange rate of DIC in karst groundwater. *Chem. Geol.* **197**, 319-336.

Grasshoff, K., Kremling, K., and Ehrhardt, M. (1999) *Methods of Seawater Analysis*. Wiley-VCH.

Green, M. A. and Aller, R. C. (1998) Seasonal patterns of carbonate diagenesis in nearshore terrigenous muds: Relation to spring phytoplankton bloom and temperature. *J. Mar. Res.* **56**, 1097-1123.

Green, M. A. and Aller, R. C. (2001) Early diagenesis of calcium carbonate in Long Island Sound sediments: Benthic fluxes of Ca^{2+} and minor elements during seasonal periods of net dissolution. *J. Mar. Res.* **59**, 769-794.

Grice, A. M., Loneragan, N. R., and Dennison, W. C. (1996) Light intensity and the interactions between physiology, morphology and stable isotope ratios in five species of seagrass. *J. Exp. Mar. Biol. Ecol.* **195**, 91-110.

Hales, B. and Emerson, S. (1997a) Calcite dissolution in sediments of the Ceara Rise: *In situ* measurements of porewater O_2, pH and CO_2 (aq). *Geochim. Cosmochim. Acta* **61**, 501-514.

Hales, B. and Emerson, S. (1997b) Evidence in support of first-order kinetics of calcite in seawater. *Earth Planet. Sci. Lett.* **148**, 317-327.

Halley, R. B. and Yates, K. K. (2004) South Florida coral reef sediment dissolution in response to elevated CO_2 (abst.) *10th International Coral Reef Symposium*, Okinawa, Japa.

Hammond, D. E., Giordani, P., Berelson, W. M., and Poletti, R. (1999) Diagenesis of carbon and nutrients and benthic exchange in sediments of the Northern Adriatic Sea. *Mar. Chem.* **66**, 53-79.

Hemminga, M. A. and Duarte, C. M. (2000) *Seagrass Ecology*. Cambridge University Press.

Hemminga, M. A. and Mateo, A. A. (1996) Stable carbon isotopes in seagrasses: variability in ratios and use in ecological studies. *Mar. Ecol. Prog. Ser.* **140**, 285-298.

Hofmann, M., Wolf-Gladrow, D. A., Takahashi, T., Sutherland, S. C., Six, K. D., and Maier-Reimer, E. (2000) Stable carbon isotope distribution of particulate organic matter in the ocean: a model study. *Mar. Chem.* **72**, 131-150.

Holmer, M., Andersen, F. O., Nielsen, S. L., and Boschker, H. T. S. (2001) The importance of mineralization based on sulfate reduction for nutrient regeneration in tropical seagrass sediments. *Aquat. Bot.* **71**, 1-17.

Hover, V. C., Walter, L. M., and Peacor, D. R. (2001) Early marine diagenesis of biogenic aragonite and Mg-calcite: new constrains from high-resolution STEM and AEM analysis of modern platform carbonate. *Chem. Geol.* **175**, 221-248.

Huettel, M. and Webster, I. T. (2001) Porewater flow in permeable sediments. In *The Benthic Boundary Layer: Transport Processes and Biogeochemistry* (eds. B. P. Boudreau and B. B. Jørgensen), Oxford University Press, pp. 144-170.

Hulthe, G., Hulth, S., and Hall, P. O. J. (1998) Effect of oxygen on degradation rate of refractory and labile organic matter in continental margin sediments. *Geochim. Cosmochim. Acta* **62**, 1319-1328.

Jahnke, R., Richards, M., Nelson, J., Robertson, C., Rao, A., and Jahnke, D. (2005) Organic matter remineralization and porewater exchange rates in permeable South Atlantic Bight continental shelf sediments. *Cont. Shelf Res.* **25**, 1433-1452.

Jahnke, R. A., Craven, D. B., and Gaillard, J.-F. (1994) The influence of organic matter diagenesis on $CaCO_3$ dissolution at the deep-sea floor. *Geochim. Cosmochim. Acta* **58**, 2799-2809.

Jahnke, R. A., Craven, D. B., McCorkle, D. C., and Reimers, C. E. (1997) $CaCO_3$ dissolution in California continental margin sediments: The influence of organic matter remineralization. *Geochim. Cosmochim. Acta* **61**, 3587-3604.

Jahnke, R. A. and Jahnke, D. B. (2004) Calcium carbonate dissolution in deep sea sediments: Reconciling microelectrode, pore water and benthic flux chamber results. *Geochim. Cosmochim. Acta* **68**, 47-59.

Jensen, H. S., McGlathery, K. J., Marino, R., and Howarth, R. W. (1998) Forms and availability of sediment phosphorus in carbonate sands of Bermuda seagrass beds. *Limnol. Oceanogr.* **43**, 799-811.

Jensen, S. I., Kühl, M., Glud, R. N., Jørgensen, L. B., and Prieme, A. (2005) Oxic microzones and radial oxygen loss from roots of *Zostera marina*. *Mar. Ecol. Prog. Ser.* **293**, 49-58.

Jones, W. B., Cifuentes, L. A., and Kaldy, J. E. (2003) Stable carbon isotope evidence for coupling between sedimentary bacteria and seagrasses in a sub-tropical lagoon. *Mar. Ecol. Prog. Ser.* **255**, 15-25.

Kanamori, S. and Ikegami, H. (1980) Computer-processed potentiometric titration for the determination of calcium and magnesium in sea water. *J. Oceanol. Soc. Jpn.* **36**, 177-184.

Keir, R. S. (1980) The dissolution kinetics of biogenic calcium carbonates in seawater. *Geochim. Cosmochim. Acta* **44**, 241-252.

Koch, E. W., Ackerman, J., Van Keulen, M., and Verduin., J. (2006) Fluid Dynamics in Seagrass Ecology: from Molecules to Ecosystems. In *Seagrasses: Biology, Ecology and Conservation* (eds. A. W. D. Larkum, R. J. Orth and C. M. Duarte), Springer, pp. 193-225.

Koch, E. W. and Gust, G. (1999) Water flow in tide- and wave-dominated beds of the seagrass *Thalassia testudinum*. *Mar. Ecol. Prog. Ser.* **184**, 63-72.

Ku, T. C. W., Walter, L. M., Coleman, M. L., Blake, R. E., and Martini, A. M. (1999) Coupling between sulfur recycling and syndepositional carbonate dissolution: evidence from oxygen and sulfur isotope composition of pore water sulfate, South Florida Platform, U.S.A. *Geochim. Cosmochim. Acta* **63**, 2529-2546.

Lewis, E. and Wallace, D. (1998) Program Developed for CO_2 System Calculations. ORNL/CDIAC-105. Carbon Dioxide Information Analysis Center, Oak Ridge National Laboratory, U.S. Department of Energy, Oak Ridge, Tennessee., Oak Ridge, Tennessee.

Lin, G., Banks, T., and Sternberg, L. S. L. O. (1991) Variation in $\delta^{13}C$ values for the seagrass *Thalassia testudinum* and its relations to mangrove carbon. *Aquat. Bot.* **40**, 333-341.

Macintyre, I. G. and Reid, R. P. (1995) Crystal alteration in a living calcareous alga (*Halimeda*): implications for studies in skeletal diagenesis. *J. Sed. Res.* **65**, 143-153.

Macintyre, I. G. and Reid, R. P. (1998) Recrystallization in living procelaneous Foraminifera (*Archaias angulatis*): textural changes without mineralogic alteration. *J. Sed. Res.* **68**, 11-19.

Mackin, J. E. and Swider, K. T. (1989) Organic matter decomposition pathways and oxygen consumption in coastal marine sediments. J. Mar. Res. 47, 681-716.

Malan, D. and McLachlan, A. (1991) In situ benthic oxygen fluxes in a nearshore coastal marine system: a new approach to quatify the effect of wave action. *Mar. Ecol. Prog. Ser.* **73**, 69-81.

Marbà, N., Holmer, M., Gacia, E., and Barrón, C. (2006) Seagrass Beds and Coastal Biogeochemistry. In *Seagrasses: Biology, Ecology and Conservation* (eds. A. W. D. Larkum, R. J. Orth and C. M. Duarte), Springer, pp. 135-157.

Martin, W. R., McNichol, A. P., and McCorkle, D. C. (2000) The radiocarbon age of calcite dissolving at the sea floor: Estimates from pore water data. *Geochim. Cosmochim. Acta* **64**, 1391-1404.

Martin, W. R. and Sayles, F. L. (1996) $CaCO_3$ dissolution in sediments of the Ceara Rise, western equatorial Atlantic. *Geochim. Cosmochim. Acta* **60**, 243-263.

Martin, W. R. and Sayles, F. L. (2003) The recycling of biogenic material at the seafloor, *Treatise on Geochemistry*. Elsevier.

McCorkle, D. C., Emerson, S. R., and Quay, P. D. (1985) Stable carbon isotopes in marine porewaters. *Earth Planet. Sci. Lett.* **74**, 13-26.

McMillan, C. (1980) $^{13}C/^{12}C$ Ratios in seagrasses. *Aquat. Bot.* **9**, 237-249.

McNichol, A. P. and Druffel, E. R. M. (1992) Variability of the $\delta^{13}C$ of dissolved inorganic carbon at a site in the north Pacific Ocean. *Geochim. Cosmochim. Acta* **56**, 3589-3592.

McNichol, A. P., Druffel, E. R. M., and Lee, C. (1991) Carbon cycling in coastal sediments: 2. An Investigation of the sources of ΣCO_2 to pore water using carbon isotopes. In *Organic Substances and Sediments in Water* (eds. R. A. Baker), Lewis Publishers, Chelsea, MI., pp. 249-272.

McNichol, A. P., Lee, C., and Druffel, E. R. M. (1988) Carbon cycling in coastal sediments: 1. A quantitative estimate of the remineralization of organic carbon in the sediments of Buzzards Bay, MA. *Geochim. Cosmochim. Acta* **52**, 1531-1543.

Melim, L. A., Westphal, H., Swart, P. K., Eberli, G. P., and Munnecke, A. (2002) Questioning carbonate diagenetic paradigms: evidence from the Neogene of the Bahamas. *Mar. Geol.* **185**, 27-53.

Millero, F. J. (2001) *Physical Chemistry of Natural Waters*. Wiley-Interscience, New York.

Milliman, J. D. (1974) *Marine Carbonates*. Springer-Verlag, New York.

Milliman, J. D. (1993) Production and accumulation of calcium carbonate in the ocean: budget of a nonsteady state. *Global Biogeochem. Cycl.* **7**, 927-957.

Milliman, J. D. and Bornhold, B. D. (1973) Peak height versus peak intensity analysis of X-ray diffraction data. *Sedimentology* **20**, 445-448.

Milliman, J. D., Freile, D., Steinen, R. P., and Wilber, R. J. (1993) Great Bahama Bank aragonite muds: mostly inorganically precipitated, mostly exported. *J. Sed. Petrol.* **63**, 589-595.

Mook, W. G. and De Vries, J. J. (2001) *Volume I: Introduction: Theory, Methods, Review. In Environmental Isotopes in the Hydrological Cycle Principles and Applications.* UNESCO/IAEA, Paris.

Morse, J. W. (1985) Kinetic control of marphology, composition, and mineralogy of abiotic sedimentary carbonates - discussion. *J. Sediment. Petrol.* **55**, 919-921.

Morse, J. W., Andersson, A. J., and Mackenzie, F. T. (2006) Initial responses of carbonate-rich shelf sediments to rising atmospheric pCO_2 and "ocean acidification": Role of high Mg-calcites. *Geochim. Cosmochim. Acta* **70**, 5814-5830.

Morse, J. W., Gledhill, D. K., and Millero, F. J. (2003) $CaCO_3$ precipitation kinetics in waters from the Great Bahama Bank: Implications for the relationship between Bank hydrochemistry and whitings. *Geochim. Cosmochim. Acta* **67**, 2819-2826.

Morse, J. W. and Mackenzie, F. T. (1990) *Geochemistry of Sedimentary Carbonates.* Elsevier.

Morse, J. W. and Mucci, A. (1984) Composition of carbonate overgrowths produced on Iceland spar calcite crystals buried in Bahamian carbonate-rich sediments. *Sediment. Geol.* **40**, 287-291.

Morse, J. W., Zullig, J. J., Bernstern, L. D., Millero, F. J., Milne, P., Mucci, A., and Choppin, G. R. (1985) Chemistry of calcium carbonate-rich shallow water sediments in the Bahamas. *Am. J. Sci.* **285**, 147-185.

Morse, J. W., Zullig, J. J., Iverson, R. L., Choppin, G. R., Mucci, A., and Millero, F. J. (1987) The influence of seagrass beds on carbonate sediments in the Bahamas. *Mar. Chem.* **22**, 71-83.

Moulin, E., Jordens, A., and Wollast, R. (1985) Influence of the aerobic bacterial respiration on the early dissolution of carbonates in coastal sediments. *Prog. Belgian Ocean. Res.*, 196-205.

Mucci, A. (1983) The solubility of calcite and aragonite in seawater at various salinities. *Am. J. Sci.* **283**, 780-799.

Mucci, A. (1986) Growth kinetics and composition of magnesian calcite overgrowths precipitated from seawater: Quantitative influence of orthophosphate ions. *Geochim. Cosmochim. Acta* **50**, 2255-2265.

Mucci, A. (1987) Influence of temperature on the composition of magnesian calcite overgrowths precipitated from seawater. *Geochim. Cosmochim. Acta* **51**, 1977-1984.

Mucci, A. and Morse, J. W. (1983) The incorporation of Mg^{2+} and Sr^{2+} into calcite overgrowths: influences of growth rate and solution composition. *Geochim. Cosmochim. Acta* **47**, 217-233.

Ogrinc, N. and Faganeli, J. (2003) Stable carbon isotopes in pore waters of coastal marine sediments (the Gulf of Trieste, N Adriatic). *Acta Chim. Slov.* **50**, 645-662.

Patterson, W. P. and Walter, L. M. (1994) Syndepositional diagenesis of modern platform carbonates: Evidence from isotopic and minor element data. *Geology* **22**, 127-130.

Pedersen, O., Borum, J., Duarte, C. M., and Fortes, M. (1998) Oxygen dynamics in the rhizophere of *Cymodocea rotundata*. *Mar. Ecol. Prog. Ser.* **169**, 283-288.

Pilson, M. E. Q. (1998) *An Introduction to the Chemistry of the Sea.* Prentice Hall, Upper Saddle River, NJ.

Plummer, L. N. and Mackenzie, F. T. (1974) Predicting mineral solubility from rate data: application to the dissolution of magnesian calcites. *Am. J. Sci.* **274**, 61-83.

Plummer, L. N. and Sprinkle, C. L. (2001) Radiocarbon dating of dissolved inorganic carbon in groundwater from confined parts of the Upper Floridan aquifer, Florida, USA. *Hydrogeol. J.* **9**, 127-150.

Presley, B. J. and Kaplan, I. R. (1968) Changes in dissolved sulfate, calcium and carbonate from interstitial water of near-shore sediments. *Geochim. Cosmochim. Acta* **32**, 1037-1048.

Rasheed, M., Wild, C., Franke, U., and Huettel, M. (2004) Benthic photosynthesis and oxygen consumption in permeable carbonate sediments at Heron Island, Great Barrier Reef, Australia. *Estuar. Coast. Shelf Sci.* **59**, 135-150.

Rasmussen, K. A., Haddad, R. I., and Neumann, A. C. (1990) Stable-isotope record of organic carbon from an evolving carbonate banktop, Bight of Abaco, Bahamas. *Geology* **18**, 790-794.

Raymond, P. A. and Cole, J. J. (2003) Increase in the export of alkalinity from North America's largest river. *Science* **371**, 88-91.

Reid, R. P. and Macintyre, I. G. (1998) Carbonate recrystallization in shallow marine environments: a widespread diagenetic process forming micritized grains. *J. Sed. Res.* **68**, 928-946.

Reid, R. P., Macintyre, I. G., and Post, J. E. (1992) Micritized skeletal grains in northern Belize lagoon: a major source of Mg-Calcite mud. *J. Sed. Petrol.* **62**, 145-156.

Reimers, C. E., Stecher, H. A., Taghon, G. L., Fuller, C. M., Huettel, M., Rusch, A., Ryckelynck, N., and Wild, C. (2004) In situ measurements of advective solute transport in permeable shelf sands. *Continental Shelf Res.* **24**, 183-201.

Robinson, P. (1980) Determination of calcium, magnesium, manganese, strontium, sodim and iron in the carbonate fraction of limestones and dolomites. *Chem. Geol.* **28**, 135-146.

Rubinson, M. (1969) Carbon-13 fractionation between aragonite and calcite. *Geochim. Cosmochim. Acta* **33**, 997-1002.

Rude, P. D. and Aller, R. C. (1991) Fluorine mobility during early diagenesis of carbonate sediment: An indicator of mineral transformation. *Geochim. Cosmochim. Acta* **55**, 2491-2509.

Rusch, A., Huettel, M., Wild, C., and Reimers, C. (2006) Benthic oxygen consumption and organic matter turnover in organic-poor, permeable shelf sands. *Aquat. Geochem.* **12**, 1-19.

Sabine, C. L. and Mackenzie, F. T. (1995) Bank-derived carbonate sediment transport and dissolution in the Hawaiian Archipelago. *Aquat. Geochem.* **1**, 189-230.

Salata, G. G., Roelke, L. A., and Cifuentes, L. A. (2000) A rapid and precise method for measuring stable carbon isotope ratios of dissolved inorganic carbon. *Mar. Chem.* **69**, 153-161.

Sampou, P. and Oviatt, C. A. (1991) Seasonal patterns of sedimentary carbon and anaerobic respiration along a simulated eutrophication gradient. *Mar. Ecol. Prog. Ser.* **72**, 271-282.

Sanders, D. (2003) Syndepositional dissolution of calcium carbonate in neritic carbonate environments: geological recognition, processes, potential significance. *J. Afr. Earth Sci.* **36**, 99-134.

Sayles, F. L. and Curry, W. B. (1988) $\delta^{13}C$, TCO_2, and the metabolism of organic carbon in deep sea sediments. *Geochim. Cosmochim. Acta* **52**, 2963-2978.

Scalan, R. S. and Morgan, T. D. (1970) Isotope ratio mass spectrometer interumentation and application to organic matter contained in recent sediments. *Int. J. Mass. Spectrom. Ion. Phys.* **4**, 267-281.

Stephens, F. C., Louchard, E. M., Reid, R. P., and Maffione, R. A. (2003) Effects of microalgal communities on reflectance spectra of carbonate sediments in subtidal optically shallow marine environments. *Limnol. Oceanogr.* **48**, 536-546.

Stoessell, R. K. (1992) Effects of sulfate reduction on $CaCO_3$ dissolution and precipitation in mixing-zone fluids. *J. Sed. Petrol.* **62**, 873-880.

Swart, P. K. and Eberli, G. (2005) The nature of the $\delta^{13}C$ of periplatform sediments: Implications for stratigraphy and the global carbon cycle. *Sediment. Geol.* **175**, 115-129.

Tribble, J. S. and Mackenzie, F. T. (1998) Recrystallization of magnesian calcite overgrowths on calcite seeds suspended in seawater. *Aquat. Geochem.* **4**, 337-360.

Turner, J. V., Anderson, T. F., Sandberg, P. A., and Goldstein, S. J. (1986) Isotopic, chemical and texural relations during the experimental alteration of biogenic high-magnesian calcite. *Geochim. Cosmochim. Acta* **50**, 495-506.

Van Tussenboek, B. I., Vonk, J. A., Stapel, J., Erftemeijer, P. L. A., Middelburg, J. J., and Zieman, J. C. (2006) The Biology of *Thalassia*: Paradigms and Recent Advances in Research. In *Seagrasses: Biology, Ecology and Conservation* (eds. A. W. D. Larkum, R. J. Orth and C. M. Duarte), Springer, pp. 409-439.

Villiers, S. D. (1999) Seawater strontium and Sr/Ca variability in the Atlantic and Pacific oceans. *Earth Planet. Sci. Lett.* **171**, 623-634.

Walter, L. M., Bischof, S. A., Patterson, W. P., and Lyons, T. W. (1993) Dissolution and recrystallization in modern shelf carbonates: evidence from pore water and solid phase chemistry. *Phil. Trans. R. Soc. Lon.* **344**, 27-36.

Walter, L. M. and Burton, E. A. (1990) Dissolution of recent platform carbonate sediments in marine pore fluids. *Am. J. Sci.* **290**, 601-643.

Walter, L. M., Ku, T. C. W., Muehlenbachs, K., Patterson, W. P., and Nonnell, L. (2006) Controls on the $\delta^{13}C$ of dissolved inorganic carbon in marine pore waters: an instructive example from biogenic carbonate sediments (South Florida Platform). ms. submitted to *Deep-Sea Res. II.*

Walter, L. M. and Morse, J. W. (1984a) Magnesian calcite stabilities: A reevaluation. *Geochim. Cosmochim. Acta* **48**, 1059-1069.

Walter, L. M. and Morse, J. W. (1984b) Reactive surface area of skeletal carbonates during dissolution: effect of grain size. *J. Sed. Petrol.* **54**, 1081-1090.

Walter, L. M. and Morse, J. W. (1985) The dissolution kinetics of shallow marine carbonates in seawater: A laboratory study. *Geochim. Cosmochim. Acta* **49**, 1503-1513.

Wang, W., Reimers, C. E., Wainright, S. C., Shahriari, M. R., and Morris, M. J. (1999) Applying fiber-optic sensors for monitoring dissolved oxygen. *Sea Technology* **40**, 69-74.

Wenzhoger, F., Adler, M., Kohls, O., Hensen, C., Strotmann, B., Boehme, S., and Schulz, H. D. (2001) Calcite dissolution driven by benthic mineralization in the deep-sea: In situ measurements of Ca^{2+}, pH, pCO_2 and O_2. *Geochim. Cosmochim. Acta* **65**, 2677-2690.

Yates, K. K. and Halley, R. B. (2006) Diurnal variations in rates of calcification and carbonate sediment dissolution in Florida Bay. *Estuar. Coast.* **29**, 24-39.

Zeebe, R. E. and Wolf-Gladrow, D. (2001) *CO_2 in Seawater: Equilibrium, Kinetics, Isotopes*. Elsevier, Amsterdam.

Zimmerman, R. C., Kohrs, D. G., Steller, D. L., and Alberte, R. S. (1997) Impacts of CO_2 enrichment on productivity and light requirements of eelgrass. *Plant Physiol.* **115**, 599-607.

Zullig, J. J. and Morse, J. W. (1988) Interaction of organic acids with carbonate mineral surfaces in seawater and related solutions: I. Fatty acid adsorption. *Geochim. Cosmochim. Acta* **52**, 1667-1678.

APPENDIX A

DERIVATION OF THE EXPRESSION FOR THE $\delta^{13}C$ OF THE DIC ADDED TO SEDIMENT PORE WATERS ($\delta^{13}C_{added}$)

I start with a solution of DIC whose concentration is $[DI^{12}C]_0 + [DI^{13}C]_0$ and add α moles of $DI^{12}C$ and β moles of $DI^{13}C$ to this solution. I can then define $\delta^{13}C_{added}$ as,

$$\delta^{13}C_{added} = 10^3[\frac{(\beta/\alpha) - R_0}{R_0}] \quad \text{(A-1)}$$

where R_0 is the $^{13}C/^{12}C$ ratio of the PDB standard. After this carbon addition, [DIC] is given by,

$$[DIC] = [DI^{12}C]_0 + [DI^{13}C]_0 + \frac{\alpha+\beta}{V} \approx [DI^{12}C]_0 + \frac{\alpha}{V} \quad \text{(A-2)}$$

since $[DI^{12}C]_0 >> [DI^{13}C]_0$ and $\alpha >> \beta$ (note that V is the volume of this solution). Similarly, the initial value of $[DIC]\cdot\delta^{13}C$ is given by

$$([DIC]\cdot\delta^{13}C)_0 \approx [DI^{12}C]_0 \cdot 10^3[\frac{([DI^{13}C]_0/[DI^{12}C]_0 - R_0}{R_0}] = 10^3[\frac{([DI^{13}C]_0 - R_0[DI^{12}C]_0}{R_0}] \quad \text{(A-3)}$$

while its value after this carbon addition is,

$$[DIC]\cdot\delta^{13}C \approx ([DI^{12}C]_0 + \frac{\alpha}{V})\cdot 10^3[\frac{\left(\frac{[DI^{13}C]_0 + \beta/V}{[DI^{12}C]_0 + \alpha/V}\right) - R_0}{R_0}] \quad \text{(A-4)}$$

$$= 10^3[\frac{([DI^{13}C]_0 + (\beta/V) - R_0[DI^{12}C]_0 - R_0(\alpha/V)}{R_0}]$$

Taking the differentials of eqns. (A-2) and (A-4) yields

$$d[DIC] = \frac{\alpha}{V} \quad \text{(A-5)}$$

$$d([DIC]\cdot\delta^{13}C) = 10^3[\frac{(\beta/V) - R_0(\alpha/V)}{R_0}] \quad \text{(A-6)}$$

This then implies that if we plot $[DIC]\cdot\delta^{13}C$ versus [DIC], the slope of the best fit line through the data ($\frac{d([DIC]\cdot\delta^{13}C)}{d[DIC]}$) will be given by

$$\frac{d([DIC]\cdot\delta^{13}C)}{d[DIC]} = \frac{10^3[\frac{(\beta/V) - R_0(\alpha/V)}{R_0}]}{\alpha/V} = 10^3[\frac{(\beta/\alpha) - R_0}{R_0}] \quad \text{(A-7)}$$

which based on eqn. (A-1) equals $\delta^{13}C_{added}$.

APPENDIX B

SEDIMENT INCUBATION PORE WATER DATA

Table B-1. Channel Marker incubation pore water data.

Incubation ID	Time (h)	Titration Salinity	Alk_T (meq/kg)	DIC (mmol/kg)	pH (NBS)	$\delta^{13}C$ (‰)	$[Ca^{2+}]$ (mmol/kg)	TDS (mmol/kg)	$[SO_4^{2-}]$ (mmol/kg)
CM-G	0	37.75	3.19	3.09	7.64	-	11.35	0.000	30.2
	10	37.86	4.38	3.64	7.63	-	11.52	0.512	30.0
	21	37.77	5.39	4.47	7.51	-	11.35	1.116	30.5
	33	37.46	6.42	5.10	7.58	-	11.61	1.590	28.9
	45	37.68	6.80	5.81	7.47	-	11.51	1.786	29.6
	58	37.54	7.98	5.79	7.52	-	11.61	2.002	28.8
	69	37.55	8.66	6.05	7.57	-	11.49	2.105	28.9
	81	37.60	8.91	7.10	7.42	-	11.76	1.798	28.3
	93	37.61	6.94	5.63	7.46	-	11.63	-	29.3
CM-P	0	37.43	3.21	3.20	7.64	-	11.28	0.074	30.2
	10	37.36	4.46	3.80	7.59	-	11.38	0.631	30.6
	21	37.37	5.60	4.51	7.46	-	11.37	1.433	29.3
	33	37.39	6.59	4.85	7.60	-	11.55	1.843	28.7
	45	37.48	7.16	5.75	7.45	-	11.44	2.024	28.8
	58	37.46	7.35	5.56	7.62	-	11.48	1.862	28.7
	69	37.40	8.12	6.50	7.64	-	11.47	2.129	28.8
	81	37.37	8.76	6.84	7.58	-	11.71	1.294	28.3
	93	37.34	7.15	5.87	7.59	-	11.58	-	28.9
CM-R	0	37.82	3.19	3.21	7.64	-	11.28	0.067	29.8
	10	37.57	4.46	3.73	7.59	-	11.40	0.554	29.3
	21	37.34	5.63	4.33	7.50	-	11.45	1.179	29.5
	33	37.55	6.42	4.98	7.62	-	11.64	1.614	29.2
	45	37.50	7.33	5.65	7.56	-	11.52	1.888	28.5
	58	37.54	7.14	5.58	7.59	-	11.64	1.639	29.7
	69	37.49	7.86	6.44	7.61	-	11.60	1.998	28.6
	81	37.60	8.27	6.68	7.52	-	11.65	1.655	28.4
	93	37.52	6.84	5.95	7.60	-	11.68	-	28.9

Table B-1. Continued.

Incubation ID	Time (h)	Titration Salinity	Alk_T (meq/kg)	DIC (mmol/kg)	pH (NBS)	$\delta^{13}C$ (‰)	$[Ca^{2+}]$ (mmol/kg)	TDS (mmol/kg)	$[SO_4^{2-}]$ (mmol/kg)
CM-B	0	37.77	3.20	3.27	7.61	-	11.20	0.124	30.9
	10	37.59	4.60	3.93	7.69	-	11.21	0.619	29.9
	21	37.26	5.55	4.63	7.57	-	11.51	1.419	29.3
	33	37.30	6.56	5.38	7.69	-	11.51	1.732	28.4
	45	37.35	6.24	5.40	7.57	-	11.48	1.663	29.8
	58	37.78	8.86	6.49	7.56	-	11.58	2.011	28.8
	69	37.64	7.71	6.62	7.67	-	11.62	2.017	28.9
	81	37.36	8.49	7.00	7.64	-	11.53	2.141	27.9
	93	37.39	6.96	6.08	7.60	-	11.70	-	28.7
CM-W	0	37.23	3.20	3.14	7.67	-	11.10	0.210	30.5
	10	37.44	4.45	3.82	7.64	-	11.35	0.508	30.9
	21	37.40	5.08	4.45	7.54	-	11.29	0.914	30.0
	33	37.35	5.90	5.11	7.64	-	11.53	1.002	28.0
	45	37.24	6.10	5.42	7.47	-	11.46	1.090	29.1
	58	37.30	6.62	5.94	7.49	-	11.63	1.007	30.0
	69	37.47	7.06	6.52	7.52	-	11.99	1.036	29.2
	81	37.24	7.60	7.17	7.37	-	12.35	0.673	29.7
	93	37.26	5.89	5.91	7.40	-	12.33	-	-

Table B-2. Halfway incubation pore water data.

Incubation ID	Time (h)	Titration Salinity	Alk_T (meq/kg)	DIC (mmol/kg)	pH (NBS)	$\delta^{13}C$ (‰)	$[Ca^{2+}]$ (mmol/kg)	TDS (mmol/kg)	$[SO_4^{2-}]$ (mmol/kg)
HW-G	0	37.34	2.62	2.39	7.76	-	11.11	0.011	29.5
	12	37.02	2.63	2.47	7.48	-	10.95	0.013	28.9
	24	37.97	3.03	3.11	7.47	-	11.09	0.012	30.0
	37	37.77	3.23	3.02	7.41	-	11.04	0.011	29.2
	48	38.10	4.20	3.54	7.41	-	11.26	0.013	29.8
	60	38.02	4.75	3.72	7.43	-	11.36	0.012	23.7
	72	38.07	4.39	3.90	7.58	-	11.61	0.012	-
	85	38.03	4.77	3.88	7.54	-	11.63	0.011	-
	97	38.11	5.60	4.35	7.50	-	11.66	0.015	30.1
	121	38.11	5.01	3.93	7.36	-	11.63	0.013	-
HW-P	0	37.99	2.83	2.58	7.63	-	11.23	0.011	30.2
	12	37.92	3.39	3.01	7.57	-	11.15	0.013	23.9
	24	38.15	3.30	3.15	7.46	-	11.15	0.013	30.7
	37	38.08	4.31	3.77	7.46	-	11.18	0.014	-
	48	38.06	5.31	4.38	7.46	-	11.21	0.015	30.0
	60	38.09	5.21	4.43	7.57	-	11.19	0.015	30.4
	72	38.74	4.88	4.11	7.63	-	11.30	0.016	29.4
	85	38.10	5.39	4.38	7.55	-	11.33	0.015	-
	97	38.07	6.07	4.87	7.52	-	11.53	0.146	23.7
	121	38.05	7.06	5.42	7.37	-	11.27	0.027	29.1
HW-R	0	38.05	2.75	2.54	7.67	-	11.20	0.013	30.6
	12	37.84	3.11	2.93	7.39	-	11.06	0.016	30.0
	24	38.06	3.49	3.31	7.44	-	11.25	0.014	30.3
	37	38.04	4.39	3.67	7.48	-	11.05	0.015	29.1
	48	37.93	4.97	4.19	7.51	-	11.40	0.017	29.8
	60	38.13	5.36	4.41	7.52	-	11.21	0.017	30.0
	72	38.14	6.42	4.80	7.64	-	11.51	0.027	29.7

Table B-2. Continued.

Incubation ID	Time (h)	Titration Salinity	AlkT (meq/kg)	DIC (mmol/kg)	pH (NBS)	δ13C (‰)	[Ca2+] (mmol/kg)	TDS (mmol/kg)	[SO42-] (mmol/kg)
	85	38.14	5.54	4.04	7.62	-	11.07	0.019	29.4
	97	38.10	5.69	4.03	7.58	-	11.40	0.016	29.2
	121	38.10	5.96	4.94	7.42	-	11.26	0.275	28.6
HW-B	0	38.14	2.59	2.27	7.63	-	11.01	0.028	30.4
	12	37.58	3.25	2.75	7.46	-	10.97	0.020	38.1
	24	37.92	3.26	3.06	7.46	-	11.07	0.019	38.1
	37	37.86	3.84	3.24	7.41	-	11.16	0.017	24.1
	48	38.04	3.87	3.04	7.45	-	11.27	0.016	24.3
	60	37.96	3.94	3.77	7.64	-	11.26	0.017	28.7
HW-B	72	38.00	4.40	3.67	7.59	-	11.26	0.020	-
	85	38.17	4.85	3.91	7.53	-	11.39	0.019	29.4
	97	37.97	5.94	4.65	7.54	-	11.33	0.301	32.2
	121	37.96	5.67	4.74	7.45	-	11.36	0.031	-

Table B-3. Ooids Shoals incubation pore water data.

Incubation ID	Time (h)	Titration Salinity	Alk_T (meq/kg)	DIC (mmol/kg)	pH (NBS)	$\delta^{13}C$ (‰)	$[Ca^{2+}]$ (mmol/kg)	TDS (mmol/kg)	$[SO_4^{2-}]$ (mmol/kg)
OS-G	0	37.65	2.46	2.24	7.76	-	11.10	0.013	30.8
	12	37.79	2.67	2.34	7.79	-	11.08	0	30.8
	21	37.78	2.85	2.79	7.66	-	11.06	0	30.6
	34	37.77	3.01	2.85	7.77	-	11.05	0	30.5
	46	37.95	3.33	3.07	7.57	-	11.28	0	27.5
	58	37.65	3.44	2.96	7.59	-	11.21	0	29.9
	70	37.82	4.51	3.21	7.61	-	11.20	0	30.0
	82	37.81	3.45	3.09	7.63	-	11.16	0	32.4
	94	37.87	3.64	3.44	7.53	-	10.99	0	31.5
	106	37.99	3.90	3.48	7.58	-	11.14	0	30.9
OS-P	0	37.60	2.47	2.27	7.81	-	11.02	0	27.4
	12	37.54	2.68	2.49	7.79	-	10.96	0	30.2
	21	37.61	2.81	2.60	7.70	-	11.05	0	28.4
	34	37.64	3.11	2.49	7.77	-	11.10	0	29.7
	46	37.69	3.27	2.97	7.52	-	11.13	0	28.8
	58	37.59	3.36	2.97	7.64	-	11.16	0	30.0
	70	38.24	3.43	3.23	7.57	-	11.03	0	30.0
	82	37.65	3.76	3.37	7.48	-	11.13	0	31.5
	94	37.76	3.69	3.48	7.55	-	11.05	0	29.9
	106	38.26	3.90	3.29	7.69	-	11.24	0	30.4
OS-R	0	38.03	2.39	2.22	7.77	-	11.04	0	29.7
	12	37.71	2.70	2.67	7.86	-	10.96	0	30.6
	21	37.57	2.88	2.70	7.74	-	10.95	0	30.2
	34	37.46	2.99	2.79	7.78	-	11.05	0	30.0
	46	37.56	3.27	3.06	7.55	-	11.12	0	29.3
	58	37.49	3.51	3.25	7.62	-	11.16	0	29.9
	70	37.52	3.94	3.25	7.58	-	11.06	0	30.7

Table B-3. Continued.

Incubation ID	Time (h)	Titration Salinity	Alk_T (meq/kg)	DIC (mmol/kg)	pH (NBS)	$\delta^{13}C$ (‰)	$[Ca^{2+}]$ (mmol/kg)	TDS (mmol/kg)	$[SO_4^{2-}]$ (mmol/kg)
	82	37.63	3.53	2.99	7.59	-	11.21	0.001	29.5
	94	37.50	3.58	3.43	7.56	-	11.13	0	30.2
	106	37.78	3.80	3.72	7.72	-	11.00	0	30.7
OS-B	0	37.87	2.40	2.24	7.72	-	11.04	0.001	29.3
	12	37.86	2.72	2.35	7.84	-	11.14	0	29.9
	21	37.77	2.80	2.67	7.75	-	10.88	0	28.9
	34	37.97	3.08	2.68	7.65	-	11.21	0	29.7
	46	37.98	3.20	2.76	7.55	-	11.13	0	29.4
	58	37.84	3.40	3.23	7.66	-	11.19	0	30.2
	70	37.83	3.49	2.95	7.58	-	11.14	0	29.7
	82	37.91	3.33	3.32	7.69	-	11.18	0	30.6
	94	38.01	3.31	3.21	7.55	-	11.24	0	30.2
	106	37.77	3.36	3.66	7.54	-	11.06	0	28.8

Table B-4. WS-3 incubation pore water data.

Incubation ID	Time (h)	Titration Salinity	Alk_T (meq/kg)	DIC (mmol/kg)	pH (NBS)	$\delta^{13}C$ (‰)	$[Ca^{2+}]$ (mmol/kg)	TDS (mmol/kg)	$[SO_4^{2-}]$ (mmol/kg)
3-N	0	36.62	2.52	2.61	7.56	-0.78	10.96	0.003	-
	15	36.64	2.69	2.77	7.41	-2.58	10.88	0.006	-
	25	36.51	3.05	3.16	7.47	-1.89	10.70	0.003	-
	38	36.62	3.29	3.39	7.41	-1.54	10.72	-	-
	48	36.62	3.53	3.62	7.34	-1.20	10.74	0.025	-
	61	36.80	3.54	3.79	7.51	-0.94	10.72	0.012	-
	72	36.54	3.54	3.65	7.24	-1.59	10.75	-	-
	88	36.66	4.07	4.15	7.54	-0.71	10.71	-	-
	96	36.63	4.17	4.25	7.31	-0.88	10.80	-	-
	109	36.45	3.84	3.93	7.35	-0.88	11.24	-	-
3-L	0	36.62	2.49	2.54	7.50	0.16	10.76	-	-
	15	36.64	3.13	3.22	7.43	-0.03	10.91	0.002	-
	25	36.51	3.47	3.50	7.45	0.22	11.06	0.007	-
	38	36.62	3.80	3.91	7.35	0.30	11.20	0.002	-
	48	36.62	4.07	4.22	7.32	0.06	11.35	-	-
	61	36.80	4.71	4.82	7.28	0.47	11.50	-	-
	72	36.54	4.61	4.81	7.25	0.23	11.50	-	-
	88	36.66	4.82	5.61	7.22	0.37	11.93	-	-
	96	36.63	5.52	5.83	7.30	0.41	11.98	-	-
	109	36.45	5.23	5.47	7.27	-0.23	11.93	-	-
3-H	0	36.62	2.51	2.59	7.55	0.25	10.56	0.003	-
	15	36.64	2.83	2.87	7.50	-0.23	10.80	0.003	-
	25	36.51	3.49	3.64	7.43	0.02	10.99	0.005	-
	38	36.62	4.23	4.33	7.38	0.12	11.13	0.004	-
	48	36.62	4.29	4.45	7.32	0.31	11.30	-	-
	61	36.80	4.69	4.86	7.35	0.13	11.38	-	-
	72	36.54	5.25	5.39	7.25	0.26	11.71	-	-

Table B-4. Continued.

Incubation ID	Time (h)	Titration Salinity	Alk_T (meq/kg)	DIC (mmol/kg)	pH (NBS)	$\delta^{13}C$ (‰)	$[Ca^{2+}]$ (mmol/kg)	TDS (mmol/kg)	$[SO_4^{2-}]$ (mmol/kg)
	88	36.66	5.91	6.13	7.30	0.59	11.59	-	-
	96	36.63	5.78	5.99	7.39	0.60	11.85	-	-
	109	36.45	5.93	6.10	7.25	0.80	12.02	-	-

Table B-5. WS-13 incubation pore water data.

Incubation ID	Time (h)	Titration Salinity	Alk_T (meq/kg)	DIC (mmol/kg)	pH (NBS)	$\delta^{13}C$ (‰)	$[Ca^{2+}]$ (mmol/kg)	TDS (mmol/kg)	$[SO_4^{2-}]$ (mmol/kg)
13-N	0	37.20	2.62	2.57	7.55	0.25	11.10	0.000	-
	8	37.07	3.12	3.22	7.44	-0.46	11.50	0.000	-
	22	36.91	3.27	3.53	7.34	-0.53	11.24	0.009	-
	33	37.17	3.69	3.39	7.37	0.37	11.51	0.008	-
	43	36.96	4.12	3.93	7.36	-0.35	11.41	0.011	-
	56	37.74	4.58	4.19	7.39	0.18	11.75	0.393	-
	69	37.33	4.69	4.51	7.28	-0.09	11.58	0.818	-
	81	37.37	4.34	4.25	7.23	-0.43	11.72	0.470	-
	93	37.59	7.16	6.15	7.43	0.22	12.01	2.338	-
	105	37.21	6.87	6.28	7.50	0.40	11.74	2.591	-
	116	37.20	5.74	5.68	7.40	-0.59	11.73	0.819	-
13-L	0	37.20	2.62	2.57	7.55	0.25	11.10	0.000	-
	8	37.07	3.05	3.20	7.42	-0.07	11.46	0.000	-
	22	36.91	3.68	3.76	7.47	0.23	11.36	0.017	-
	33	37.17	4.03	4.22	7.41	0.61	11.40	0.005	-
	43	36.96	4.43	4.61	7.35	0.49	11.50	0.005	-
	56	37.74	5.31	5.36	7.35	0.62	12.15	0.006	-
	69	37.33	4.65	4.84	7.17	0.05	12.19	0.006	-
	81	37.37	4.98	5.25	7.25	0.18	11.94	0.010	-
	93	37.59	6.21	6.33	7.33	0.38	12.02	0.045	-
	105	37.21	6.60	6.77	7.37	0.29	12.35	0.029	-
	116	37.20	6.29	6.55	7.34	0.26	11.43	0.005	-
13-H	0	37.20	2.62	2.57	7.55	0.25	11.10	0.000	-
	8	37.07	3.29	3.23	7.58	0.56	11.41	0.000	-
	22	36.91	3.98	4.07	7.39	0.57	11.72	0.006	-
	33	37.17	4.54	4.63	7.46	0.64	12.11	0.005	-
	43	36.96	5.15	5.33	7.28	0.43	12.35	0.004	-
	56	37.74	5.92	6.06	7.30	0.63	12.53	0.005	-

Table B-5. Continued.

Incubation ID	Time (h)	Titration Salinity	Alk_T (meq/kg)	DIC (mmol/kg)	pH (NBS)	$\delta^{13}C$ (‰)	$[Ca^{2+}]$ (mmol/kg)	TDS (mmol/kg)	$[SO_4^{2-}]$ (mmol/kg)
13-H	69	37.37	5.27	5.52	7.24	0.09	12.20	0.004	-
	81	37.59	6.35	6.60	7.29	0.30	12.64	0.005	-
	93	37.21	7.19	7.23	7.32	0.12	12.21	0.002	-
	105	37.20	8.07	8.31	7.33	-0.21	12.15	0.002	-
	116	37.20	8.10	8.25	7.37	0.05	13.15	0.003	-

APPENDIX C
ACTIVATION ENERGY OF AEROBIC RESPIRATION IN LSI SEDIMENTS

Newly collected CM sediments were incubated with seawater in sealed 42 ml vials, and O_2 concentration in the vials was monitored using an optical O_2 sensor. Concentration changes were linear with time, and the slope of this line was used to estimate the rate of O_2 consumption. O_2 consumption rates were measured at 10, 17, 23, 25, 30°C and the measured rates were normalized against the wet volume of the sediments.

From the Arrhenius law, $-\frac{E_a}{R}(\frac{1}{T_1}-\frac{1}{T_2}) = \ln(\frac{r_1}{r_2})$ (Mackin and Swider, 1989), in which E_a is apparent activation energy, R is the gas constant (8.314 J/mol/K), T is absolute temperature (K), and r is reaction rate (μmol/h/g sediment), the E_a value of the O_2 consumption reaction is 74.9±8.2 kJ/mol (see Fig. C-1 below). This result agrees well with that of anaerobic respiration reactions (71-109 kJ/mol) in other coastal sediments (Mackin and Swider, 1989), but is greater than the value of 33-53 kJ/mol in coastal environments based on temperature-dependent DIC and O_2 fluxes (Forja et al., 2004).

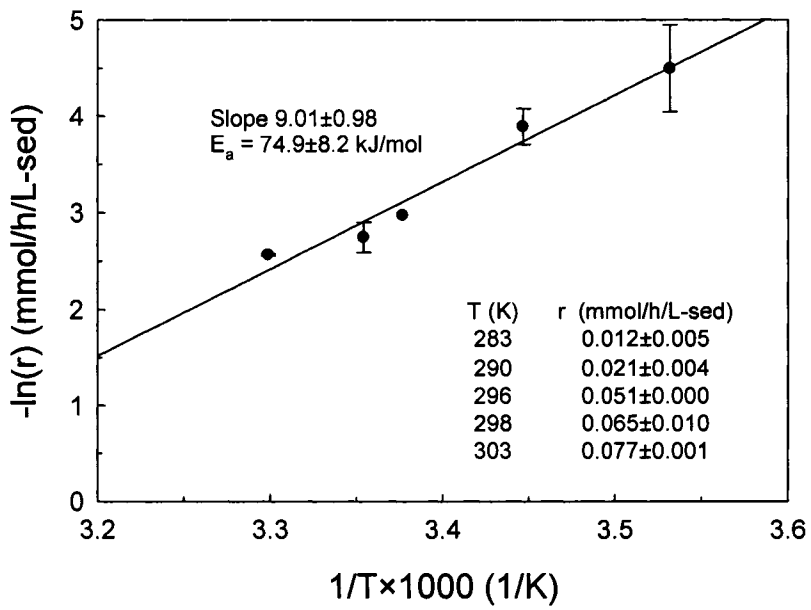

Fig. C-1. Activation energy of O_2 consumption reaction in LSI sediments

APPENDIX D

2004 BAHAMAS BANK SEDIMENT PORE WATER DATA

Table D-1. WS-1 pore water data.

Depth (cm)	Salinity	Alkalinity (meq/kg)	DIC (mmol/kg)	pH_{NBS}	$\delta^{13}C$ (‰)	TDS (mmol/kg)	Sulfate (mmol/kg)	$[Ca^{2+}]$ (mmol/kg)	$[O_2]$ (µmmol/kg)
0	36.7	3.56	2.24	7.97	-	0.00	30.5	10.91	242
1	36.8	4.64	2.09	8.12	-	0.01	29.7	10.82	219
2	36.7	1.33	2.07	8.09	-	0.00	30.3	10.96	244
4	36.8	2.33	2.34	7.73	-	-	-	10.95	109
5	36.7	1.13	2.31	7.56	-	0.07	30.5	10.93	100
8	36.8	1.42	2.24	7.05	-	0.01	28.5	11.05	84
10	36.8	1.45	2.29	7.76	-	-	31.1	10.97	107
15	36.7	2.63	2.56	7.59	-	0.00	32.0	11.02	70
20	36.7	1.29	2.37	6.92	-	0.01	31.8	10.98	96
1	36.8	1.19	2.08	8.16	-	-	30.1	11.14	207
2	36.7	2.36	2.14	8.14	-	-	32.0	10.97	-
4	36.8	-	-	-	-	-	-	10.95	-
5	36.7	1.03	2.31	7.35	-	-	29.1	10.88	-
8	36.8	2.36	2.27	7.7	-	-	30.0	10.90	89
10	36.8	-	-	-	-	-	-	10.93	-
15	36.7	2.43	-	7.03	-	-	-	11.01	-
20	36.7	1.80	2.28	7.71	-	-	30.1	11.10	-
1	36.8	2.26	2.13	8.23	-	-	29.0	10.90	224
2	36.7	2.19	2.15	8.09	-	-	-	10.97	237
4	36.8	2.42	2.32	7.69	-	-	29.7	10.95	117
5	36.7	2.62	2.52	7.38	-	-	-	12.63	92
8	36.8	1.21	2.50	7.25	-	-	31.1	11.00	79
10	36.8	1.20	2.36	7.35	-	-	30.7	10.90	87
15	36.7	2.92	3.05	7.53	-	-	29.5	12.62	28
20	36.7	2.38	2.43	7.63	-	-	30.6	10.89	88

Table D-2. WS-2 pore water data.

Sample	Salinity	Alkalinity (meq/kg)	DIC (mmol/kg)	pH_{NBS}	$\delta^{13}C$ (‰)	TDS (mmol/kg)	Sulfate (mmol/kg)	$[Ca^{2+}]$ (mmol/kg)	$[O_2]$ (µmol/kg)
0	36.5	2.40	2.02	8.35	-	0.00	29.6	11.12	226
0	36.5	1.98	2.04	8.40	2.10	0.00	30.1	10.74	219
0	36.5	1.50	2.03	8.11	2.29	0.00	31.1	11.02	223
1	36.6	2.44	2.15	8.08	-	0.02	31.4	10.91	195
2	36.9	2.36	2.05	7.78	-	0.01	31.6	11.21	195
4	36.6	3.04	2.86	7.97	-	0.10	32.6	11.35	118
5	36.5	3.93	3.66	7.99	-	0.02	30.7	11.21	7
8	36.6	4.68	4.35	7.86	-	0.07	30.6	11.54	40
10	36.7	3.86	3.60	7.85	-	0.09	30.6	11.20	33
15	36.5	5.05	4.63	7.80	-	0.26	30.1	11.75	70
20	36.5	3.35	3.12	7.05	-	0.09	-	10.80	77
1	36.6	2.57	2.40	8.17	-	-	30.1	10.96	167
2	36.9	2.35	2.14	8.33	-	-	31.3	10.74	-
4	36.6	3.14	2.99	7.9	-	-	29.2	11.14	-
5	36.5	4.04	3.87	7.92	-	-	26.6	11.57	-
8	36.6	3.27	3.14	7.84	-	-	30.0	11.16	26
10	36.7	3.27	3.17	7.84	-	-	29.3	11.15	-
15	36.5	3.33	3.22	7.87	-	-	30.7	11.26	-
20	36.5	3.05	2.96	7.87	-	-	31.6	10.80	-
1	36.6	2.38	2.06	8.42	2.11	-	30.3	10.83	202
2	36.9	2.38	2.09	8.41	1.41	-	29.9	10.73	211
4	36.6	4.37	4.16	7.82	1.49	-	29.4	11.57	34
5	36.5	2.43	2.41	7.95	1.09	-	29.6	11.42	58
8	36.6	7.21	6.66	7.76	1.64	-	28.5	12.29	2
10	36.7	4.16	3.98	7.80	1.19	-	29.9	11.57	22
15	36.5	3.92	3.86	7.81	1.58	-	31.4	11.51	0
20	36.5	2.53	2.44	7.93	1.44	-	29.9	10.80	76

Table D-3. WS-3 pore water data.

Sample	Salinity	Alkalinity (meq/kg)	DIC (mmol/kg)	pH_{NBS}	$\delta^{13}C$ (‰)	TDS (mmol/kg)	Sulfate (mmol/kg)	$[Ca^{2+}]$ (mmol/kg)	$[O_2]$ (µmmol/kg)
0	36.4	2.34	2.07	8.23	0.66	0.00	29.2	10.70	213
0	36.4	2.34	2.09	8.25	0.66	0.01	26.6	10.79	212
0	36.4	2.33	2.05	8.27	0.66	0.00	29.2	10.73	214
1	36.3	2.30	2.08	8.35	-	0.01	26.6	10.72	223
2	36.4	2.33	2.28	7.93	-	0.01	27.5	10.95	122
4	36.3	2.53	2.42	7.87	-	0.01	26.4	10.83	78
5	36.3	2.37	2.04	7.86	-	0.00	-	10.74	-
8	36.3	2.49	2.39	7.84	-	0.01	26.3	11.05	84
10	36.4	2.46	2.40	7.80	-	0.01	27.3	10.82	68
15	36.3	2.71	2.74	7.80	-	0.02	27.8	10.86	102
20	36.4	2.53	2.45	7.90	-	0.01		10.82	108
1	36.3	2.33	2.07	8.36	0.48	-	29.9	10.70	216
2	36.4	2.73	2.62	7.86	-0.56	-	27.6	10.76	51
4	36.3	2.63	2.48	7.92	-0.28	-	27.4	10.62	86
5	36.3	2.59	2.52	7.79	-0.02	-	27.4	10.76	41
8	36.3	2.77	2.71	7.83	0.02	-	26.8	10.74	41
10	36.4	2.78	2.55	7.57	0.46	-	27.1	11.03	77
15	36.3	2.78	2.72	7.83	0.56	-	25.6	11.01	77
20	36.4	2.55	2.51	7.86	0.70	-	24.2	11.00	72
1	36.3	2.31	2.09	8.40	0.734	-	26.4	10.62	238
2	36.4	2.30	2.25	8.08	0.662	-	26.9	10.69	137
4	36.3	2.63	2.72	7.79	0.206	-	26.8	10.97	126
5	36.3	2.35	2.32	7.96	0.222	-	26.6	10.72	56
8	36.3	2.49	2.46	7.89	0.216	-	28.1	10.92	61
10	36.4	2.45	2.41	7.86	0.031	-	27.2	10.78	49
15	36.3	2.67	2.63	7.87	0.054	-	-	10.93	42
20	36.4	2.52	2.48	7.93	0.054	-	28.6	10.65	52

Table D-4. WS-3 2nd cast pore water data.

Sample	Salinity	Alkalinity (meq/kg)	DIC (mmol/kg)	pH_{NBS}	$\delta^{13}C$ (‰)	TDS (mmol/kg)	Sulfate (mmol/kg)	$[Ca^{2+}]$ (mmol/kg)	$[O_2]$ (µmmol/kg)
0	36.4	2.32	2.06	8.05	0.00	0.00	29.4	10.75	230
0	36.4	2.30	2.06	8.07	1.84	0.00	29.3	10.60	234
0	36.4	2.29	2.05	8.11	1.85	0.00	29.8	10.58	230
1	36.5	2.35	2.04	8.20	-	0.00	29.0	10.57	232
2	36.4	2.29	2.15	7.93	-	0.00	28.0	10.64	149
4	36.4	2.34	2.24	7.84	-	0.00	28.9	10.70	108
5	36.3	2.29	2.06	8.27	-			10.55	
8	36.3	2.44	2.42	7.75	-	0.01	28.6	10.74	59
10	36.4	2.61	2.34	7.74	-	0.01	29.9	10.61	50
15	36.4	2.53	2.49	7.76	-	0.01	29.0	10.68	45
20	36.5	2.34	2.08	8.28	-	0.01	28.4	10.64	
1	36.5	2.30	2.05	8.32	1.89	-	28.8	10.55	- 237
2	36.4	2.30	2.03	8.33	2.16	-		10.68	230
4	36.4	2.37	2.30	7.93	0.95	-		10.54	113
5	36.3	2.48	2.43	7.78	1.15	-	29.7	10.54	
8	36.3	2.44	2.34	7.81	1.38	-	28.8	10.53	42
10	36.4	2.59	2.49	7.85	1.59	-	29.1	10.69	63
15	36.4	2.50	2.44	7.87	1.52	-	28.8	10.60	46
20	36.5	2.49	2.40	7.85	1.64	-	29.2	10.64	91
1	36.5	2.28	2.06	8.31	-	-	-	10.60	-
2	36.4	2.27	2.08	8.32	-	-	29.3	10.72	58
4	36.4	2.26	2.16	7.92	-	-	28.7	10.49	72
5	36.3	2.51	2.43	7.79	-	-	29.7	10.56	44
8	36.3	2.41	2.37	7.83	-	-	29.3	10.81	73
10	36.4	2.49	2.39	7.71	-	-	29.5	10.75	82
15	36.4	2.57	2.49	7.86	-	-	28.9	10.60	52
20	36.5	2.51	2.46	7.75	-	-	29.3	10.64	67

Table D-5. WS-4 pore water data.

Sample	Salinity	Alkalinity (meq/kg)	DIC (mmol/kg)	pH_{NBS}	$\delta^{13}C$ (‰)	TDS (mmol/kg)	Sulfate (mmol/kg)	$[Ca^{2+}]$ (mmol/kg)	$[O_2]$ (µmmol/kg)
0	36.3	2.26	2.08	7.95	0.00	0.00	29.88	10.70	212
0	36.3	2.16	2.08	8.17	1.01	0.00	30.65	10.67	211
0	36.3	2.27	2.07	8.17	1.12	0.00	28.59	10.75	208
1	36.8	2.26	2.08	8.19	-	0.00	28.86	10.71	219
2	36.5	2.24	2.07	8.17	-	0.00	-	10.84	206
4	36.6	2.26	2.11	8.01	-	0.01	27.41	11.15	145
5	36.4	2.41	2.37	7.82	-	0.00	28.46	10.75	117
8	36.4	2.82	2.83	7.73	-	0.01	29.56	10.87	71
10	36.4	2.41	2.38	7.83	-	0.00	29.08	10.75	78
15	36.4	2.50	2.43	7.85	-	0.01	30.03	11.40	108
20	36.6	2.44	2.45	7.87	-	0.01	-	10.80	94
1	36.8	2.30	2.09	8.34	1.41	-	-	10.70	222
2	36.5	2.24	2.07	8.33	1.48	-	-	10.72	225
4	36.6	2.24	2.08	8.15	1.06	-	29.42	10.92	162
5	36.4	2.48	2.39	7.96	0.83	-	29.05	10.74	115
8	36.4	2.50	2.44	7.84	1.08	-	29.48	11.66	93
10	36.4	2.36	2.25	7.9	1.31	-	-	10.74	119
15	36.4	2.42	2.37	7.9	1.61	-	-	10.64	112
20	36.6	2.48	2.38	7.96	1.53	-	28.28	12.30	94
1	36.8	2.30	2.06	8.35	-	-	29.433	10.64	222
2	36.5	2.31	2.03	8.30	-	-	29.308	10.68	226
4	36.6	2.27	2.07	8.29	-	-	29.506	10.70	180
5	36.4	2.31	2.12	8.22	-	-	29.871	10.79	155
8	36.4	2.66	2.62	7.81	-	-	28.814	10.78	74
10	36.4	2.54	2.51	7.81	-	-	29.956	10.72	56
15	36.4	2.86	2.77	7.80	-	-	29.340	11.02	55
20	36.6	2.53	2.49	7.84	-	-	29.493	10.78	90

Table D-6. WS-5 pore water data.

Sample	Salinity	Alkalinity (meq/kg)	DIC (mmol/kg)	pH_{NBS}	$\delta^{13}C$ (‰)	TDS (mmol/kg)	Sulfate (mmol/kg)	$[Ca^{2+}]$ (mmol/kg)	$[O_2]$ (µmmol/kg)
0	36.9	2.37	2.02	8.13	0.00	0.00	29.3	10.69	218
0	36.9	2.31	2.06	8.12	2.64	0.00	29.8	10.86	209
0	36.9	2.31	2.06	8.11	2.47	0.00	30.4	10.78	206
1	36.6	2.29	2.02	8.14	-	0.00	29.5	10.74	226
2	36.7	2.32	2.08	8.05	-	0.00	29.7	10.68	220
4	37.6	2.60	2.49	7.65	-	0.02	29.1	12.38	51
5	36.6	2.51	2.37	7.69	-	0.02	32.8	10.68	69
8	36.7	2.80	2.63	7.62	-	0.08	28.9	10.80	39
10	37.6	2.46	2.36	7.68	-	0.02	30.4	10.72	45
15	36.8	2.43	2.35	7.65	-	0.01	28.7	10.75	77
20	37.3	2.40	2.28	7.61	-	0.01	31.8	11.75	64
1	36.6	2.29	2.01	8.13	-	-	28.7	10.64	214
2	36.7	2.30	2.05	8.12	-	-	26.4	10.71	192
4	37.6	2.36	2.47	7.94	-	-	-	11.58	-
5	36.6	2.43	2.31	7.76	-	-	29.4	10.71	82
8	36.7	2.60	2.46	7.72	-	-	28.7	10.99	59
10	37.6	2.48	2.32	7.87	-	-	28.1	11.41	24
15	36.8	2.40	2.31	7.7	-	-	-	10.52	33
20	37.3	2.64	2.60	7.65	-	-	31.4	11.72	58
1	36.6	2.28	2.05	8.14	2.60	-	29.3	10.89	212
2	36.7	2.51	2.38	7.77	1.48	-	27.5	10.75	72
4	37.6	2.63	2.45	7.86	1.04	-	30.1	10.78	35
5	36.6	2.59	2.43	7.79	1.24	-	29.0	10.75	-
8	36.7	2.46	2.35	7.78	1.41	-	30.3	10.70	51
10	37.6	2.67	2.53	7.69	1.09	-	29.1	10.77	26
15	36.8	2.35	2.24	7.63	1.61	-	28.7	11.14	62
20	37.3	2.26	2.20	7.70	1.39	-	29.0	11.78	42

Table D-7. WS-6 pore water data.

Sample	Salinity	Alkalinity (meq/kg)	DIC (mmol/kg)	pH_{NBS}	$\delta^{13}C$ (‰)	TDS (mmol/kg)	Sulfate (mmol/kg)	$[Ca^{2+}]$ (mmol/kg)	$[O_2]$ (µmmol/kg)
0	36.7	2.34	2.06	8.05	0.00	0.00	30.9	10.75	207
0	36.7	2.33	2.06	8.06	2.60	0.00	30.1	10.64	205
0	36.7	2.31	2.05	8.06	2.60	0.00	28.0	10.79	209
1	36.8	2.33	2.06	8.04	-	0.00	29.3	10.86	215
2	36.7	2.42	2.16	7.89	-	0.00	29.0	10.85	166
4	37.0	3.71	3.18	7.64	-	0.74	29.1	11.09	0
5	37.4	2.93	2.59	7.75	-	0.31	29.9	11.35	15
8	37.5	2.98	2.85	7.59	-	0.07	24.8	11.11	27
10	37.0	2.88	2.53	7.63	-	0.47	24.7	10.96	59
15	37.6	4.04	3.81	7.48	-	0.34	28.7	11.27	9
20	37.1	3.04	2.66	7.65	-	0.63	29.3	11.01	2
1	36.8	2.28	2.10	8.06	2.62	-	29.5	10.66	215
2	36.7	2.42	2.30	7.89	2.11	-	30.2	10.58	135
4	37.0	2.51	2.33	7.82	2.04	-	29.7	10.74	58
5	37.4	2.65	2.35	7.7	1.48	-	30.1	11.56	6
8	37.5	3.08	2.70	7.67	1.38	-	36.7	11.15	8
10	37.0	2.80	2.61	7.62	1.64	-	28.2	10.85	40
15	37.6	3.16	2.72	7.66	1.45	-	28.3	12.49	17
20	37.1	3.37	3.04	7.65	1.81	-	30.0	11.05	0
1	36.8	2.45	2.24	7.96	-	-	31.2	11.64	173
2	36.7	2.32	2.06	8.07	-	-	29.8	11.41	206
4	37.0	2.86	2.66	7.77	-	-	28.9	11.04	20
5	37.4	2.57	2.34	7.67	-	-	29.1	11.20	31
8	37.5	2.75	2.58	7.68	-	-	29.3	11.13	0
10	37.0	2.69	2.40	7.65	-	-	29.6	10.80	28
15	37.6	2.87	2.69	7.63	-	-	30.2	11.88	1
20	37.1	3.18	2.74	7.66	-	-	30.1	11.19	2

Table D-8. WS-8 pore water data.

Sample	Salinity	Alkalinity (meq/kg)	DIC (mmol/kg)	pH_{NBS}	$\delta^{13}C$ (‰)	TDS (mmol/kg)	Sulfate (mmol/kg)	$[Ca^{2+}]$ (mmol/kg)	$[O_2]$ (µmmol/kg)
0	36.9	2.33	2.09	8.04	-	0.00	30.0	10.78	221
0	36.9	2.34	2.07	8.04	1.56	-	30.0	11.06	215
0	36.9	2.35	2.06	8.07	1.10	-	30.7	11.04	216
1	36.7	2.50	2.35	7.80	-	0.03	29.1	10.78	128
2	37.3	4.19	3.99	7.44	-	0.01	31.4	11.69	22
4	37.0	3.16	2.92	7.43	-	0.39	30.0	11.08	11
5	36.9	3.42	3.20	7.46	-	0.37	29.1	10.82	17
8	36.9	3.01	2.83	7.55	-	0.31	28.7	10.95	57
10	36.8	4.46	4.24	7.43	-	0.61	26.4	11.37	38
15	37.6	4.15	3.86	7.54	-	0.78	29.1	11.28	5
20	37.0	4.60	4.41	7.44	-	0.77	28.6	11.18	0
1	36.7	2.34	2.06	8.08	1.28	-	29.0	10.82	159
2	37.3	2.99	2.82	7.58	-0.30	-	30.9	11.10	68
4	37.0	3.14	2.93	7.57	-	-		11.59	151
5	36.9	3.28	3.04	7.56	0.70	-	28.9	11.10	72
8	36.9	4.34	3.98	7.55	0.45	-	28.8	11.42	34
10	36.8	3.35	3.13	7.57	1.02	-	28.6	11.05	32
15	37.6	4.05	3.76	7.55	0.76	-	29.3	12.56	11
20	37.0	4.43	4.09	7.46	0.82	-	29.0	11.70	8
1	36.7	2.41	2.18	7.98	-	-	29.7	11.07	190
2	37.3	2.92	2.66	7.56	-	-	29.5	11.23	31
4	37.0	3.67	3.50	7.57	-	-	29.3	12.09	2
5	36.9	3.16	2.97	7.47	-	-	30.9	11.09	19
8	36.9	3.45	3.24	7.66	-	-	26.9	11.11	46
10	36.8	3.14	2.92	7.59	-	-	28.7	11.21	6
15	37.6	3.24	3.12	7.55	-	-	28.5	11.33	9
20	37.0	3.22	3.07	7.55	-	-	30.1	11.10	16

Table D-9. WS-9 pore water data.

Sample	Salinity	Alkalinity (meq/kg)	DIC (mmol/kg)	pH_{NBS}	$\delta^{13}C$ (‰)	TDS (mmol/kg)	Sulfate (mmol/kg)	$[Ca^{2+}]$ (mmol/kg)	$[O_2]$ (µmmol/kg)
0	38.2	2.23	2.07	7.94	-	0.00	30.5	11.08	212
0	38.2	2.26	2.05	7.90	1.54	-	31.6	11.10	208
0	38.2	2.26	2.03	8.02	1.40	-	32.2	11.19	208
1	38.0	2.30	2.05	7.99	-	0.00	31.8	11.03	191
2	37.8	2.38	2.26	7.72	-	0.01	30.9	11.68	64
4	37.8	3.19	2.85	7.74	-	0.53	29.9	11.14	2
5	37.6	2.28	2.15	7.71	-	0.02	31.1	10.89	33
8	37.5	2.66	2.53	7.61	-	0.06	30.0	11.00	53
10	37.6	3.10	2.89	7.55	-	0.24	31.1	10.80	7
15	37.4	3.36	2.99	7.61	-	0.67	29.8	11.09	3
20	37.3	3.65	3.36	7.58	-		31.0	11.09	1
1	38.0	2.70	2.11	7.88	1.30	-	30.6	11.05	159
2	37.8	2.38	2.14	7.96	1.44	-	31.9	11.05	136
4	37.8	2.67	2.20	7.690	0.32	-	30.7	11.09	16
5	37.6	2.38	2.26	7.7	0.86	-	30.8	11.19	15
8	37.5	2.64	2.48	7.67	0.60	-	29.8	11.05	16
10	37.6	2.24	2.11	7.65	0.51	-	30.3	10.92	44
15	37.4	2.52	2.34	7.67	0.83	-	30.5	11.09	28
20	37.3	2.70	2.49	7.59	1.47	-	30.7	11.11	32
1	38.0	2.56	2.05	7.97	-	-	31.1	11.01	188
2	37.8	2.29	2.16	7.94	-	-	30.6	11.36	148
4	37.8	2.31	2.15	7.83	-	-	30.5	11.05	63
5	37.6	2.53	2.35	7.74	-	-	27.3	11.00	15
8	37.5	2.47	2.28	7.70	-	-	28.9	11.03	18
10	37.6	2.66	2.42	7.64	-	-	31.1	11.05	8
15	37.4	2.69	2.39	7.61	-	-	27.8	11.09	21
20	37.3	2.66	2.48	7.54	-	-	30.4	11.14	10

Table D-10. WS-10 pore water data.

Sample	Salinity	Alkalinity (meq/kg)	DIC (mmol/kg)	pH_{NBS}	$\delta^{13}C$ (‰)	TDS (mmol/kg)	Sulfate (mmol/kg)	$[Ca^{2+}]$ (mmol/kg)	$[O_2]$ (μmol/kg)
0	37.8	2.32	2.07	8.12	-	0.00	29.4	11.20	198
0	37.8	2.31	2.07	8.12	1.57	-	30.3	11.12	200
0	37.8	2.32	2.05	8.11	1.61	-	31.1	11.00	214
1	37.4	2.32	2.07	8.08	-	0.00	25.2	11.04	194
2	37.4	2.41	2.19	7.97	-	0.03	30.2	11.06	179
4	37.5	2.46	2.32	7.74	-	0.05	30.2	11.06	25
5	37.3	2.43	2.29	7.72	-	0.01	31.2	10.86	64
8	37.3	2.61	2.48	7.68	-	0.03	30.5	11.60	21
10	37.3	2.42	2.38	7.70	-	0.02	30.6	11.14	29
15	37.1	2.68	2.62	7.56	-	0.07	30.3	12.25	34
20	37.2	2.37	2.31	7.70	-	0.02	29.5	11.07	66
1	37.4	2.30	2.04	8.15	-	-	30.3	11.02	217
2	37.4	2.22	2.06	7.84	1.84	-	30.9	11.03	152
4	37.5	2.44	2.30	7.75	0.65	-	30.0	11.06	97
5	37.3	2.75	2.54	7.87	0.17	-	30.0	11.16	44
8	37.3	2.39	2.26	7.68	0.69	-	30.4	10.95	43
10	37.3	2.47	2.38	7.65	-0.26	-	31.0	11.14	39
15	37.1	2.61	2.45	7.69	0.09	-	28.4	11.65	37
20	37.2	2.60	2.47	7.63	-0.01	-	30.6	11.12	50
1	37.4	2.33	2.06	8.12	0.80	-	30.4	11.07	218
2	37.4	2.20	2.05	8.04	-	-	30.7	11.39	219
4	37.5	2.47	2.33	7.64	-	-		11.06	87
5	37.3	2.23	2.17	7.74	0.14	-	30.3	11.01	50
8	37.3	2.36	2.33	7.69	0.39	-	29.5	11.28	42
10	37.3	2.49	2.42	7.64	0.01	-	29.4	11.13	26
15	37.1	2.36	2.27	7.65	0.07	-	30.0	11.06	24
20	37.2	2.64	2.53	7.63	0.09	-	30.4	11.18	40

Table D-11. WS-11 pore water data.

Sample	Salinity	Alkalinity (meq/kg)	DIC (mmol/kg)	pH_{NBS}	$\delta^{13}C$ (‰)	TDS (mmol/kg)	Sulfate (mmol/kg)	$[Ca^{2+}]$ (mmol/kg)	$[O_2]$ (µmol/kg)
0	37.0	2.34	2.07	8.05	-	0.00	29.9	10.55	218
0	37.0	2.37	2.11	8.02	2.01	-	29.6	10.50	207
0	37.0	2.32	2.07	8.02	2.07	-	29.3	10.56	210
1	37.0	2.19	2.06	8.03	-	0.00	29.2	-	212
2	37.0	2.33	2.10	8.03	-	0.00	29.8	10.71	
4	37.3	2.98	2.77	7.55	-	0.11	30.1	-	41
5	37.3	2.90	3.20	7.51	-	0.26	29.9	10.89	23
8	37.3	3.83	3.62	7.49	-	0.35	30.0	-	36
10	37.5	3.81	3.30	7.39	-	0.34	29.3	11.65	45
15	36.9	4.25	3.98	7.51	-	0.69	29.8	11.44	0
20	37.5	4.20	3.94	7.57	-	0.55	33.4	-	2
1	37.0	2.33	2.08	8.03	2.34	-	29.0		198
2	37.0	2.79	2.63	7.58	1.38	-	29.2	10.76	33
4	37.3	2.59	2.59	7.52	1.40	-	29.8	-	40
5	37.3	3.66	3.49	7.47	1.29	-	30.2	11.56	21
8	37.3	4.17	3.96	7.51	1.27	-	29.1	-	8
10	37.5	4.02	3.82	7.54	1.38	-	29.4	11.32	4
15	36.9	4.16	3.85	7.52	1.66	-	30.2	11.15	74
20	37.5	5.03	4.87	7.46	1.40	-	29.0		4
1	37.0	2.06	2.04	7.46	-	-	30.1	11.38	107
2	37.0	2.38	2.30	7.71	-	-	29.9	10.59	80
4	37.3	2.42	2.38	7.60	-	-	37.9	-	21
5	37.3	3.07	2.91	7.56	-	-	-	11.60	21
8	37.3	2.92	2.69	7.54	-	-	29.6	10.90	35
10	37.5	2.93	2.78	7.56	-	-	29.6	11.48	12
15	36.9	2.76	2.62	7.48	-	-	29.3	10.86	55
20	37.5	4.07	3.78	7.48	-	-	29.8	11.86	8

Table D-12. WS-12 pore water data.

Sample	Salinity	Alkalinity (meq/kg)	DIC (mmol/kg)	pH_{NBS}	$\delta^{13}C$ (‰)	TDS (mmol/kg)	Sulfate (mmol/kg)	$[Ca^{2+}]$ (mmol/kg)	$[O_2]$ (µmol/kg)
0	37.0	2.28	2.07	8.01	-	0.00	29.3	10.75	207
0	37.0	2.31	2.07	8.09	1.57	-	29.8	10.80	214
0	37.0	2.31	2.07	8.09	1.51	-	29.5	10.73	218
1	36.9	2.23	2.06	8.07	-	0.00	29.6	10.78	217
2	36.9	2.33	2.07	8.10	-	0.00	30.6	10.74	-
4	36.9	2.34	2.23	7.74	-	0.00	28.9	10.76	81
5	36.9	2.25	2.17	7.54	-	0.00	29.8	10.85	52
8	36.9	2.38	2.31	7.65	-	0.01	30.6	10.79	45
10	36.7	2.35	2.21	7.69	-	0.00	29.1	10.63	62
15	36.8	2.31	2.29	7.51	-	0.01	30.3	10.81	18
20	36.8	2.43	2.34	7.46	-	0.03	29.3	11.30	66
1	36.9	2.32	2.04	7.95	-	-	30.4	10.71	219
2	36.9	2.31	2.06	8.1	-	-	29.3	10.73	209
4	36.9	2.32	2.22	7.82	-	-	-	10.76	135
5	36.9	2.36	2.31	7.49	-	-	29.3	11.06	46
8	36.9	2.44	2.36	7.6	-	-	29.3	11.51	51
10	36.7	2.35	2.29	7.63	-	-	29.3	10.72	60
15	36.8	2.46	2.40	7.58	-	-	30.1	10.81	54
20	36.8	2.29	2.23	7.64	-	-	30.0	11.02	74
1	36.9	2.30	2.08	8.06	1.20	-	29.4	10.85	212
2	36.9	2.36	2.04	8.07	1.52	-	30.1	10.69	210
4	36.9	2.20	2.13	7.76	1.14	-	29.2	10.76	79
5	36.9	2.40	2.36	7.57	1.40	-	28.6	10.95	45
8	36.9	2.36	2.37	7.58	1.36	-	28.9	11.06	74
10	36.7	2.33	2.33	7.49	2.07	-	29.4	10.91	63
15	36.8	2.47	2.37	7.47	2.00	-	29.1	10.81	50
20	36.8	2.36	2.33	7.53	1.40	-	29.4	10.74	56

Table D-13. WS-13 pore water data.

Sample	Salinity	Alkalinity (meq/kg)	DIC (mmol/kg)	pH_{NBS}	$\delta^{13}C$ (‰)	TDS (mmol/kg)	Sulfate (mmol/kg)	$[Ca^{2+}]$ (mmol/kg)	$[O_2]$ (µmmol/kg)
0	36.7	2.35	2.09	7.96	-	0.00	29.7	10.955	211
0	36.7	2.31	2.08	8.02	1.10	-	29.9	10.801	210
0	36.7	2.33	2.10	7.93	0.85	-	30.1	10.771	219
1	36.8	2.32	2.02	8.02	-	0.00	31.8	10.88	222
2	36.7	2.64	2.50	7.72	-	0.01	30.5	11.01	121
4	36.8	2.78	2.68	7.59	-	-	-	11.08	-
5	36.7	2.92	2.86	7.45	-	0.02	29.6	11.13	13
8	36.9	3.23	3.14	7.44	-	0.02	29.1	11.78	18
10	36.7	4.66	4.42	7.36	-	-	29.7	11.48	14
15	36.8	3.33	3.29	7.39	-	0.02	29.5	11.19	16
20	36.7	6.98	6.68	7.26	-	1.31	28.5	12.43	7
1	36.8	2.34	2.08	8.05	1.61	-	30.1	10.87	217
2	36.7	2.66	2.57	7.68	1.07	-	30.5	11.36	91
4	36.8	3.10	2.99	7.48	-	-	29.9	11.13	21
5	36.7	2.45	2.36	7.61	0.93	-	30.1	10.74	68
8	36.9	2.86	2.79	7.52	1.32	-	27.3	11.47	29
10	36.7	5.80	5.29	7.39	1.43	-	29.2	11.60	7
15	36.8	3.49	3.38	7.41	-	-	30.8	11.23	42
20	36.7	6.23	5.90	7.33	1.05	-	30.1	12.43	6
1	36.8	2.31	2.16	8.08	0.25	-	29.6	10.85	227
2	36.7	2.79	2.58	7.70	0.73	-	29.6	11.18	96
4	36.8	2.67	2.57	7.55	0.96	-	29.3	11.03	20
5	36.7	4.15	4.01	7.46	1.10	-	29.4	10.93	18
8	36.9	3.38	3.19	7.53	0.86	-	29.5	11.17	19
10	36.7	3.82	3.60	7.45	1.00	-	28.3	11.46	22
15	36.8	4.72	4.39	7.42	0.41	-	29.8	11.21	6
20	36.7	5.35	5.26	7.38	0.88	-	29.5	12.43	8

Table 14. WS-14 pore water data.

Sample	Salinity	Alkalinity (meq/kg)	DIC (mmol/kg)	pH_{NBS}	$\delta^{13}C$ (‰)	TDS (mmol/kg)	Sulfate (mmol/kg)	$[Ca^{2+}]$ (mmol/kg)	$[O_2]$ (µmmol/kg)
0	36.7	2.35	2.07	8.03	-	0.00	30.4	10.80	220
0	36.7	2.33	2.05	7.99	2.14	-	30.7	10.80	214
0	36.7	2.31	2.08	8.00	2.00	-	30.1	10.84	220
1	36.9	2.30	2.08	8.01	-	0.01	29.3	10.88	210
2	36.9	3.61	3.43	7.48	-	0.27	27.2	11.73	46
4	36.7	5.16	4.85	7.37	-	0.85	28.8	11.63	6
5	37.0	5.49	5.19	7.37	-	0.85	28.9	11.91	10
8	36.6	5.70	5.52	7.36	-	0.66	30.0	12.14	11
10	37.0	5.37	5.13	7.44	-	0.81	-	11.98	6
15	37.4	6.39	6.14	7.38	-	1.10	29.9	12.11	1
20	36.8	5.34	5.09	7.46	-	0.82	29.3	11.93	4
1	36.9	2.38	2.17	8.02	0.98	-	30.5	10.88	209
2	36.9	3.34	3.22	7.65	0.64	-	29.8	11.26	45
4	36.7	5.94	5.26	7.35	-0.18	-	29.9	11.63	1
5	37.0	5.20	4.94	7.54	0.48	-	30.2	11.77	2
8	36.6	3.40	3.29	7.52	0.75	-	31.2	11.50	16
10	37.0	4.48	4.40	7.49	0.89	-	30.1	11.80	5
15	37.4	7.08	7.11	7.42	0.33	-	29.5	12.10	0
20	36.8	4.02	3.95	7.65	0.90	-	29.1	11.86	1
1	36.9	2.32	2.10	8.02	-	-	29.7	10.89	201
2	36.9	2.80	2.62	7.88	-0.148	-	30.3	11.10	126
4	36.7	4.92	4.68	7.58	-0.758	-	30.6	11.63	1
5	37.0	4.12	3.88	7.49	0.805	-	32.0	11.97	13
8	36.6	5.80	5.47	7.42	-0.291	-	29.1	11.82	1
10	37.0	4.28	4.23	7.45	0.927	-	29.5	11.62	9
15	37.4	5.41	5.13	7.51	-	-	28.3	12.09	1
20	36.8	5.33	5.25	7.53	1.106	-	28.7	11.78	6

Table D-15. WS-15 pore water data.

Sample	Salinity	Alkalinity (meq/kg)	DIC (mmol/kg)	pH_{NBS}	$\delta^{13}C$ (‰)	TDS (mmol/kg)	Sulfate (mmol/kg)	$[Ca^{2+}]$ (mmol/kg)	$[O_2]$ (µmmol/kg)
0	36.7	2.30	2.09	7.99	-	0.00	29.6	10.78	203
0	36.7	2.31	2.06	8.02	1.47	-	30.1	10.70	204
0	36.7	2.31	2.08	8.00	1.50	-	29.2	10.74	208
1	36.8	2.26	2.09	8.02	-	-	31.2	10.79	204
2	36.7	3.26	3.07	7.65	-	-	29.5	11.20	108
4	36.7	5.06	4.90	7.38	-	0.15	28.5	11.73	4
5	36.6	3.55	3.46	7.39	-	0.15	29.7	11.52	24
8	36.8	5.84	5.70	7.26	-	1.57	31.0	12.41	8
10	36.8	4.53	4.39	7.39	-	0.15	29.4	11.89	2
15	36.7	5.39	5.25	7.35	-	1.53	29.1	11.95	3
20	36.9	4.35	4.30	7.47	-	0.15	29.2	11.46	2
1	36.8	2.23	2.13	8	1.90	-	29.8	10.72	185
2	36.7	2.97	2.93	7.62	1.34	-	29.6	11.20	69
4	36.7	4.06	3.90	7.52	-	-	28.9	11.36	34
5	36.6	7.00	6.79	7.3	1.17	-	-	12.30	0
8	36.8	4.90	4.62	7.47	1.78	-	26.9	11.72	37
10	36.8	5.58	5.46	7.42	1.91	-	-	11.51	11
15	36.7	7.02	6.85	7.38	1.69	-	-	12.13	2
20	36.9	6.44	6.38	7.42	1.78	-	29.3	11.84	0
1	36.8	2.28	2.09	8.03	-	-	29.7	10.65	208
2	36.7	2.68	2.55	7.82	1.35	-	29.1	10.95	137
4	36.7	4.77	4.57	7.51	-	-	29.5	11.55	4
5	36.6	2.53	2.49	7.55	0.67	-	30.3	10.90	46
8	36.8	3.60	3.53	7.45	2.03	-	29.5	12.06	52
10	36.8	3.98	3.85	7.53	2.08	-	29.2	11.13	36
15	36.7	6.15	6.10	7.36	-	-	30.0	12.30	5
20	36.9	4.79	4.78	7.44	1.18	-	30.1	12.21	10

Table D-16. WS-16 pore water data.

Sample	Salinity	Alkalinity (meq/kg)	DIC (mmol/kg)	pH_{NBS}	$\delta^{13}C$ (‰)	TDS (mmol/kg)	Sulfate (mmol/kg)	$[Ca^{2+}]$ (mmol/kg)	$[O_2]$ (µmmol/kg)
0	36.9	2.34	2.09	8.04	-	0.00	30.1	10.93	224
0	36.9	2.32	2.08	8.01	1.66	-	30.5	10.89	208
0	36.9	2.30	2.07	8.01	1.70	-	29.6	10.88	222
1	37.0	2.33	2.09	8.02	-	0.00	29.9	10.83	220
2	37.1	2.23	2.07	7.89	-	0.00	27.0	11.06	178
4	37.1	2.39	2.34	7.71	-	0.00	28.4	10.80	56
5	37.0	2.55	2.46	7.54	-	0.01	30.1	10.72	19
8	36.9	2.51	2.38	7.60	-	0.01	30.3	10.76	43
10	36.9	2.44	2.33	7.67	-	0.00	29.7	10.86	66
15	36.8	2.36	2.26	7.64	-	0.00	29.4	10.87	32
20	36.9	2.49	2.38	7.64	-	0.01	28.8	11.03	36
1	37.0	2.31	2.06	8	1.79	-	29.5	10.86	216
2	37.1	2.30	2.07	8.05	1.60	-	30.1	10.79	228
4	37.1	2.40	2.26	7.7	1.46	-	30.2	10.80	62
5	37.0	2.38	2.28	7.68	1.31	-	-	10.77	99
8	36.9	2.36	2.27	7.56	0.91	-	30.7	10.74	34
10	36.9	2.31	2.23	7.67	0.88	-	29.5	10.84	69
15	36.8	2.30	2.23	7.65	0.52	-	-	10.87	72
20	36.9	2.30	2.23	7.65	0.43	-	31.1	10.77	66
1	37.0	2.30	2.08	8.03	1.66	-	30.2	10.80	225
2	37.1	2.32	2.10	7.98	1.38	-	30.0	10.89	191
4	37.1	2.38	2.35	7.61	1.00	-	29.1	10.80	54
5	37.0	2.26	2.16	7.71	-	-	29.0	10.83	78
8	36.9	2.67	2.57	7.65	1.40	-	29.5	10.78	30
10	36.9	2.40	2.33	7.63	0.82	-	31.6	10.85	32
15	36.8	2.55	2.47	7.64	0.83	-	29.8	10.87	23
20	36.9	2.307	2.256	7.64	1.26	-	30.7	10.75	47

Table D-17. WS-17 pore water data.

Sample	Salinity	Alkalinity (meq/kg)	DIC (mmol/kg)	pH_{NBS}	$\delta^{13}C$ (‰)	TDS (mmol/kg)	Sulfate (mmol/kg)	$[Ca^{2+}]$ (mmol/kg)	$[O_2]$ (µmmol/kg)
0	36.9	2.163	2.132	8.00	-	0.04	33.3	11.13	218
0	36.9	2.051	2.106	7.99	1.58	-	29.3	10.92	208
0	36.9	2.276	2.088	8.00	1.58	-	27.1	10.70	212
1	36.7	2.280	2.092	7.99	-	-	30.2	10.86	219
2	37.0	2.189	2.079	7.93	-	0.04	30.3	10.71	203
4	36.8	2.246	2.134	7.79	-	0.04		11.59	162
5	36.8	2.252	2.208	7.61	-	0.04	29.3	10.77	53
8	36.9	2.323	2.264	7.49	-	0.04	29.4	10.85	37
10	36.7	2.358	2.377	7.43	-	0.04	29.4	10.90	56
15	36.8	2.378	2.394	7.43	-	-	29.9	10.73	36
20	36.7	2.387	2.392	7.47	-	0.04	30.2	12.38	46
1	36.7	2.314	2.074	7.98	-	-	-	10.82	201
2	37.0	2.241	2.056	7.99	-	-	-	10.76	233
4	36.8	2.171	2.108	7.65	-	-	-	10.74	135
5	36.8	2.304	2.275	7.57	-	-	29.3	10.89	45
8	36.9	2.293	2.213	7.47	-	-	29.5	10.72	53
10	36.7	2.284	2.303	7.51	-	-	30.1	10.67	56
15	36.8	2.514	2.528	7.45	-	-	-	10.73	39
20	36.7	2.361	2.468	7.49	-	-	-	10.88	92
1	36.7	2.291	2.221	7.81	1.82	-	-	10.78	151
2	37.0	2.347	2.362	7.78	0.85	-	29.8	10.85	141
4	36.8	2.229	2.226	7.55	-	-	30.3	10.87	117
5	36.8	2.410	2.380	7.55	0.34	-	30.5	12.85	51
8	36.9	2.338	2.388	7.45	0.28	-	-	11.13	62
10	36.7	2.337	2.380	7.54	0.14	-	-	10.93	82
15	36.8	2.361	2.361	7.52	-	-	29.7	10.73	57
20	36.7	2.135	2.406	7.41	0.77	-	29.6	11.63	75

Table D-18. WS-18 pore water data.

Sample	Salinity	Alkalinity (meq/kg)	DIC (mmol/kg)	pH_{NBS}	$\delta^{13}C$ (‰)	TDS (mmol/kg)	Sulfate (mmol/kg)	$[Ca^{2+}]$ (mmol/kg)	$[O_2]$ (µmmol/kg)
0	37.4	2.35	2.12	8.02	-	0.00	28.6	11.03	218
0	37.4	2.35	2.11	8.00	0.75	-	29.5	11.04	217
0	37.4	2.35	2.11	8.01	1.22	-	29.7	10.91	216
1	37.4	2.32	2.12	8.01	-	0.00	29.2	10.94	209
2	37.6	2.70	2.62	7.56	-	0.01	30.1	11.19	67
4	37.8	3.13	2.96	7.39	-	0.19		11.15	19
5	37.4	3.48	3.25	7.42	-	0.31	29.2	11.20	29
8	37.6	4.62	4.35	7.33	-	0.85	28.8	11.70	26
10	37.1	4.53	4.55	7.30	-	0.42	29.2	11.84	3
15	37.4	6.75	6.75	7.19	-	0.99	28.3	12.01	0
20	37.5	5.40	5.25	7.30	-	0.66	29.7	11.97	2
1	37.4	2.34	2.11	8.01	1.21	0.00	31.9	10.97	217
2	37.6	2.50	2.38	7.61	-	0.01	30.4	10.73	133
4	37.8	3.05	2.93	7.54		0.19	30.2	11.19	31
5	37.4	2.73	2.69	7.46	0.77	0.31	30.2	11.14	12
8	37.6	3.67	3.33	7.43	0.68	0.85	30.0	11.24	43
10	37.1	4.55	4.46	7.33	1.29	0.42	28.9	11.84	54
15	37.4	3.50	3.44	7.43	-	0.99	30.4	11.34	10
20	37.5	5.63	5.61	7.34	0.95	0.66	28.0	12.29	0
1	37.4	2.36	2.12	7.82	1.05	-	31.6	10.91	176
2	37.6	2.31	2.15	7.93	1.41	-	30.1	11.65	195
4	37.8	2.96	2.89	7.47	0.14	-	28.6	11.17	42
5	37.4	3.39	3.18	7.51	0.14	-	31.6	11.26	12
8	37.6	3.12	3.00	7.46	0.27	-	29.0	12.10	24
10	37.1	3.39	3.18	7.50	0.28	-	29.1	11.84	13
15	37.4	4.23	4.21	7.50	0.66	-	33.0	11.67	6
20	37.5	5.12	5.06	7.51	0.04	-	28.8	12.09	0

Table D-19.WS-20 pore water data.

Sample	Salinity	Alkalinity (meq/kg)	DIC (mmol/kg)	pH_{NBS}	$\delta^{13}C$ (‰)	TDS (mmol/kg)	Sulfate (mmol/kg)	$[Ca^{2+}]$ (mmol/kg)	$[O_2]$ (µmmol/kg)
0	37.8	2.30	2.02	7.94	-	0.00	30.6	11.19	227
0	37.8	2.31	2.03	7.95	1.04	-	31.0	11.01	229
0	37.8	2.32	2.04	7.98	1.04	-		11.39	229
1	37.4	2.28	2.01	8.00	-	0.00	30.4	10.91	230
2	37.5	2.30	2.02	7.96	-	0.00	-	10.98	217
4	37.6	2.31	2.22	7.56	-	-	29.7	11.01	67
5	37.5	2.40	2.38	7.52	-	-	28.5	11.07	27
8	37.4	2.31	2.24	7.61	-	0.00	27.9	11.23	85
10	37.3	2.34	2.33	7.50	-	0.00	-	11.13	60
15	37.2	2.38	2.27	7.51	-	0.00	30.3	11.03	45
20	37.2	2.47	2.44	7.44	-	0.02	30.6	11.01	38
1	37.4	2.33	2.07	8.04	-	-	30.8	10.92	222
2	37.5	2.35	2.08	8.03	1.53	-	29.8	11.01	231
4	37.6	2.26	2.20	7.61	-	-	30.9	10.93	59
5	37.5	2.40	2.38	7.48	1.19	-	29.7	11.01	38
8	37.4	2.40	2.41	7.52	1.14	-	29.9	11.23	42
10	37.3	2.38	2.38	7.54	1.03	-	29.2	11.13	65
15	37.2	2.27	2.36	7.52	1.07	-	29.2	11.03	47
20	37.2	2.32	2.39	7.5	1.18	-	28.9	10.89	56
1	37.4	2.23	2.12	8.01	-	-	29.8	11.01	231
2	37.5	2.28	2.12	8.03	-	-	31.2	10.96	229
4	37.6	2.35	2.44	7.63	-	-	31.4	11.02	53
5	37.5	2.34	2.24	7.69	-	-	32.2	10.95	121
8	37.4	2.29	2.39	7.45	-	-	29.8	11.23	59
10	37.3	2.39	2.44	7.47	-	-	31.3	11.13	51
15	37.2	2.36	2.38	7.49	-	-	31.0	11.03	61
20	37.2	2.30	2.36	7.50	-	-	31.0	10.89	56

Table D-20. WS-21 pore water data.

Sample	Salinity	Alkalinity (meq/kg)	DIC (mmol/kg)	pH_{NBS}	$\delta^{13}C$ (‰)	TDS (mmol/kg)	Sulfate (mmol/kg)	$[Ca^{2+}]$ (mmol/kg)	$[O_2]$ (µmmol/kg)
0	37.3	2.25	2.04	8.01	-	0.00	30.1	10.76	213
0	37.3	2.25	2.05	7.97	-	-	30.0	10.75	224
0	37.3	2.28	2.04	8.00	-	-	30.1	10.83	-
1	37.5	2.28	2.07	7.97	-	-	30.3	10.68	207
2	37.2	2.30	2.15	7.85	-	0.00	29.7	10.89	162
4	37.3	2.68	2.52	7.69	-	-	29.4	10.64	
5	37.6	3.05	2.89	7.53	-	-	30.0	11.07	11
8	37.5	4.33	4.09	7.35	-	0.24	-	11.19	5
10	37.6	2.28	2.24	7.55	-	-	30.1	10.68	60
15	37.8	5.20	4.94	7.37	-	0.65	29.2	11.80	0
20	37.6	3.25	3.02	7.45	-	0.08	29.6	11.31	32
1	37.5	2.28	2.07	7.99	-	-	30.1	11.23	213
2	37.2	2.29	2.16	7.835	-	-	29.8	10.57	-
4	37.3	2.81	2.52	7.605	-	-	-	10.92	44
5	37.6	3.07	2.89	7.455	-	-	-	11.37	5
8	37.5	3.22	2.91	7.5	-	-	28.6	10.99	-
10	37.6	4.48	4.01	7.48	-	-	29.2	11.41	6
15	37.8	5.70	5.19	7.47	-	-	29.7	11.64	8
20	37.6	3.79	3.67	7.55	-	-	29.9	11.35	0
1	37.5	2.28	2.07	7.98	-	-	-	10.90	143
2	37.2	2.28	2.16	7.82	-	-	29.9	11.08	142
4	37.3	2.95	2.52	7.52	-	-	-	11.26	43
5	37.6	3.08	2.89	7.38	-	-	29.9	10.78	34
8	37.5	3.06	2.86	7.48	-	-	29.5	11.39	58
10	37.6	2.48	2.37	7.45	-	-	31.6	10.96	16
15	37.8	3.68	5.13	7.58	-	-	30.5	11.96	0
20	37.6	5.60	3.69	7.46	-	-	30.1	11.30	-

Table D-22. WS-24 pore water data.

Sample	Salinity	Alkalinity (meq/kg)	DIC (mmol/kg)	pH_{NBS}	$\delta^{13}C$ (‰)	TDS (mmol/kg)	Sulfate (mmol/kg)	$[Ca^{2+}]$ (mmol/kg)	$[O_2]$ (µmmol/kg)
0	36.4	2.28	2.04	8.08	-	0.00	32.9	10.70	219
0	36.4	2.08	2.05	8.08	1.74	-	29.1	10.75	222
0	36.4	2.30	2.02	8.07	1.76	-	28.9	10.65	218
1	36.4	2.31	2.19	7.92	-	0.00	27.9	11.07	164
2	36.4	2.50	2.54	7.77	-	0.01	29.1	10.66	88
4	36.5	2.63	2.54	7.61	-	0.00	28.8	11.01	42
5	36.6	2.21	2.13	7.67	-	0.00	32.4	10.67	90
8	36.6	2.95	2.81	7.61	-	0.03	29.0	11.52	34
10	36.7	2.72	2.57	7.61	-	0.05	33.9	11.31	19
15	36.7	2.61	2.56	7.63	-	0.01	30.0	10.98	56
20	36.5	2.29	2.23	7.65	-	0.00	30.4	10.67	44
1	36.4	2.42	2.22	7.96	-	-	31.4	10.69	162
2	36.4	2.59	2.24	7.76	-	-	30.1	10.72	50
4	36.5	2.38	2.30	7.57	-	-	-	10.71	52
5	36.6	2.67	2.53	7.74	-	-	27.4	10.89	12
8	36.6	2.71	2.59	7.66	-	-	29.4	10.72	36
10	36.7	2.59	2.53	7.67	-	-	26.4	10.75	36
15	36.7	2.78	2.66	7.63	-	-	28.9	10.98	26
20	36.5	2.52	2.47	7.63	-	-		10.87	40
1	36.4	2.29	2.08	8.07	1.70	-	28.7	11.43	225
2	36.4	2.24	2.14	7.82	1.31	-	37.5	10.44	159
4	36.5	2.33	2.53	7.63	0.77	-	28.3	10.72	31
5	36.6	2.90	2.52	7.69	0.74	-	28.6	10.76	22
8	36.6	2.53	2.69	7.64	1.09	-	32.2	10.84	31
10	36.7	2.43	2.44	7.64	1.38	-	28.2	11.31	13
15	36.7	2.69	2.62	7.62	1.32	-	27.8	10.98	46
20	36.5	2.52	2.48	7.70	0.73	-	29.2	10.56	8

Table D-23. WS-25 pore water data.

Sample	Salinity	Alkalinity (meq/kg)	DIC (mmol/kg)	pH_{NBS}	$\delta^{13}C$ (‰)	TDS (mmol/kg)	Sulfate (mmol/kg)	$[Ca^{2+}]$ (mmol/kg)	$[O_2]$ (µmmol/kg)
0	36.6	2.38	2.03	8.02	-	0.00	29.8	10.70	231
0	36.6	2.31	2.03	8.05	1.60	-	29.9	10.66	225
0	36.6	2.28	2.03	8.05	1.68	-	30.7	10.65	227
1	36.9	2.26	2.10	8.08	-	-	30.0	10.65	227
2	36.8	2.47	2.36	7.83	-	-	29.6	10.75	131
4	36.6	3.15	3.07	7.56	-	0.20	28.9	11.21	51
5	36.6	2.62	2.58	7.75	-	0.00	29.6	10.93	35
8	36.8	3.17	3.16	7.53	-	0.00	30.2	11.27	6
10	36.7	3.30	3.30	7.50	-	-	30.6	11.13	20
15	36.8	3.11	3.06	7.49	-	0.00	29.7	10.96	31
20	37.0	2.76	2.77	7.59	-	0.07	30.1	11.19	43
1	36.9	2.36	2.14	8.05	1.86	-	-	10.78	219
2	36.8	2.34	2.29	7.79	1.46	-	30.2	10.79	131
4	36.6	2.57	2.47	7.66	1.41	-	29.8	10.71	47
5	36.6	2.30	2.37	7.66	1.39	-	31.3	10.69	53
8	36.8	2.68	2.64	7.56	0.96	-	30.5	11.00	25
10	36.7	2.49	2.44	7.65	1.43	-	30.7	10.81	55
15	36.8	2.41	2.47	7.52	1.22	-	31.2	10.99	55
20	37.0	2.36	2.33	7.62	1.49	-	29.4	10.77	39
1	36.9	2.31	2.06	8.14	-	-	29.1	11.01	220
2	36.8	2.35	2.27	7.76	-	-	33.0	10.77	77
4	36.6	2.70	2.66	7.60	-	-	29.9	10.90	30
5	36.6	2.52	2.54	7.58	-	-	29.8	10.79	41
8	36.8	2.93	3.11	7.61	-	-	27.3	10.88	44
10	36.7	2.94	2.61	7.64	-	-	29.4	10.92	38
15	36.8	2.83	2.85	7.58	-	-	-	10.98	47
20	37.0	2.37	2.46	7.58	-	-	30.5	10.96	51

APPENDIX E
MATLAB SCRIPT FOR THE PORE WATER ADVECTION-DIFFUSION-REACTION MODEL

```
clear all;

tic
d=xlsread('ws_data_fitting.xls'); %Load data file

for j= 1:9:181
X=d(j:j+8,1);                          %Define depth variable

% --- Create fit for alkalinity profile
Y1=d(j:j+8,2);
fo1 =
fitoptions('method','NonlinearLeastSquares','Algorithm','Levenberg-
Marquardt',...
    'MaxFunEvals',1000000,'MaxIter',10000,'TolFun',1e-012,'TolX',1e-
012);
ok1 = ~(isnan(X) | isnan(Y1));
st1 = [1 1 1 -1 ];
set(fo1,'Startpoint',st1);
ft1 = fittype('a1+b1/(1+c1*exp(d1*x))' ,...
     'dependent',{'y'},'independent',{'x'},...
     'coefficients',{'a1', 'b1', 'c1', 'd1'});

% Fit this model using new data
cf1 = fit(X(ok1),Y1(ok1),ft1 ,fo1);

%Plot this fit
figure(1)
subplot(221);
plot(X,Y1,'ob'), title('Alkalinity'),axis ([0 25 0 6]); %plot original
data points
hold on;
h1 = plot(cf1,'fit',0.95);                                %plot fitted
curve
set(h1(1),'Color',[1 0 0],...
     'LineStyle','-', 'LineWidth',2,...
    'Marker','none', 'MarkerSize',6);
xlabel ('Depth (cm)');
ylabel ('Alkalinity (meq/L)');
hold off;

% --- Create fit for DIC profile
Y2=d(j:j+8,3);
fo2 =
fitoptions('method','NonlinearLeastSquares','Algorithm','Levenberg-
Marquardt',...
    'MaxFunEvals',1000000,'MaxIter',10000,'TolFun',1e-012,'TolX',1e-
012);
ok2 = ~(isnan(X) | isnan(Y2));
st2 = [1 1 1 -1 ];
set(fo2,'Startpoint',st2);
ft2 = fittype('a2+b2/(1+c2*exp(d2*x))' ,...
     'dependent',{'y'},'independent',{'x'},...
     'coefficients',{'a2', 'b2', 'c2', 'd2'});

% Fit this model using new data
cf2 = fit(X(ok2),Y2(ok2),ft2 ,fo2);
```

```
%Plot this fit
subplot(222);
plot(X,Y2,'sg'), title('DIC'),axis ([0 25 0 6]);
hold on;
h2 = plot(cf2,'fit',0.95);
set(h2(1),'Color',[0 0 1],...
     'LineStyle','-', 'LineWidth',2,...
    'Marker','none', 'MarkerSize',6);
xlabel ('Depth (cm)');
ylabel ('DIC (mM)');
hold off;

% --- Create fit for Ca2+ profile
Y3=d(j:j+8,4);
fo3 =
fitoptions('method','NonlinearLeastSquares','Algorithm','Levenberg-
Marquardt',...
    'MaxFunEvals',1000000,'MaxIter',10000,'TolFun',1e-012,'TolX',1e-
012);
ok3 = ~(isnan(X) | isnan(Y3));
st3 = [1 1 1 0];
set(fo3,'Startpoint',st3);
ft3 = fittype('a3+b3/(1+c3*exp(d3*x))' ,...
     'dependent',{'y'},'independent',{'x'},...
     'coefficients',{'a3', 'b3', 'c3', 'd3'});

% Fit this model using new data
cf3 = fit(X(ok3),Y3(ok3),ft3,fo3);

%Plot this fit
subplot(223);
plot(X,Y3,'dk'), title('Ca2+'),axis ([0 25 10 15]);
hold on;
h3 = plot(cf3,'fit',0.95);
set(h3(1),'Color',[0 0 0],...
     'LineStyle','-', 'LineWidth',2,...
    'Marker','none', 'MarkerSize',6);
xlabel ('Depth (cm)');
ylabel ('Ca2+ (mM)');
hold off;

%legend ('alkalinity', '','DIC','','Ca2+',''); % Add legend to the
profile plots, '' represent the data point

%% --- Create fit for O2 profile
Y4=d(j:j+8,5);
fo4 =
fitoptions('method','NonlinearLeastSquares','Algorithm','Levenberg-
Marquardt',...
    'MaxFunEvals',1000000,'MaxIter',10000,'TolFun',1e-012,'TolX',1e-
012);
ok4 = ~(isnan(X) | isnan(Y4));
st4 = [1 200 0 0.1 ];
set(fo4,'Startpoint',st4);
ft4 = fittype('a4+b4/(1+c4*exp(d4*x))' ,...
```

```
     'dependent',{'y'},'independent',{'x'},...
     'coefficients',{'a4', 'b4', 'c4', 'd4'});

% Fit this model using new data
cf4 = fit(X(ok4),Y4(ok4),ft4 ,fo4);

%Plot this fit
subplot(224);
plot(X,Y4,'vm'), title('O2'),axis ([0 25 0 250]);
hold on;
h4 = plot(cf4,'fit',0.95);
set(h4(1),'Color',[0 1 1],...
     'LineStyle','-', 'LineWidth',2,...
     'Marker','none', 'MarkerSize',6);
xlabel ('Depth (cm)');
ylabel ('O2 (micro-M)');
hold off;

%%%%%%%%%%%%%%%%%%%%%%%%%%%%%%%%%%%%%%%%%%%%%%%
%Spline fitting of seagrass O2 input
sg=xlsread('seagrass_biomass.xls');
sg_depth=sg(:,1);      %seagrass depth
sg_biomass=sg(:,2);    %seagrass biomass

%Calculate second order derivatives of all solutes, their diffusive
fluxes
%and fitted concentration profiles
v=0:0.1:20;       %define a array of 201 elements for 0.1 step size
N=length(v);
DAlk=d(j,9);      %cm2/day
DDIC=d(j,10);     %cm2/day
DCa=d(j,11);      %cm2/day
DOxy=d(j,12);     %cm2/day
x=zeros(N,1);
Alk2=zeros(N,1);
Alk_diff=zeros(N,1);
Alk_conc=zeros(N,1);
DIC2=zeros(N,1);
DIC_diff=zeros(N,1);
DIC_conc=zeros(N,1);
Ca2=zeros(N,1);
Ca_diff=zeros(N,1);
Ca_conc=zeros(N,1);
Oxy2=zeros(N,1);
Oxy_diff=zeros(N,1);
Oxy_conc=zeros(N,1);
seagrass_biomass_cal=zeros(N,1);
seagrass_input=zeros(N,1);

for i=1:1:N
    x(i)=(i-1)*1d-1;

Alk2(i)=2*(cf1.b1)/(1+cf1.c1*exp(cf1.d1*x(i)))^3*(cf1.c1)^2*(cf1.d1)^2*
exp(cf1.d1*x(i))^2-....
cf1.b1/(1+cf1.c1*exp(cf1.d1*x(i)))^2*(cf1.c1)*(cf1.d1)^2*exp(cf1.d1*x(i
));
```

```
Alk_diff(i)=DAlk*Alk2(i);
Alk_conc(i)=cf1.a1+cf1.b1/(1+cf1.c1*exp(cf1.d1*x(i)));


DIC2(i)=2*(cf2.b2)/(1+cf2.c2*exp(cf2.d2*x(i)))^3*(cf2.c2)^2*(cf2.d2)^2*
exp(cf2.d2*x(i))^2....
    -
cf2.b2/(1+cf2.c2*exp(cf2.d2*x(i)))^2*(cf2.c2)*(cf2.d2)^2*exp(cf2.d2*x(i
));
DIC_diff(i)=DDIC*DIC2(i);
DIC_conc(i)=cf2.a2+cf2.b2/(1+cf2.c2*exp(cf2.d2*x(i)));


Ca2(i)=2*(cf3.b3)/(1+cf3.c3*exp(cf3.d3*x(i)))^3*(cf3.c3)^2*(cf3.d3)^2*e
xp(cf3.d3*x(i))^2....
    -
cf3.b3/(1+cf3.c3*exp(cf3.d3*x(i)))^2*(cf3.c3)*(cf3.d3)^2*exp(cf3.d3*x(i
));
Ca_diff(i)=DCa*Ca2(i);
Ca_conc(i)=cf3.a3+cf3.b3/(1+cf3.c3*exp(cf3.d3*x(i)));


Oxy2(i)=2*(cf4.b4)/(1+cf4.c4*exp(cf4.d4*x(i)))^3*(cf4.c4)^2*(cf4.d4)^2*
exp(cf4.d4*x(i))^2....
    -
cf4.b4/(1+cf4.c4*exp(cf4.d4*x(i)))^2*(cf4.c4)*(cf4.d4)^2*exp(cf4.d4*x(i
));
Oxy_diff(i)=DOxy*Oxy2(i);
Oxy_conc(i)=cf4.a4+cf4.b4/(1+cf4.c4*exp(cf4.d4*x(i)));

%Seagrass biomass
    seagrass_biomass_cal(i)=interp1(sg_depth,sg_biomass,x(i),'spline');

%Seagrass underground biomass interpolation at 0.1 cm depth interval
    seagrass_input(i)=d(j,8)*seagrass_biomass_cal(i)/100;
end

    biomass=trapz(x,seagrass_biomass_cal); %Seagrass biomass
integration
    seagrass_input_corr=seagrass_input/biomass*100;

biomass=trapz(x,seagrass_biomass_cal);   %trapzoidal approximation of
total biomass in % value, number is 102%
oxy_input_non_irr=Oxy_diff+seagrass_biomass_cal*d(j,8)/100/biomass*100;
%O2 input through seagrass plant and diffusion only, plant input is
corrected by calculated seagrass biomass integrated value above

%figure(2)
plot(x,oxy_input_non_irr,x,Oxy_diff), title('O2 input through diffusion
and seagrass pumping')

Alk_irr=zeros(N,1);
DIC_irr=zeros(N,1);
Ca_irr=zeros(N,1);
Oxy_irr=zeros(N,1);
```

```
fval=zeros(2001,101);
for k=1:1:2001
     for mm=1:1:101
%%%%%%%%%%%%%%%%%%%%%%%%%%%%%%%%%%%%%%%%%%%%%%%%%%%%%%%%%%%%%%%%%%%%%%%%%%%%
Trial of result searching, linear gradient within the literature
reported values%
%%%%%%%%%%%%%%%%%%%%%%%%%%%%%%%%%%%%%%%%%%%%%%%%%%%%%%%%%%%%%%%%%%%%%%%%%%%%

    alpha0=[(k-1)*0.01,(mm-1)*0.01];

for i=1:1:N
    x(i)=(i-1)*1d-1;
    Alk_irr(i)=alpha0(1)*exp(-alpha0(2)*x(i))*(Alk_conc(i)-Alk_conc(1));
    DIC_irr(i)=alpha0(1)*exp(-alpha0(2)*x(i))*(DIC_conc(i)-DIC_conc(1));
    Ca_irr(i)=alpha0(1)*exp(-alpha0(2)*x(i))*(Ca_conc(i)-Ca_conc(1));
    Oxy_irr(i)=alpha0(1)*exp(-alpha0(2)*x(i))*(Oxy_conc(i)-Oxy_conc(1));
end

    Alk_prod=trapz(x,(-Alk_diff+Alk_irr))*d(j,7)*10000/1000;
    DIC_prod=trapz(x,(-DIC_diff+DIC_irr))*d(j,7)*10000/1000;
    Ca_prod=trapz(x,(-Ca_diff+Ca_irr)   )*d(j,7)*10000/1000;
    Oxy_cons=trapz(x,(Oxy_diff-Oxy_irr+seagrass_input_corr))*d(j,7)/100;

    F=zeros(3,1);
    F(1)=abs((2*Oxy_cons-Alk_prod)/(2*Oxy_cons+Alk_prod)*2);
    F(2)=abs((2*Oxy_cons-DIC_prod)/(2*Oxy_cons+DIC_prod)*2);
    F(3)=abs((Alk_prod-DIC_prod)/(Alk_prod+DIC_prod)*2);
    fval(k,mm)=mean(F);

     end
end

%Get minimum value from the matrix
SizeData = size(fval);
Vec = reshape(fval, [prod(SizeData), 1]);
[Min, MinInd] = min(Vec);

ND = length(SizeData);

StrCom = '[I1 ';
for Idim=2:1:ND,
   StrTemp = sprintf('I%d ',Idim);
   StrCom  = [StrCom,',',StrTemp];
end
StrInd = [StrCom,']'];
StrCom = [StrInd,'=ind2sub(SizeData,MinInd);'];
eval(StrCom);
MinIndVec=eval(StrInd);
fval(I1,I2)

%Calculate production and consumption rate of each species using the
obtained parameters

    alpha1=[(I1-1)*0.01,(I2-1)*0.01];
```

```
for i=1:1:N
    x(i)=(i-1)*1d-1;
    Alk_irr(i)=alpha1(1)*exp(-alpha1(2)*x(i))*(Alk_conc(i)-Alk_conc(1));
    DIC_irr(i)=alpha1(1)*exp(-alpha1(2)*x(i))*(DIC_conc(i)-DIC_conc(1));
    Ca_irr(i)=alpha1(1)*exp(-alpha1(2)*x(i))*(Ca_conc(i)-Ca_conc(1));
    Oxy_irr(i)=alpha1(1)*exp(-alpha1(2)*x(i))*(Oxy_conc(i)-Oxy_conc(1));
end

    Alk_prod=trapz(x,(-Alk_diff+Alk_irr))*d(j,7)*10000/1000;
    DIC_prod=trapz(x,(-DIC_diff+DIC_irr))*d(j,7)*10000/1000;
    Ca_prod=trapz(x,(-Ca_diff+Ca_irr))*d(j,7)*10000/1000;
    Oxy_cons=trapz(x,(Oxy_diff-Oxy_irr+seagrass_input_corr))*d(j,7)/100;
    Oxy_cons_diff=trapz(x,(Oxy_diff))*d(j,7)/100;
    Oxy_cons_irr=trapz(x,(-Oxy_irr))*d(j,7)/100;

%Modeling result output

%Curve fitting coefficient
Fitting_coefs={'A_alk','B_alk','C_alk','D_alk';cf1.a1,cf1.b1,cf1.c1,cf1
.d1;...
    'A_DIC','B_DIC','C_DIC','D_DIC';cf2.a2,cf2.b2,cf2.c2,cf2.d2;...
    'A_Ca','B_Ca','C_Ca','D_Ca';cf3.a3,cf3.b3,cf3.c3,cf3.d3;...
    'A_Oxy','B_Oxy','C_Oxy','D_Oxy';cf4.a4,cf4.b4,cf4.c4,cf4.d4};

%Production or consumption rates of each species
Prod_Cons={'Alkalinity production',Alk_prod;'DIC
production',DIC_prod;'Ca production',Ca_prod;...
    'Oxygen consumption',Oxy_cons;'err',fval(I1,I2)};

%Oxygen input by all three mechanisms
Oxy_inputs={'Total
consumption',Oxy_cons;'Irrigation',Oxy_cons_irr;'Diffusion',Oxy_cons_di
ff;'Plant Input', d(j,8)*d(j,7)/100};

%Advection coefficient
Irr_coef={'alpha',(I1-1)*0.01;'beta',(I2-1)*0.01};

%Result ouput
xlswrite('ws_data_fitting.xls',Fitting_coefs',(j+8)/9+1,'B2')
xlswrite('ws_data_fitting.xls',Prod_Cons,(j+8)/9+1,'G12')
xlswrite('ws_data_fitting.xls',Oxy_inputs,(j+8)/9+1,'G18')
xlswrite('ws_data_fitting.xls',Irr_coef,(j+8)/9+1,'K18')
end
```

APPENDIX F

THE LETTER OF REPRINT PERMISSION

ELSEVIER

3 January 2007 Our ref: CT/SS/Jan 07/J004

Xinping Hu
Old Dominion University
OEAS Department
Norfolk, VA 23529 USA

Dear Dr. Hu

GEOCHIMICA ET COSMOCHIMICA ACTA, Vol 71, No 1, 2007, pp 129-144, Hu & Burdige, "Enriched stable carbon..."

As per your letter dated 20 December 2006, we hereby grant you permission to reprint the aforementioned material at no charge **in your thesis** subject to the following conditions:

1. If any part of the material to be used (for example, figures) has appeared in our publication with credit or acknowledgement to another source, permission must also be sought from that source. If such permission is not obtained then that material may not be included in your publication/copies.

2. Suitable acknowledgment to the source must be made, either as a footnote or in a reference list at the end of your publication, as follows:

   "Reprinted from Publication title, Vol number, Author(s), Title of article, Pages No., Copyright (Year), with permission from Elsevier".

3. Your thesis may be submitted to your institution in either print or electronic form.

4. Reproduction of this material is confined to the purpose for which permission is hereby given.

5. This permission is granted for non-exclusive world **English** rights only. For other languages please reapply separately for each one required. Permission excludes use in an electronic form other than submission. Should you have a specific electronic project in mind please reapply for permission.

6. This includes permission for UMI to supply single copies, on demand, of the complete thesis. Should your thesis be published commercially, please reapply for permission.

Yours sincerely

C. Truter

Clare Truter
Rights Manager, S&T

VITA

XINPING HU
Department of Ocean, Earth, and Atmospheric Sciences
Old Dominion University
Norfolk, Virginia, 23529-0276, USA

EDUCATION

Ph.D., Oceanography, May 2007
Old Dominion University, Norfolk, Virginia
Dissertation: Seagrass mediated carbonate dissolution and early diagenesis in Bahamas Bank sediments (Defended on Jan. 10th, 2007)

B.S., Chemistry, July, 1997
Beijing University, Beijing, China

PROFESSIONAL EXPERIENCE

Old Dominion University, Norfolk, Virginia
Research Assistant, 2000-present

Institute of Oceanology, Chinese Academy of Sciences, Qingdao, Shandong, China
Research Assistant, 1997-2000

AWARDS

Dominion Scholar Award 2000-2002
OEAS Special Research Scholarship 2005

PUBLICATIONS

Hu, X. and Burdige, D. J., 2007. Enriched stable carbon isotopes in the pore waters of carbonate sediments dominated by seagrasses: evidence for coupled carbonate dissolution and reprecipitation. *Geochim. Cosmochim. Acta* **71**, 129-144.